Mechanisms of *GBA1* related PD in hiPSC derived neurons

Dissertation

zur Erlangung des Grades eines
Doktors der Naturwissenschaften

der Mathematisch-Naturwissenschaftlichen Fakultät
und
der Medizinischen Fakultät
der Eberhard-Karls-Universität Tübingen

vorgelegt
von

David Schöndorf
aus Neustadt an der Weinstraße, Deutschland

Juli - 2017

Tag der mündlichen Prüfung: .....18.07.2018.....

Dekan der Math.-Nat. Fakultät: Prof. Dr. W. Rosenstiel
Dekan der Medizinischen Fakultät: Prof. Dr. I. B. Autenrieth

1. Berichterstatter: Prof. PD Dr. Thomas Gasser
2. Berichterstatter: Prof. PD Dr. Stefan Liebau

Prüfungskommission: Prof. Dr. Andrea Wizenmann
Jun. Prof. PD Dr. / Dr. Michela Deleidi

Erklärung / Declaration:

Ich erkläre, dass ich die zur Promotion eingereichte Arbeit mit dem Titel:

„Mechanisms of GBA1 related PD in hiPSC derived neurons“

selbständig verfasst, nur die angegebenen Quellen und Hilfsmittel benutzt und wörtlich oder inhaltlich übernommene Stellen als solche gekennzeichnet habe. Ich versichere an Eides statt, dass diese Angaben wahr sind und dass ich nichts verschwiegen habe. Mir ist bekannt, dass die falsche Abgabe einer Versicherung an Eides statt mit Freiheitsstrafe bis zu drei Jahren oder mit Geldstrafe bestraft wird.

I hereby declare that I have produced the work entitled “……”, submitted for the award of a doctorate, on my own (without external help), have used only the sources and aids indicated and have marked passages included from other works, whether verbatim or in content, as such. I swear upon oath that these statements are true and that I have not concealed anything. I am aware that making a false declaration under oath is punishable by a term of imprisonment of up to three years or by a fine.

Tübingen, den 20.7.2017 .....

Datum / Date Unterschrift /Signature

"Mechanisms of *GBA1* related PD in hiPSC derived neurons"

Table of Contents

Chapter 1: Introduction:

Parkinson's disease

Parkinson's disease (PD) is the second most common neurodegenerative disorder after Alzheimer's disease, affecting around 6 million people worldwide (Lesage & Brice, 2009). PD is, except rare cases of early onset, primarily a disease of the elderly which affects 1-2% of the population over 65 and 5% of the population over 85 years of age (Alves, 2008). It was first described by James Parkinson in 1817 in the work "An assay on the Shaking palsy" where he describes the disease as: " Involuntary tremulous motions, with lessened muscular power (...) with a propensity to bend the trunk forwards, and to pass from a walking to a running pace: the senses and intellects being un-injured" (Parkinson, 1817, re-published in 2002). Today the clinical representation of PD can be separated in motor and non-motor symptoms. Classical motor symptoms include resting tremor, bradykinesia, shuffling gait and postural instability. The symptoms are progressive but the age of onset and the rate of progression is variable (Hauser, 2012). Besides classical motor symptoms, non-motor symptoms include cognitive, behavioural or neuropsychatric disturbances which are known to accompany 90% of all PD patients during the course of the disease (Löhle, 2009). Non-motor symptoms can deteriorate quality of life massively since they do not respond as well to current therapies as motor symptoms (Lim & Lang, 2010) and include depression or anxiety, which occur in 20% to over 50% of all PD cases (J. J. Chen & Marsh, 2014). Further, the risk to develop dementia over the course of PD is increased 6 times and occurs usually later in the disease (Aarsland, 2001).

During lifetime, PD is defined on the basis of clinical parkinsonian symptoms of the patient but a definite diagnosis is possible only by post mortem analysis of the patient brain. The identification of cytoplasmic inclusion bodies, spindle-like Lewy neuritis (LNs) or more globular Lewy bodies (LBs), is a mandatory prerequisite for the diagnosis. These cellular inclusion bodies consist of protein aggregates containing mainly alpha-synuclein (α-syn), neurofilaments and ubiquitin (Spillantini, 1997). The pathology is not restricted to the midbrain but spreads with time course

of the disease. This process affects just certain subtypes of neurons and can be divided in six stages starting in the medulla oblongata in the brain stem spreading over the midbrain and mesocortex until affecting the neocortex. The progression of protein accumulation in different brain areas correlates well with the clinical manifestation of symptoms in PD patients (Braak, 2003). In addition to LB pathology, PD is defined by a loss of dopaminergic neurons in the *substantia nigra pars compacta* (SNPc) in the midbrain (mDA neurons). Dopaminergic neurons in the SNPc are characterized by the production of neuromelanin, which results in dark pigmentation of such cells and depigmentation as consequence in PD brains when dopaminergic neurons are dying (Marsden, 1983). Loss of these neurons leads to a depletion of dopamine (DA) in the areas of their projections, mainly in the putamen. This imbalance in dopamine leads to striatal dysfunction and the progression of PD related motor symptoms (Kish, 1988). Interestingly, first motor symptoms only occur when already 60-70% of dopaminergic cells have died (Sulzer, 2007) which indicates compensatory mechanisms such as upregulation of dopamine synthesis and downregulation of dopamine transporters in the affected regions of the putamen (Nandhagopal, 2011). It is important to notice that neurodegeneration is not restricted to dopaminergic neurons, but also affects noradrenergic, cholinergic and serotonergic neurons in different brain areas like the olfactory bulb, cerebral cortex or hippocampus, which could explain the high rate of dementia and other non-motor symptoms accompanying PD (Dauer & Przedborski, 2003).

The molecular pathomechanisms underlying PD are still not completely understood. There is emerging evidence that pathogenic pathways like protein aggregation, impairment of the ubiquitin-proteasomal or autophagosomal system, elevated oxidative stress and mitochondrial dysfunction could represent common mechanisms underlying both familial and sporadic forms of PD (Moore, 2005).

Initial causes of such defects are not well known, but aging, environmental factors or familial genetic predisposition are proposed to contribute to the multifactorial etiology of PD.

Risk factors for PD:

Neurodegenerative disorders, like PD, are the result of complex interactions between aging, which represents the strongest risk factor to develop such diseases, environmental factors and genetic predisposition. On a molecular level aging is considered to be a partly predictable process of cellular alterations that lead to accumulation of unrepaired cellular damage, caused by a weakening of cellular repair and compensatory mechanisms (Kirkwood, 2003). Underlying mechanisms are for example mitochondrial dysfunction, which in turn leads to excessive production of reactive oxygen species (ROS), free radical formation, DNA mutations and genomic instability. An age related decline in activity of the proteasomal-autophagosomal system can lead to an aberrant accumulation of cellular proteins. Further associated is an elevation in inflammation, activation of microglia and the complement system as well as a reduced response to beneficial neurotrophic factors (Cherra & Chu, 2008) (Hindle, 2010).

Environmental factors such as viral infection have long been proposed to cause PD, however even though they can induce parkinsonian like symptoms, clinical and pathological characteristics can differ from PD (H. Jang, 2009). This changed in 1982 when researchers observed cases of acute parkinsonism in patients after intake of the meperidine analogue 1-methyl-4-phenyl-1,2,3,6-tetrahydropyridine (MPTP). Importantly MPTP-induced disease fully recapitulated PD characteristics which include a dramatic improvement of the symptoms after the application of L-dopa (Ballard, 1985). Further tests in animal models, using squirrel monkeys, revealed a specific destruction of nigral dopaminergic neurons after MPTP application (Langston, 1984). Since that time several other compounds, mainly pesticides, have been found to induce PD in a MPTP related manner. Such toxins include for example Rotenone, Paraquat, organochlorine pesticides or hexachlorohexanes. For many substances the mechanisms of action are not completely understood, however mitochondrial dysfunction and excessive ROS production seem to play a common role, which lead to cell death of dopaminergic neurons (Goldman, 2014). Beside pesticides, further environmental factors which increase the risk to develop PD have been suggested, including increased exposure to certain metals (iron, manganese, mercury), polychlorinated biphenyls (used extensively as lubricants and coolants in 1930-1970) or increased levels of air

pollution (Goldman, 2014). Interestingly there have been also life style factors described which correlate inversely with the risk to develop PD. In this context it has been shown that the risk for smokers is approximately half compared to non-smokers. Further, caffeine and coffee consumption reduce markedly the risk for PD (Hernán, 2002). However evidence if and how the risk to develop PD is influenced remains still uncertain for many of such factors. One major complication is that the impact of acute or long term exposure of factors can lead to the disease many years later which makes it very complicated to determine the influence of single events or factors during life time on the disease progression.

Genetics of PD:

In the last decades the view on the etiology of PD has changed considerably. While it was thought before that PD as a disease relies almost only on environmental factors, it gets more and more clear, that the genetic predisposition plays a major role for the risk to develop PD. To our current knowledge > 85% of all PD cases are idiopathic or late onset and do not seem to have a familiar background, however by studying families with mendelian inheritance pattern of PD (<10%) multiple genes could be identified which provides insight into the molecular pathomechanisms of PD (Corti, 2011). Up to now at least 16 genetic loci (PARK1-16) have been identified to be implicated in familiar forms of PD, or in syndromes where parkinsonism is a prominent feature. Besides, there is a constantly growing list of genetic loci which contribute risk to develop idiopathic forms of PD (Brug, 2015).

SNCA:

The first mapped PD gene was *SNCA* in 1997 (Polymeropoulos, 1997) coding for the α-syn protein. Since then, 2 categories of genomic alterations have been discovered in *SNCA*: point mutations which lead to amino acid alterations or multiplications of the whole genomic locus. Consequently it has been found that the severity of the phenotype depends on the copy number of the SNCA locus in a dose dependent manner (Ibáñez, 2009) (J. Fuchs, 2007). Based on the finding that α-syn toxicity increases linearly with the number of copies, a range of overexpression models have been created to recapitulate PD pathology (Mochizuki, 2006) (Feany & Bender, 2000). The physiological function of α-syn is still not completely understood. Intracellular, α-syn was shown to be mainly located at the presynaptic nerve terminal, associated to synaptic vesicles (Kahle et al., 2000). It is suggested that α-syn plays a major role in proper assembly of the SNARE complex, which facilitates synaptic vesicle release (Burré, 2010). Mutations as well as elevated expression of α-syn lead to an increase in α-syn oligomerization and the formation of insoluble LBs, which are one of the hallmarks of LBD and PD. This suggests rather a gain-of-function mechanism then the loss of membrane binding capacity to be responsible for the pathology. It is however not fully clear if aggregates of α-syn are the toxic species or if this represents a mechanism of the cell to protect itself against potentially toxic α-syn intermediate oligomers (Levy, 2009). Exact mechanisms linking protein aggregation, cellular dysfunction and cell death in PD are still unknown, however there is the hypothesis that α-syn might spread in a prion-like manner (Hawkes, 2007). On a cellular level it has been shown that α-syn aggregates can be released in exosomes and correspondingly be taken up by recipient cells, inducing further α-syn toxicity (Danzer, 2012). The strongest evidence for this hypothesis has been observed in PD patients who received embryonic cell transplants in an attempt to restore dopaminergic neuronal transmission, as Lewy pathology could be observed in the transplanted grafts decades later (Li, 2008).

LRRK2:

Besides *SNCA* and *VPS35*, mutations in *Leucin rich repeat kinase 2 (LRRK2),* which corresponds to the PARK8 locus, have been clearly linked to autosomal dominant forms of PD so far (Zimprich, 2004). LRRK2 belongs to the ROCO family of proteins because of the presence of a RAS-of-complex (ROC) GTPase domain adjacent to a C-terminal-of-ROC (COR) linker. It further consists of a serine/threonine protein kinase and a leucine rich repeat (LRR) domain flanking the ROCO catalytic region. A lot of research has been done to investigate exact LRRK2 interaction partners and corresponding molecular pathways ranging from translational control, vesicular trafficking, cytoskeletal regulation, neurite outgrowth and autophagy (reviewed in Tsika & Moore, 2012). On a cellular level, LRRK2 is present in the whole cytoplasm, mainly described to be localized to intracellular membranes in particular endosomes, lysosomes, microtubule associated vesicles, mitochondrial membranes, or multivesicular bodies (Biskup, 2006), suggesting participation of LRRK2 in vesicular transport as well as cytoskeleton organisation. This hypothesis was confirmed by quantitative immunoprecipitation experiments following mass spectrometry analysis using endogenous LRRK2 expression in murine cells where it was shown that the LRRK2 interactome comprises actin isoforms as well as other proteins involved in cytoskeletal organization (Meixner, 2011).

Many pathogenic genetic variations are described over the whole *LRRK2* locus. Among those, the G2019S mutation, which is located in the kinase domain, is the most common mutation with frequencies of 4% in familial and 1% in sporadic cases of PD (Gilks, 2005). Importantly, the clinical features of patients with this mutation are almost indistinguishable from sporadic PD cases including late age of onset, slow progression and good responsiveness to L-Dopa treatment, making the G2019S mutation an interesting target of research also for mechanisms linked to sporadic forms of PD (Healy, 2008). This finding proposes modulation of LRRK2 kinase activity as an attractive target to treat PD and indeed, inhibition of LRRK2 kinase activity has been shown to ameliorate pathogenic effects of the G2019S mutation and to be neuroprotective in models of PD (Ramsden, 2011). It is however noteworthy, that other pathogenic mutations in the ROC-COR domain of LRRK2 like the I2020T or R1441C/G mutation do not show any alterations in kinase activity

(Greggio & Cookson, 2009). This contradicts the hypothesis of enhanced kinase activity being the major pathogenic output of LRRK2 and rather suggests distinct pathogenic mechanisms for distinct mutations in LRRK2.

PINK-1/Parkin:

In addition to the genetically dominant forms of PD, mutations in the genes *Parkin* (PARK2), *PINK-1* (PARK 6) or *DJ1* (PARK 7) are associated with recessive parkinsonism. Patients with such mutations have an earlier onset of the disease compared to idiopathic cases, usually show classical symptoms of PD and respond well to L-Dopa treatment. Of those genes, mutations in *Parkin* are the most common cause of early onset PD (<40 years of age) and the frequency decreases rapidly with increasing age of onset (Lücking, 2000). So far, over 170 different pathogenetic alterations have been identified including missense mutations, multiplications and small insertions or deletions (Nuytemans, 2010). Functionally, Parkin is part of the E3 ubiquitin ligase family consisting of a N-terminal ubiquitin like domain and a C-terminal ubiquitin ligase domain catalysing the transfer of activated ubiquitin onto substrate proteins (Hristova, 2009). This leads to various functional consequences, including proteasomal degradation or alteration of cellular location and protein interactions of target molecules (reviewed in Pickart & Eddins, 2004). Interestingly, mutations in *Parkin* are hypothesised to rather affect the solubility of the protein then resulting in an enzymatic loss of function of the protein (reviewd in Corti & Brice, 2007).

Compound heterozygous and homozygous mutations in *PINK-1* are the second most common cause of autosomal recessive forms of PD. It was first described in 2001 with patients showing a clinical appearance indistinguishable from sporadic PD (Valente, 2002). The 581 amino acid long protein PINK-1 harbours a C-terminal kinase domain, as well as an N-terminal mitochondrial targeting sequence suggesting mitochondrial localization inside the cells (Valente, 2004). Interestingly, both proteins, PINK-1 and Parkin have been associated with mitochondrial integrity and are acting in the same pathway even though PINK-1 is located at the outer mitochondrial membrane (MOM) whereas Parkin mainly remains cytosolic (Clark, 2006). Under normal conditions, PINK-1 is rapidly imported through transporters of

the outer mitochondria (TOM) and then cleaved by mitochondrial processing peptidases (MPP) (Greene, 2012) resulting in a constant low level of PINK-1 on the MOM. However upon loss of mitochondrial membrane potential (MMP) due to mitochondrial dysfunction, the import is disrupted and PINK-1 accumulates on the MOM, where its kinase activity is required for Parkin translocation to mitochondria. Parkin then ubiquitinates damaged mitochondria to initiate their selective removal by autophagy (mitophagy) (Narendra, 2008). Pathogenic mutations in *PINK-1* or *Parkin* however prevent PINK-1 mediated recruitment of parkin, resulting in disrupted mitophagy and accumulation of dysfunctional mitochondria in the cell (Geisler, 2010) supporting the hypothesis of the involvement of mitochondrial dysfunction in the pathogenesis of PD.

GBA1:

Besides autosomal dominant and recessive loci, there have also been genetic risk factors described to be associated with PD. Interestingly, the most common risk factor was identified in clinical studies of patients with the rare lysosomal storage disorder Gaucher's disease (GD). GD, which was first described by Philippe Gaucher in 1882, is an autosomal recessive inherited lysosomal storage disorder that primarily affects the mononuclear phagocyte system where lysosomes in macrophages get overwhelmed with stored lipids, resulting in typical clinical manifestations like hepatosplenomegaly, anaemia or thrombocytopenia (Zimran, 2011). The clinical spectrum of GD is however very heterogenous, which leads to the classification into 3 categories upon the absence (type 1) or the involvement of neurological symptoms (type 2, 3). Type 1 represents the mildest form of the disease with a very wide spectrum of symptoms, which are usually sensitive to enzyme replacement therapy (ERT). GD type 2 and 3 progress more severe and show neuronopathic features like learning disabilities or myoclonic epilepsy in case of type 3 and rapid neurological degeneration, which can lead to death in a few days after birth in case of form 2 (Sidransky & Lopez, 2012). It is worth mentioning however that the clinical spectrum is considered to be a continuum, ranging from asymptomatic patients to prenatal death *in utero*. The main pathomolecular feature

of GD is the loss of activity of the lysosomal enzyme ß-glucocerebrosidase (GCase), genetically represented by the *GBA1* locus. It is located on chromosome 1 adjacent to a *GBA1* pseudogene, which shares 96% homology and significantly complicates sequencing and detection of pathogenic mutations.

GCase, an around 60kDa big protein located in the lysosome, has its primary function in cleaving the ß-glucosidic bound of glucocerebroside and contributing to the glycolipid metabolism. So far about 300 mutations have been detected in *GBA1* where the N370S mutation counts for 70% of the mutant alleles among Askhenazi Jews (Beutler,1992). The phenotype – genotype correlation is however incomplete suggesting further disease modifying factors to be present.

Interestingly, a subset of GD patients develop features of parkinsonism similar to those of idiopathic PD including LB pathology, dementia and a favourable response to levodopa. In 2003 a screening of 17 GD patients with parkinsonian symptoms revealed the common GD type 1 mutation N370S in 82% of the cases (Tayebi, 2003). Following further multiple small genetic screens, a large cooperative study was done including 5691 PD patients and 4898 control individuals. Screening for the 2 most common *GBA1* mutations, the N370S and the L444P mutation, revealed a frequency of 3% - 15% of such mutations in PD patients depending on the ethnic origin. Sequencing of the whole *GBA1* locus in a subset of 1700 PD patients revealed in 7% of all cases *GBA1* mutations (in controls <1%), confirming that mutations in this locus represent a common genetic risk factor to develop PD (Sidransky , 2009). PD patients with *GBA1* mutations are clinically similar to idiopathic cases, however present an earlier age of onset of the disease, a higher prevalence of dementia and non-motor symptoms (Brockmann & Berg, 2014). Further, GCase activity has been shown to be reduced in the aging brain (Rocha, 2015) and in sporadic cases of PD (Murphy, 2014). Together with the clinical similarity of *GBA1* related and idiopathic PD this proposes *GBA1* as a very interesting target for pathomechanistic and therapeutic related PD research.

Using hiPSCs to model PD in vitro

Human *in vitro* models of PD have greatly contributed to our basic understanding of PD. Such models enable the study of molecular pathomechanisms in human cells involving single genes and proteins very detailed, fast and with a high reproducibility. Further, such models comprise a prefect platform for initial chemical compound screens to develop drugs for PD.
Depending on the research question, the choice of the correct *in vitro* model of PD is crucial. Widely used models of PD are based on the use of neuroblastoma cell lines, optimally with the option to display features of neuronal and dopaminergic cells such as SH-SY5Y or LUHMES. Such lines however are transformed cell lines, which display genomic instability and differentially regulated metabolism compared to primary dopaminergic neurons. One further disadvantage is the inability to study patient specific mechanisms or single genomic mutations on endogenous level. Such questions can be assessed using for example patient derived cells such as fibroblasts, which however show again differentially regulated cellular gene expression profiling and metabolism compared to neuronal cells.

Induced pluripotent stem cells:

The way to obtain non-transformed human dopaminergic neurons was cleared by the first isolation of human embryonic stem (ES) cells from human embryos in 1998 (Thomson, 1998). Studying such cells lead to further understanding of human development, tissue formation and differentiation and had the potential to model diseases or ultimately enable cell therapies.
The derivation of such cells however led to big ethical controversies in the scientific and non-scientific community in the US, ultimately leading to the governmental restriction of funding in 2001. Even though since then the regulations were loosened, allowing research using the already generated ES lines, the diversity of lines available is too small to answer emerging questions related to disease modelling and treatment and did not solve the issue of the lack of patient specificity.

An elegant alternative came up in 2006 where Takahashi and Yamanaka announced the successful generation of induced pluripotent stem cells (iPSCs) by the retroviral introduction of the four stem cell markers, the so called Yamanaka factors, *Oct4, Sox2, Klf4* and *c-Myc* in mouse fibroblasts. Such cells expressed typical ES markers like SSEA-3, SSEA-4, tumor-related antigen (TRA)-1-60, TRA-1-81, alkaline phosphatase, and NANOG. Further, iPSCs could be differentiated in cell types of all three germ layers (mesoderm, ectoderm, endoderm) *in vivo* and *in vitro* (Takahashi & Yamanaka, 2006). Shortly after, this could be validated in different species, including human fibroblasts (Takahashi et al., 2007), resulting in the development and refinement of differentiation protocols to generate cell types to study various diseases including cardiac disorders, neurodegenerative diseases, diabetes and multiple mono-or polygenetic disorders (reviewed in Gunaseeli, Doss, Antzelevitch, Hescheler, & Sachinidis, 2010). Such cells harbour a great potential on one side to model various diseases and investigate underlying pathomechanisms and on the other side provide a personalized source for cell replacement therapies (Figure 1).

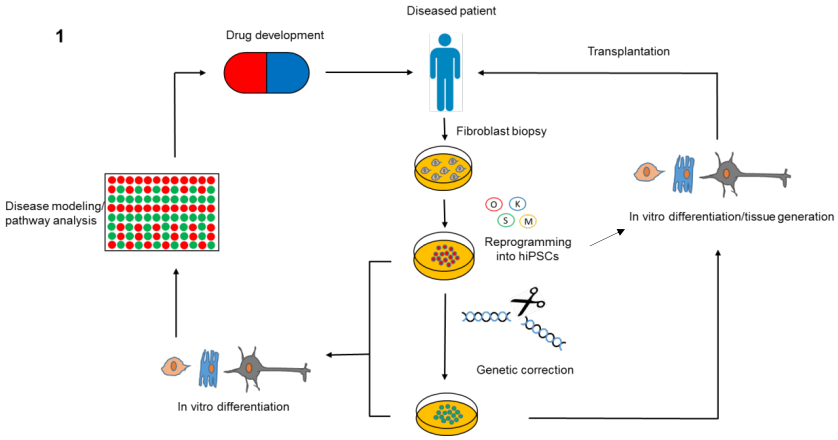

Figure1: Potential applications of hiPSCs for disease modelling and therapy. Fibroblasts from diseased patients can be reprogrammed to hiPSCs by utilization of the Yamanaka factors (Oct4, Sox2, Klf4, c-myc). Such cells can be genetically corrected to obtain isogenic controls and differentiated into various cell types which are then either suited for direct transplantation into patients or for disease modelling and disease pathways analysis, potentially resulting in the development of novel drugs.

Proof that differentiated cells derived from human iPSCs (hiPSCs) can successfully integrate in the brain and ameliorate disease associated phenotypes has been shown in rat models of PD (Wernig et al., 2008), however there are currently safety concerns regarding potential tumorigenicity associated to hiPSC derived transplantations which have to be assessed in order to process to human clinical trials.

Basic research on neurological disorders on the other hand has benefited already a lot from hiPSC based modelling since affected human cell types, like neurons or astroglia, were so far just available from post-mortem samples. Since PD includes mainly the degeneration of mDA neurons, multiple generation protocols to obtain such cell types by targeted differentiation have been described and constantly refined. Early differentiation protocols produced high numbers of TH+ neurons from hES cells grown on stromal feeder cells, however lacking expression of markers of regional midbrain specificity like FOXA2 or LMX1A (Perrier et al., 2004). This was first achieved by forced overexpression of *LMX1A* in addition to treatment with the growth factors Sonic Hedgehog (SHH), a morphogen defining the ventral region of the neural plate and fibroblast growth factor 8 (FGF8), important in setting up the midbrain-hindbrain border during early development (Friling et al., 2009). Further, an early temporal implementation and recapitulation of morphogenic signals important in mDA patterning could be achieved by the use of dual SMAD inhibitors in the first days of differentiation, inhibiting TGF-ß, nodal, activin and BMP signalling which results in a high level of neural induction without the need of feeder cells (Chambers et al., 2009). Finally, completely correct midbrain specification was achieved when WNT/ß-catenin signalling pathways were targeted by GSK3-ß inhibition, resulting in high levels of FOXA2 and TH+ neurons derived from hESCs. Such cells displayed gene expression patterns and electrophysiological activity of mature mDA neurons and successfully integrated in the rodent brain (Kriks et al., 2012).

In terms of PD research, somatic cells from patients carrying mutations in *SNCA*, *LRRK2*, *PINK1*, *Parkin* and *GBA1* mutations have been successfully reprogrammed to hiPSCs and differentiated into mDA neurons. For *SNCA,* Soldner et al. described the generation of hiPSCs from fibroblasts of an A53T mutation carrier following genetic correction of the mutation by the use of zinc finger nucleases (ZFNs). Further, using the same technique it was also possible to introduce the A53T

mutation artificially into the wild type genome of hES cells (Soldner et al., 2011). Besides, in the same year, the generation of hiPSCs from a patient carrying a *SNCA* triplication was described. Interestingly, when such cells were differentiated into mDA neurons, the overall α-syn levels were approximately doubled, recapitulating one of the hallmarks of PD (Devine et al., 2011). HIPSC models for *LRRK2*, mainly with focus on the G2019S mutation, have been described by multiple groups, focusing on different pathomechanisms and phenotypes. Nguyen et al. described the first PD related phenotypes including oxidative and proteasomal stress proofing that hiPSCs could indeed serve as an important tool to model PD *in vitro.* Further studies have revealed additional pathomechanisms including mitochondrial dysfunction, morphological abnormalities and alterations in macroautophagy (Zhao et al., 2014). In 2011, first hiPSCs from patients harbouring *PINK1* mutations were generated. Derived mDA neurons from such hiPSCs showed impaired recruitment of Parkin to depolarized mitochondria, increased PGC1α activation and an increase in mitochondrial copy number (Seibler et al., 2011). Further it was shown, that mDA neurons with *PINK1* mutations show reduced levels of parkin and subsequent impairment of mitophagy due to insufficient ubiquitination potential (Rakovic et al., 2013). Those models are valuable tools for PD research since the molecular pathophysiology observed in PD patients with such mutations can be closely recapitulated. HIPSC derived neurons from PD patients with *Parkin* mutations were reported to show dysfunction in dopamine uptake and release as well as increased intracellular ROS levels due to mitochondrial dysfunction suggesting parkin to play a role in the protection from oxidative stress and dopamine transmission (Jiang et al., 2012). In addition such cells showed decreased neurite complexity and length due to destabilized microtubules, which could be rescued by overexpression of wild type parkin and indicating the importance of parkin in neuronal health in PD (Ren et al., 2015). In 2012 Panicker et al. described the generation of hiPSCs from patients with type 1,2 and 3 GD however with focus on differentiation into macrophages. Such cells showed typical hallmarks of GD including low GCase activity, sphingolipid accumulation and a defective lysosomal system (Panicker et al., 2012). The latter could be reproduced in an elegant study using hiPSC derived mDA neurons from GD patients, showing that autophagic dysfunction leads to the accumulation of α-syn resulting in neurotoxicity by direct stabilization of α-syn oligomers by Glc-Cer. On the other hand, increased levels of α-syn inhibit lysosomal

activity of wild type GCase suggesting a bidirectional link between α-syn and GCase (Mazzulli et al., 2011). In a follow up study it was shown afterwards that accumulated α-syn inhibits intracellular trafficking of GCase by disrupting the ER-Golgi localization of Rab1a, which is a major mediator of vesicle trafficking in the cell (Mazzulli, Zunke, Isacson, Studer, & Krainc, 2016). Such misprocessing of GCase associated with ER stress and aberrant cellular lipid profiles could also be shown in hiPSC derived mDA neurons from PD patients with *GBA* mutations compared to unrelated controls (Fernandes et al., 2016b).

Gene editing:

Overall, the use of patient derived hiPSC gains more and more attention for disease modelling purposes, since for the first time it is possible to investigate pathomechanisms in human cell types directly affected by the disease. One drawback however, compared to working with mouse strains or established cell lines, is that the genomic heterogeneity can mask disease specific effects comparing patient derived cells with unrelated controls. To assess this issue, it is possible to change single bases in the genome and by this create isogenic perfect controls, harbouring the exact genomic background except the mutation of interest. This technique named “genome editing” had its beginning in 1996 where the endonuclease Fok-I was first described to cut DNA double strands *in vitro* (Y. G. Kim, Cha, & Chandrasegaran, 1996). Combining this chimeric enzyme with zinc-finger domains, which recognize specific DNA triplets, lead to the generation of zinc-finger-nucleases (ZFNs) and was the basis of gene editing tools in different cultured cells and organisms including animal models, plants and pluripotent stem cells (Bibikova, Golic, Golic, & Carroll, 2002) (Townsend et al., 2009) (Hockemeyer et al., 2009). On a molecular level, the underlying system is based on dimerization and subsequent activation of two Fok-I monomers, which leads to the induction of a DNA double strand break (DSB) at the genomic site determined by the DNA binding motifs. The resulting lesion can be repaired by either non-homologous end joining (NHEJ) or homology directed repair (HDR), depending on the presence or absence of a repair template in the cell. Even though the cellular DNA repair machinery can work quite precisely, NHEJ eventually results in the formation of either small DNA

deletions or insertions (indels) resulting in frameshift mutations and subsequently either loss of the mRNA due to nonsense-mediated-decay or the generation of truncated proteins. In comparison, HDR allows precise modification of the genome by cloning and transfection of a custom made DNA template. Such templates usually consist of the modified region of interest flanked by two homologous arms guiding the template to the site of the DSB. The type of insert specifies the outcome of the DSB repair, resulting for example in genetic corrections (Urnov et al., 2005) or fluorescent tagging of proteins endogenously (Doyon et al., 2011). The ZNF technique however harbours disadvantages limiting the use in *in vitro* and *in vivo* studies. The construction of protein domains is very laborious and cost-intensive for every single genomic locus and usually has to be outsourced. Further, since every zinc finger domain targets one fixed DNA triplet, the range in genomic loci accessible is restricted. This issue was overcome by the generation of Transcription activator – like effector nucleases (TALENs). Similar to ZFNs, TALENs consist of a central domain responsible for DNA binding, a nuclear localization signal and a fused Fok-I nuclease, which has to be present as a dimer at the site where the DSB is induced. In contrast to ZFNs however, the DNA binding domain consist of an alignment of single monomers of 34 amino acids, which can bind single specific nucleotides over repeat variable residues (RVDs). Such consecutive monomers can be cloned easily in vectors containing Fok-I and a nuclear localization signal and by this it is possible to target any genomic sequence and induce DSBs at any site of interest (Cermak et al., 2011). Similar to ZFNs, multiple cell lines and organisms have been genetically edited using TALEN technology, which will not be discussed further at that point. Distinct from the site specific nucleases mentioned, an alternative way to efficiently edit the genome is the use of clustered regulatory interspaced short palindromic repeats (CRISPR) paired with an RNA guided endonuclease (eg. Cas9). This system was discovered in bacteria, providing acquired immunity against invading foreign DNA by detecting and cleaving the latter (Wiedenheft, Sternberg, & Doudna, 2012). In type II CRISPR/Cas systems, short fragments of foreign DNA are integrated into the genomic CRISPR locus and transcribed into CRISPR RNA (crRNA). Such RNA pieces can directly anneal to trans-activating crRNAs (tracrRNA) and guide the Cas9 protein to the pathogenic DNA, which is then cleaved and silenced. The only restriction for target recognition by Cas9 is the presence of a conserved dinucleotide containing protospacer

adjacent motif (PAM) upstream of the crRNA binding site (Jinek et al., 2012). In *in vitro* experiments it was possible to combine crRNA and tracrRNA into one single guide RNA (sgRNA), allowing the generation of custom made sgRNA pieces targeting and cleaving nearly any DNA sequence of choice. Importantly, the CRISPR/Cas system has been shown to be directly transferable into cells by delivering all necessary components via plasmid transfection or viral integration (Jinek et al., 2013). Since then a range of experimental strategies have been implicated using CRIPSR/Cas ranging from targeted HDR in hiPSCs (Mali et al., 2013), multiplexed gene disruption by simultaneous delivery of multiple gRNAs (González et al., 2014) or delivery into zebrafish (Hwang et al., 2013).

The combination of gene editing technologies and hiPSCs harbours great potential for patient specific pathomechanistic research. Genetic corrections or full gene knock outs allow the assessment of the impact of one specific SNPs or genes on disease pathogenesis in an isogenic genetic background. Endogenous tagging of genes enables imaging or purification of single proteins independent of antibody associated limitations like specificity and efficiency. Multiple genomic cuts (by eg. application of two sgRNAs) can be used to generate truncated proteins or complete gene knock outs (Figure 2).

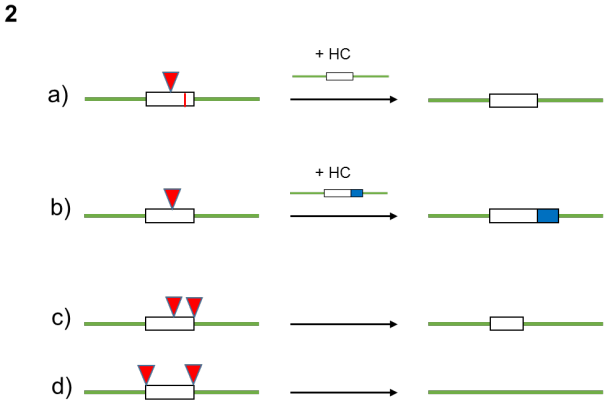

Figure2: Schematic overview of potential genome editing strategies. Green lines and white boxed represent introns and exons respectively, red arrows indicate nuclease cutting sites. a) Genetic correction of a point mutation (red bar) is possible by co-application of nuclease and a homologous construct (HC) harbouring the wild type sequence. b) Introduction of an endogenous tag (eg. a fluorophore) can be achieved by corresponding design of the homologous construct. c) Application of 2 nucleases enables the generation of truncated proteins or complete knock outs (d).

GBA1 related pathomechanisms

The exact pathomechanisms of *GBA1* related parkinsonism still remain elusive. In general, autosomal recessive forms of PD (eg. mutations in *parkin* and *PINK1*) are associated with loss of function mechanisms, whereas dominant forms (eg mutations in *LRRK2* or *SNCA*) are considered to follow gain of function pathways (Hardy, 2009). Since *GBA1* related PD however does not follow a clear mendelian pattern and both, gain and loss of function hypothesis have been postulated.

Loss of function hypothesis are supported by the fact that *GBA1* null mutations are found in a subset of *GBA1* PD patients where GCase is completely absent (Aharon-Peretz, 2004). Further, inhibition of GCase by the chemical inhibitor condruitol-β-epoxide (CBE) was shown to induce α-syn accumulation in cell culture models (Cleeter, 2013) and mice harbouring *GBA1* null mutations showed severe mitochondrial phenotypes as well as autophagic dysfunction and α-syn accumulation (Osellame & Duchen, 2013). Besides, it was reported that reduced GCase activity results in in lysosomal dysfunction, subsequent accumulation of α-syn and neurotoxicity. Increased levels of α-syn on the other hand compromise the function of normal lysosomal GCase leading to further autophagic dysfunction (Mazzulli, 2011), forming a pathogenic loop. Loss of GCase function can also alter the lipid metabolism of the cell, resulting in dysregulated lipid raft function or interference with the membrane curvature with altered affinity to α-syn (Hein, 2008) (Auluck, 2010).

Gain of function hypotheses on the other hand are suggested since just a small subset of GD patients actually develops PD despite low GCase activity. Most *GBA1* PD patients harbour heterozygous mutations where one allele is still intact and at least 50% of the enzyme activity is preserved. Further, most pathogenic mutations in the *GBA1* gene are missense mutations leading to misfolded GCase. Such misfolded proteins have been shown to directly interact with α-syn, leading to accumulation of the latter (Sidransky & Lopez, 2012) or to be held back in the endoplasmic reticulum (ER) leading to ER stress (ERS) burdening the cellular proteasomal and lysosomal degradation system (Fernandes, 2016). The exact pathomechanisms underlying *GBA1* related PD however still remain unclear and will be further discussed in this work.

Autophagy

Autophagy is an evolutionary conserved mechanism of the cell to react to fluctuations of metabolic parameters. It involves sequestration of cytoplasmic components including complete organelles (like dysfunctional mitochondria) or protein aggregates which makes autophagy a key mechanism in neurodegenerative disorders. Structures targeted for degradation are engulfed by a doublemembrane, the so-called autophagosome, which fuses with lysosomes for final degradation of the cargo. Multiple autophagy-related genes have been identified functioning at different stages of the autophagic process, namely initiation, elongation and fusion of the phagosome with the lysosome. In the initiation phase, a double membrane, derived from the ER, Golgi, mitochondria or the cell membrane, is formed, the so called phagophore. This phagophore grows in size during the elongation phase and utilizes the microtubule-associated protein light chain 3 (LC3) for lysosomal fusion. Generally spoken, autophagy can be induced by conditions like limited ATP availability, lack of nutrients or the accumulation of specific metabolites (Galluzzi, 2014). When ATP is not synthesized by oxidative phosphorylation or glycolysis, AMP accumulates, activating AMP activated protein kinase (AMPK) which in turn stimulates autophagy (Hardie, 2012). Interestingly, AMPK can also be modulated by intracellular Ca^{2+} levels suggesting multiple levels of regulation (Hawley, 2005). When phosphorylated itself, AMPK is a master regulator of autophagy by phosphorylating and activating ULK1 (J. Kim, 2011) as well as inhibiting mTORC1 by phosphorylating components of this enzymatic complex (Hardie, 2012). mTORC1 itself is an enzymatic complex which, when activated, positively regulates protein translation by phosphorylating eukaryotic translation initiation factor 4E binding protein 1 (EIF4EBP1) and ribosomal protein S6 kinase (RPS6K) promoting protein synthesis (Shimobayashi & Hall, 2014). Further, activated mTORC1 suppresses autophagy by phosphorylating and inhibiting ULK1 and transcription factor EB (TFEB) (Settembre, 2013). When dephosphorylated on the other hand, TFEB can translocate into the nucleus and induce the transcription of lysosomal genes by binding to the CLEAR (Coordinated Lysosomal Expression and Regulation) element (Sardiello, 2009) (Settembre, 2011). Interestingly, TFEB signalling has been shown to be disturbed in mDA neurons form rats expressing the parkin Q311X mutation resulting in impaired autophagy and mitochondrial quality

control. Further, targeting the TFEB pathway can rescue mDA cells from α-synuclein pathology (Decressac, 2013) and APP/PS1 mice from Aß accumulation and amyloid pathogenesis (Xiao, 2015). In the context of *GBA1*, TFEB signalling has been shown to be disturbed in hiPSC derived neurons from GD patients (Awad, 2015). Being a lysosomal glucosidase, mutated *GBA1* has also been proposed to be involved in autophagic dysfunction. Overexpression of the D409A *GBA1* mutation has been shown to lead to accumulation of the lysosomal substrate α-syn, which importantly could be reversed by application of the autophagy inducer rapamycin (Cullen, 2011). Furthermore, in an *in vivo* mouse model of GD, accumulation of the lysosomal marker LAMP2 and the lysosomal cargo protein p62 suggests an impaired autophagic clearance (Sun & Grabowski, 2010). The autophagosomal-lysosomal flux has been reported to be disturbed in primary cells of a *GBA1* knock out mouse model (Osellame, 2013). Such findings suggest that the autophagosomal-lysosomal system is disturbed in models of homozygous *GBA1* mutations, if this is however also valid for heterozygous PD related *GBA1* mutations we will further investigate in this work.

ER Stress and UPR

The ER is a highly dynamic organelle fulfilling crucial functions in protein translation, protein folding, lipid metabolism and Ca^{2+} storage. Disturbance of the integrity of the ER by perturbations in Ca^{2+} homeostasis, redox balance or protein folding defects can lead to the excessive accumulation of misfolded proteins in the ER resulting in ER Stress (ERS). Upon acute ERS, the cell activates an orchestrated signalling system including activation of the unfolded protein response (UPR), ER-associated degradation (ERAD), autophagy or mitochondrial biogenesis.

UPR is a very well defined response to restore cellular homeostasis following accumulation of misfolded proteins (Rutkowski & Hegde, 2010). Three ER membrane anchored proteins act as sensitive sensors for UPR induction, RNA-activated protein kinase like ER kinase (PERK), activating transcription factor 6 (ATF6) and inositol-requiring enzyme 1 (IRE1). Following well defined signalling

cascades, those mediating proteins then directly activate the transcription of chaperones, redox enzymes or cell death programs. Under conditions of ER stress, the molecular chaperone BIP/GRP78 dissociates from PERK and IRE1 leading to phosphorylation of those proteins. Phosphorylated IRE1 then leads to splicing of X-box protein 1 (Xbp1s) which on the other hand induces expression of proteins involved in protein folding, ERAD or lipogenesis. Phosphorylated PERK itself phosphorylates and inactivates elongation initiation factor 2 alpha (eIF2α), resulting in cellular translational attenuation and the specific translation of ATF4 mRNA. This leads to expression of enzymes involved in balancing redox homeostasis and the induction of apoptosis in cooperation with C/EBP homologous protein (CHOP). ER stress and the subsequent activation of the UPR were reported in various LSDs, including GM1-gangliosidosis and infantile neuronal ceroid lipofuscinosis due to loss of function of ß-galactosidase or palmitoyl-protein thioesterase respectively (Tessitore, 2004) (Z. Zhang, 2006).

There is evidence that *GBA1* mutations can lead to ER stress and the subsequent activation of the UPR. In fibroblasts from GD patients and in a *Drosophila* model with homozygous N370S or L444P mutations, elevated expression of UPR related genes like ATF6, BIP and Xbp1s, an increase in phospho-eif2α as well as resulting locomotor deficits and neuronal cell death was reported (Maor, 2013) (Sanchez-Martinez, 2016). Similar results could also be shown in a *GBA1*-PD model using hiPSC derived neurons (Fernandes, 2016), however if such observations are a result of gain-or loss of function mechanisms of mutant *GBA1* still needs to be investigated.

Mitochondria and mitochondrial dysfunction

Mitochondria arose when alpha-proteobacteria was engulfed by eukaryotic progenitors around 2 billion years ago (Lane & Martin, 2010). They are comprised of 2 functionally distinct doublemembrane layers, namely outer (OM) and inner membranes (IM) and their main task in the cell is the production of ATP via oxidative phosphorylation (Oxphos). In the Krebs cycle electron carriers like NADH and

$FADH_2$ are generated which transfer electrons to the electron transport chain (ETC), a series of 5 protein supercomplexes localized in the inner mitochondrial membrane. The main task of complex I-IV is to pump hydrogen protons across the inner mitochondrial membrane into the inter membrane space generating a difference in charge between this compartment and the inner mitochondrial matrix. This mitochondrial membrane potential (MMP) is the driving force to generate ATP by complex V phosphorylating ADP and producing H_2O as a side product (Stock, 1999). It becomes more and more clear that besides the production of ATP, mitochondria fulfill various different functions necessary for cellular homeostasis. Complex I (C I) and III are producing ROS, which can influence homeostatic signalling pathways, control differentiation and proliferation of cells and which can contribute to internal stress signalling (Hamanaka & Chandel, 2010). Mitochondrial ROS is generated as a side product of oxidative phosphorylation and dysregulation of the latter can subsequently lead to excessive generation of free radicals and nitrosative stress, causing lipid or protein peroxidation or oxidative DNA damage. The delicate balance of pro-and anti-oxidative reactions is therefore crucial in living organisms and dysregulation can lead to a variety of diseases (Adly, 2010).

Besides ROS regulation, mitochondria regulate levels of amino acids, cellular metabolites and various enzymes including histone deacetylases. Importantly, mitochondria also take part in Ca^{2+} homeostasis by buffering Ca^{2+} arising from ER or the plasma membrane (De Stefani, 2011). This property is especially useful in neurons which have to regulate their Ca^{2+} levels very tight to control neurogenesis, neuronal plasticity and neurotransmitter release. Mitochondrial Ca^{2+} uptake plays a key role in various intracellular functions. A tightly regulated increase in mitochondrial Ca^{2+} can activate mitochondrial respiration and subsequent ATP production, prolonged Ca^{2+} influx however leads to apoptosis by opening of the mitochondrial permeability transition pore and cytochrome c release (Giorgi, 2008). Importantly, mitochondria carry their own circular genome, of which the biggest part was transferred to the eucaryotic nucleus during evolution. The mitochondrial genome encodes for 13 proteins, corresponding to approximately 1% of all mitochondrial genes. Nuclear encoded proteins required for proper mitochondrial function must therefore be imported mainly by translocases of the outer and inner mitochondrial membrane (Wiedemann, 2004). Mitochondrial DNA is mainly transmitted maternally in a non-mendelian mechanism, since paternal mitochondria

are actively destroyed immediately after fertilization probably by proteolysis (Cummins, 2000). Mutations in mitochondrial DNA can be linked to various diseases in all fields of medicine. Related disorders are very heterogeneous and mutations in the same mitochondrial complexes can lead to different clinical manifestations. Deficiency in C I for example can lead from isolated myopathy up to neonatal death (Kirby, 1999). This phenotypic variability linked to mitochondrial DNA mutations can be explained by the high copy number of mitochondria in eukaryotic cells. When cells are dividing during embryogenesis, healthy and diseased mitochondria might be apportioned asymmetrically to their daughter cells. This situation, called heteroplasmy (Holt, 1988), can subsequently result in tissue specific phenotypes of mitochondrial DNA mutations.

Mitochondria undergo a variety of dynamic alterations including fusion, fission and mitochondrial motility. Such processes can regulate mitochondrial shape, recruit mitochondria to specific subcellular compartments or favor exchange of content, including ROS or mitochondrial DNA, between mitochondria (H. Chen & Chan, 2009). Besides, alterations in dynamics are important for mitochondrial quality control. Fission is a key mechanism preceding translocation of dysfunctional mitochondria to lysosomes and subsequent degradation (Kim, 2007). Mitochondrial fusion on the other hand might buffer and therefore compensate partially for intra-mitochondrial defects or transient stress. Loss of function of such dynamic processes can lead to dysfunctional mitochondria and related disorders (H. Chen, 2007).

Due to their high energy demand and post-mitotic character, neurons are dependent on proper mitochondrial functioning and are vulnerable to dysfunction of respiration. Accordingly, various neurodegenerative disorders have been linked to mitochondrial dysfunction including AD, PD, HD or ALS. In aging, homeostasis of oxidative stress responses is disturbed leading to increased ROS levels generated by defective mitochondria (Wang, 2013). In case of PD, post mortem brain tissue shows markedly reduced C I activity in the *substantia nigra* (Schapira, 1989). Dopaminergic neurons are especially exposed to elevated levels of ROS due to their dopaminergic character itself. Dopamine is a very unstable neurotransmitter undergoing auto-oxidation producing ROS as a result (Slivka & Cohen, 1985). That mitochondrial dysfunction is closely linked to PD pathogenesis is proven by the fact that the neurotoxin MPTP, which inhibits specifically C I, leads preferentially to

cytotoxicity in dopaminergic neurons in animal models (Betarbet, 2002). Further evidence comes from genetic analyses linking the mitochondrial associated proteins *DJ-1*, *Parkin* and *PINK-1* to familial forms of PD. Lastly it was shown that dopaminergic neurons in the *substantia nigra pars compacta* of PD patients show elevated levels of mitochondrial DNA mutations (Bender, 2008) and that mutations in the enzyme polymerase gamma (POLG), which replicates the mitochondrial genome, can lead to forms of parkinsonism (Luoma, 2004).

Very little has been reported about mitochondrial dysfunction in *GBA1* related PD. In loss of functions models, loss of GCase activity in SH-SY5Y cells by CBE treatment and knock down of *GBA1* using shRNA increased ROS formation, decreased the MMP and consequently inhibited ADP phosphorylation (Cleeter, 2013). A *GBA1* knock out mouse model was showing similar phenotypes including reduction of the activity of mitochondrial C I, II/III, decrease in oxygen consumption and fragmentation of mitochondria (Osellame, 2013). In case of *GBA1* mutations, fibroblasts from homozygous L444P-GD patients showed impaired respiration, reduced ATP levels and increased ROS formation (de la Mata, 2015). Accordingly, in a homozygous D409H mouse model of GD similar phenotypes could be observed including loss of mitochondrial cristae (Xu, 2014). Such findings suggest mitochondrial function to be affected in GD pathogenesis, however if the same is true for *GBA1* PD remains however still elusive and will be object of the current work.

Targeting the oxidative metabolism by NAD+ modulation

Nicotinamide dinucleotide (NAD+) first came in the spotlight of research when it became clear that a deficiency of the latter is responsible for the disease pellagra due to malnutrition. Under normal conditions, NAD+ can be synthesized from multiple precursors, for example tryptophan (Trp) over an eight step de-novo pathway and nicotinamide (NAM), nicotinic acid (NA) or nicotinamide riboside (NR) over salvage pathways. In mitochondria, the oxidized form NAD+ or NADP is recycled back and forth to the reduced forms NADH or NADPH feeding the respiratory chain with electrons. Further, NAD+ is an important co-substrate for

multiple NAD+ consuming enzymes. Such enzymes break the glycolytic bond between NAM and the ADP ribose residue resulting in various downstream processes. The enzyme poly-ADP-ribose-polymerase (PARP) for example transfers NAD+ derived ADP-ribose to histones and other proteins at sites of DNA damage, facilitating genomic stability and integrity (Chambon, 1963). The ectoenzymes CD38/157 hydrolyze NAD+ extracellularly by generating cyclic ADPribose which acts as a strong Ca^{2+} inducer (De Flora, 2004). However, the best described class of enzymes utilizing NAD+ as a co-substrate is the deacetylase family of sirtuins (Sirt). Here, NAD+ cleavage facilitates the removal of acetyl groups from lysine residues of target proteins, accompanied by their transfer to ADP-ribose (Imai, 2000). Sirtuins are described to play major roles in multiple metabolic processes such as dietary restriction or oxidative stress. Sirt1 has been shown to deacetylate and activate the transcription factor proliferator-activated receptor gamma coactivator 1 alpha (PGC1α) (Rodgers, 2005), which is a key regulator of glucose production in the liver through activation of the glucogenic pathway (Yoon, 2001). PGC1α itself modulates the activity of multiple metabolic associated genes such as estrogen related receptors (ERRs) (Schreiber, 2003), myocyte enhancer factor-2 (MEF2) (Michael, 2001) and the family of forkhead O-box (FOXO) transcription factors (Puigserver, 2003) and is induced by situations where energy is required such as cold, exercise, or fasting (Puigserver, 1998) (Mootha, 2004). Interestingly, an increase in NAD+ levels (or subsequent decrease in NADH) was shown to mediate an extension of life span induced by caloric restriction (Lin, 2004). Further, enhancing NAD+ levels and subsequent Sirt1 activity was protective against metabolic abnormalities in a mouse model of obesity (Cantó, 2012). Sirt1 has been described to have an impact on mitochondrial function and biogenesis. An increase in PGC1α activity drastically increases the expression of mitochondrial uncoupling protein 1 (UCP1) (Puigserver, 1998) and mitochondrial biogenesis mainly by modulating the transcriptional activity and downstream expression of targets of nuclear respiration factors (NRFs). NRF1 and PGC1α can act as co-activators to regulate expression of transcription factor A, mitochondrial (TFAM), which is mainly responsible for replicating genes from the mitochondrial genome (Wu, 1999). Interestingly, the expression of UCP2 has also been linked to increased PGC1α levels (Calegari, 2011), providing an intracellular mechanism to reduce mitochondrial ROS formation and sustain mitochondrial health.

Besides improving mitochondrial biogenesis and function, Sirt1 has also been shown to be able to enhance autophagy by activating the FOXO pathway (Hariharan, 2010) or directly interacting with components of the autophagic machinery like Atg5, Atg7 or Atg8 where Sirt1 is able to directly deacetylate such proteins in a NAD+ dependent manner. To further confirm this discovery, it has been shown that autophagy is impaired in Sirt1 knock-out mice, which leads to an aberrant accumulation of dysfunctional organelles including mitochondria (Lee, 2008).

Interestingly, activated AMPK also positively influences mitochondrial biogenesis through PGC1α and NRF1 (Bergeron, 2001). Additionally, AMPK has also been shown to indirectly regulate Sirt1 activity by enhancing transcription of nicotinamide phosphoribosyltransferase (NAMPT), an enzyme involved in the production of NAD+ (Cantó, 2009). Viceversa, Sirt1 activity is required for AMPK activation and the subsequent beneficial effects on mitochondrial function (Price, 2012).

Aging remains as the strongest risk factor for the development of neurodegenerative diseases associated with metabolic changes including mitochondrial dysfunction and disturbance in autophagy (Shigenaga,1994) (Brunk & Terman, 2002). A decline in Sirt1 activity has been reported to be accompanied with aging (Chang & Guarente, 2013) (Gomes, 2013) (Ramsey, 2008) and respectively, reduced NAD+ levels have been found in mouse and *C.elegans* models of aging (Mouchiroud, 2013). Moreover, reduced NAD+ levels were also reported in models of methylmercury induced toxicity (Caito & Aschner, 2016), high fat high sucrose diet (Gariani, 2015) and mitochondrial myopathy (Khan, 2014). Accordingly mitochondrial dysfunction has been described in corresponding models such as increase in mitochondrial oxidative stress (Caito & Aschner, 2016), disturbance in respiration (Long, 2015), O_2 consumption (Gariani, 2015), cristae structure (Khan, 2014) and upregulation of the mitochondrial unfolded protein response (mtUPR) (Gariani, 2015).

Importantly, such dysregulations could be reversed by increasing intracellular NAD+ concentrations. Genetic knock out of NAD+ consuming enzymes like CD38 (Barbosa, 2007) or PARP1 (Bai, 2011) result in increased NAD+ levels and subsequent activation of the Sirt1-PGC1α-axis leading to increased mitochondrial biogenesis.

Pharmacological approaches to modulate NAD+ levels for disease treatment include the application of NAD+ boosting compounds such as the NAD+ precursors

NMN or NR or even NAD+ directly. The application of NR (Vitamin B3) displays a very high potency of increasing intracellular NAD+ levels by up to 270% of untreated controls in different cellular models (Yang, 2007). NR was used in multiple studies to investigate the effect of NAD+ boosting agents for a variety of diseases. Improvements were described in different *C.elegans*, cell culture and mouse models and were not restricted to disease predispositions but also improved wild type conditions. In a mouse model of obesity, NR had the potential to activate the Sirt1 and Sirt3 pathway resulting in lower cholesterol levels and increased oxidative function including expression of mitochondrial markers and an increased mitochondrial cristae density (Cantó, 2012). In a model of mitochondrial myopathy, NR was shown to increase mitochondrial biogenesis in muscle, reverse mitochondrial ultrastructure abnormalities and abolished the hallmarks of the disease (Khan, 2014). Beneficial effects of NAD+ replenishment have also been shown in models of neurodegeneration, in particular in AD. Gong reported an increase of NAD+ in brains of transgenic mice after NR application, providing evidence that NR is potent to penetrate into the brain. PGC1α induced degradation of BACE1 leadsto decreased Aß production resulting in an improvement in cognitive function and synaptic plasticity in AD mice (Gong, 2013). In a second study, administration of NAM resulted in improved mitochondrial functioning and a fission-fusion shift of mitochondria in an APP/PS1 transgenic mouse model (Long, 2015).
Further, modulating NAD+ metabolism has been shown to improve autophagic defects. Elevating NAD+ levels by application of NAM proved to decrease the mitochondrial content and increase LC3 positive punctae and mitochondrial fragmentation in human fibroblasts (Jang, 2012). This effect is accompanied by a decrease in levels of Complex V and an increase in LC3-II. Blocking autophagy by pharmacological inhibition was able to reverse such effects (Kang & Hwang, 2009). Further, in a model of xeroderma pigmentosum group A (XPA), where patients show besides dermatological symptoms signs of neurodegeneration and a decrease of the NAD+-Sirt1-PGC1α axis triggered defective mitophagy which could be reversed by application of NAD+ precursors (Fang, 2014).
Such results combined with the finding that even prolonged administration of high doses of NR do not lead to toxicity in rodent models (Conze, 2016) make NR an interesting candidate for clinical trials to treat diseases like muscular dystrophy or neurodegenerative disorders. First promising test in healthy controls have shown

that even a single dose of orally administrated NR can increase the level of NAD+ almost 3 fold in the blood (Trammell, 2016), however long term effects and especially the impact on disorders in humans still have to be investigated.

Chapter 2: Using patient fibroblast derived hiPSCs and gene editing tools to model LRRK2 related PD

Reinhardt, Schmid et al. Cell Stem Cell, 2013

Mutations in the LRRK2 gene represent the most common genetic cause for familiar forms of PD, the exact mechanisms however how mutations in LRRK2 are contributing to the disease are not fully understood. Multiple pathomolecular pathways were described in the context of LRRK2 ranging from translational control and vesicular trafficking over cytoskeletal regulation to neurite outgrowth and autophagy (reviewed in Tsika & Moore, 2012). One reason for this ambiguity might be the use of non-suited model-systems to study LRRK2 related pathogenesis. On this basis we decided to generate human iPSCs (hiPSCs) from PD patients who harbour the G2019S mutation which represents the most frequent LRRK2 mutation up to date. 2 patient and 4 healthy control fibroblast lines were transduced with the "Yamanaka factors" *Oct4, Sox2, Klf4* and *c-myc* to obtain patient specific hiPSCs. Immunocytochemical staining revealed that such cells are positive for pluripotency markers like NANOG, OCT4, SSEA4 and TRA1-81. Further quantitative PCR proved that reprogrammed hiPSCs express stem cell markers on a level comparable to hESCs and that the exogenously introduced Yamanaka factors are silenced in expression. Further, all lines were tested for the ability to differentiate into all three germ layers in vitro via embryoid body mediated differentiation and in vivo by teratoma formation in immune-compromised mice, proving the successful generation of bona fide hiPSCs. Multiple genetic variants are associated with PD, explaining partly the variety in phenotypes associated with PD patients who harbour *LRRK2* G2019S mutations (Simón-Sánchez, 2009). To overcome this problem and to investigate exclusively mechanisms related to the *LRRK2* G2019S mutation we further generated genetically isogenic control by ZFN technology. In this context, a donor construct was cloned, homologous to the wild type genomic sequence located at exon 41 of the *LRRK2* gene. Co-application of this plasmid together with vectors encoding two ZFN monomers which generate a DSB in exon 41, lead then to HDR of the DNA strand at the site of mutation, generating gene corrected controls from G2019S mutated hiPSCs. Additionally, we generated a plasmid for homologous recombination containing the G2019S mutation itself, enabling us to integrate this mutation in healthy hiPSCs using the same strategy. Importantly, global gene expression profiling revealed that such isogenic lines cluster much closer together with their parental hiPSCs then with unrelated gender and aged matched controls, underlining the importance of using genetic corrections for disease modelling. Phenotypic analysis revealed that correcting the G2019S

mutation results in amelioration of defects in neurite outgrowth, autophagy and the sensitivity to oxidative stress observed in hiPSC derived mDA neurons. Further, gene corrected neurons displayed reduced levels of α-syn and tau which are prone to aggregate in the disease. In summary, our study shows the importance of using patient derived hiPSCs in combination with gene editing approaches to model PD, to study underlying disease mechanisms and to investigate potential treatment possibilities.

Chapter 3: hiPSC-derived neurons from *GBA1*-associated Parkinson's disease patients show autophagic defects and dysregulation of Calcium homeostasis

Schöndorf et al, Nature Communications, 2014

Mutations in the *GBA1* gene represent the most common genetic risk factor to develop PD. Recent animal and cell culture models, including hiPSC derived cells

of GD patients show pathomechanistic features like reduced GCase activity, sphingolipid and α-syn accumulation as well as aberrant microglial activation (Mazzulli, 2011) (Panicker, 2012) (Keatinge, 2015). For *GBA1* related PD however, no patient derived neurons had been generated yet at this point and it was largely unknown if such cells would recapitulate PD related features *in vitro*. The objective of our study was to generate hiPSC derived neurons from PD and GD patients with *GBA1* mutations, to characterize such cells in regard to disease related features and to investigate underlying pathomechanisms.

Generation of hiPSCs, gene corrected lines and differentiation into mDA neurons

We obtained fibroblasts from 2 healthy controls, 4 Parkinson's disease patients with heterozygous *GBA1* mutations (N370S, L444P, RecNcil) as well as 4 homozygous GD patients (N370S, L444P). Cells were reprogrammed to hiPSCs, using retroviral transduction of the Yamanaka factors. After 2-4 weeks first stem cell colonies formed which were then characterized by immunostaining for the stem cell markers SSEA4, TRA1-81, TRA1-60, OCT4, LIN28 and NANOG. Further, such cells did not show any transgene expression after multiple passages but an upregulation of expression of endogenous stem cell markers and the potential to differentiate into all 3 germ layers (meso-, ecto-, and endoderm) in vitro and in vivo after transplantation into kidney and testis of immunodeficient mice.
Since multiple genetic variants can be associated to the development of PD (Simón-Sánchez, 2009) it is very challenging to assign disease relevant phenotypes to single mutations in PD related genes. Genetic corrections using gene editing technologies such as ZFN, TALEN or CRISPR/Cas provide a valuable tool to study single genetic mutations in diseased and control cells with identical genetic background. In our study we corrected all 3 PD relevant mutations in *GBA1* using a single ZFN pair and a homologous wild type construct. The ZFN introduces a double strand break between exon 9 and 10 of *GBA1* where all three pathogenic mutations used in our study are located. By application of a homologous wild type construct spanning exon 9 and 10 is was possible to correct the mutations.

Since PD is mainly affecting dopaminergic neurons in the *substantia nigra pars compacta* in the ventral midbrian, we differentiated the generated hiPSC to mDA neurons following a published protocol (Kriks, 2011). This protocol is based on the induction of floor plate precursors by dual SMAD inhibition and subsequent activation of Wnt and SHH signalling which leads to around 70% ßIII-tub+ and 15-20% TH+ cells at DIV 65 which co expressed typical mDA markers like FOXA2, NURR1, GIRK2 or VMAT2. Importantly, such cells showed punctate synapsin immunofluorescence staining indicating the establishment of synaptic connections. Due to the heterogeneity of differentiation efficiency we included an additional neuronal enrichment step using FACS. Sorting for the markers CD24+, CD29-, CD184-, CD44- and CD15- resulted in a highly enriched neuronal population, which could be kept in vitro for 3 weeks, showed electrophysiological activity and released dopamine in the medium supernatant.

Characterization of hiPSC derived mDA neurons

In order to verify that hiPSC derived neurons are a suitable model system to study disorders related to sphingolipid accumulation we assessed the polyganglioside content in differentiated neurons. The content and composition of polygangliosides changes over embryonal development and the highest contents can actually be found in the brain (Svennerholm, 1989). After metabolic labelling and subsequent radio imaging analysis, parental fibroblasts and hiPSCs showed low levels of mainly the monosialic ganglioside GM3. This pattern however changed upon differentiation with an increase in the overall levels of gangliosides and a shift to a more diverse pattern. Neuronal FACS enrichment further specified the ganglioside pattern comparable to what can be observed in the human and rodent CNS (Ngamukote, 2007). Different expression patterns and activity of glycohydrolases can be attributed to specific levels of sphingolipids. In hiPSC derived mDA neurons at DIV 65 the activities of the hydrolases GCase, GBA2 (non-lysosomal), ß-galactosidase and ß-hexosaminidase, which all represent major hydrolases involved in glycolipid metabolism, were increased compared to fibroblasts and hiPSC. As expected, mRNA expression and protein levels of such hydrolases were upregulated in

neurons compared to hiPSC. Taken together, the sphingolipid metabolism in hiPSC derived mDA neurons is comparable to the adult brain, which makes such neurons a powerful tool to study glycosphingolipid related disorders and associated neurodegeneration in vitro.

Disease associated phenotypes in mutant GBA1 hiPSC derived neurons

In order to model PD using *GBA1* mutant hiPSC derived mDA neurons, disease relevant phenotypes were investigated. In hiPSC based models for GD, it has been shown that macrophages and neurons derived from homozygous mutant *GBA1* hiPSCs show deficiency in GCase activity and subsequently accumulation of glycosphingolipids (Panicker, 2012). Liquid chromatography and tandem mass spectrometry (LC-MS/MS) revealed an increase in Glc-Cer in hiPSC derived neurons from GD and PD patients with *GBA1* mutations. Importantly, gene corrected lines showed reduced level of Glc-Cer. Correspondingly, protein levels and the enzymatic activity of GCase were significantly reduced in mutant hiPSC derived neurons but not in corresponding isogenic controls. Interestingly, the enzymatic activities of the hydrolases GBA2 and ß-galactosidase were reduced as well in mutant neurons compared to gene corrected controls suggesting a molecular crosstalk of such enzymes with GCase as suggested before (Körschen, 2013).

There is evidence linking *GBA1* mutations to an increase in α- syn accumulation. In the absence of GCase or in the presence of *GBA1* mutations in GD models accumulation of α-syn was reported (Manning-Boğ, 2009). In hiPSC derived neurons from *GBA1* PD or GD patients we found an increase in overall levels of α-syn. Interestingly such differences were just significant when comparing *GBA1* mutants to corresponding gene corrected controls but, except for L444P mutated *GBA1*, not comparing mutants to unrelated controls. This finding reflects the heterogeneity of basal α-syn levels in the overall population due to genetic variation (Julia Fuchs, 2008) and further underlines the importance of using isogenic controls for modelling of synucleinopathies.

Since α-syn is also partly degraded by the autophagosomal-lysosomal system, lysosomal dysfunction has been reported being associated to α-syn accumulation

(reviewed in Bourdenx, 2014). Immunofluorescent staining of the lysosomal marker LAMP1 revealed an increased accumulation of lysosomes in *GBA1* mutant hiPSC derived neurons. Number as well as average size of lysosomes was significantly increased compared to isogenic and unrelated controls suggesting a defective clearance of lysosomes in such cells. Further, assessment of macroautophagy by immunocytochemical staining revealed a significant increase in LC3-II positive particles in hiPSC derived neurons from *GBA1*-PD patients. This finding could be confirmed by Western blot analysis, showing accumulation of LC3-II at basal conditions as well as disturbance in the autophagic flux after inhibition of lysosomal degradation by Leupeptin/NH_4Cl. Further, co-staining of LC3-II and LAMP1 revealed a decreased co-localization of those markers suggesting a disturbed autophagosomal-lysosomal fusion in *GBA1*-PD cells compared to controls.
Taken together hiPSC derived neurons from PD patients with *GBA1* mutations and GD patients show decreased hydrolase activities and associated dysregulated sphingolipid metabolism. Further we observed an increase in α-syn accumulation in mutant cells and dysfunction of the autophagosomal-lysosomal system. Those findings suggest potential interactions of loss of GCase function, lipid metabolism, α-syn accumulation and autophagic dysfunction on multiple levels contributing to *GBA1* related pathogenesis in PD.

Dysfunction of Calcium homeostasis in GBA1 mutated hiPSC derived mDA neurons

In an unbiased experimental approach, we used LC-MS/MS comparing *GBA1* mutant neurons to controls in order to identify dysregulated genes and pathways, which might be implicated in *GBA1* associated pathogenesis. Overall, 7069 proteins were identified in FACS enriched neurons. The top hit NECAB2 was 1.9 fold higher expressed in *GBA1* mutated neurons compared to controls. NECAB2 is part of the family of the EF-hand calcium binding proteins with a mainly neuronal expression pattern (Sugita, 2002). On a molecular level it can interact with the A2A receptor (Canela, 2007) and has been reported to potentially regulate mGluR5 signalling (Canela, 2009). Dysregulation of calcium (Ca^{2+}) homeostasis and related excitotoxicity has been proposed to play a role in the pathogenesis of PD (Surmeier,

2012). Further, mDA neurons possess pacemaker activity which is dependent on L-type Ca^{2+} currents responsible for depolarization (Harris, 1989).

By performing calcium-imaging analysis using the Ca^{2+} sensitive dye Fura2, we observed an increase in basal Ca^{2+} levels in *GBA1* mutated neurons.

In post mortem brain it has been described that agonist induced Ca^{2+} release by stimulation of RyR resulted in elevated Ca^{2+} release from the ER in GD patients compared to controls (Pelled, 2005). Therefore, we applied Caffeine, which is a RyR agonist and releases Ca^{2+} from the ER into the cytoplasm to hiPSC derived neurons with *GBA1* mutations and controls. Interestingly we observed a significantly elevated cytoplasmatic Ca^{2+} burst in cells derived from PD and GD patients compared to isogenic and unrelated controls. This suggests *GBA1* having an influence on regulating intracellular levels of Ca^{2+}. Interestingly, this finding could be replicated recently in fibroblasts derived from PD and GD patients with *GBA1* mutations. However, pure loss of GCase activity by pharmacological inhibition did not lead to an increase of ER related Ca^{2+} suggesting a gain of function mechanism of mutated *GBA1* (Kilpatrick, 2016). Importantly, dysregulation of Ca^{2+} homeostasis in *GBA1* mutated neurons was associated with an increase in vulnerability to cellular stressors. Compared to isogenic controls, mutated cells showed increased release of lactate dehydrogenase (LDH) release after application of A23187, which is a Ca^{2+} ionophore inducing ER stress by elevating cytosolic Ca^{2+} concentrations, or rotenone. Besides, knock down of NECAB2 further potentiated the cellular toxicity, suggesting a protective effect by its potential Ca^{2+} binding properties.

Taken together, we show that intracellular Ca^{2+} homeostasis is dysregulated in hiPSC derived neurons from PD and GD patients compared to controls and that this is accompanied by increased susceptibility to ER stress of such by intracellular elevation of Ca^{2+}.

Chapter 4: The NAD+ Precursor Nicotinamide Riboside Rescues Mitochondrial Defects and Neuronal Loss in iPSC and Fly Models of Parkinson's Disease

Schöndorf et al. Cell Reports 2018

Mitochondrial dysfunction is one of the major molecular pathologic hallmarks of PD and especially the contribution to *GBA1* related PD remains unclear. In this context it is unclear whether mitochondria are actual disease drivers and if boosting mitochondrial function and biogenesis might have beneficial effects in PD pathogenesis. Further, the potential involvement of gain and loss of function of mutated *GBA1* in such PD pathogenic mechanisms is still not fully understood. Interestingly, in a global unbiased gene transcription analysis comparing hiPSC derived mDA neurons of PD patients with *GBA1* mutations with controls, pathways associated to the phagosomal system, mitochondrial function and protein synthesis were significantly dysregulated. The aim of our study was to elucidate the involvement of gain and loss of function mechanisms of mutant *GBA1,* also in the context of mitochondrial function and dysfunction. To this end we generated *GBA1* knockout ($^{-/-}$) cells and included such cells in the study. Further, we investigated the NAD+ metabolism in *GBA1*-PD cells and, in order to assess potential treatment possibilities for mitochondrial dysfunction, applied the NAD+ precursor NR on *GBA1* PD cells and in *in vivo* models of *GBA1* PD.

Generation and characterization of GBA1$^{-/-}$ hiPSC derived neurons

To elucidate the question if gain or loss of function mechanisms of mutated *GBA1* associated mutations are present in PD and how such mechanisms are contributing to mitochondrial dysfunctions in PD pathogenesis, we generated *GBA1*$^{-/-}$ hiPSCs by CRISPR/Cas9 technology. Previous groups addressing this question in fibroblasts from GD patients described impaired oxygen consumption, increased formation of ROS as well as reduced MMP (de la Mata, 2015). In context of PD, this

model however has the major drawback of using a non-affected cell type in the disease. Further, homozygous *GBA1* mutated cells show remaining GCase activity and accumulation of misfolded GCase in the ER, mimicking as well gain of function mechanisms then purely loss of function phenotypes. In a different study, a *GBA1*$^{-/-}$ mouse model was generated and mitochondrial dysfunction could be observed in neurons and astrocytes including increased mitochondrial fragmentation and impaired mitochondrial respiration (Osellame, 2013). First evidence for the implication of loss of function mechanisms in human cells was derived from a study where SH-SY5Y cells were treated with the chemical GCase inhibitor CBE. These cells showed reduction of the MMP, increase in ROS production and mitochondrial fragmentation (Cleeter, 2013). The findings could be replicated using shRNA mediated knock down of GCase in the same cell model system. Artificial chemical or shRNA mediated knock down systems however are not fully precise, leaving residual GCase activity which might be sufficient to sustain basic physiological functions of the enzyme. Due to such reasons we decided to generate *GBA1*$^{-/-}$ hiPSC using CRISPR-Cas technology. 2 different guide RNAs were delivered in the cell causing a genomic deletion between exon 3 and 4 of the *GBA1* gene leading to a coding frameshift and an early stop codon. The cells showed complete ablation of *GBA1* protein and GCase enzyme activity. Further, analysis of dopaminergic differentiation potential revealed that dopaminergic differentiation of *GBA1*$^{-/-}$ hiPSC result in similar number of ßIII-tubulin and TH positive cells compared to maternal control hiPSCs. We recently described accumulation of α-syn in hiPSC derived neurons after GCase inhibition due to CBE application (Schöndorf, 2014). As expected, neurons derived from *GBA1*$^{-/-}$ hiPSC showed elevated levels of α-syn compared to their maternal lines.

GBA1-PD neurons display intraorganellar defects including ERS and mitochondrial dysfunction with involvement of gain and loss of function mechanisms

Transcriptomic analysis comparing *GBA1* PD and control hiPSC derived neurons revealed phagosome formation, mitochondrial function as well as eif2α signalling dysregulated in *GBA1* PD. eif2α is closely linked to protein translation and

interestingly, translational attenuation can be a result of elevated induction of ERS and has been described in models of neurodegeneration (Moreno, 2012). The induction of ERS and activation of the UPR on the other hand have been described in various models of GD and *GBA1* related PD (Sanchez-Martinez, 2016) (Braunstein, 2016) (Fernandes, 2016). However if GCase loss of function is sufficient for *GBA1* related ERS induction in this context is not clear. Interestingly, *GBA1* PD but not gene corrected or GBA$^{-/-}$ neurons showed elevated ERS including increased levels of BIP, elevated expression of phosphorylated eif2α and phosphorylated PERK as well as Xbp1s transcription, assigning this effect for the first time to a potential gain of function mechanism of mutant *GBA1* in PD. Importantly, we also observe a reduction in the expression of the mitophagy adaptor protein NIX/BNIP3L in *GBA1* PD cells. This is in line with reduced TFEB translocation in *GBA1* PD cells and the above described dysfunction in the autophagosomal-lysosomal system (Schöndorf, 2014). According to the reduced expression of NIX/BNIP3L, transcriptomic analysis revealed mitochondrial dysfunction as a major dysregulated pathway in *GBA1* PD, which can also be a result of impaired mitophagy. In order to study mitochondrial dysfunction in *GBA1* PD and GBA1$^{-/-}$ cells, we first compared the overall mitochondrial mass of the cells. Citrate synthase activity measurements showed that the mitochondrial mass was similar in *GBA1* PD, *GBA1*$^{-/-}$ as well genetic control neurons. Deficiency of activity of the mitochondrial electron transport complex I can be observed in post mortem tissue of PD patients (Schapira, 1989). Interestingly, *GBA1* PD and *GBA1* $^{-/-}$ hiPSC derived neurons showed a reduction in C I activity compared to isogenic controls in a biochemical assay. Dysfunction of the mitochondrial electron transport chain can lead to impaired respiration and ROS production. Excessive generation of ROS was described in models of *GBA1* inhibition (Cleeter, 2013) and GD (de la Mata, 2015). Using FACS analysis we found that *GBA1* PD and *GBA1*$^{-/-}$ neurons exhibited increased levels of MitoSox fluorescence corresponding to increased generation of mitochondrial ROS (mROS) compared to isogenic controls. Disrupted mitochondrial cristae structure was observed in nigral neurons form PD patients (Anglade, 1997) and it has been shown that elevated levels of α-syn can trigger mitochondrial cristae rearrangement (Martin, 2006) but an association to *GBA1* related PD has not been described yet. Electron microscopy analysis revealed that the morphology of the

inner mitochondrial cristae of *GBA1*-PD and *GBA1*$^{-/-}$ mitochondria presented higher levels of disorganization whereas cristae of isogenic control mitochondria appear to be more lamellar. Mitochondrial dysfunction can also occur as a result of impaired clearance of dysfunctional mitochondria. Comparing mitochondrial lysosomal co-localization we found that mitophagy is impaired in *GBA1* PD and *GBA1*$^{-/-}$ neurons compared to isogenic controls. This finding is in line with results of the transcriptomic analysis presenting phagosomal pathways dysregulated in *GBA1* PD and findings of our previous work describing dysfunction of the autophagosomal-lysosomal system in such cells (Schöndorf, 2014). Measurement of the cellular oxygen consumption rate (OCR) by a Seahorse XF analyzer revealed deficits of *GBA1* PD and *GBA1*$^{-/-}$ neurons in mitochondrial respiration. The spare respiratory capacity (SRC) was significantly lower in such cells compare to isogenic controls. Importantly *GBA1* PD neurons further showed reduced levels of basal and maximal respiration as well as ATP production compared to *GBA1*$^{-/-}$ neurons and isogenic controls. Considering this discrepancy together with the lack of a gene-dose effect on mitochondrial function parameters, this finding suggests different implicated pathomechanisms in *GBA1* PD compared to *GBA1* $^{-/-}$ cells. Taken together our results show for the first time that *GBA1* PD hiPSC derived neurons show mitochondrial dysfunction and results from *GBA1*$^{-/-}$ cells suggest that loss of *GBA1* function and subsequent lysosomal dysfunction and α-syn accumulation might play a role in this observation. Further, due to the implication of ERS exclusively in *GBA1* PD not in *GBA1*$^{-/-}$ hiPSC derived neurons, an involvement of both gain and loss of function mechanisms in *GBA1* PD pathology is likely.

In summary we observe multi-organelle dysfunction in *GBA1* PD including the autophagosomal and mitochondrial system as well as the ER. In a mechanistic context of mutant *GBA1* both, gain- and loss of function models could be involved in the mitochondrial dysfunction observed.

Treatment with the NAD+ precursor NR restores pathogenic phenotypes and neuroprotection in GBA1 PD hiPSC derived neurons and in a Drosophila model of PD.

Decline of intracellular NAD+ levels have been associated to ageing and mitochondrial dysfunction and elevation of intracellular levels of NAD+ have been shown to ameliorate such defects (Mouchiroud, 2013) (H. Zhang, 2016) (Khan, 2014). Nicotinamide Riboside (NR) is a potent NAD+ precursor which has been shown to improve deficits related to mitochondrial dysfunction in mouse models of mitochondrial disease (Cerutti, 2014), myopathy (Khan, 2014) or high fat related obesity (Cantó, 2012). The exact role of NAD+ metabolism in, and the effect of NR on neurodegenerative disorders modelled by hiPSC derived neurons however is unknown. Given the potential role of *GBA1* mutations in ageing, we investigated effects of mitochondrial dysfunction and ERS on NAD+ metabolism in *GBA1* PD and *GBA1*$^{-/-}$ hiPSC derived neurons. We found that mRNA levels of the enzyme mononucleotide adenylyltransferase 2 (NMNAT2), which is involved in NAD+ biosynthesis, are significantly reduced in *GBA1* PD compared to isogenic controls and *GBA1*$^{-/-}$ cells. LC-MS analysis revealed unaltered levels of NAD+ in all *GBA1* variants. To rule out the possibility however, that the heterogeneity of the cellular composition might influence this result, we also applied the fluorescent sensor Peredox to measure the NAD+/NADH ration in neuronal cells specifically (Hung, 2011). Importantly, the NAD+/NADH ratio was significantly reduced in *GBA1* PD hiPSC derived neurons suggesting an alteration of NAD+ metabolism and subsequent reduced levels of available NAD+.

To investigate potential beneficial effects of elevating NAD+ levels, we applied NR to *GBA1* PD cells. Measuring the NAD+ content after treatment, we found that application of 24h 250µM NR increased intracellular levels of NAD+ approximately 2.7 fold, proving that NR can be taken up by cells *in vitro* and can be effectively further converted to NAD+ intracellularly.

In animal models, multiple studies describe an increase in Sirt1 dependent transcription of mitochondrial biogenesis related genes like TFAM and ERR-alpha or mitochondrial chaperones like HSP60 or ClpP (Cerutti, 2014) (Mouchiroud, 2013) (Mootha, 2004). Q-RT-PCR analysis in *GBA1*-PD hiPSC derived neurons revealed that treatment with NR upregulates the expression of markers like TFAM, ERR-

alpha and Hsp60 significantly. These effects can mainly be attributed to an increase in Sirt1 and subsequent PGC1α activity, which serve as direct transcriptional regulator of those genes (Onyango, 2010). Importantly, in accordance with the literature, the expression of Sirt1 and PGC1α itself stays unaltered (Cerutti, 2014) (Cantó, 2012) ,suggesting that NR might influence Sirt1 activity by increasing the bioavailability of NAD+ leading to a direct deacetylation following activation of PGC1α (Rodgers, 2005). Mitochondrial mass was increased after NR treatment in *GBA1*-PD hiPSC derived neurons as shown by Western Blot and mitochondrial copy number analysis. Next we analyzed the mitochondrial ultrastructure of *GBA1* PD neurons after NR treatment. EM analysis revealed a significant increase in the number of mitochondria with lamellar cristae in NR treated *GBA1* PD cells, whereas the inner structure of untreated cell was more disorganized, suggesting also functional improvement of mitochondria, which is in accordance with previously published work (Cantó, 2012). Indeed, measurement of mitochondrial ROS production revealed a significant decrease of the latter in cells treated with NR, suggesting improved functionality of mitochondria and consequently reduced oxidative stress.

Interestingly, in mouse embryonic fibroblasts it has been shown that Sirt1 activation increases expression of members of the ATG family resulting in an increase of the autophagic potential (Lee, 2008) which could be confirmed by a study in human fibroblasts showing that elevation of the NAD+/NADH ratio results in an increase in the autophagic flux (Jang, 2012). In hiPSC derived neurons from *GBA1* PD patients, NR treatment lead to lower expression but to an increase of translocation of TFEB from the cytoplasm to the nucleus indicating an increase in lysosomal homeostasis and consequently autophagic induction. Indeed, NR treated cells showed increased levels of LC3-II after lysosomal inhibition suggesting an increase in lysosomal generation.

Importantly, the increase in autophagy could also be linked to increased levels of degradation of mitochondria shown by an increase in mitochondrial-lysosomal co-localization after treatment of *GBA1* PD neurons with NR.

After proving the efficiency of NR treatment in hiPSC derived neurons on mitochondrial dysfunction, we were interested if NR treatment could also ameliorate *GBA1* related pathology *in vivo*.

Recently, Sanchez-Martinez published the generation of a *Drosophila* model of mutant *GBA1* describing loss of dopaminergic neuronal loss, induction of ERS and impaired locomotor function (Sanchez-Martinez, 2016). Interestingly, feeding of NR significantly reduced neuronal loss and improved locomotor function, confirming protective effects of NAD+ elevation *in vivo*.

Taken together, our results show that an increase of intracellular NAD+ levels has beneficial effects in hiPSC derived neuronal as well as in Drosophila models of *GBA1* related PD. Our data suggest that multiple mechanisms might contribute to the beneficial effects of NR on hiPSC derived neurons. Besides increasing mitochondrial mass and functionality and the induction of markers of the mitochondrial UPR, clearance of dysfunctional mitochondria by elevated mitophagy might also contribute to decreased levels of mitochondrial ROS production and due to this to an improved intracellular oxidation status.

Chapter 5: Discussion

Choosing the right cell type is crucial for modelling neurodegenerative disorders *in vitro*. Existing models like patient fibroblasts or neuroblastoma cell lines, however do not represent the disease relevant cell type or lack patient specificity. The generation of hiPSCs and subsequent neuronal differentiation enables researchers for the first time to investigate neurodegenerative disorders in a patient and cell type specific context.

We show that hiPSC derived neurons from PD patients recapitulate disease relevant phenotypes including high levels of α-syn or increased sensitivity against toxins. The choice of proper controls is very important in this context. Due to the different genetic background of individuals, physiological functions are variable and the expression of α-syn for example varies significantly in the population. mRNA expression profiling revealed that gene corrected hiPSCs cluster in terms of gene expression much closer to their parental diseased lines compared to unrelated age and gender matched controls which are often used in studies.

Underlining the potential of hiPSCs to model neurodegenerative disorders we show that over the time course of differentiation from hiPSCs to mDA neurons, the polyganglioside pattern of cells is changing, recapitulating the shift in gangliosides observed during brain development. Comparing the ganglioside composition in sorted and unsorted neurons, we found that unsorted cultures contain high levels of GM3 and GD3 which is mainly present in the early developing brain but decrease during development (Ngamukote, 2007). FACS sorted neurons on the other side displayed a higher abundance of gangliosides found in the developed brain such as GM1, GD1a, GD1b, GT1b (Kracun, 1984). This underlines the importance of sorting neuronal populations differentiated from hiPSC cultures to reduce background and misinterpretation of data due to the presence of non-neuronal or undifferentiated cell types. However, due to high cell quantities required for certain biochemical assays, it is not always applicable to FACS sort neurons. An alternative hereby is the investigation of single cells from heterogeneous cultures for example by immunofluorescent staining. Corresponding to the shift in the ganglioside pattern over differentiation we could also observe an increase in the expression of glycohydrolases GCase, GBA2, ß-hexosaminidase or ß-galactosidase, proposing expression of such enzymes as a key in neuronal development.

As a result of decrease and loss of GCase enzymatic activity in *GBA1* PD and *GBA1*$^{-/-}$ hiPSC derived neurons respectively, we find an increase in accumulation of Glc-Cer by LC-MS/MS analysis. This has also been shown in post mortem tissue of GD patients, in a neuronopathic mouse model of GD as well as in a RNAi *GBA1* knock down model (Nilsson & Svennerholm, 1982) (Enquist, 2007) (Mazzulli, 2011) but not in models of *GBA1* PD before.

Physiologically, GCase is a lysosomal enzyme which fulfils important functions in the sphingolipid metabolism of the cell. Correspondingly, and in accordance with our observations, loss of GCase function leads to autophagic dysfunction and dysregulation of the lipid metabolism. It has been shown that the intracellular lipid content can also influence the autolysosomal system (Koga, 2010) and sphingolipids and ceramide have been proposed to regulate autophagy (Harvald, 2015) connecting lipid accumulation and autophagic dysfunction on a functional level.

We find α-syn accumulated in *GBA1* PD and *GBA1*$^{-/-}$ neurons. Interestingly, α-syn accumulation, dysregulation of lipid homeostasis and lysosomal dysfunction can be linked in common pathways. α-syn has been shown to interact with cellular membranes (Kamp & Beyer, 2006) and lipid rafts can induce α- syn aggregation (Drescher, 2010). It also has been suggested that loss of GCase activity can trigger α-syn accumulation as a secondary effect of lysosomal dysfunction, which on the other hand can inhibit trafficking of GCase to the lysosome, forming a pathogenic loop (Mazzulli, 2011).

It was reported that pharmacological inhibition of GCase results in accumulation of α-syn *in vitro* and *in vivo* (Cleeter, 2013) (Manning-Boğ, 2009) linking α-syn accumulation to a loss of function mechanism of *GBA1* in PD. Contrarily, in a gain of function manner, misfolded GCase has also been shown to directly interact with α-syn, enhancing its aggregation, and is besides present in LBs (Goker-Alpan, 2010). In our model *GBA1*-PD hiPSC derived neurons show already increased α-syn levels compared to isogenic controls and interestingly such an elevation was even more evident in isogenic *GBA1*$^{-/-}$ cells suggesting a gene dose dependent effect and contribution of loss of function mechanisms of *GBA1* in our findings.

Investigating lysosomal dysfunction in *GBA1* mutations carriers on a mechanistic level, we found that the nuclear translocation of the lysosomal master gene TFEB was reduced in *GBA1* PD neurons compared to isogenic controls. Interestingly, the mRNA levels of TFEB were higher in *GBA1* mutant cells suggesting an effort of the cell to compensate for reduced TFEB induction. Importantly, TFEB is directly regulated by mTOR activity, which has been described to be dysregulated in post mortem brain tissue of PD patients (Wills, 2012) and further, reduced stability of TFEB has been shown in a hiPSC model of GD (Awad, 2015). Consequently, modulation of TFEB could be a potent strategy to ameliorate lysosomal dysfunction in various neurodegenerative disorders. Interestingly, TFEB signalling has been shown to be disturbed in mDA neurons form rats expressing the parkin Q311X mutation resulting in impaired autophagy and mitochondrial quality control (Siddiqui, 2015). In line with such results we observe reduced mitochondrial-lysosomal co-localization as well as reduced expression of the mitophagy adaptor protein NIX/BNIP3L suggesting defective mitophagy in *GBA1* PD hiPSC derived neurons.

Mitochondrial dysfunction is one of the key pathological features of PD. In post mortem brain tissue of PD patients Complex I activity in the *substantia nigra* was found to be markedly reduced (Schapira, 1989). Further, mitochondrial dysfunction has been described in various models of PD and ultimately it has been shown that mutations in mitochondrial related genes such as *PINK1* or *parkin* can lead to the development of familiar forms of PD. For the first time we describe the involvement of mitochondrial dysfunction in *GBA1* related PD. Mitochondrial respiration parameters like basal respiration, SRC and ATP production were reduced in *GBA1* PD neurons compared to isogenic controls. These findings suggest that mitochondria in *GBA1* PD or *GBA1*$^{-/-}$ neurons lack the capacity to upregulate ATP production under stress situations potentially resulting in increased vulnerability to cellular stress (Hill, 2009). Accordingly, by electron microscopy analysis, we observe disorganized mitochondrial cristae structure, which is the site of respiratory chain supercomplex assembly. In line with our results, structural alteration in the shape of this inner mitochondrial membranes has been linked to impaired respiration (Cogliati, 2013). Further we observe an increase in mitochondrial ROS production in *GBA1* PD. UCP2 expression was shown to reduce mROS production, however at the cost of ATP production (Garlid, 2000) (Zhang, 2001). Interestingly

GBA1 PD cells showed reduced levels of UCP2, which might be a cellular response to enhance defective respiration observed in such neurons and consequently results in increased mROS production. In this context we also observed reduced C I activity in both *GBA1* PD and *GBA1* $^{-/-}$, which can be reason as well as result of increased levels of ROS (Tretter, 2004) and is in line with results described by Schapira et al.

Transcriptomic analysis further revealed eif2α signalling as one of the major dysregulated pathways in *GBA1* PD neurons. Dysregulation of protein translation has been described in various disorders including prion neurodegeneration (Moreno, 2012) and is closely related to increased ERS in such cells. In various other lysosomal storage disorders it has been shown that loss of glycohydrolase activity and subsequent substrate accumulation is sufficient to trigger ERS (Tessitore, 2004) (Zhang, 2006). Comparing *GBA1* PD and *GBA1* $^{-/-}$ neurons, we show however for the first time that mechanisms linked to ERS induction are uniquely linked to *GBA1* PD associated mutations and are absent upon deletion of GCase. The ER is one of the major Ca^{2+} stores in the cell and ERS has been shown to potentially lead to alteration in Ca^{2+} homeostasis and subsequent apoptosis by dysregulation of IP_3R assembly (Higo, 2010). Importantly, proteomic analysis revealed increased expression of the Ca^{2+} binding protein NECAB2 in *GBA1* PD neurons compared to isogenic controls suggesting dysregulated Ca^{2+} homeostasis in *GBA1* PD. Dysregulated Ca^{2+} homeostasis has been described in various neurodegenerative disorders including PD (Surmeier, 2012). We find elevated basal levels of Ca^{2+} in *GBA1* PD neurons, which are raising even higher after application of Caffeine, which releases Ca^{2+} from the ER by activation of the RyR receptor. This is in line with previous results showing that in neuronopathic models of GD, Glc-Cer leads to over-activation of the RyR receptor on the ER (Pelled, 2005). Importantly, this is also linked to increased neuronal toxicity after application of Rotenone or the ER stressor A23187. NECAB2 knockdown aggravates such toxicity, suggesting a novel, protective role of NECAB2 by its Ca^{2+} binding properties. ER and mitochondria are also connected on a cellular functional level by the exchange of Ca^{2+} and lipids, and we propose that this connection might be disturbed in *GBA1* PD. PERK, which we find enhanced phosphorylated in *GBA1* PD cells is an important component of the

MAMs and has been shown to modulate ER mitochondrial connectivity (Verfaillie, 2012). Further, both BNIP3L and UCP2 are linked to this intracellular communication and are dysregulated in *GBA1* PD hiPSC derived neurons. BNIP3L can propagate mitochondrial associated cell death signals residing at the ER (Kitsis & Molkentin, 2010) and UCP2 has been described to be essential for mitochondria Ca^{2+} uptake from the ER (Trenker, 2007). Direct evidence however that mitochondrial dysfunction results from ERS and disturbed mitochondrial ER interaction in *GBA1* PD still has to be obtained. Electron micrographs can give information about the physical distance between ER and mitochondria. Changes in the MAM composition can lead to altered distance between ER and mitochondria, which on the other side has an influence on mitochondrial Ca^{2+} loading from the ER which can be measured by mitochondrial localized Ca^{2+} sensitive dyes such as Rhod2 AM. Mitochondrial Ca^{2+} is crucial for proper mitochondrial homeostasis including respiration and the regulation of apoptosis (reviewed in Rizzuto, 2009). Further, a defined distance between ER and mitochondria is crucial for the generation and transfer of phospholipids, which is fundamental for proper mitochondrial membrane composition and homeostasis (Tatsuta, 2014). Lipidomic analysis of mitochondria from *GBA1* PD and gene corrected neurons, which however requires high amounts of purified mitochondria, might give information about the composition of mitochondrial membranes in this context.

In summary, data from transcriptomic analysis as well as functional assays suggest multi-organelle dysfunction in *GBA1* PD hiPSC derived neurons including ER, mitochondria and autophagosomes/lysosomes. All of such organelles were described to play a role in PD and importantly, all 3 organelles can be connected on a functional level. ER derived Ca^{2+} for example is important in lysosomal functioning and ER stress can lead to the modulation of autophagic induction (reviewed in Sano & Reed, 2013). Further, ER and mitochondria form MAMs, which are required for the transfer of Ca^{2+}, which is necessary for proper mitochondrial homeostasis. The lipid composition of MAMs is highly dependent on orchestrated mitochondrial – ER interactions (Raturi & Simmen, 2013), resulting in the generation of lipid rafts highly enriched in glycosphingolipids. This can also have an important impact on mitochondrial metabolism as it has been shown in yeast models (Birner, 2001). Mitochondria and lysosomes on the other hand are connected on different

levels in terms of signalling (Baixauli, 2015) or the clearance of defective mitochondria (Youle & Narendra, 2011) assuring proper cellular homeostasis.

In a mechanistic context of mutant *GBA1* both, gain- and loss of function models could be involved in the multi organelle dysfunction observed. Loss of GCase activity leads to substrate accumulation in lysosomes and subsequently to autophagic-lysosomal dysfunction. Further, loss of GCase is associated with disturbed sphingolipid metabolism, which can disturb ER-mitochondrial connections and affect various cellular functions such as Ca^{2+} signalling, lipid homeostasis, mitochondrial dynamics or apoptosis. Further, autophagic impairment resulting from loss of GCase function can lead to the accumulation of α-syn, dysfunctional mitochondria and subsequent elevation in ROS production. Gain of function mechanisms of misfolded GCase on the other hand can lead to ERS and activation of the UPR, which in turn can result in pathological modulation of MAMs and impaired ER-lysosomal interactions. Further, ER retention of mutant *GBA1* could also change the lipid composition of the ER resulting in similar, MAM related effects.

Our data suggest the involvement of both gain and loss of function mechanisms of mutant GCase in *GBA1* PD. *GBA1* PD but not *GBA1* $^{-/-}$ iPSC derived neurons show ERS and subsequent activation of the UPR. This could be linked mechanistically to mitochondrial dysfunction, which however is also evident in *GBA1* $^{-/-}$ cells, suggesting an influence of loss of function mechanisms. Supporting this, a-syn accumulation and also mROS productionis more aggravated in *GBA1* $^{-/-}$ cells compared to *GBA1* PD and isogenic controls. On the other side, no gene dose effect is evident when comparing *GBA1* PD and *GBA1* $^{-/-}$ on the level of mitochondrial phenotypes like cristae arrangement or mitophagy. Contrarily, *GBA1* PD neurons show the highest cellular respiration deficiency when comparing all 3 genotypes. These findings suggest the involvement of both gain and loss of function of mutant GCase in PD. In this context however, the exact influence of gain of function mechanisms in *GBA1* PD still have to be investigated. Artificial expression of wildtype *GBA1* or application of recombinant GCase (Imiglucerase) in the background of hetero- or homozygous *GBA1* mutations could give exclusive information of potential gain of function mechanisms of misfolded GCase.

Alterations in the intracellular NAD+ levels have been associated to various ageing related disorders (Imai & Guarente, 2014). LC-MS/MS analysis revealed that in *GBA1* PD and *GBA1*$^{-/-}$ heterogenous hiPSC derived neuronal cultures and brain homogenates from *GBA1*$^{+/-}$ and *GBA1*$^{-/-}$ zebrafish, NAD+ levels were maintained. The intracellular NAD+ content however can be highly variable in different tissues and in different cell types inside the same tissue. Therefore we analysed the NAD+/NADH ratio in hiPSC derived neurons using a fluorescent NADH sensitive sensor. Interestingly, *GBA1* PD neurons showed decreased NAD+/NADH ratios. Such reduced NAD+/NADH levels can be explained by increased oxidative stress, which was shown to lead to an increase in the activity of NAD+ consuming enzymes such as PARP (Luo & Kraus, 2012), reducing the cellular bioavailability of NAD+. Further, dysfunction of the NADH dehydrogenase Complex I leads to a reduction of the NAD+/NADH ratio, which has been shown to reduce the activity of Sirt3 (Karamanlidis, 2013). The reduced levels of NMNAT2 expression further support an important role of the alteration of NAD+ metabolism in *GBA1* PD. Besides its crucial role as an enzyme involved in cellular NAD+ synthesis, NMNAT2 also displays chaperone function and its overexpression has been shown to be beneficial in models of AD (Ali, 2016). Reduced NMNAT2 levels can therefore be involved in the increase in proteotoxic stress observed in *GBA1* PD neurons. NAD+ is an important coenzyme in the regulation of the activity of the sirtuin family, which is implicated in regulating cellular homeostasis including autophagy, mitophagy, mitochondrial function, biogenesis and ERS (Tang, 2016) (Ng & Tang, 2013) (Fiorentino, 2015). We therefore suggest that reduced levels of NAD+ might play a crucial role in the development of *GBA1* PD related pathogenesis and that NAD+ boosting strategies might have beneficial impact on the latter. Elevation of NAD+ levels has been shown to be beneficial in various disease models, including mitochondrial myopathy and metabolic disorders (Khan, 2014) (Cantó, 2012). Further, application of NAD+ precursors has been described to increase lifespan and to ameliorate ageing associated phenotypes in *C.elegans* (Mouchiroud, 2013) but if elevation in NAD+ is beneficial in models of PD is not known. Due to its high bioavailability and its potency to cross the blood brain barrier, we decided to apply NR in hiPSC derived neurons. Importantly, NR increased mitochondrial biogenesis and function and reduced mitochondrial ROS production. An elevation in NAD+ levels has been shown to improve expression and activity of single mitochondrial

complexes as well as to increase the mitochondrial UPR and expression of antioxidant related genes such as SOD2 (Cerutti, 2014) (Cantó, 2012) (Pirinen, 2014). If a single mechanism or a combination of such is contributing to the observed effects of NR treatment in *GBA1* PD hiPSC derived neurons has still to be elucidated. Further, application of NR increased autophagic capacity and consistent with those findings we also observed increased mitophagy after NR application. Furthermore we also observe reduced TFEB expression and an increase in nuclear translocation of the latter. This is implicating that NR treatment is normalizing dysregulated TFEB signalling and is boosting autophagy in hiPSC derived *GBA1* PD neurons. To underline the protective effects of NAD+ elevation, we further show that NR improves locomotor deficits and mDA neuronal cell survival of a *Drosophila in vivo* model of *GBA1* related PD.
Contrary to the beneficial effects of NR application on mitochondrial function and autophagy, we could not observe and effect on ERS in hiPSC derived neurons. Even though ERS and UPR activation have been described to play a role in various neurodegenerative diseases (Lindholm, 2006), the exact role in disease pathogenesis is unknown. In this context it is important to emphasize that UPR induction has also been shown to regulate important physiological functions in neuronal development and plasticity (Hayashi, 2007) or neuroprotection upon cellular stress (Valdés, 2014).

To conclude, we present *GBA1* PD hiPSC derived neurons as a powerful tool for PD research, recapitulating major hallmarks of the disease like α-syn accumulation and autophagic-lysosomal dysfunction. Genetic modifications of such cells enables the investigation of novel *GBA1* related disease pathomechanisms such as disturbed Ca^{2+} homeostasis and mitochondrial dysfunction and implicates the involvement of both gain and loss of function mechanisms of mutated *GBA1*. Further, our findings suggest a key role of NAD+ metabolism in the neurodegenerative process. Given the clinical similarity of *GBA1* PD and sporadic PD patients, elevating NAD+ levels by application of NAD+ precursors can be adapted as a therapeutic strategy not only for genetic but also sporadic PD as well as other neurodegenerative disorders.

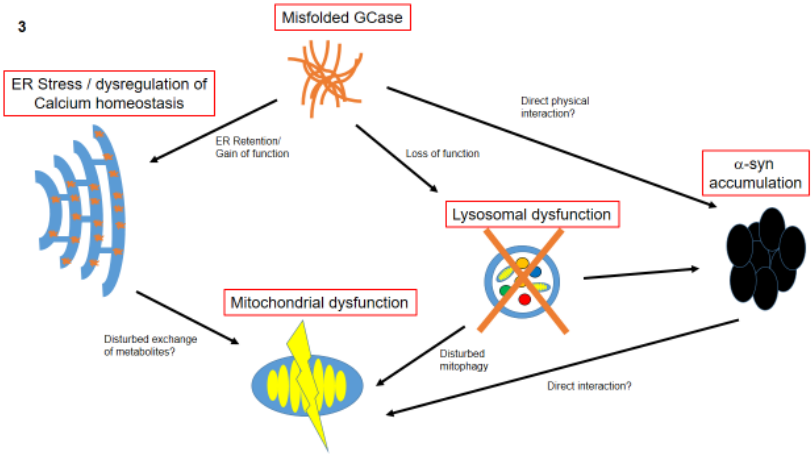

Figure3: Potential mechanisms how mutations in GBA1 can contribute to disease pathogenesis in PD. Following gain of function mechanisms, misfolded GCase remains in the ER which leads to induction of ER Stress and might be responsible for dysregulation of calcium homeostasis. This on the other side might affect mitochondria by disturbed exchange of lipids or Calcium which then leads to mitochondrial dysfunction. Following loss of function mechanisms, loss of GCase function leads to lysosomal dysfunction, which as a result can disturb mitophagy or lead to accumulation of a-syn. Further misfolded GCase has been reported to interact physically with a-syn which enhances aggregation. Either single pathways or combined effects of multiple mechanisms might be responsible for GBA1 related disease progression in PD.

References

Aarsland, D., Andersen, K., Larsen, J. P., Lolk, A., Nielsen, H., & Kragh-Sorensen, P. (2001). Risk of dementia in Parkinson's disease: a community-based, prospective study. *Neurology*, *56*(6), 730–736. https://doi.org/10.1212/WNL.56.6.730

Adly, A. A. M. (2010). Oxidative stress and disease: An updated review. *Research Journal of Immunology*. https://doi.org/10.3923/rji.2010.129.145

Aharon-Peretz, J., Rosenbaum, H., & Gershoni-Baruch, R, et al. (2004). Mutations in the glucocerebrosidase gene and Parkinson's disease in Ashkenazi Jews. *The New England Journal of Medicine*, *351*(19), 1972–1977. https://doi.org/10.1056/NEJMoa033277

Ali, Y. O., Allen, H. M., Yu, L., Li-Kroeger, D., Bakhshizadehmahmoudi, D., Hatcher, A., … Lu, H. C. (2016). NMNAT2:HSP90 Complex Mediates Proteostasis in Proteinopathies. *PLoS Biology*, *14*(6). https://doi.org/10.1371/journal.pbio.1002472

Alves, G., Forsaa, E. B., Pedersen, K. F., Dreetz Gjerstad, M., & Larsen, J. P. (2008). Epidemiology of Parkinson's disease. In *Journal of Neurology* (Vol. 255, pp. 18–32). https://doi.org/10.1007/s00415-008-5004-3

Anglade, P. (1997). Apoptosis and autophagy in nigral neurons of patients with Parkinson's disease. *Histology and Histopathology*, *12*(1), 25–31.

Arensdorf, A. M., McCabe, D. D., Kaufman, R. J., & Thomas Rutkowski, D. (2013). Temporal clustering of gene expression links the metabolic transcription factor HNF4?? to the ER stress-dependent gene regulatory network. *Frontiers in Genetics*, *4*(SEP). https://doi.org/10.3389/fgene.2013.00188

Auluck, P. K., Caraveo, G., & Lindquist, S. (2010). α-Synuclein: Membrane Interactions and Toxicity in Parkinson's Disease. *Annu. Rev. Cell Dev. Biol*, *26*, 211–33. https://doi.org/10.1146/annurev.cellbio.042308.113313

Awad, O., Sarkar, C., Panicker, L. M., Miller, D., Zeng, X., Sgambato, J. A., … Feldman, R. A. (2015). Altered TFEB-mediated lysosomal biogenesis in Gaucher disease iPSC-derived neuronal cells. *Human Molecular Genetics*, *24*(20), 5775–5788. https://doi.org/10.1093/hmg/ddv297

B'Chir, W., Maurin, A. C., Carraro, V., Averous, J., Jousse, C., Muranishi, Y., … Bruhat, A. (2013). The eIF2α/ATF4 pathway is essential for stress-induced autophagy gene expression. *Nucleic Acids Research*, *41*(16), 7683–7699. https://doi.org/10.1093/nar/gkt563

Bai, P., Cantó, C., Oudart, H., Brunyánszki, A., Cen, Y., Thomas, C., … Auwerx, J. (2011). PARP-1 inhibition increases mitochondrial metabolism through SIRT1 activation. *Cell Metabolism*, *13*(4), 461–468. https://doi.org/10.1016/j.cmet.2011.03.004

Baixauli, F., Acín-Pérez, R., Villarroya-Beltrí, C., Mazzeo, C., Nuñez-Andrade, N., Gabandé-Rodriguez, E., … Mittelbrunn, M. (2015). Mitochondrial respiration controls lysosomal function during inflammatory t cell responses. *Cell Metabolism*, *22*(3), 485–498. https://doi.org/10.1016/j.cmet.2015.07.020

Ballard, P. A., Tetrud, J. W., & Langston, J. W. (1985). Permanent human parkinsonism due to 1-methyl-4-phenyl-1,2,3,6-tetrahydropyridine (MPTP): seven cases. *Neurology*, *35*(7), 949–956. https://doi.org/10.1212/WNL.35.7.949

Barbosa, M. T. P., Soares, S. M., Novak, C. M., Sinclair, D., Levine, J. a, Aksoy, P., & Chini, E. N. (2007). The enzyme CD38 (a NAD glycohydrolase, EC 3.2.2.5) is necessary for the development of diet-induced obesity. *The FASEB Journal : Official Publication of the Federation of American Societies for Experimental Biology*, *21*(13), 3629–3639. https://doi.org/10.1096/fj.07-8290com

Bender, A., Schwarzkopf, R. M., McMillan, A., Krishnan, K. J., Rieder, G., Neumann, M., … Klopstock, T. (2008). Dopaminergic midbrain neurons are the prime target for

mitochondrial DNA deletions. *Journal of Neurology*, *255*(8), 1231–1235. https://doi.org/10.1007/s00415-008-0892-9

Bergeron, R., Ren, J. M., Cadman, K. S., Moore, I. K., Perret, P., Pypaert, M., … Shulman, G. I. (2001). Chronic activation of AMP kinase results in NRF-1 activation and mitochondrial biogenesis. *American Journal of Physiology. Endocrinology and Metabolism*, *281*(6), E1340-6. https://doi.org/10.1016/j.bbabio.2012.02.033

Betarbet, R., Sherer, T. B., & Greenamyre, J. T. (2002). Animal models of Parkinson's disease. *BioEssays : News and Reviews in Molecular, Cellular and Developmental Biology*, *24*(4), 308–18. https://doi.org/10.1002/bies.10067

Beutler, E., Gelbart, T., Kuhl, W., Zimran, A., & West, C. (1992). Mutations in Jewish patients with Gaucher disease. *Blood*, *79*, 1662–1666.

Bibikova, M., Golic, M., Golic, K. G., & Carroll, D. (2002). Targeted chromosomal cleavage and mutagenesis in Drosophila using zinc-finger nucleases. *Genetics*, *161*(3), 1169–1175.

Birner, R., Bürgermeister, M., Schneiter, R., & Daum, G. (2001). Roles of phosphatidylethanolamine and of its several biosynthetic pathways in Saccharomyces cerevisiae. *Mol. Biol. Cell*, *12*(4), 997–1007. https://doi.org/10.1371/journal.pone.0077380

Biskup, S., Moore, D. J., Celsi, F., Higashi, S., West, A. B., Andrabi, S. A., … Dawson, V. L. (2006). Localization of LRRK2 to membranous and vesicular structures in mammalian brain. *Annals of Neurology*, *60*(5), 557–569. https://doi.org/10.1002/ana.21019

Bouman, L., Schlierf, a, Lutz, a K., Shan, J., Deinlein, a, Kast, J., … Winklhofer, K. F. (2011). Parkin is transcriptionally regulated by ATF4: evidence for an interconnection between mitochondrial stress and ER stress. *Cell Death and Differentiation*, *18*(5), 769–782. https://doi.org/10.1038/cdd.2010.142

Bourdenx, M., Bezard, E., & Dehay, B. (2014). Lysosomes and α-synuclein form a dangerous duet leading to neuronal cell death. *Frontiers in Neuroanatomy*, *8*(August), 83. https://doi.org/10.3389/fnana.2014.00083

Braak, H., Del Tredici, K., Rüb, U., De Vos, R. A. I., Jansen Steur, E. N. H., & Braak, E. (2003). Staging of brain pathology related to sporadic Parkinson's disease. *Neurobiology of Aging*, *24*(2), 197–211. https://doi.org/10.1016/S0197-4580(02)00065-9

Braunstein, H., Maor, G., Chicco, G., Filocamo, M., Zimran, A., & Horowitz, M. (2016). UPR activation and CHOP mediated induction of GBA1 transcription in Gaucher disease. *Blood Cells, Molecules, and Diseases*. https://doi.org/10.1016/j.bcmd.2016.10.025

Brockmann, K., & Berg, D. (2014). The significance of GBA for Parkinson's disease. *Journal of Inherited Metabolic Disease*, *37*, 643–648. https://doi.org/10.1007/s10545-014-9714-7

Brug, M. van der. (2015). Parkinson's disease: From human genetics to clinical trials. *Science Translational …*, *8*(305). Retrieved from http://stm.sciencemag.org/content/7/305/305ps20.abstract

Brunk, U. T., & Terman, A. (2002). The mitochondrial-lysosomal axis theory of aging. *European Journal of Biochemistry*, *269*(8), 1996–2002. https://doi.org/10.1046/j.1432-1033.2002.02869.x

Burré, J., Sharma, M., Tsetsenis, T., Buchman, V., Etherton, M. R., & Südhof, T. C. (2010). Alpha-synuclein promotes SNARE-complex assembly in vivo and in vitro. *Science (New York, N.Y.)*, *329*(5999), 1663–7. https://doi.org/10.1126/science.1195227

Caito, S. W., & Aschner, M. (2016). NAD + supplementation attenuates methylmercury dopaminergic and mitochondrial toxicity in Caenorhabditis elegans, (718).

Calegari, V. C., Zoppi, C. C., Rezende, L. F., Silveira, L. R., Carneiro, E. M., & Boschero, A. C. (2011). Endurance training activates AMP-activated protein kinase, increases expression of uncoupling protein 2 and reduces insulin secretion from rat pancreatic islets. *The Journal of Endocrinology*, *208*(3), 257–264. https://doi.org/10.1530/JOE-10-0450

Canela, L., Fernández-Dueñas, V., Albergaria, C., Watanabe, M., Lluís, C., Mallol, J., …

Ciruela, F. (2009). The association of metabotropic glutamate receptor type 5 with the neuronal Ca2+-binding protein 2 modulates receptor function. *Journal of Neurochemistry*, *111*(2), 555–567. https://doi.org/10.1111/j.1471-4159.2009.06348.x

Canela, L., Lujan, R., Lluis, C., Burgueno, J., Mallol, J., Canela, E. I., … Ciruela, F. (2007). The neuronal Ca(2+)-binding protein 2 (NECAB2) interacts with the adenosine A(2A) receptor and modulates the cell surface expression and function of the receptor. *Molecular and Cellular Neurosciences*, *36*(1), 1–12. https://doi.org/10.1016/j.mcn.2007.05.007

Cantó, C., Gerhart-Hines, Z., Feige, J. N., Lagouge, M., Noriega, L., Milne, J. C., … Auwerx, J. (2009). AMPK regulates energy expenditure by modulating NAD+ metabolism and SIRT1 activity. *Nature*, *458*(7241), 1056–1060. https://doi.org/10.1038/nature07813

Cantó, C., Houtkooper, R. H., Pirinen, E., Youn, D. Y., Oosterveer, M. H., Cen, Y., … Auwerx, J. (2012). The NAD+ Precursor Nicotinamide Riboside Enhances Oxidative Metabolism and Protects against High-Fat Diet-Induced Obesity. *Cell Metabolism*, *15*(6), 838–847. https://doi.org/10.1016/j.cmet.2012.04.022

Cermak, T., Doyle, E. L., Christian, M., Wang, L., Zhang, Y., Schmidt, C., … Voytas, D. F. (2011). Efficient design and assembly of custom TALEN and other TAL effector-based constructs for DNA targeting. *Nucleic Acids Research*, *39*(12), e82. https://doi.org/10.1093/nar/gkr218

Cerutti, R., Pirinen, E., Lamperti, C., Marchet, S., Sauve, A. a., Li, W., … Zeviani, M. (2014). NAD+-dependent activation of Sirt1 corrects the phenotype in a mouse model of mitochondrial disease. *Cell Metabolism*, *19*(6), 1042–1049. https://doi.org/10.1016/j.cmet.2014.04.001

Chambers, S. M., Fasano, C. a, Papapetrou, E. P., Tomishima, M., Sadelain, M., & Studer, L. (2009). Highly efficient neural conversion of human ES and iPS cells by dual inhibition of SMAD signaling. *Nature Biotechnology*, *27*(3), 275–80. https://doi.org/10.1038/nbt.1529

Chambon, P. Weill, JD. Mandel, P. (1963) . Nicotinamide mononucleotide activation of new DNA-dependent polyadenylic acid synthsizing nuclear enzyme. *Biochem Biophys Res Commun, 2(*11*), 39-43*

Chang, H. C., & Guarente, L. (2013). XSIRT1 mediates central circadian control in the SCN by a mechanism that decays with aging. *Cell*, *153*(7). https://doi.org/10.1016/j.cell.2013.05.027

Chen, H., & Chan, D. C. (2009). Mitochondrial dynamics-fusion, fission, movement, and mitophagy-in neurodegenerative diseases. *Human Molecular Genetics*, *18*(R2), 169–176. https://doi.org/10.1093/hmg/ddp326

Chen, H., McCaffery, J. M., & Chan, D. C. (2007). Mitochondrial Fusion Protects against Neurodegeneration in the Cerebellum. *Cell*, *130*(3), 548–562. https://doi.org/10.1016/j.cell.2007.06.026

Chen, J. J., & Marsh, L. (2014). Anxiety in Parkinson's disease: identification and management. *Therapeutic Advances in Neurological Disorders*, *7*(1), 52–59. https://doi.org/10.1177/1756285613495723

Cherra, S. J., & Chu, C. T. (2008). Autophagy in neuroprotection and neurodegeneration: A question of balance. *Future Neurol*, *3*(3), 309–323. https://doi.org/10.2217/14796708.3.3.309

Clark, I. E., Dodson, M. W., Jiang, C., Cao, J. H., Huh, J. R., Seol, J. H., … Guo, M. (2006). Drosophila pink1 is required for mitochondrial function and interacts genetically with parkin. *Nature*, *441*(7097), 1162–1166. https://doi.org/10.1038/nature04779

Cleeter, M. W. J., Chau, K. Y., Gluck, C., Mehta, A., Hughes, D. a., Duchen, M., … Schapira, A. H. (2013). Glucocerebrosidase inhibition causes mitochondrial dysfunction and free radical damage. *Neurochemistry International*, *62*(1), 1–7. https://doi.org/10.1016/j.neuint.2012.10.010

Cogliati, S., Frezza, C., Soriano, M. E., Varanita, T., Quintana-Cabrera, R., Corrado, M., … Scorrano, L. (2013). Mitochondrial cristae shape determines respiratory chain supercomplexes assembly and respiratory efficiency. *Cell*, *155*(1), 160–171. https://doi.org/10.1016/j.cell.2013.08.032

Conze, D. B., Crespo-Barreto, J., & Kruger, C. L. (2016). Safety assessment of nicotinamide riboside, a form of vitamin B3. *Human & Experimental Toxicology*. https://doi.org/10.1177/0960327115626254

Corti, O., & Brice, A. (2007). Of Parkin and Parkinson's: light and dark sides of a multifaceted E3 ubiquitin-protein ligase. *Drug Discovery Today: Disease Mechanisms*. https://doi.org/10.1016/j.ddmec.2007.11.002

Corti, O., Lesage, S., & Brice, a. (2011). What Genetics Tells us About the Causes and Mechanisms of Parkinson's Disease. *Physiological Reviews*, *91*(4), 1161–1218. https://doi.org/10.1152/physrev.00022.2010

Cullen, V., Sardi, S. P., Ng, J., Xu, Y. H., Sun, Y., Tomlinson, J. J., … Schlossmacher, M. G. (2011). Acid ??-glucosidase mutants linked to gaucher disease, parkinson disease, and lewy body dementia alter ??-synuclein processing. *Annals of Neurology*, *69*(6), 940–953. https://doi.org/10.1002/ana.22400

Cummins, J. M. (2000). Fertilization and elimination of the paternal mitochondrial genome. *Human Reproduction (Oxford, England)*, *15 Suppl 2*, 92–101. https://doi.org/10.1093/humrep/15.suppl_2.92

Danzer, K. M., Kranich, L. R., Ruf, W. P., Cagsal-Getkin, O., Winslow, A. R., Zhu, L., … McLean, P. J. (2012). Exosomal cell-to-cell transmission of alpha synuclein oligomers. *Molecular Neurodegeneration*, *7*(1), 42. https://doi.org/10.1186/1750-1326-7-42

Dauer, W., & Przedborski, S. (2003). Parkinson's Disease. *Neuron*, *39*(6), 889–909. https://doi.org/10.1016/S0896-6273(03)00568-3

De Flora, A., Zocchi, E., Guida, L., Franco, L., & Bruzzone, S. (2004). Autocrine and paracrine calcium signaling by the CD38/NAD+/cyclic ADP-ribose system. *Ann N Y Acad Sci*, *1028*, 176–191. https://doi.org/1028/1/176 [pii]\r10.1196/annals.1322.021

de la Mata, M., Cotán, D., Oropesa-Ávila, M., Garrido-Maraver, J., Cordero, M. D., Villanueva Paz, M., … Sánchez-Alcázar, J. a. (2015). Pharmacological Chaperones and Coenzyme Q10 Treatment Improves Mutant β-Glucocerebrosidase Activity and Mitochondrial Function in Neuronopathic Forms of Gaucher Disease. *Scientific Reports*, *5*(April), 10903. https://doi.org/10.1038/srep10903

De Stefani, D., Raffaello, A., Teardo, E., Szabò, I., & Rizzuto, R. (2011). A forty-kilodalton protein of the inner membrane is the mitochondrial calcium uniporter. *Nature*, *476*(7360), 336–40. https://doi.org/10.1038/nature10230

Decressac, M., Mattsson, B., Weikop, P., Lundblad, M., Jakobsson, J., & Björklund, A. (2013). TFEB-mediated autophagy rescues midbrain dopamine neurons from α-synuclein toxicity. *Proceedings of the National Academy of Sciences of the United States of America*, *110*(19), E1817-26. https://doi.org/10.1073/pnas.1305623110

Devine, M. J., Ryten, M., Vodicka, P., Thomson, A. J., Burdon, T., Houlden, H., … Kunath, T. (2011). Parkinson's disease induced pluripotent stem cells with triplication of the α-synuclein locus. *Nature Communications*, *2*, 440. https://doi.org/10.1038/ncomms1453

Doyon, J. B., Zeitler, B., Cheng, J., Cheng, A. T., Cherone, J. M., Santiago, Y., … Drubin, D. G. (2011). Rapid and efficient clathrin-mediated endocytosis revealed in genome-edited mammalian cells. *Nature Cell Biology*, *13*(3), 331–337. https://doi.org/10.1038/ncb2175

Drescher, M., Van Rooijen, B. D., Veldhuis, G., Subramaniam, V., & Huber, M. (2010). A stable lipid-induced aggregate of ??-synuclein. *Journal of the American Chemical Society*, *132*(12), 4080–4082. https://doi.org/10.1021/ja909247j

Duplan, E., Giaime, E., Viotti, J., Sévalle, J., Corti, O., Brice, A., … Alves da Costa, C. (2013).

ER-stress-associated functional link between Parkin and DJ-1 via a transcriptional cascade involving the tumor suppressor p53 and the spliced X-box binding protein XBP-1. *J Cell Sci.*, *126*(Pt 9), 2124–33. https://doi.org/10.1242/jcs.127340

Enquist, I. B., Lo Bianco, C., Ooka, A., Nilsson, E., Månsson, J.-E., Ehinger, M., … Karlsson, S. (2007). Murine models of acute neuronopathic Gaucher disease. *Proceedings of the National Academy of Sciences of the United States of America*, *104*(44), 17483–8. https://doi.org/10.1073/pnas.0708086104

Fang, E. F., Scheibye-Knudsen, M., Brace, L. E., Kassahun, H., Sengupta, T., Nilsen, H., … Bohr, V. A. (2014). Defective mitophagy in XPA via PARP-1 hyperactivation and NAD +/SIRT1 reduction. *Cell*, *157*(4), 882–896. https://doi.org/10.1016/j.cell.2014.03.026

Feany, M. B., & Bender, W. W. (2000). A Drosophila model of Parkinson's disease. *Nature*, *404*(6776), 394–8. https://doi.org/10.1038/35006074

Fernandes, H. J. R., Hartfield, E. M., Christian, H. C., Emmanoulidou, E., Zheng, Y., Booth, H., … Wade-Martins, R. (2016a). ER Stress and Autophagic Perturbations Lead to Elevated Extracellular α-Synuclein in GBA-N370S Parkinson's iPSC-Derived Dopamine Neurons, (February). https://doi.org/10.1016/j.stemcr.2016.01.013

Fernandes, H. J. R., Hartfield, E. M., Christian, H. C., Emmanoulidou, E., Zheng, Y., Booth, H., … Wade-Martins, R. (2016b). ER Stress and Autophagic Perturbations Lead to Elevated Extracellular α-Synuclein in GBA-N370S Parkinson's iPSC-Derived Dopamine Neurons. *Stem Cell Reports*, *6*(3), 342–356. https://doi.org/10.1016/j.stemcr.2016.01.013

Fiorentino, T. V, Procopio, T., Mancuso, E., Arcidiacono, G. P., Andreozzi, F., Arturi, F., … Sesti, G. (2015). SRT1720 counteracts glucosamine-induced endoplasmic reticulum stress and endothelial dysfunction. *Cardiovasc Res*, *107*(2), 295–306. https://doi.org/10.1093/cvr/cvv169

Friling, S., Andersson, E., Thompson, L. H., Jönsson, M. E., Hebsgaard, J. B., Nanou, E., … Ericson, J. (2009). Efficient production of mesencephalic dopamine neurons by Lmx1a expression in embryonic stem cells. *Proceedings of the National Academy of Sciences of the United States of America*, *106*(18), 7613–8. https://doi.org/10.1073/pnas.0902396106

Fuchs, J., Nilsson, C., Kachergus, J., Munz, M., Larsson, E. M., Sch??le, B., … Farrer, M. J. (2007). Phenotypic variation in a large Swedish pedigree due to SNCA duplication and triplication. *Neurology*, *68*(12), 916–922. https://doi.org/10.1212/01.wnl.0000254458.17630.c5

Fuchs, J., Tichopad, A., Golub, Y., Munz, M., Schweitzer, K. J., Wolf, B., … Gasser, T. (2008). Genetic variability in the SNCA gene influences alpha-synuclein levels in the blood and brain. *The FASEB Journal*, *22*(5), 1327–34. https://doi.org/10.1096/fj.07-9348com

Galluzzi, L., Pietrocola, F., Levine, B., & Kroemer, G. (2014). Metabolic Control of Autophagy. *Cell*, *159*(6), 1263–1276. https://doi.org/10.1016/j.cell.2014.11.006

Gariani, K., Menzies, K. J., Ryu, D., Wegner, C. J., Wang, X., Ropelle, E. R., … Auwerx, J. (2015). Eliciting the mitochondrial unfolded protein response via NAD + repletion reverses fatty liver disease. *Hepatology*, 1–13. https://doi.org/10.1002/hep.28245

Garlid, K. D., Jabůrek, M., Ježek, P., & Vařecha, M. (2000). How do uncoupling proteins uncouple? *Biochimica et Biophysica Acta - Bioenergetics*, *1459*(2–3), 383–389. https://doi.org/10.1016/S0005-2728(00)00175-4

Geisler, S., Holmstr??m, K. M., Treis, A., Skujat, D., Weber, S. S., Fiesel, F. C., … Springer, W. (2010). The PINK1/Parkin-mediated mitophagy is compromised by PD-associated mutations. *Autophagy*, *6*(7), 871–878. https://doi.org/10.4161/auto.6.7.13286

Gilks, W. P., Abou-Sleiman, P. M., Gandhi, S., Jain, S., Singleton, A., Lees, A. J., … Wood, N. W. (2005). A common LRRK2 mutation in idiopathic Parkinson's disease. *Lancet*, *365*(9457), 415–416. https://doi.org/10.1016/S0140-6736(05)17830-1

Giorgi, C., Romagnoli, A., Pinton, P., & Rizzuto, R. (2008). Ca2+ signaling, mitochondria and cell death. *Current Molecular Medicine*, *8*(2), 119–130. https://doi.org/10.2174/156652408783769571

Goker-Alpan, O., Stubblefield, B. K., Giasson, B. I., & Sidransky, E. (2010). Glucocerebrosidase is present in ??-synuclein inclusions in Lewy body disorders. *Acta Neuropathologica*, *120*(5), 641–649. https://doi.org/10.1007/s00401-010-0741-7

Goldman, S. M. (2014). Environmental toxins and Parkinson's disease. *Annu Rev Pharmacol Toxicol*, *54*, 141–164. https://doi.org/10.1146/annurev-pharmtox-011613-135937

Gomes, A. P., Price, N. L., Ling, A. J. Y., Moslehi, J. J., Montgomery, M. K., Rajman, L., … Sinclair, D. A. (2013). Declining NAD+ induces a pseudohypoxic state disrupting nuclear-mitochondrial communication during aging. *Cell*, *155*(7), 1624–1638. https://doi.org/10.1016/j.cell.2013.11.037

Gong, B., Pan, Y., Vempati, P., Zhao, W., Knable, L., Ho, L., … Pasinetti, G. M. (2013). Nicotinamide riboside restores cognition through an upregulation of proliferator-activated receptor-γ coactivator 1α regulated β-secretase 1 degradation and mitochondrial gene expression in Alzheimer's mouse models. *Neurobiology of Aging*, *34*(6), 1581–1588. https://doi.org/10.1016/j.neurobiolaging.2012.12.005

González, F., Zhu, Z., Shi, Z.-D., Lelli, K., Verma, N., Li, Q. V, & Huangfu, D. (2014). An iCRISPR Platform for Rapid, Multiplexable, and Inducible Genome Editing in Human Pluripotent Stem Cells. *Cell Stem Cell*, 1–12. https://doi.org/10.1016/j.stem.2014.05.018

Greene, A. W., Grenier, K., Aguileta, M. a, Muise, S., Farazifard, R., Haque, M. E., … Fon, E. a. (2012). Mitochondrial processing peptidase regulates PINK1 processing, import and Parkin recruitment. *EMBO Reports*, *13*(4), 378–385. https://doi.org/10.1038/embor.2012.14

Greggio, E., & Cookson, M. R. (2009). Leucine-rich repeat kinase 2 mutations and Parkinson's disease: three questions. *ASN Neuro*, *1*(1), 13–24. https://doi.org/10.1042/AN20090007

Gunaseeli, I., Doss, M. X., Antzelevitch, C., Hescheler, J., & Sachinidis, a. (2010). Induced pluripotent stem cells as a model for accelerated patient- and disease-specific drug discovery. *Current Medicinal Chemistry*, *17*(8), 759–766. https://doi.org/10.2174/092986710790514480

Hamanaka, R. B., & Chandel, N. S. (2010). Mitochondrial reactive oxygen species regulate cellular signaling and dictate biological outcomes. *Trends in Biochemical Sciences*. https://doi.org/10.1016/j.tibs.2010.04.002

Hardie, D. G., Ross, F. a, & Hawley, S. a. (2012). AMPK: a nutrient and energy sensor that maintains energy homeostasis. *Nature Reviews. Molecular Cell Biology*, *13*(4), 251–62. https://doi.org/10.1038/nrm3311

Hardy, J., Lewis, P., Revesz, T., Lees, A., & Paisan-Ruiz, C. (2009). The genetics of Parkinson's syndromes: a critical review. *Current Opinion in Genetics and Development*. https://doi.org/10.1016/j.gde.2009.03.008

Hariharan, N., Maejima, Y., Nakae, J., Paik, J., Depinho, R. A., & Sadoshima, J. (2010). Deacetylation of FoxO by Sirt1 plays an essential role in mediating starvation-induced autophagy in cardiac myocytes. *Circulation Research*, *107*(12), 1470–1482. https://doi.org/10.1161/CIRCRESAHA.110.227371

Harris, N. C., Webb, C., & Greenfield, S. A. (1989). A possible pacemaker mechanism in pars compacta neurons of the guinea-pig substantia nigra revealed by various ion channel blocking agents. *Neuroscience*, *31*(2), 355–362. https://doi.org/10.1016/0306-4522(89)90379-5

Harvald, E. B., Olsen, A. S. B., & Færgeman, N. J. (2015). Autophagy in the light of sphingolipid metabolism. *Apoptosis*. https://doi.org/10.1007/s10495-015-1108-2

Hauser, R. A., Lyons, K. E., & McClain, T. A. (2012). Parkinson Disease. *Medscape*

Reference, 650–656. https://doi.org/10.1097/SMJ.0b013e318273a60d
Hawkes, C. H., Del Tredici, K., & Braak, H. (2007). Parkinson's disease: A dual-hit hypothesis. *Neuropathology and Applied Neurobiology*. https://doi.org/10.1111/j.1365-2990.2007.00874.x
Hawley, S. A., Pan, D. A., Mustard, K. J., Ross, L., Bain, J., Edelman, A. M., … Hardie, D. G. (2005). Calmodulin-dependent protein kinase kinase-beta is an alternative upstream kinase for AMP-activated protein kinase. *Cell Metabolism*, *2*(1), 9–19. https://doi.org/10.1016/j.cmet.2005.05.009
Hayashi, A., Kasahara, T., Iwamoto, K., Ishiwata, M., Kametani, M., Kakiuchi, C., … Kato, T. (2007). The role of Brain-derived Neurotrophic Factor (BDNF)-induced XBP1 splicing during brain development. *Journal of Biological Chemistry*, *282*(47), 34525–34534. https://doi.org/10.1074/jbc.M704300200
Healy, D. G., Falchi, M., O'Sullivan, S. S., Bonifati, V., Durr, A., Bressman, S., … Wood, N. W. (2008). Phenotype, genotype, and worldwide genetic penetrance of LRRK2-associated Parkinson's disease: a case-control study. *The Lancet Neurology*, *7*(7), 583–590. https://doi.org/10.1016/S1474-4422(08)70117-0
Hein, L. K., Duplock, S., Hopwood, J. J., & Fuller, M. (2008). Lipid composition of microdomains is altered in a cell model of Gaucher disease. *Journal of Lipid Research*, *49*(8), 1725–1734. https://doi.org/10.1194/jlr.M800092-JLR200
Hernán, M. A., Takkouche, B., Caamaño-Isorna, F., & Gestal-Otero, J. J. (2002). A meta-analysis of coffee drinking, cigarette smoking, and the risk of Parkinson's disease. *Annals of Neurology*, *52*(3), 276–284. https://doi.org/10.1002/ana.10277
Higo, T., Hamada, K., Hisatsune, C., Nukina, N., Hashikawa, T., Hattori, M., … Mikoshiba, K. (2010). Mechanism of ER Stress-Induced Brain Damage by IP3 Receptor. *Neuron*, *68*(5), 865–878. https://doi.org/10.1016/j.neuron.2010.11.010
Hill, B. G., Dranka, B. P., Zou, L., Chatham, J. C., & Darley-Usmar, V. M. (2009). Importance of the bioenergetic reserve capacity in response to cardiomyocyte stress induced by 4-hydroxynonenal. *The Biochemical Journal*, *424*(1), 99–107. https://doi.org/10.1042/BJ20090934
Hindle, J. V. (2010). Ageing, neurodegeneration and Parkinson's disease. *Age and Ageing*, *39*(2), 156–161. https://doi.org/10.1093/ageing/afp223
Hockemeyer, D., Soldner, F., Beard, C., Gao, Q., Mitalipova, M., DeKelver, R. C., … Jaenisch, R. (2009). Efficient targeting of expressed and silent genes in human ESCs and iPSCs using zinc-finger nucleases. *Nature Biotechnology*, *27*(9), 851–7. https://doi.org/10.1038/nbt.1562
Holt, I. J., Harding, A. E., & Morgan-Hughes, J. A. (1988). Deletions of muscle mitochondrial DNA in patients with mitochondrial myopathies. *Nature*, *331*(6158), 717–719. https://doi.org/10.1038/331717a0
Hristova, V. A., Beasley, S. A., Rylett, R. J., & Shaw, G. S. (2009). Identification of a novel Zn2+ -binding domain in the autosomal recessive juvenile Parkinson-related E3 ligase parkin. *Journal of Biological Chemistry*, *284*(22), 14978–14986. https://doi.org/10.1074/jbc.M808700200
Hung, Y. P., Albeck, J. G., Tantama, M., & Yellen, G. (2011). Imaging Cytosolic NADH-NAD+ Redox State with a Genetically Encoded Fluorescent Biosensor. *Cell Metabolism*, *14*(4), 545–554. https://doi.org/10.1016/j.cmet.2011.08.012
Hwang, W. Y., Fu, Y., Reyon, D., Maeder, M. L., Tsai, S. Q., Sander, J. D., … Joung, J. K. (2013). Efficient genome editing in zebrafish using a CRISPR-Cas system. *Nat Biotechnol*, *31*(3), 227–229. https://doi.org/10.1038/nbt.2501
Ibáñez, P., Lesage, S., Janin, S., Lohmann, E., Durif, F., Destée, A., … Brice, A. (2009). Alpha-synuclein gene rearrangements in dominantly inherited parkinsonism: frequency,

phenotype, and mechanisms. *Archives of Neurology*, *66*(1), 102–8. https://doi.org/10.1001/archneurol.2008.555
Imai, S., Armstrong, C. M., Kaeberlein, M., & Guarente, L. (2000). Transcriptional silencing and longevity protein Sir2 is an NAD-dependent histone deacetylase. *Nature*, *403*(6771), 795–800. https://doi.org/10.1038/35001622
Imai, S. I., & Guarente, L. (2014). NAD+ and sirtuins in aging and disease. *Trends in Cell Biology*, *24*(8), 464–471. https://doi.org/10.1016/j.tcb.2014.04.002
James Surmeier, D., Guzman, J. N., Sanchez, J., & Schumacker, P. T. (2012). Physiological phenotype and vulnerability in Parkinson's disease. *Cold Spring Harbor Perspectives in Medicine*. https://doi.org/10.1101/cshperspect.a009290
Jang, H., Boltz, D. A., Webster, R. G., & Smeyne, R. J. (2009). Viral parkinsonism. *Biochimica et Biophysica Acta - Molecular Basis of Disease*. https://doi.org/10.1016/j.bbadis.2008.08.001
Jang, S. Y., Kang, H. T., & Hwang, E. S. (2012). Nicotinamide-induced mitophagy: Event mediated by high NAD+/NADH ratio and SIRT1 protein activation. *Journal of Biological Chemistry*, *287*(23), 19304–19314. https://doi.org/10.1074/jbc.M112.363747
Jiang, H., Ren, Y., Yuen, E. Y., Zhong, P., Ghaedi, M., Hu, Z., … Feng, J. (2012). Parkin controls dopamine utilization in human midbrain dopaminergic neurons derived from induced pluripotent stem cells. *Nature Communications*, *3*, 668. https://doi.org/10.1038/ncomms1669
Jinek, M., Chylinski, K., Fonfara, I., Hauer, M., Doudna, J. A., & Charpentier, E. (2012). A programmable dual-RNA-guided DNA endonuclease in adaptive bacterial immunity. *Science (New York, N.Y.)*, *337*(6096), 816–21. https://doi.org/10.1126/science.1225829
Jinek, M., East, A., Cheng, A., Lin, S., Ma, E., & Doudna, J. (2013). RNA-programmed genome editing in human cells. *eLife*, *2013*(2). https://doi.org/10.7554/eLife.00471
Kahle, P. J., Neumann, M., Ozmen, L., Muller, V., Jacobsen, H., Schindzielorz, a, … Haass, C. (2000). Subcellular localization of wild-type and Parkinson's disease-associated mutant alpha -synuclein in human and transgenic mouse brain. *The Journal of Neuroscience : The Official Journal of the Society for Neuroscience*, *20*(17), 6365–6373. https://doi.org/20/17/6365 [pii]
Kamp, F., & Beyer, K. (2006). Binding of ??-synuclein affects the lipid packing in bilayers of small vesicles. *Journal of Biological Chemistry*, *281*(14), 9251–9259. https://doi.org/10.1074/jbc.M512292200
Kang, H. T., & Hwang, E. S. (2009). Nicotinamide enhances mitochondria quality through autophagy activation in human cells. *Aging Cell*, *8*(4), 426–438. https://doi.org/10.1111/j.1474-9726.2009.00487.x
Karamanlidis, G., Lee, C. F., Garcia-Menendez, L., Kolwicz, S. C., Suthammarak, W., Gong, G., … Tian, R. (2013). Mitochondrial complex i deficiency increases protein acetylation and accelerates heart failure. *Cell Metabolism*, *18*(2), 239–250. https://doi.org/10.1016/j.cmet.2013.07.002
Keatinge, M., Bui, H., Menke, A., Chen, Y., Sokol, A. M., Bai, Q., … Unit, G. (2015). *Glucocerebrosidase 1 deficient Danio rerio mirror key pathological aspects of human Gaucher disease and provide evidence of early microglial activation preceding alpha-synuclein-independent neuronal cell death*.
Khan, N. a., Auranen, M., Paetau, I., Pirinen, E., Euro, L., Forsström, S., … Suomalainen, A. (2014). Effective treatment of mitochondrial myopathy by nicotinamide riboside, a vitamin B3. *EMBO Molecular Medicine*, *6*(6), 721–731. https://doi.org/10.1002/emmm.201403943
Kilpatrick, B. S., Magalhaes, J., Beavan, M. S., McNeill, A., Gegg, M. E., Cleeter, M. W. J., … Patel, S. (2016). Endoplasmic reticulum and lysosomal Ca2+ stores are remodelled in

GBA1-linked Parkinson disease patient fibroblasts. *Cell Calcium*, *59*(1), 12–20. https://doi.org/10.1016/j.ceca.2015.11.002
Kim, I., Rodriguez-Enriquez, S., & Lemasters, J. J. (2007). Selective degradation of mitochondria by mitophagy. *Archives of Biochemistry and Biophysics*. https://doi.org/10.1016/j.abb.2007.03.034
Kim, J., Kundu, M., Viollet, B., & Guan, K.-L. (2011). AMPK and mTOR regulate autophagy through direct phosphorylation of Ulk1. *Nature Cell Biology*, *13*(2), 132–41. https://doi.org/10.1038/ncb2152
Kim, Y. G., Cha, J., & Chandrasegaran, S. (1996). Hybrid restriction enzymes: zinc finger fusions to Fok I cleavage domain. *Proc Natl Acad Sci U S A*, *93*(3), 1156–1160. https://doi.org/10.1073/pnas.93.3.1156
Kirby, D. M., Crawford, M., Cleary, M. A., Dahl, H. H., Dennett, X., & Thorburn, D. R. (1999). Respiratory chain complex I deficiency: an underdiagnosed energy generation disorder. *Neurology*, *52*(6), 1255–64. https://doi.org/10.1212/WNL.52.6.1255
Kirkwood, T. B. L. (2003). The most pressing problem of our age. *BMJ : British Medical Journal*, *326*, 1297–1299. https://doi.org/10.1136/bmj.326.7402.1297
Kish, S. J., Shannak, K., & Hornykiewicz O. (1988). Uneven patterns of dopamine loss in the striatum of patients with idiopathic Parkinson's disease. *New England Journal of Medicine*, *318*, 876–880.
Kitsis, R. N., & Molkentin, J. D. (2010). Apoptotic cell death "Nixed" by an ER-mitochondrial necrotic pathway. *Proceedings of the National Academy of Sciences of the United States of America*, *107*(20), 9031–9032. https://doi.org/10.1073/pnas.1003827107
Koga, H., Kaushik, S., & Cuervo, A. M. (2010). Altered lipid content inhibits autophagic vesicular fusion. *FASEB Journal : Official Publication of the Federation of American Societies for Experimental Biology*, *24*(8), 3052–65. https://doi.org/10.1096/fj.09-144519
Körschen, H. G., Yildiz, Y., Raju, D. N., Schonauer, S., Bönigk, W., Jansen, V., … Wachten, D. (2013). The non-lysosomal β-glucosidase GBA2 is a non-integral membrane-associated protein at the endoplasmic reticulum (ER) and Golgi. *Journal of Biological Chemistry*, *288*(5), 3381–3393. https://doi.org/10.1074/jbc.M112.414714
Kra??un, I., R??sner, H., ??osovi??, C., & Stavljeni??, A. (1984). Topographical Atlas of the Gangliosides of the Adult Human Brain. *Journal of Neurochemistry*, *43*(4), 979–989. https://doi.org/10.1111/j.1471-4159.1984.tb12833.x
Kriks, S., Shim, J.-W., Piao, J., Ganat, Y. M., Wakeman, D. R., Xie, Z., … Studer, L. (2011). Dopamine neurons derived from human ES cells efficiently engraft in animal models of Parkinson's disease. *Nature*, *480*(7378), 547–51. https://doi.org/10.1038/nature10648
Kriks, S., Shim, J.-W., Piao, J., Ganat, Y. M., Wakeman, D. R., Xie, Z., … Studer, L. (2012). Floor plate-derived dopamine neurons from hESCs efficiently engraft in animal models of PD. *Nature*, *480*(7378), 547–551. https://doi.org/10.1038/nature10648.Floor
Lane, N., & Martin, W. (2010). The energetics of genome complexity. *Nature*, *467*(7318), 929–34. https://doi.org/10.1038/nature09486
Lee, I. H., Cao, L., Mostoslavsky, R., Lombard, D. B., Liu, J., Bruns, N. E., … Finkel, T. (2008). A role for the NAD-dependent deacetylase Sirt1 in the regulation of autophagy. *Proceedings of the National Academy of Sciences of the United States of America*, *105*(9), 3374–9. https://doi.org/10.1073/pnas.0712145105
Lesage, S., & Brice, A. (2009). Parkinson's disease: From monogenic forms to genetic susceptibility factors. *Human Molecular Genetics*, *18*(R1), 48–59. https://doi.org/10.1093/hmg/ddp012
Levy, O. A., Malagelada, C., & Greene, L. A. (2009). Cell death pathways in Parkinson's disease: Proximal triggers, distal effectors, and final steps. *Apoptosis*. https://doi.org/10.1007/s10495-008-0309-3

Li, J.-Y., Englund, E., Holton, J. L., Soulet, D., Hagell, P., Lees, A. J., … Brundin, P. (2008). Lewy bodies in grafted neurons in subjects with Parkinson's disease suggest host-to-graft disease propagation. *Nature Medicine*, *14*(5), 501–503. https://doi.org/10.1038/nm1746

Lim, S. Y., & Lang, A. E. (2010). The nonmotor symptoms of Parkinson's disease-An overview. *Movement Disorders*, *25*(SUPPL. 1). https://doi.org/10.1002/mds.22786

Lin, S. J., Ford, E., Haigis, M., Liszt, G., & Guarente, L. (2004). Calorie restriction extends yeast life span by lowering the level of NADH. *Genes and Development*, *18*(1), 12–16. https://doi.org/10.1101/gad.1164804

Lindholm, D., Wootz, H., & Korhonen, L. (2006). ER stress and neurodegenerative diseases. *Cell Death and Differentiation*, *13*(3), 385–92. https://doi.org/10.1038/sj.cdd.4401778

Löhle, M., Storch, A., & Reichmann, H. (2009). Beyond tremor and rigidity: Non-motor features of Parkinson's disease. *Journal of Neural Transmission*, *116*(11), 1483–1492. https://doi.org/10.1007/s00702-009-0274-1

Long, A. N., Owens, K., Schlappal, A. E., Kristian, T., Fishman, P. S., & Schuh, R. a. (2015). Effect of nicotinamide mononucleotide on brain mitochondrial respiratory deficits in an Alzheimer's disease-relevant murine model. *BMC Neurology*, *15*(1), 1–14. https://doi.org/10.1186/s12883-015-0272-x

Lücking, C. B., Dürr, a, Bonifati, V., Vaughan, J., De Michele, G., Gasser, T., … Brice, a. (2000). Association between early-onset Parkinson's disease and mutations in the parkin gene. *The New England Journal of Medicine*, *342*(21), 1560–1567. https://doi.org/10.1056/NEJM200005253422103

Luo, X., & Lee Kraus, W. (2012). On par with PARP: Cellular stress signaling through poly(ADP-ribose) and PARP-1. *Genes and Development*, *26*(5), 417–432. https://doi.org/10.1101/gad.183509.111

Luoma, P., Melberg, A., Rinne, J. O., Kaukonen, J. a, Nupponen, N. N., Chalmers, R. M., … Suomalainen, A. (2004). Parkinsonism, premature menopause, and mitochondrial DNA polymerase gamma mutations: clinical and molecular genetic study. *Lancet*, *364*(9437), 875–882. https://doi.org/10.1016/S0140-6736(04)16983-3

Mali, P., Yang, L., Esvelt, K. M., Aach, J., Guell, M., DiCarlo, J. E., … Church, G. M. (2013). RNA-guided human genome engineering via Cas9. *Science (New York, N.Y.)*, *339*(6121), 823–6. https://doi.org/10.1126/science.1232033

Manning-Boğ, A. B., Schüle, B., & Langston, J. W. (2009). Alpha-synuclein-glucocerebrosidase interactions in pharmacological Gaucher models: A biological link between Gaucher disease and parkinsonism. *NeuroToxicology*, *30*(6), 1127–1132. https://doi.org/10.1016/j.neuro.2009.06.009

Maor, G., Rencus-Lazar, S., Filocamo, M., Steller, H., Segal, D., & Horowitz, M. (2013). Unfolded protein response in Gaucher disease: from human to Drosophila. *Orphanet Journal of Rare Diseases*, *8*, 140. https://doi.org/10.1186/1750-1172-8-140

Marsden, C. D. (1983). Neuromelanin and Parkinson's disease. *Journal of Neural Transmission. Supplementum*, *19*, 121–41. Retrieved from http://www.ncbi.nlm.nih.gov/pubmed/6321645

Martin, L. J., Pan, Y., Price, A. C., Sterling, W., Copeland, N. G., Jenkins, N. A., … Lee, M. K. (2006). Parkinson's disease alpha-synuclein transgenic mice develop neuronal mitochondrial degeneration and cell death. *The Journal of Neuroscience : The Official Journal of the Society for Neuroscience*, *26*(1), 41–50. https://doi.org/10.1523/JNEUROSCI.4308-05.2006

Mazzulli, J. R., Xu, Y.-H., Sun, Y., Knight, A. L., McLean, P. J., Caldwell, G. a, … Krainc, D. (2011). Gaucher disease glucocerebrosidase and α-synuclein form a bidirectional pathogenic loop in synucleinopathies. *Cell*, *146*(1), 37–52. https://doi.org/10.1016/j.cell.2011.06.001

Mazzulli, J. R., Zunke, F., Isacson, O., Studer, L., & Krainc, D. (2016). *α-Synuclein–induced lysosomal dysfunction occurs through disruptions in protein trafficking in human midbrain synucleinopathy models*. *Proceedings of the National Academy of Sciences* (Vol. 113). https://doi.org/10.1073/pnas.1520335113

Meixner, A., Boldt, K., Van Troys, M., Askenazi, M., Gloeckner, C. J., Bauer, M., … Ueffing, M. (2011). A QUICK screen for Lrrk2 interaction partners--leucine-rich repeat kinase 2 is involved in actin cytoskeleton dynamics. *Molecular & Cellular Proteomics : MCP*, *10*(1), M110.001172. https://doi.org/10.1074/mcp.M110.001172

Michael, L. F., Wu, Z., Cheatham, R. B., Puigserver, P., Adelmant, G., Lehman, J. J., … Spiegelman, B. M. (2001). Restoration of insulin-sensitive glucose transporter (GLUT4) gene expression in muscle cells by the transcriptional coactivator PGC-1. *Proceedings of the National Academy of Sciences of the United States of America*, *98*(7), 3820–3825. https://doi.org/10.1073/pnas.061035098

Mochizuki, H., Yamada, M., & Mizuno, Y. (2006). Alpha-synuclein overexpression model. *J Neural Transm Suppl*.

Moore, D. J., West, A. B., Dawson, V. L., & Dawson, T. M. (2005). Molecular Pathophysiology of Parkinson'S Disease. *Annual Review of Neuroscience*, *28*(1), 57–87. https://doi.org/10.1146/annurev.neuro.28.061604.135718

Mootha, V. K., Handschin, C., Arlow, D., Xie, X., St Pierre, J., Sihag, S., … Spiegelman, B. M. (2004). Erralpha and Gabpa/b specify PGC-1alpha-dependent oxidative phosphorylation gene expression that is altered in diabetic muscle. *Proceedings of the National Academy of Sciences of the United States of America*, *101*(17), 6570–6575. https://doi.org/10.1073/pnas.0401401101

Moreno, J., Radford, H., Peretti, D., Steinert, Verity, N., Martin, M., … Mallucci, G. (2012). Sustained translational repression by eIF2α-P mediates prion neurodegeneration. *Nature*, *485*(7399), 507–511. https://doi.org/10.1038/nature11058

Mouchiroud, L., Houtkooper, R. H., Moullan, N., Katsyuba, E., Ryu, D., Cantó, C., … Auwerx, J. (2013). XThe NAD+/sirtuin pathway modulates longevity through activation of mitochondrial UPR and FOXO signaling. *Cell*, *154*(2). https://doi.org/10.1016/j.cell.2013.06.016

Mu??oz, J. P., Ivanova, S., S??nchez-Wandelmer, J., Mart??nez-Crist??bal, P., Noguera, E., Sancho, A., … Zorzano, A. (2014). Erratum: Mfn2 modulates the UPR and mitochondrial function via repression of PERK (EMBO Journal 32 (2348-2361) DOI 10.1038/emboj.2013.168). *EMBO Journal*. https://doi.org/10.1002/embj.201470050

Murphy, K. E., Gysbers, A. M., Abbott, S. K., Tayebi, N., Kim, W. S., Sidransky, E., … Halliday, G. M. (2014). Reduced glucocerebrosidase is associated with increased -synuclein in sporadic Parkinson's disease. *Brain*, awt367-. https://doi.org/10.1093/brain/awt367

Nandhagopal, R., Kuramoto, L., Schulzer, M., Mak, E., Cragg, J., McKenzie, J., … Stoessl, A. J. (2011). Longitudinal evolution of compensatory changes in striatal dopamine processing in Parkinson's disease. *Brain*, *134*(11), 3290–3298. https://doi.org/10.1093/brain/awr233

Narendra, D., Tanaka, A., Suen, D. F., & Youle, R. J. (2008). Parkin is recruited selectively to impaired mitochondria and promotes their autophagy. *Journal of Cell Biology*, *183*(5), 795–803. https://doi.org/10.1083/jcb.200809125

Ng, F., & Tang, B. L. (2013). Sirtuins' modulation of autophagy. *Journal of Cellular Physiology*, *228*(12), 2262–2270. https://doi.org/10.1002/jcp.24399

Ngamukote, S., Yanagisawa, M., Ariga, T., Ando, S., & Yu, R. K. (2007). Developmental changes of glycosphingolipids and expression of glycogenes in mouse brains. *Journal of Neurochemistry*, *103*(6), 2327–2341. https://doi.org/10.1111/j.1471-4159.2007.04910.x

Nilsson, O., & Svennerholm, L. (1982). Accumulation of Glucosylceramide and

Glucosylsphingosine (Psychosine) in Cerebrum and Cerebellum in Infantile and Juvenile Gaucher Disease. *Journal of Neurochemistry*, *39*(3), 709–718. https://doi.org/10.1111/j.1471-4159.1982.tb07950.x

Nuytemans, K., Theuns, J., Cruts, M., & Van Broeckhoven, C. (2010). Genetic etiology of Parkinson disease associated with mutations in the SNCA, PARK2, PINK1, PARK7, and LRRK2 genes: A mutation update. *Human Mutation*. https://doi.org/10.1002/humu.21277

Onyango, I. G., Lu, J., Rodova, M., Lezi, E., Crafter, A. B., & Swerdlow, R. H. (2010). Regulation of neuron mitochondrial biogenesis and relevance to brain health. *Biochimica et Biophysica Acta (BBA) - Molecular Basis of Disease*, *1802*(1), 228–234. https://doi.org/10.1016/j.bbadis.2009.07.014

Osellame, L. D., & Duchen, M. R. (2013). Defective quality control mechanisms and accumulation of damaged mitochondria link Gaucher and Parkinson diseases. *Autophagy*, *9*(10), 1633–1635. https://doi.org/10.4161/auto.25878

Osellame, L. D., Rahim, A. a, Hargreaves, I. P., Gegg, M. E., Richard-Londt, A., Brandner, S., … Duchen, M. R. (2013). Mitochondria and quality control defects in a mouse model of Gaucher disease--links to Parkinson's disease. *Cell Metabolism*, *17*(6), 941–53. https://doi.org/10.1016/j.cmet.2013.04.014

Panicker, L. M., Miller, D., Park, T. S., Patel, B., Azevedo, J. L., Awad, O., … Feldman, R. a. (2012). Induced pluripotent stem cell model recapitulates pathologic hallmarks of Gaucher disease. *Proceedings of the National Academy of Sciences of the United States of America*, *109*(44), 18054–9. https://doi.org/10.1073/pnas.1207889109

Parkinson, J. (2002). An essay on the shaking palsy. 1817. *The Journal of Neuropsychiatry and Clinical Neurosciences*, *14*(2), 223–236; discussion 222. https://doi.org/10.1176/appi.neuropsych.14.2.223

Pelled, D., Trajkovic-Bodennec, S., Lloyd-Evans, E., Sidransky, E., Schiffmann, R., & Futerman, A. H. (2005). Enhanced calcium release in the acute neuronopathic form of Gaucher disease. *Neurobiology of Disease*, *18*(1), 83–88. https://doi.org/10.1016/j.nbd.2004.09.004

Perrier, A. L., Tabar, V., Barberi, T., Rubio, M. E., Bruses, J., Topf, N., … Studer, L. (2004). Derivation of midbrain dopamine neurons from human embryonic stem cells. *Proceedings of the National Academy of Sciences of the United States of America*, *101*(34), 12543–8. https://doi.org/10.1073/pnas.0404700101

Pickart, C. M., & Eddins, M. J. (2004). Ubiquitin: Structures, functions, mechanisms. *Biochimica et Biophysica Acta - Molecular Cell Research*. https://doi.org/10.1016/j.bbamcr.2004.09.019

Pirinen, E., Cant??, C., Jo, Y. S., Morato, L., Zhang, H., Menzies, K. J., … Auwerx, J. (2014). Pharmacological inhibition of poly(ADP-ribose) polymerases improves fitness and mitochondrial function in skeletal muscle. *Cell Metabolism*, *19*(6), 1034–1041. https://doi.org/10.1016/j.cmet.2014.04.002

Polymeropoulos, M. H., Lavedan, C., Leroy, E., Ide, S. E., Dehejia, A., Dutra, A., … Nussbaum, R. L. (1997). Mutation in the alpha-synuclein gene identified in families with Parkinson's disease. *Science (New York, N.Y.)*, *276*(5321), 2045–2047. https://doi.org/doi: 10.1126/science.276.5321.2045

Price, N. L., Gomes, A. P., Ling, A. J. Y., Duarte, F. V., Martin-Montalvo, A., North, B. J., … Sinclair, D. A. (2012). SIRT1 is required for AMPK activation and the beneficial effects of resveratrol on mitochondrial function. *Cell Metabolism*, *15*(5), 675–690. https://doi.org/10.1016/j.cmet.2012.04.003

Puigserver, P., Rhee, J., Donovan, J., Walkey, C. J., Yoon, J. C., Oriente, F., … Spiegelman, B. M. (2003). Insulin-regulated hepatic gluconeogenesis through FOXO1-PGC-1alpha interaction. *Nature*, *423*(6939), 550–5. https://doi.org/10.1038/nature01667

Puigserver, P., Wu, Z., Park, C. W., Graves, R., Wright, M., & Spiegelman, B. M. (1998). A cold-inducible coactivator of nuclear receptors linked to adaptive thermogenesis. *Cell*, *92*(6), 829–839. https://doi.org/10.1016/S0092-8674(00)81410-5

Rakovic, A., Shurkewitsch, K., Seibler, P., Gr??newald, A., Zanon, A., Hagenah, J., … Klein, C. (2013). Phosphatase and tensin homolog (PTEN)-induced Putative Kinase 1 (PINK1)-dependent ubiquitination of endogenous parkin attenuates mitophagy: Study in human primary fibroblasts and induced pluripotent stem cell-derived neurons. *Journal of Biological Chemistry*, *288*(4), 2223–2237. https://doi.org/10.1074/jbc.M112.391680

Ramsden, N., Perrin, J., Ren, Z., Lee, B. D., Zinn, N., Dawson, V. L., … Hopf, C. (2011). Chemoproteomics-based design of potent LRRK2-selective lead compounds that attenuate Parkinson's disease-related toxicity in human neurons. *ACS Chemical Biology*, *6*(10), 1021–1028. https://doi.org/10.1021/cb2002413

Ramsey, K. M., Mills, K. F., Satoh, A., & Imai, S. I. (2008). Age-associated loss of Sirt1-mediated enhancement of glucose-stimulated insulin secretion in beta cell-specific Sirt1-overexpressing (BESTO) mice. *Aging Cell*, *7*(1), 78–88. https://doi.org/10.1111/j.1474-9726.2007.00355.x

Raturi, A., & Simmen, T. (2013a). Where the endoplasmic reticulum and the mitochondrion tie the knot: The mitochondria-associated membrane (MAM). *Biochimica et Biophysica Acta - Molecular Cell Research*. https://doi.org/10.1016/j.bbamcr.2012.04.013

Raturi, A., & Simmen, T. (2013b). Where the endoplasmic reticulum and the mitochondrion tie the knot: The mitochondria-associated membrane (MAM). *Biochimica et Biophysica Acta - Molecular Cell Research*, *1833*(1), 213–224. https://doi.org/10.1016/j.bbamcr.2012.04.013

Reinhardt, P., Schmid, B., Burbulla, L. F., Schöndorf, D. C., Wagner, L., Glatza, M., … Sterneckert, J. (2013). Genetic correction of a LRRK2 mutation in human iPSCs links parkinsonian neurodegeneration to ERK-dependent changes in gene expression. *Cell Stem Cell*, *12*(3), 354–67. https://doi.org/10.1016/j.stem.2013.01.008

Ren, Y., Jiang, H., Hu, Z., Fan, K., Wang, J., Janoschka, S., … Feng, J. (2015). Parkin mutations reduce the complexity of neuronal processes in iPSC-derived human neurons. *Stem Cells*, *33*(1), 68–78. https://doi.org/10.1002/stem.1854

Rizzuto, R., Marchi, S., Bonora, M., Aguiari, P., Bononi, A., De Stefani, D., … Pinton, P. (2009). Ca2+ transfer from the ER to mitochondria: When, how and why. *Biochimica et Biophysica Acta - Bioenergetics*, *1787*(11), 1342–1351. https://doi.org/10.1016/j.bbabio.2009.03.015

Rocha, E. M., Smith, G. A., Park, E., Cao, H., Brown, E., Hayes, M. A., … Isacson, O. (2015). Glucocerebrosidase gene therapy prevents α-synucleinopathy of midbrain dopamine neurons. *Neurobiology of Disease*. https://doi.org/10.1016/j.nbd.2015.09.009

Rodgers, J. T., Lerin, C., Haas, W., Gygi, S. P., Spiegelman, B. M., & Puigserver, P. (2005). Nutrient control of glucose homeostasis through a complex of PGC-1a and SIRT1. *Nature*, *434*(7029), 113–118. https://doi.org/10.1038/nature03314.1.

Rutkowski, D. T., & Hegde, R. S. (2010). Regulation of basal cellular physiology by the homeostatic unfolded protein response. *Journal of Cell Biology*. https://doi.org/10.1083/jcb.201003138

Sanchez-Martinez, A., Beavan, M., Gegg, M. E., Chau, K.-Y., Whitworth, A. J., & Schapira, A. H. V. (2016). Parkinson disease-linked GBA mutation effects reversed by molecular chaperones in human cell and fly models. *Scientific Reports*, *6*(August), 31380. https://doi.org/10.1038/srep31380

Sano, R., & Reed, J. C. (2013). ER stress-induced cell death mechanisms. *Biochimica et Biophysica Acta - Molecular Cell Research*, *1833*(12), 3460–3470. https://doi.org/10.1016/j.bbamcr.2013.06.028

Sardiello, M., Palmieri, M., di Ronza, A., Medina, D. L., Valenza, M., Gennarino, V. A., … Schieweck, . (2009). A gene network regulating lysosomal biogenesis and function. *Science (New York, N.Y.)*, *325*(5939), 473–7. https://doi.org/10.1126/science.1174447

Schapira, a H., Cooper, J. M., Dexter, D., Jenner, P., Clark, J. B., & Marsden, C. D. (1989). Mitochondrial complex I deficiency in Parkinson's disease. *Lancet*, *1*(8649), 1269. https://doi.org/10.1016/S0140-6736(89)92366-0

Schapira, a H., Mann, V. M., Cooper, J. M., Dexter, D., Daniel, S. E., Jenner, P., … Marsden, C. D. (1990). Anatomic and disease specificity of NADH CoQ1 reductase (complex I) deficiency in Parkinson's disease. *Journal of Neurochemistry*, *55*(6), 2142–2145. https://doi.org/10.1016/0140-6736(91)92989-F

Schöndorf, D. C., Aureli, M., McAllister, F. E., Hindley, C. J., Mayer, F., Schmid, B., … Deleidi, M. (2014a). iPSC-derived neurons from GBA1-associated Parkinson's disease patients show autophagic defects and impaired calcium homeostasis. *Nature Communications*, *5*(May), 4028. https://doi.org/10.1038/ncomms5028

Schöndorf, D. C., Aureli, M., McAllister, F. E., Hindley, C. J., Mayer, F., Schmid, B., … Deleidi, M. (2014b). iPSC-derived neurons from GBA1-associated Parkinson's disease patients show autophagic defects and impaired calcium homeostasis. *Nature Communications*, *5*(May), 4028. https://doi.org/10.1038/ncomms5028

Schreiber, S. N., Knutti, D., Brogli, K., Uhlmann, T., & Kralli, A. (2003). The transcriptional coactivator PGC-1 regulates the expression and activity of the orphan nuclear receptor estrogen-related receptor alpha (ERRalpha). *The Journal of Biological Chemistry*, *278*(11), 9013–8. https://doi.org/10.1074/jbc.M212923200

Seibler, P., Graziotto, J., Jeong, H., Simunovic, F., Klein, C., & Krainc, D. (2011). Mitochondrial Parkin recruitment is impaired in neurons derived from mutant PINK1 induced pluripotent stem cells. *The Journal of Neuroscience : The Official Journal of the Society for Neuroscience*, *31*(16), 5970–6. https://doi.org/10.1523/JNEUROSCI.4441-10.2011

Settembre, C., Di Malta, C., Polito, V. A., Garcia Arencibia, M., Vetrini, F., Erdin, S., … Ballabio, A. (2011). TFEB links autophagy to lysosomal biogenesis. *Science (New York, N.Y.)*, *332*(6036), 1429–33. https://doi.org/10.1126/science.1204592

Settembre, C., Fraldi, A., Medina, D. L., & Ballabio, A. (2013). Signals from the lysosome: a control centre for cellular clearance and energy metabolism. *Nature Reviews. Molecular Cell Biology*, *14*(5), 283–96. https://doi.org/10.1038/nrm3565

Shigenaga, M. K., Hagen, T. M., & Ames, B. N. (1994). Oxidative damage and mitochondrial decay in aging. *Proceedings of the National Academy of Sciences of the United States of America*, *91*(23), 10771–8. https://doi.org/10.1073/pnas.91.23.10771

Shimobayashi, M., & Hall, M. N. (2014). Making new contacts: the mTOR network in metabolism and signalling crosstalk. *Nature Reviews. Molecular Cell Biology*, *15*(3), 155–62. https://doi.org/10.1038/nrm3757

Siddiqui, A., Bhaumik, D., Chinta, S. J., Rane, A., Rajagopalan, S., Lieu, C. A., … Andersen, J. K. (2015). Mitochondrial Quality Control via the PGC1α-TFEB Signaling Pathway Is Compromised by Parkin Q311X Mutation But Independently Restored by Rapamycin. *Journal of Neuroscience*, *35*(37), 12833–12844. https://doi.org/10.1523/JNEUROSCI.0109-15.2015

Sidransky, E., & Lopez, G. (2012). The link between the GBA gene and parkinsonism. *The Lancet Neurology*, *11*(11), 986–998. https://doi.org/10.1016/S1474-4422(12)70190-4

Sidransky, E., Nalls, M. A., Aasly, J. O., Aharon-Peretz, J., Annesi, G., Barbosa, E. R., … Ziegler, S. G. (2009). Multicenter Analysis of Glucocerebrosidase Mutations in Parkinson's Disease. *New England Journal of Medicine*, *361*(17), 1651–1661. https://doi.org/10.1056/NEJMoa0901281

Simón-Sánchez, J., Schulte, C., Bras, J. M., Sharma, M., Gibbs, J. R., Berg, D., … Gasser, T. (2009). Genome-wide association study reveals genetic risk underlying Parkinson's disease. *Nature Genetics*, *41*(12), 1308–12. https://doi.org/10.1038/ng.487

Slivka, A., & Cohen, G. (1985). Hydroxyl radical attack on dopamine. *Journal of Biological Chemistry*, *260*(29), 15466–15472.

Soldner, F., Lagani??re, J., Cheng, A. W., Hockemeyer, D., Gao, Q., Alagappan, R., … Jaenisch, R. (2011). Generation of isogenic pluripotent stem cells differing exclusively at two early onset parkinson point mutations. *Cell*, *146*(2), 318–331. https://doi.org/10.1016/j.cell.2011.06.019

Spillantini, M. G., Schmidt, M. L., Lee, V. M., Trojanowski, J. Q., Jakes, R., & Goedert, M. (1997). Alpha-synuclein in Lewy bodies. *Nature*, *388*(6645), 839–840. https://doi.org/10.1038/42166

Stock, D., Leslie, A. G., & Walker, J. E. (1999). Molecular architecture of the rotary motor in ATP synthase. *Science (New York, N.Y.)*, *286*(5445), 1700–5. https://doi.org/10.1126/science.286.5445.1700

Sugita, S., Ho, A., & Südhof, T. C. (2002). NECABs: A family of neuronal Ca2+-binding proteins with an unusual domain structure and a restricted expression pattern. *Neuroscience*, *112*(1), 51–63. https://doi.org/10.1016/S0306-4522(02)00063-5

Sulzer, D. (2007). Multiple hit hypotheses for dopamine neuron loss in Parkinson's disease. *Trends in Neurosciences*, *30*(5), 244–250. https://doi.org/10.1016/j.tins.2007.03.009

Sun, Y., & Grabowski, G. A. (2010). Impaired autophagosomes and lysosomes in neuronopathic Gaucher disease. *Autophagy*. https://doi.org/10.4161/auto.6.5.12047

Svennerholm, L., Boström, K., Fredman, P., Månsson, J. E., Rosengren, B., & Rynmark, B. M. (1989). Human brain gangliosides: developmental changes from early fetal stage to advanced age. *Biochimica et Biophysica Acta*, *1005*(2), 109–17. https://doi.org/10.1016/0005-2760(89)90175-6

Takahashi, K., Tanabe, K., Ohnuki, M., Narita, M., Ichisaka, T., Tomoda, K., & Yamanaka, S. (2007). Induction of pluripotent stem cells from adult human fibroblasts by defined factors. *Cell*, *131*(5), 861–72. https://doi.org/10.1016/j.cell.2007.11.019

Takahashi, K., & Yamanaka, S. (2006). Induction of Pluripotent Stem Cells from Mouse Embryonic and Adult Fibroblast Cultures by Defined Factors. *Cell*, *126*(4), 663–676. https://doi.org/10.1016/j.cell.2006.07.024

Tang, B. L. (2016). Sirt1 and the Mitochondria. *Molecules and Cells*, *39*(2), 87–95. https://doi.org/10.14348/molcells.2016.2318

Tatsuta, T., Scharwey, M., & Langer, T. (2014). Mitochondrial lipid trafficking. *Trends in Cell Biology*. https://doi.org/10.1016/j.tcb.2013.07.011

Tayebi, N., Walker, J., Stubblefield, B., Orvisky, E., LaMarca, M. E., Wong, K., … Sidransky, E. (2003). Gaucher disease with parkinsonian manifestations: Does glucocerebrosidase deficiency contribute to a vulnerability to parkinsonism? *Molecular Genetics and Metabolism*, *79*(2), 104–109. https://doi.org/10.1016/S1096-7192(03)00071-4

Tessitore, A., Martin, M. D. P., Sano, R., Ma, Y., Mann, L., Ingrassia, A., … D'Azzo, A. (2004). GM1-ganglioside-mediated activation of the unfolded protein response causes neuronal death in a neurodegenerative gangliosidosis. *Molecular Cell*, *15*(5), 753–766. https://doi.org/10.1016/j.molcel.2004.08.029

Thomson, J. A. (1998). Embryonic Stem Cell Lines Derived from Human Blastocysts. *Science*, *282*(5391), 1145–1147. https://doi.org/10.1126/science.282.5391.1145

Townsend, J. a, Wright, D. a, Winfrey, R. J., Fu, F., Maeder, M. L., Joung, J. K., & Voytas, D. F. (2009). High-frequency modification of plant genes using engineered zinc-finger nucleases. *Nature*, *459*(7245), 442–5. https://doi.org/10.1038/nature07845

Trammell, S. A. J., Schmidt, M. S., Weidemann, B. J., Redpath, P., Jaksch, F., Dellinger, R.

W., … Lau, D. T. (2016). Nicotinamide riboside is uniquely and orally bioavailable in mice and humans. *Nature Communications*, *7*, 12948. https://doi.org/10.1038/ncomms12948

Trenker, M., Malli, R., Fertschai, I., Levak-Frank, S., & Graier, W. F. (2007). Uncoupling proteins 2 and 3 are fundamental for mitochondrial Ca2+ uniport. *Nature Cell Biology*, *9*(4), 445–52. https://doi.org/10.1038/ncb1556

Tretter, L., Sipos, I., & Adam-Vizi, V. (2004). Initiation of Neuronal Damage by Complex I Deficiency and Oxidative Stress in Parkinson's Disease. *Neurochemical Research*. https://doi.org/10.1023/B:NERE.0000014827.94562.4b

Tsika, E., & Moore, D. J. (2012). Mechanisms of LRRK2-mediated neurodegeneration. *Current Neurology and Neuroscience Reports*, *12*(3), 251–60. https://doi.org/10.1007/s11910-012-0265-8

Urnov, F. D., Miller, J. C., Lee, Y. L., Beausejour, C. M., Rock, J. M., Augustus, S., … Holmes, M. C. (2005). Highly efficient endogenous human gene correction using designed zinc-finger nucleases. *Nature*, *435*(7042), 646–651. https://doi.org/10.1038/nature03556

Valdés, P., Mercado, G., Vidal, R. L., Molina, C., Parsons, G., Court, F. a, … Hetz, C. (2014). Control of dopaminergic neuron survival by the unfolded protein response transcription factor XBP1. *Proceedings of the National Academy of Sciences of the United States of America*, *111*(18), 6804–9. https://doi.org/10.1073/pnas.1321845111

Valente, E. M., Abou-Sleiman, P. M., Caputo, V., Muqit, M. M., Harvey, K., Gispert, S., … Wood, N. W. (2004). Hereditary early-onset Parkinson's disease caused by mutations in PINK1. *Science*, *304*(5674), 1158–1160. https://doi.org/10.1126/science.1096284

Valente, E. M., Brancati, F., Caputo, V., Graham, E. A., Davis, M. B., Ferraris, A., … Wood, N. W. (2002). PARK6 is a common cause of familial parkinsonism. *Neurological Sciences*, *23*(SUPPL. 2). https://doi.org/10.1007/s100720200097

van Vliet, A. R., Verfaillie, T., & Agostinis, P. (2014). New functions of mitochondria associated membranes in cellular signaling. *Biochimica et Biophysica Acta - Molecular Cell Research*. https://doi.org/10.1016/j.bbamcr.2014.03.009

Velayati, A., Yu, W. H., & Sidransky, E. (2010). The role of glucocerebrosidase mutations in parkinson disease and lewy body disorders. *Current Neurology and Neuroscience Reports*. https://doi.org/10.1007/s11910-010-0102-x

Verfaillie, T., Rubio, N., Garg, A., Bultynck, G., Rizzuto, R., Decuypere, J.-P., … Agostinis, P. (2012). PERK is required at the ER-mitochondrial contact sites to convey apoptosis after ROS-based ER stress. *Cell Death and Differentiation*, *19*(10), 1880–1891. https://doi.org/10.1038/cdd.2012.74

Wang, C.-H., Wu, S.-B., Wu, Y.-T., & Wei, Y.-H. (2013). Oxidative stress response elicited by mitochondrial dysfunction: implication in the pathophysiology of aging. *Experimental Biology and Medicine (Maywood, N.J.)*, *238*(5), 450–60. https://doi.org/10.1177/1535370213493069

Wernig, M., Zhao, J.-P., Pruszak, J., Hedlund, E., Fu, D., Soldner, F., … Jaenisch, R. (2008). Neurons derived from reprogrammed fibroblasts functionally integrate into the fetal brain and improve symptoms of rats with Parkinson's disease. *Proceedings of the National Academy of Sciences*, *105*(15), 5856–5861. https://doi.org/10.1073/pnas.0801677105

Wiedemann, N., Frazier, A. E., & Pfanner, N. (2004). The Protein Import Machinery of Mitochondria. *Journal of Biological Chemistry*. https://doi.org/10.1074/jbc.R400003200

Wiedenheft, B., Sternberg, S. H., & Doudna, J. a. (2012). RNA-guided genetic silencing systems in bacteria and archaea. *Nature*, *482*(7385), 331–338. https://doi.org/10.1038/nature10886

William Langston, J., Forno, L. S., Rebert, C. S., & Irwin, I. (1984). Selective nigral toxicity after systemic administration of 1-methyl-4-phenyl-1,2,5,6-tetrahydropyrine (MPTP) in

the squirrel monkey. *Brain Research*, *292*(2), 390–394. https://doi.org/10.1016/0006-8993(84)90777-7

Wills, J., Credle, J., Oaks, A. W., Duka, V., Lee, J. H., Jones, J., & Sidhu, A. (2012). Paraquat, but not maneb, induces synucleinopathy and tauopathy in striata of mice through inhibition of proteasomal and autophagic pathways. *PLoS ONE*, *7*(1). https://doi.org/10.1371/journal.pone.0030745

Wu, Z., Puigserver, P., Andersson, U., Zhang, C., Adelmant, G., Mootha, V., … Spiegelman, B. M. (1999). Mechanisms controlling mitochondrial biogenesis and respiration through the thermogenic coactivator PGC-1. *Cell*, *98*(1), 115–124. https://doi.org/10.1016/S0092-8674(00)80611-X

Xiao, Q., Yan, P., Ma, X., Liu, H., Perez, R., Zhu, A., … Lee, J.-M. (2015). Neuronal-Targeted TFEB Accelerates Lysosomal Degradation of APP, Reducing Aβ Generation and Amyloid Plaque Pathogenesis. *The Journal of Neuroscience : The Official Journal of the Society for Neuroscience*, *35*(35), 12137–51. https://doi.org/10.1523/JNEUROSCI.0705-15.2015

Xu, Y. H., Xu, K., Sun, Y., Liou, B., Quinn, B., Li, R. H., … Grabowski, G. A. (2014). Multiple pathogenic proteins implicated in neuronopathic Gaucher disease mice. *Human Molecular Genetics*, *23*(15), 3943–3957. https://doi.org/10.1093/hmg/ddu105

Yang, T., Chan, N. Y. K., & Sauve, A. A. (2007). Syntheses of nicotinamide riboside and derivatives: Effective agents for increasing nicotinamide adenine dinucleotide concentrations in mammalian cells. *Journal of Medicinal Chemistry*, *50*(26), 6458–6461. https://doi.org/10.1021/jm701001c

Yoon, J. C., Puigserver, P., Chen, G., Donovan, J., Wu, Z., Rhee, J., … Spiegelman, B. M. (2001). Control of hepatic gluconeogenesis through the transcriptional coactivator PGC-1. *Nature*, *413*(6852), 131–138. https://doi.org/10.1038/35093050

Youle, R. J., & Narendra, D. P. (2011). Mechanisms of mitophagy. *Nat Rev Mol Cell Biol*, *12*(1), 9–14. https://doi.org/10.1038/nrm3028

Zhang, C. Y., Baffy, G., Perret, P., Krauss, S., Peroni, O., Grujic, D., … Lowell, B. B. (2001). Uncoupling protein-2 negatively regulates insulin secretion and is a major link between obesity, beta cell dysfunction, and type 2 diabetes. *Cell*, *105*(6), 745–755. https://doi.org/S0092-8674(01)00378-6 [pii]

Zhang, H., Zhang, H., Ryu, D., Wu, Y., Gariani, K., Wang, X., … Menzies, K. J. (2016). NAD + repletion improves mitochondrial and stem cell function and enhances life span in mice, *2693*(April).

Zhang, Z., Lee, Y. C., Kim, S. J., Choi, M. S., Tsai, P. C., Xu, Y., … Mukherjee, A. B. (2006). Palmitoyl-protein thioesterase-1 deficiency mediates the activation of the unfolded protein response and neuronal apoptosis in INCL. *Human Molecular Genetics*, *15*(2), 337–346. https://doi.org/10.1093/hmg/ddi451

Zhao, P., Luo, Z., Tian, W., Yang, J., Ibáñez, D. P., Huang, Z., … Fan, W. (2014). Solving the puzzle of Parkinson's disease using induced pluripotent stem cells. *Exp. Biol. Med.*, 1421–1432. https://doi.org/10.1177/1535370214538588

Zimprich, A., Biskup, S., Leitner, P., Lichtner, P., Farrer, M., Lincoln, S., … Gasser, T. (2004). Mutations in LRRK2 cause autosomal-dominant parkinsonism with pleomorphic pathology. *Neuron*, *44*(4), 601–607. https://doi.org/10.1016/j.neuron.2004.11.005

Zimran, A. (2011). How I treat Gaucher disease. *Blood*. https://doi.org/10.1182/blood-2011-04-308890

Appendix:

Statement of contributions to individual publications:

"Genetic Correction of a LRRK2 Mutation in Human iPSCs Links Parkinsonian Neurodegeneration to ERK-Dependent Changes in Gene Expression" (Cell Stem cell, 2013)

D.S took part in characterization and gene editing of hiPSC lines. Further D.S performed Western Blot experiments.

"iPSC-derived neurons from GBA1-associated Parkinson's disease patients show autophagic
defects and impaired calcium homeostasis" (Nat. Comm., 2014)

D.S. performed gene editing of hiPSCs,measured GBA activity, performed Western Blot experiments, Immunofluorescent stainings, Toxicity assays and NECAB knockdown experiments. Further, D.S. took part in data analysis and writing of the manuscript.

"The NAD+ Precursor Nicotinamide Riboside Rescues Mitochondrial Defects and Neuronal Loss in iPSC and Fly Models of Parkinson's Disease" (Cell Reports, 2018)

D.S. supervised gene editing of hiPSCs. Further D.S. performed Q-RT-PCRs, GBA activity assays, Western Blots, Immunofluorescent stainings, Seahorse measurements, NAD measurements, Mitosox experiments, TMRM analysis, Citrate synthase measurements and prepared cells for EM analysis/MSMS/Lipidomic analysis. D.S. participated in planning of experiments, data analysis and writing of the manuscript

List of publications

"Genetic Correction of a LRRK2 Mutation in Human iPSCs Links Parkinsonian Neurodegeneration to ERK-Dependent Changes in Gene Expression" (Cell Stem cell, 2013)

"iPSC-derived neurons from GBA1-associated Parkinson's disease patients show autophagic defects and impaired calcium homeostasis" (Nat. Comm., 2014)

"The NAD+ Precursor Nicotinamide Riboside Rescues Mitochondrial Defects and Neuronal Loss in iPSC and Fly Models of Parkinson's Disease" (Cell Reports, 2018)

Cell Stem Cell
Article

Genetic Correction of a LRRK2 Mutation in Human iPSCs Links Parkinsonian Neurodegeneration to ERK-Dependent Changes in Gene Expression

Peter Reinhardt,[1,10] Benjamin Schmid,[2,10] Lena F. Burbulla,[2] David C. Schöndorf,[2,4] Lydia Wagner,[1] Michael Glatza,[1] Susanne Höing,[1] Gunnar Hargus,[1,4] Susanna A. Heck,[2] Ashutosh Dhingra,[2,5] Guangming Wu,[1] Stephan Müller,[3] Kathrin Brockmann,[2] Torsten Kluba,[6] Martina Maisel,[2] Rejko Krüger,[2] Daniela Berg,[2] Yaroslav Tsytsyura,[7] Cora S. Thiel,[7] Olympia-Ekaterini Psathaki,[1] Jürgen Klingauf,[7] Tanja Kuhlmann,[4] Marlene Klewin,[8] Heiko Müller,[8] Thomas Gasser,[2,*] Hans R. Schöler,[1,9,*] and Jared Sterneckert[1]

[1]Department of Cell and Developmental Biology, Max Planck Institute for Molecular Biomedicine, Röntgenstrasse 20, 48149 Münster, Germany
[2]Department of Neurodegenerative Diseases
[3]Department of Epileptology
Hertie Institute for Clinical Brain Research, University of Tübingen, and German Center for Neurodegenerative Diseases, 72076 Tübingen, Germany
[4]Institute of Neuropathology, University Hospital Münster, Albert-Schweitzer-Campus 1, Gebäude A7, 48149 Münster, Germany
[5]Graduate School of Cellular & Molecular Neuroscience
[6]Department of Orthopaedic Surgery
University of Tübingen, 72076 Tübingen, Germany
[7]Cellular Biophysics Group, Institute for Medical Physics and Biophysics, Westfälische Wilhelms-Universität Münster, Robert-Koch Str. 31, 41849 Münster, Germany
[8]Department of Pharmacology, Lead-Discovery-Center GmbH, Otto-Hahn-Strasse 15, 44227 Dortmund, Germany
[9]Medical Faculty, University of Münster, Domagkstrasse 3, 48149 Münster, Germany
[10]These authors contributed equally and share first authorship
*Correspondence: thomas.gasser@uni-tuebingen.de (T.G.), office@mpi-muenster.mpg.de (H.R.S.)
http://dx.doi.org/10.1016/j.stem.2013.01.008

SUMMARY

The *LRRK2* mutation G2019S is the most common genetic cause of Parkinson's disease (PD). To better understand the link between mutant *LRRK2* and PD pathology, we derived induced pluripotent stem cells from PD patients harboring *LRRK2* G2019S and then specifically corrected the mutant *LRRK2* allele. We demonstrate that gene correction resulted in phenotypic rescue in differentiated neurons and uncovered expression changes associated with *LRRK2* G2019S. We found that *LRRK2* G2019S induced dysregulation of *CPNE8*, *MAP7*, *UHRF2*, *ANXA1*, and *CADPS2*. Knockdown experiments demonstrated that four of these genes contribute to dopaminergic neurodegeneration. *LRRK2* G2019S induced increased extracellular-signal-regulated kinase 1/2 (ERK) phosphorylation. Transcriptional dysregulation of *CADPS2*, *CPNE8*, and *UHRF2* was dependent on ERK activity. We show that multiple PD-associated phenotypes were ameliorated by inhibition of ERK. Therefore, our results provide mechanistic insight into the pathogenesis induced by mutant *LRRK2* and pointers for the development of potential new therapeutics.

INTRODUCTION

Parkinson's disease (PD) is the second most common neurodegenerative disease worldwide and affects an estimated 1 in 1,000 people in Europe (European Brain Council, 2011). Although most cases of PD are sporadic, about 5%–10% of patients have familial PD (fPD) following an autosomal-recessive or -dominant inheritance pattern (Schiesling et al., 2008). These two inheritance forms appear to have different pathologies (Schiesling et al., 2008). Unlike patients with autosomal-recessive fPD, patients with autosomal-dominant fPD typically show extensive formation of Lewy bodies in different parts of the brain. Alpha-synuclein (αSYN), the protein encoded by the gene *SNCA*, is the major component of Lewy bodies, indicating that αSYN plays a central role in the pathogenesis of PD (Spillantini et al., 1997). *SNCA* was the first gene identified as being mutated in patients with fPD (Polymeropoulos et al., 1997).

In 2004, two research groups simultaneously discovered mutations in the *Leucine-rich repeat kinase 2* (*LRRK2*) gene in patients with fPD (Paisán-Ruíz et al., 2004; Zimprich et al., 2004). Like *SNCA* mutations, *LRRK2* mutations result in autosomal-dominant fPD. Mutations in *LRRK2* have been found in about 2% of patients with sporadic PD (Berg et al., 2005), with much higher prevalence rates in some populations, e.g., Ashkenazi Jews (Ozelius et al., 2006). Patients with PD with *LRRK2* mutations most often exhibit Lewy body pathology, and experiments in the mouse model have suggested a link between *LRRK2* and *SNCA* (Lin et al., 2009; Ross et al., 2006). G2019S

is the most common mutation of *LRRK2*, and mutations in *LRRK2*, including G2019S, have been suggested to lead to increased expression of *SNCA* (Carballo-Carbajal et al., 2010; Nguyen et al., 2011). Therefore, *LRRK2* mutations are thought to confer susceptibility to PD through *SNCA* (Cookson, 2010). However, it should be noted that although most patients with PD harboring *LRRK2* mutations manifest alpha-synucleinopathy, patients with nigral degeneration without αSYN aggregation have been reported (Cookson et al., 2008).

Several lines of evidence suggest a role for TAU in PD pathology. Genome-wide association studies have demonstrated that polymorphisms at the *Microtubule-associated protein TAU* (*MAPT)* locus, which encodes TAU, are associated with PD. In addition, it has been shown that the *MAPT* haplotype influences age at onset in *LRRK2* mutation carriers (Golub et al., 2009), and there has been at least one documented case of a *LRRK2* G2019S carrier having TAU pathology (Rajput et al., 2006). Interestingly, it has been suggested that TAU may colocalize with αSYN in a subset of Lewy bodies (Ishizawa et al., 2003).

Human induced pluripotent stem cell (hiPSC) technology offers a unique opportunity to study the mechanism of PD pathogenesis induced by *LRRK2* G2019S, which could enable the development of new therapies. In 2006, Shinya Yamanaka demonstrated that expression of four genes in fibroblasts induced the formation of pluripotent stem cells, with the same self-renewal and differentiation potential as embryonic stem cells (Takahashi and Yamanaka, 2006). Nguyen et al. (2011) first demonstrated that this technology could be used to generate iPSC lines from patients with PD harboring *LRRK2* G2019S. It was reported that differentiated midbrain dopaminergic (mDA) neurons, which are preferentially lost in patients with PD, were more susceptible to oxidative stress and had increased levels of αSYN. Subsequently, Sánchez-Danés et al. (2012) showed increased αSYN and aberrant autophagy in mDA neurons differentiated from iPSC lines of PD patients with and without *LRRK2* G2019S. However, PD phenotypes are affected by polymorphisms at multiple loci. For example, patients with *LRRK2* mutations will exhibit variable phenotypes when additional polymorphisms are present in either *SNCA* or *MAPT* (Botta-Orfila et al., 2012; Golub et al., 2009). As a result, it is unclear whether these observed phenotypes in iPSC-derived neurons were specifically due to *LRRK2* G2019S. Because of the large variability in the genetic background between individuals, it is very difficult to detect and study molecular changes resulting from a specific allele such as *LRRK2* G2019S.

Gene correction of iPSCs from patients with known genetic mutations is a powerful tool for overcoming this limitation of the use of iPSCs. Here, we report mechanistic insights for mDA neurodegeneration induced by *LRRK2* G2019S by using cultures of mDA neurons differentiated from isogenic iPSC lines. We show that targeted correction of *LRRK2* G2019S ameliorated a deficit in neurite outgrowth and a defect in basal autophagy and increased αSYN, TAU, and susceptibility to oxidative stress. In addition, we demonstrate that targeted insertion of *LRRK2* G2019S into iPSCs from a healthy donor was sufficient to recapitulate the disease phenotypes. With isogenic cultures, we were able to detect dysregulation of *Copine VIII* (*CPNE8*), *Annexin A1* (*ANXA1*), *Microtubule-associated protein 7* (*MAP7*), *Calcium-dependent activator protein for secretion 2* (*CADPS2*), and *Ubiquitin-like with PHD and ring finger domains 2* (*UHRF2*), which are involved in other neurodegenerative pathologies but have not previously been associated with PD. Pharmacological inhibition of LRRK2 kinase activity corrected these gene expression changes and rescued PD-associated phenotypes. Knockdown experiments demonstrated that dysregulation of four of these genes significantly contributed to mDA neurodegeneration under oxidative stress. Finally, we demonstrate that *LRRK2* G2019S was associated with increased activation of ERK and that inhibition of ERK ameliorated mDA neurodegeneration, neurite outgrowth, and the dysregulation of *CADPS2*, *CPNE8*, and *UHRF2*. Therefore, these results reveal molecular details for the pathogenesis of mutant *LRRK2* and possible new targets for the development of new therapeutics for patients with PD.

RESULTS

Generation and Gene Correction of iPSCs

We derived iPSCs from two patients harboring the *LRRK2* mutation G2019S (Table S1 available online). The samples used in this study were derived from two female patients with PD born in 1958 and 1931 (designated L1 and L2, respectively). As nonisogenic healthy controls, we used iPSC lines derived from four healthy women born in 1959, 1931, 1943, and 1932 (designated C1, C2, C3, and C4, respectively) (Table S1). Dermal fibroblasts from skin punch biopsies of patients with PD or healthy controls were expanded and infected with retroviral expression vectors containing the genes indicated and iPSCs were generated (Takahashi et al., 2007). Individual clonal iPSC lines derived from L1 and L2 were designated L1-1 and L2-1, respectively (Table S1).

Multiple assays were used to confirm the reprogramming of fibroblasts into all the iPSC lines used in this study. Immunostaining demonstrated that the iPSC lines expressed the pluripotent markers NANOG, OCT4, SSEA4, and TRA1-81 (Figures 1A and S1A). Real-time quantitative PCR (qRT-PCR) analysis showed that iPSCs expressed pluripotency markers at levels comparable with human embryonic stem cells (hESCs) (Figures 1B and S1B) and silencing of the retroviral vectors, which is a hallmark of bona fide iPSCs (Figure S1C; Hotta and Ellis, 2008). Pluripotent differentiation potential of each iPSC line was tested in vitro via embryoid body (EB)-mediated differentiation and in vivo via teratoma formation (Figures 1C, 1D, S2A, and S2B). Each line was verified to be euploid via microarray profiling of single-nucleotide polymorphisms.

Genome-wide association studies have revealed that multiple genetic variants are associated with PD (Simón-Sánchez et al., 2009). Therefore, given the variable phenotypes associated with specific *LRRK2* mutations, it is very likely that variants in other genetic loci modify the phenotype induced by *LRRK2* G2019S. To account for this, we gene-corrected iPSC lines from both patients to obtain three isogenic lines per patient that differed only in this mutation. A correction vector was inserted site specifically by cotransfecting it with zinc finger nucleases (ZFNs) designed to introduce a double-strand break adjacent to the G2019S mutation of the *LRRK2* gene. Because *LRRK2* mutations are inherited dominantly, our patients with PD are heterozygous for the G2019S mutation. As such, only

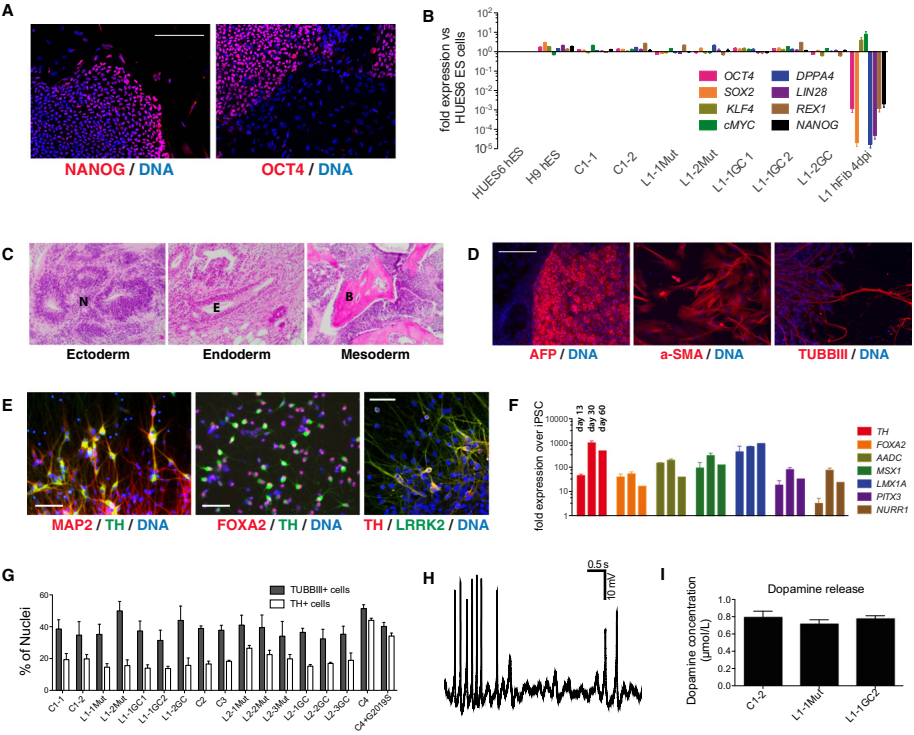

Figure 1. iPSC Line Derivation and Differentiation into Functional mDA Neurons

(A) Immunostaining for the indicated markers was performed along with nuclear counterstaining by Hoechst. See also Figure S1A.

(B) qRT-PCR analysis of the indicated iPSC lines for the expression of the indicated pluripotency markers relative to HUES6 hESCs. Fibroblasts from patient 1 at 4 days after retroviral infection are also shown. See also Figures S1B and S1C. Error bars give variation from using *GAPDH* and *BACT* as housekeeping genes.

(C) Teratomas formed from subcutaneous injection of iPSCs into immunodeficient mice were isolated and stained with hematoxylin and eosin. N, neural rosettes; E, gut-like epithelium; B, bone; M, muscle. See also Figure S2.

(D) iPSCs were differentiated in vitro via embryoid bodies and immunostained for AFP (endoderm), alpha-SMA (mesoderm), and TUBBIII (ectoderm). See also Figure S2.

(E) The differentiation protocol efficiently produces midbrain dopaminergic neurons, shown by immunostaining for TH, MAP2, and FOXA2. See also Figures S3–S5.

(F) qRT-PCR for the indicated markers on the indicated days of differentiation of the iPSC line C3. Error bars show the variation of duplicate experiments. See also Figure S3.

(G) Differentiation efficiencies for all lines, given as percentage of cells, identified by nuclei, positive for the indicated marker. n = 3–5 for each line, error bars indicate SEM.

(H) Exemplary recording of spontaneous firing of APs in current-clamp mode. See Figure S5 for further characterization.

(I) mDA neuron cultures contain mature dopamine-producing neurons, shown by dopamine release upon stimulation of the given lines. Error bars show the variance between two independent differentiation cultures. See also Figures S1–S5 as well as Tables S1 and S2.

All scale bars represent 100 µm.

half of the targeted cell lines would be expected to target the correct allele. We used DNA sequencing of iPSCs and differentiated neurons to confirm correction of the G2019S mutation (Figures S2C and S2D). As an additional experimental control, the ZFNs were used to introduce the G2019S mutation into one of the *LRRK2* loci of the control iPSC line C4, which was derived from a healthy individual. Appropriate expression of the artificially mutated allele was confirmed through quantification by pyro-sequencing with cDNA (Figure S2E). Therefore, through both patient selection and gene targeting, we have a complete set of iPSC lines to study the mechanisms of PD pathogenesis induced by mutant *LRRK2* (Table S1). All

gene-targeted subclones were fully characterized and confirmed to be euploid and pluripotent in vitro and in vivo (Figures S1 and S2).

Gene Correction Ameliorates PD-Associated Phenotypes in mDA Neurons

Because PD is characterized by the degeneration of mDA neurons, we directed the differentiation of iPSCs into this neuronal subtype. After 10 days of differentiation, we observed efficient formation of OTX2 and FOXA2 double-positive cells, which are markers of mDA neural progenitors (Figures S3A and S3B). Additional developmental markers associated with the specification of mDA neurons were detected by qRT-PCR after 13, 30, and 60 days of differentiation, including *TH*, *FOXA2*, *AADC*, *MSX1*, *LMX1A*, *PITX3*, and *NURR1* (Figures 1F, S3C, and S3D). Immunostaining demonstrated frequent formation of FOXA2 and TH as well as TH and LRRK2 double-positive cells (Figures 1E and S4). The efficiency of mDA neuron formation was approximately 20% of the total cells and 50% of all neurons after plating them as single cells on day 30 of differentiation (Figure 1G). Cultures of differentiated mDA neurons stained positively for NURR1, which is a marker of mDA neurons, as well as NeuN, MAP2, and SYNAPTOPHYSIN, which are markers of mature neurons (Figures 1E, S5A, and S5B). Analysis of electrophysiology and dopamine release upon chemical stimulation confirmed that the differentiated neurons were functionally mature after 30–35 days of differentiation (Figures 1H, 1I, and S5C–S5G).

Next, we sought to determine whether the gene correction of *LRRK2* G2019S resulted in functional phenotypic correction. Neurite shortening and sensitivity to neurotoxins are phenotypes associated with *LRRK2* G2019S (MacLeod et al., 2006; Nguyen et al., 2011; Sánchez-Danés et al., 2012). We observed a statistically significant ($p < 0.001$) reduction in the velocity of outgrowing neurites harboring *LRRK2* G2019S compared to wild-type controls (Figures 2A–2C). Targeted gene correction of *LRRK2* G2019S rescued this phenotype to a level equal to the wild-type controls (Figures 2A and 2B). Immunostaining showed that about 20% of outgrowing neurites were TH positive, suggesting that this is a general neuronal phenotype and not specific to mDA neurons (Figure 2D).

Previously, Sánchez-Danés et al. (2012), reported that *LRRK2* G2019S was associated with aberrant autophagy in neurons differentiated from iPSCs. Consistent with this report, we found that basal autophagy was significantly reduced by about 20% (Figures S6A and S6B) and increased numbers of autophagosomes were observed in cultures harboring *LRRK2* G2019S (Figures S6C). Similarly, cultures of differentiated mDA neurons were significantly more sensitive to oxidative stress when cultured in N2 medium without the supplement B27 (Figures 3 and 4A), which contains antioxidant proteins such as Catalase and Superoxide Dismutase (Brewer et al., 1993). Addition of the neurotoxins rotenone or 6-hydroxydopamine (6-OHDA) resulted in a small increase in the number of TH and cleaved CASPASE3 double-positive cells in differentiated cultures harboring *LRRK2* G2019S compared to gene-corrected isogenic controls (Figures 3, 4A, 4B, S6D, and S6E). Immunostaining showed that more than 80% of the cells positive for cleaved CASPASE3 also expressed TH (Figure 4C). To further assess the specificity of neurodegeneration, we differentiated iPSCs into peripheral sensory neurons (Greber et al., 2011), cultured them under conditions of oxidative stress, and immunostained for cleaved CASPASE3 and BRN3A, which mark apoptotic sensory neurons. Compared to mDA neurons, fewer sensory neurons were positive for cleaved CASPASE3, and there was no increase associated with *LRRK2* G2019S (Figure S6F). These results demonstrate that apoptosis was preferentially induced in mDA neurons. In another experiment, we tested whether *LRRK2* G2019S is sufficient to increase sensitivity of mDA neurons to B27 withdrawal and to 6-OHDA- and rotenone-induced toxicity. To do this, we repeated the above assays with neurons derived from the iPSC lines C4 and C4+G2019S, in which we had inserted the G2019S mutation into the *LRRK2* locus of an iPSC line derived from a healthy control. The increase in cytotoxicity was comparable in magnitude with the decrease in cytotoxicity observed after gene correction for mutant *LRRK2* iPSC lines (Figures 3A and 4A). We conclude that mutant *LRRK2* is sufficient to induce increased sensitivity of human mDA neurons to oxidative stress.

To address the question of whether the G2019S mutation results in a gain or loss of function, we repeated the cytotoxicity experiments in the presence of LRRK2-IN1, which is a small molecule inhibitor of LRRK2 kinase activity. We observed a statistically significant increase in mDA neuron survival as measured by cleaved CASPASE3 and TH in the presence of the inhibitor compared to controls (Figures 4D and S6G). A similar trend was observed when cell death was quantified by lactate dehydrogenase (LDH) release (Figures 4E and S6H). These data suggest that *LRRK2* G2019S results in a gain of kinase function, which is consistent with previous reports (Gloeckner et al., 2006; West et al., 2005). Therefore, multiple phenotypic assays confirm that gene correction of *LRRK2* G2019S resulted in functional phenotypic correction.

LRRK2 G2019S Causes PD-Associated Changes in TAU and αSYN

Because multiple lines of evidence suggest a role for TAU in PD pathogenesis, we characterized *MAPT* transcription and TAU protein levels. qRT-PCR analysis on triplicate samples on day 30 of differentiation demonstrated that *MAPT* was significantly downregulated by 39% in cultures of mDA neurons containing wild-type *LRRK2* compared with isogenic cultures with G2019S *LRRK2* (Figure 5A). Western blotting confirmed that TAU protein and phospho-Thr181 TAU were significantly lower in cultures of mDA neurons harboring gene-corrected *LRRK2* compared to isogenic cultures with *LRRK2* G2019S (Figures 5B, 5C, and S7A). Immunostaining confirmed that neurons expressing TH were also positive for TAU and phospho-TAU (Figure S7B). These data are consistent with previously published data showing a link between patients with PD, *MAPT*, and *LRRK2*. Interestingly, it has been shown that TAU enhances αSYN aggregation and toxicity (Badiola et al., 2011). It is also significant to note that increased levels of Thr181-phosphorylated TAU correlate with neurite retraction (Maldonado et al., 2008, 2011), and, as such, could contribute to the neurite outgrowth phenotype in *LRRK2* G2019S neurons.

Because αSYN pathology is present in most patients with PD harboring mutant *LRRK2*, we assessed the level of *SNCA* mRNA

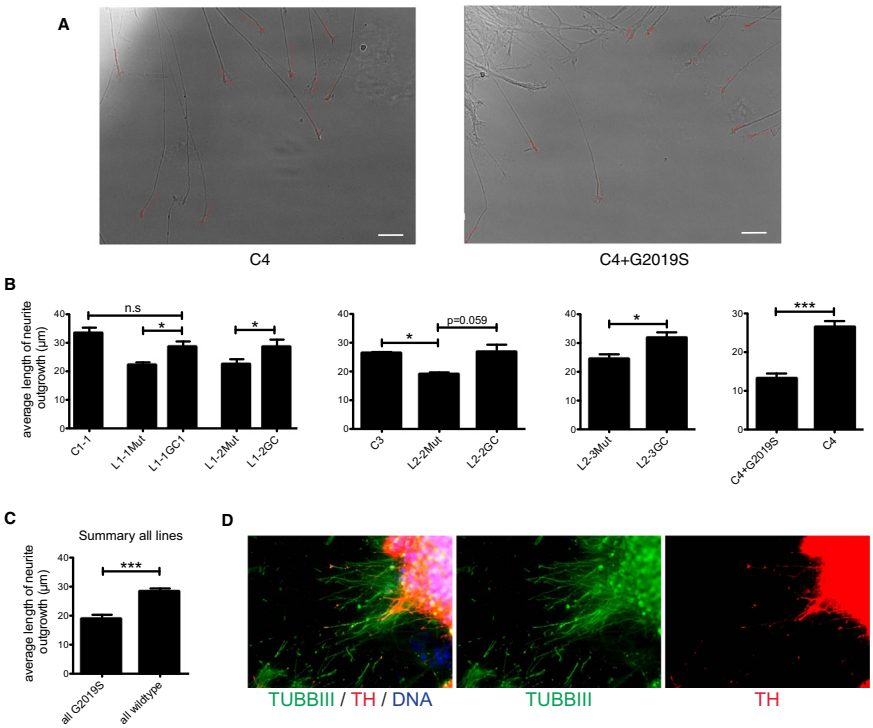

Figure 2. Gene Correction of *LRRK2* G2019S Ameliorates Neurite Outgrowth Phenotype

(A) Sample pictures from a neurite outgrowth experiment for neurons differentiated from the indicated isogenic wild-type (left) and G2019S (right) *LRRK2* iPSC line. Red dots indicate the end of the neurite, which was determined every 5 min. Scale bars represent 50 µm.

(B) Individual neurite outgrowth speeds for the indicated lines measured from triplicate cultures, Error bars represent the standard error of the mean (SEM). *$p < 0.05$, ***$p < 0.001$.

(C) When combined, the results show a significantly lower neurite outgrowth speed in neuron cultures with *LRRK2* G2019S compared to wild-type. Error bars indicate SEM.

(D) The neurite outgrowth reduction is a general neuronal phenotype, as only about 20% of the fastest outgrowing neurons are positive for TH.

and αSYN protein by mDA neurons that had been differentiated from iPSCs. qRT-PCR showed that isogenic cultures of mDA neurons differentiated for 30 and 60 days expressed comparable levels of *SNCA* (Figure 5D). Immunostaining showed that αSYN protein in neurons differentiated for 30 days displayed a punctate staining pattern that colocalized with SYNAPTOPHSYIN, which is a marker of mature neurons (Figure S5B). Western blots confirmed the presence of monomeric αSYN protein in cultures of differentiated mDA neurons (Figure 5E). Because it has been suggested that *LRRK2* G2019S results in increased levels of αSYN protein (Nguyen et al., 2011), we quantified the level of αSYN normalized to GAPDH protein levels (Figure S7A). When we initially compared all cultures of mDA neurons with either wild-type or G2019S *LRRK2* without taking into account matching lines from gene correction, we found no significant difference in αSYN protein levels between groups. In contrast, when the data was reanalyzed directly comparing the level of αSYN present in gene-corrected cultures to the respective isogenic cultures with *LRRK2* G2019S, we found that cultures of mDA neurons harboring gene-corrected *LRRK2* contained about 30% less αSYN protein, which was statistically significant, compared to cultures differentiated from isogenic G2019S *LRRK2* lines (Figure 5F). This is in agreement with human pathophysiological data, which shows extensive αSYN pathology in PD patients carrying *LRRK2* G2019S (Schiesling et al., 2008). These results are also in agreement with previously published

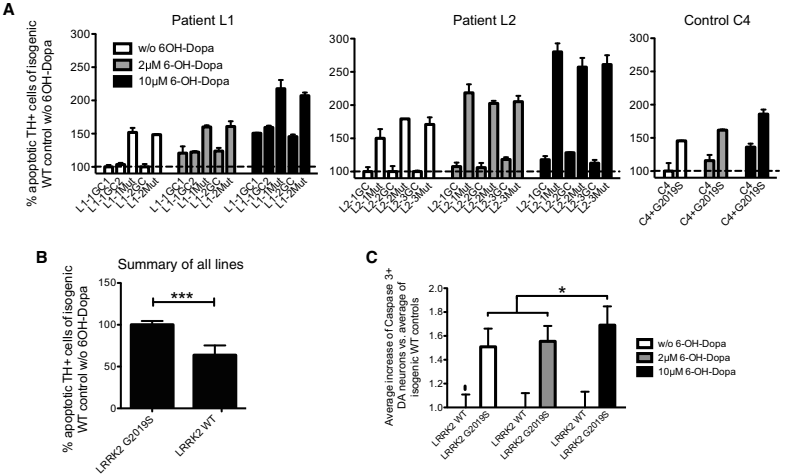

Figure 3. *LRRK2* G2019S Causes 6-Hydroxydopamine Sensitivity in Human mDA Neurons

(A) Relative frequency of cleaved CASPASE3 and TH double-positive cells after treating the mDA neurons differentiated from the indicated iPSC line with the indicated concentration of 6-OHDA in N2 medium (n = 2). Error bars represent the variation. Data are presented after normalization on the *LRRK2* WT isogenic line that was treated with N2 medium only to correct for basal level of cell death caused by replating and N2 medium alone. For individual primary results, see Figure S6. mDA neurons harboring *LRRK2* G2019S were more susceptible to apoptosis compared to wild-type when cultured only in N2 medium. The magnitude of the difference increased when 6-OHDA was added.

(B) All results together, after normalization by setting all mutant *LRRK2* cultures to 100, show that *LRRK2* G2019S causes a higher sensitivity to cytotoxic stress when comparing mutant to their isogenic wild-type samples. Error bars show the standard deviation. ***$p < 0.001$ according to t test.

(C) Treatment with 10 μM 6-OHDA leads to a faster increase of cell death in LRRK2 G2019S DA neurons, compared to the isogenic LRRK2 WT controls. *$p < 0.05$, according to the t test. Error bars indicate SEM.

results (Nguyen et al., 2011; Sánchez-Danés et al., 2012). However, we found that the difference in the level of αSYN was not significant when comparing nonisogenic cultures because of the high variation within the "healthy" neurons. This suggests that the increase in αSYN protein levels induced by *LRRK2* G2019S cannot reliably be distinguished from the variance already present in our cultures from patients without PD.

Gene Correction Enables Identification of Novel Genes Dysregulated by *LRRK2* G2019S

To identify possible changes in gene expression caused by *LRRK2* G2019S, we compared the global gene expression profile of cultures after 30 days of differentiation. Three independent hiPSC lines harboring *LRRK2* G2019S were differentiated alongside their isogenic gene-corrected hiPSC lines. In addition, two hiPSC lines derived from age- and sex-matched control patients were differentiated. RNA was harvested and analyzed with Illumina gene expression microarray on day 30 of differentiation. The cluster dendrogram demonstrated that the gene expression profiles of cultures differentiated from a hiPSC line with *LRRK2* G2019S was most closely related to its isogenic gene-corrected culture in each of the three cases (Figure 6A). In addition, we found that cultures of mDA neurons differentiated from the healthy control hiPSC line C1-1 clustered more closely to cultures differentiated from hiPSC lines derived from patient 2 than to those from patient 1. This was unexpected because the donor for hiPSC line C1-1 was age and gender matched to patient 1. Moreover, the gene expression of cultures differentiated from control line C2, which was derived from a patient age and gender matched to patient 2, was significantly different from all other samples. This clearly shows that derivation of hiPSC lines from patients that are age and gender matched does not result in closely related gene expression patterns after differentiation even though the overall differentiation efficiencies were comparable between all hiPSC lines. In contrast, gene correction resulted consistently in extremely similar expression patterns with the isogenic *LRRK2* G2019S hiPSC line after differentiation. Given the large effect of genetic background on gene expression, our data suggest that it is possible to detect changes specifically associated with *LRRK2* G2019S only through gene correction.

To gain further mechanistic insight into the development of *LRRK2*-related phenotypes, we sought to identify genes whose expression levels were changed by the presence of *LRRK2* G2019S. By using our previous global gene expression profiles, we filtered for genes that were expressed at a minimum threshold level and either up- or downregulated by at least 1.2-fold in the same direction in all three cultures of mDA neurons

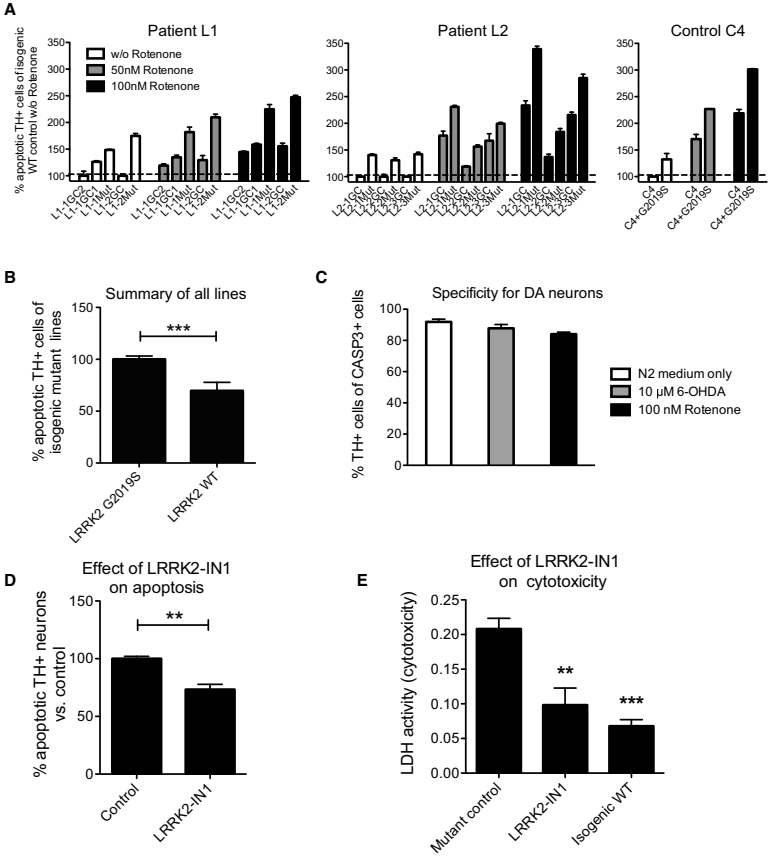

Figure 4. Gene Correction of *LRRK2* G2019S Ameliorates Sensitivity of Human mDA Neurons to Rotenone

(A) Relative frequency of cleaved CASPASE3 and TH double-positive cells after treating the mDA neurons of the indicated lines with the indicated concentration of rotenone in N2 medium (n = 2). Error bars represent the variation. Data are normalized to the *LRRK2* WT isogenic line treated with N2 medium alone. mDA neurons harboring *LRRK2* G2019S were more susceptible to apoptosis compared to wild-type when cultured in only N2 medium. The magnitude of the difference increased when rotenone was added.

(B) *LRRK2* G2019S causes a higher sensitivity to cytotoxic stress when compared with the wild-type isogenic line caused by rotenone. Error bars show the standard deviation. These are combined data for isogenic lines L1-1, L1-2, L2-2, L2-3, and C4 at all concentrations used.

(C) Cleaved CASPASE3 was preferentially in cells expressing TH after treatment with the indicated conditions. Error bars indicate variation.

(D and E) 1.5 μM LRRK2-IN1, which inhibits LRRK2 kinase activity, rescued mDA neurons from apoptosis. Cultures were differentiated in triplicate from L1-1Mut and C4+G2019S, stressed with 50 nM rotenone, and immunostaining for cleaved CASPASE3 and TH double-positive cells (D) and LDH release (E) compared to DMSO-treated controls. Error bars indicate SEM.

**p < 0.01 and ***p < 0.001 according to t test. See also Figure S6.

differentiated for 30 days from hiPSCs containing *LRRK2* G2019S compared to gene-corrected *LRRK2*. Subsequently, we differentiated these and additional hiPSC lines in independent triplicate cultures for 30 days followed by qRT-PCR validation. Six genes could be corroborated by further samples by qRT-PCR as significantly and consistently dysregulated

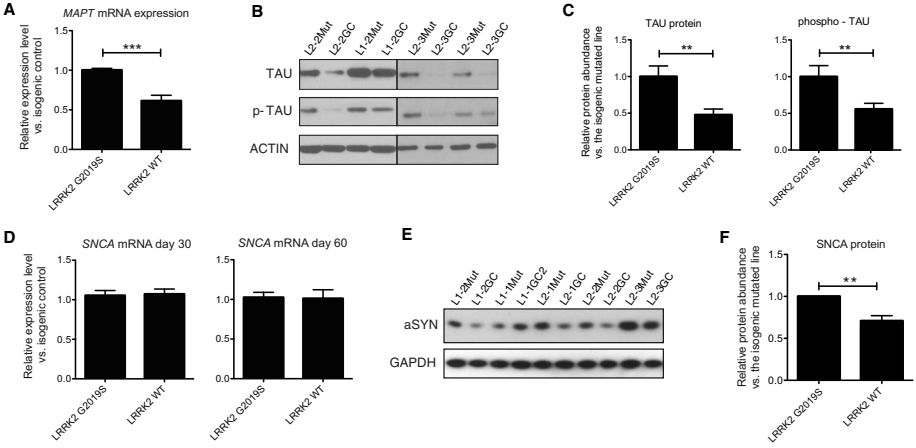

Figure 5. *LRRK2* G2019S Mutation Leads to Increased Expression of *MAPT* mRNA and TAU Protein as well as Increased αSYN Protein

(A) *MAPT* mRNA levels are significantly decreased when comparing triplicate cultures differentiated from *LRRK2* wild-type to isogenic mutant lines. n = 6 lines wild-type, n = 5 mutant, including C4 and C4+G2019S.

(B) Representative western blot results for the given mDA neuron cultures. Independent replicate experiments are shown for lines L2-3Mut and L2-3GC.

(C) Reduced TAU and phospho-TAU (Thr181) protein is found in cultures differentiated from *LRRK2* wild-type compared to isogenic mutant lines. This is an average of individual results shown in Figure S7.

(D) No change in expression is detected by qRT-PCR analysis of *SNCA* expression in mDA neuron cultures differentiated in independent replicate cultures comparing all targeted lines to their isogenic mutant line. n = 3–5 for each line at day 30, n = 2–3 for each line at day 60 of differentiation.

(E) Representative western blot results for the given mDA neuron cultures for αSYN protein showing lower levels in wild-type compared to isogenic mutant samples. αSYN protein levels were normalized using GAPDH as a housekeeping gene.

(F) Average αSYN protein abundance showing a significant decrease in gene-corrected lines compared to their mutant isogenic lines. n = 9, individual results are shown in Figure S7.

Error bars indicate SEM in all panels. *$p < 0.05$, **$p < 0.01$, ***$p < 0.001$ according to t test.

by *LRRK2* G2019S in cultures of mDA neurons. The first four that we identified were *CPNE8, ANXA1*, *MAP7*, and *CADPS2*, which were downregulated by about 38%, 40%, 30%, and 29%, respectively, in cultures of mDA neurons harboring gene-corrected *LRRK2* compared to isogenic cultures with the G2019S mutation (Figure 6B). In addition, we identified *UHRF2* as significantly upregulated by 16% in cultures of mDA neurons harboring gene-corrected *LRRK2* compared with the isogenic cultures with the G2019S mutation (Figure 6B). To confirm the effect of *LRRK2* G2019S on the expression of these genes, we repeated the experiment with cultures differentiated from the hiPSC line C4, which was derived from a healthy control patient, and from the hiPSC line C4-G2019S, in which the mutation G2019S had been specifically introduced into one endogenous *LRRK2* allele. The results were consistent with the gene-corrected cultures (Figure 6C). Western blotting demonstrated that protein levels of CPNE8, CADPS2, ANXA1, and MAP7 were significantly altered in cultures with mutant *LRRK2* compared with isogenic controls (Figures 6D and 6E). *UHRF2* was lower in *LRRK2* G2019S samples compared with isogenic controls with a p value of 0.0533 (Figures 6D and 6E). Inhibition of LRRK2 kinase activity with LRRK2-IN1 rescued the dysregulation of these genes (Figure S6I). Therefore, isogenic cultures enabled the detection of multiple genes that were specifically dysregulated by *LRRK2* G2019S.

Knockdown experiments were used to assess the contributions of *CPNE8*, *ANXA1*, *MAP7*, *CADPS2*, and *UHRF2* to mDA neurodegeneration under oxidative stress. Cultures of mDA neurons differentiated from iPSC line L1-1Mut were treated with Accell siRNA SMARTpool targeting one of the identified dysregulated genes. qRT-PCR demonstrated that the target gene expression was decreased by 50%–80% (Figure 6F). After exposure to oxidative stress via B27 withdrawal alone or in combination with 50 nM rotenone, neurodegeneration was assessed by LDH release and double-immunostaining for cleaved CASPASE3 and TH. We found that knockdown of *CPNE8*, *CADPS2*, and *MAP7* resulted in a statistically significant decrease in the number of cleaved CASPASE3 and TH double-positive neurons (Figures 6G and 6H). In contrast, we found that knockdown of *UHRF2* resulted in small, but significant, increase in the number of cleaved CASPASE3 and TH double-positive neurons (Figures 6G and 6H). No significant change was observed with the knockdown of *ANXA1* (Figures 6G and 6H). Knockdown of *CPNE8*, *CADPS2*, and *MAP7* was also protective when we used LDH release as a measure of cytotoxicity (Figures S6J and S6K). These results demonstrate that the upregulation of *CPNE8*,

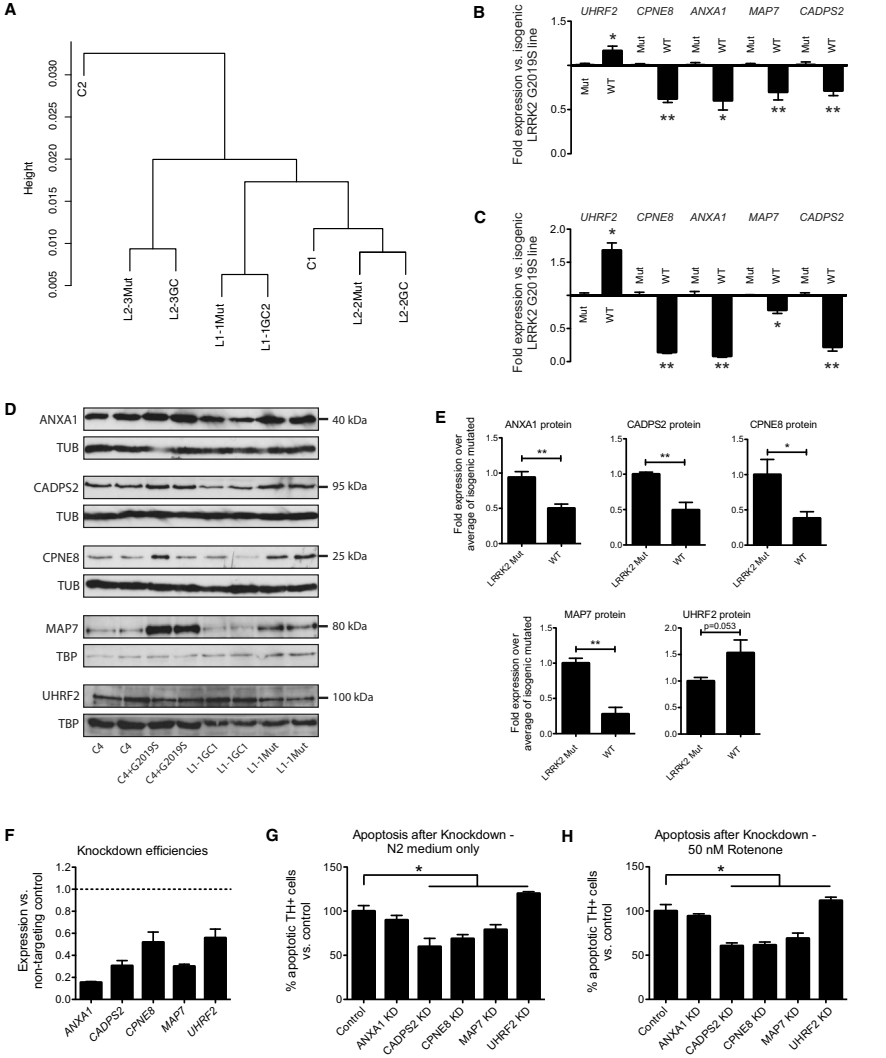

Figure 6. Identification and Validation of Novel Genes Contributing to PD-Associated Phenotypes Induced by *LRRK2* G2019S

(A) Cluster analysis of the whole-genome expression profile after 30 days differentiation of the indicated cell lines. Only isogenic iPSC lines give extremely comparable differentiation outcome. Interestingly, C1 clusters closer to L2 and C2 closer to L1, which is opposite to their matches based upon age and gender.

(B) Candidate genes dysregulated by *LRRK2* G2019S from the microarray data were validated by qRT-PCR on mDA neuronal cultures differentiated for 30 days in triplicates from isogenic hiPSC lines L1-1Mut with L1-1GC1 and L1-1GC2, L1-2Mut and L1-2GC, L2-2Mut and L2-2GC, L2-3Mut and L2-3GC.

(C) hiPSC line C4 and the isogenic line C4+G2019S were differentiated and analyzed by qRT-PCR for the candidate genes. Error bars represent SEM.

(legend continued on next page)

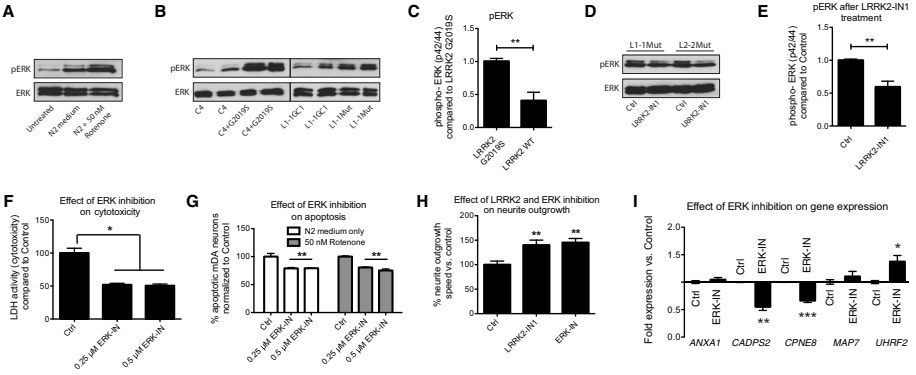

Figure 7. *LRRK2* G2019S Causes Increased ERK Phosphorylation that Is Responsible for Some of the Observed Phenotypes

(A) Western blot for phosphorylated ERK1/2 (pERK) and ERK1/2 (ERK) on neurons differentiated for 30 days and cultured under the indicated conditions for 2 days.

(B) Representative western blot images of pERK and ERK of mDA neuronal cultured differentiated in duplicate for 30 days from the indicated lines.

(C) Quantification of the data from (B) showing significantly increased pERK in cultures harboring *LRRK2* G2019S compared to isogenic controls.

(D) Representative western blot for the indicated marker for differentiated cultures from the indicated lines treated for 6 days with 1.5 μM LRRK2-IN1 alongside the DMSO-treated control.

(E) Quantification of the effect of LRRK2-IN1 on pERK with lines L1-1Mut, L2-2Mut, L2-3Mut, and C4+G2019S in duplicates of treatment, alongside their DMSO-treated controls for 6 days.

(F and G) mDA cultures of the line L1-1Mut at day 30 of differentiation were treated for 2 days with PD0325901 (ERK-IN), an ERK phosphorylation-inhibitor, at the given concentrations, which reduced cytotoxicity from stress with 50 nM rotenone as measured by LDH release (F) and cleaved CASPASE3 and TH double-positive cells (G) compared to DMSO-treated controls.

(H) Neurite outgrowth assay on neurons differentiated for 30 days and treated with the indicated compounds compared to DMSO-treated controls.

(I) qRT-PCR for the indicated genes on neurons differentiated for 30 days and treated with ERK-IN relative to DMSO-treated controls.

*p < 0.05, **p < 0.01, ***p < 0.001 according to t test. Error bars represent SEM in all panels.

CADPS2, and *MAP7* by *LRRK2* G2019S contributes to the mDA neurodegenerative phenotype observed. The small, but significant, increase in mDA degeneration resulting from *UHRF2* knockdown is consistent with the small decrease in *UHRF2* expression observed in cultures with *LRRK2* G2019S. Western blotting after knockdown of MAP7 reduced αSYN by about 50% in cultures differentiated from iPSCs harboring *LRRK2* G2019S (Figures S7C and S7D). Knockdown of *CADP2* and *CPNE8* had mildly reduced αSYN, but knockdown of *UHRF2* and *ANXA1* had no effect (Figures S7C and S7D).

Higher Sensitivity of *LRRK2* G2019S Neurons to Oxidative Stress Involves the Activation of ERK

Previously, it was shown that *LRRK2* G2019S causes abnormalities in basal autophagy in fibroblasts through activation of ERK1/2 (ERK) (Bravo-San Pedro et al., 2013). In addition, neurite shortening by *LRRK2* G2019S has been linked to ERK signaling (Plowey et al., 2008). For these reasons, we performed western blotting to quantify the level of phosphorylated ERK1/2 (pERK), which is the active form of ERK. Cultures of mDA neurons had increased pERK levels after B27 withdrawal compared to controls, and addition of rotenone further increased levels of pERK (Figure 7A). Untreated mDA cultures harboring wild-type *LRRK2* had 50% less pERK compared to isogenic cultures with *LRRK2* G2019S (Figures 7B and 7C). When cultures of mDA neurons were treated with LRRK2-IN1, pERK levels were significantly decreased by more than 40% (Figures 7D and 7E). Treatment with PD0325901 (hereafter ERK-IN), an inhibitor of ERK phosphorylation, rescued cultures of mDA neurons from degeneration and reduced overall

(D) Representative western blot pictures for the newly identified genes from the indicated lines taken at day 30 of duplicate differentiation cultures from the indicated isogenic lines. TBP and α-TUBULIN (TUB) were used as loading controls.

(E) Densitometric quantification of the western blots from (D). For ANXA1 and CADPS2, duplicate cultures differentiated from L2-2Mut and L2-3Mut were additionally used. Error bars indicate SEM.

(F) Knockdown efficiency was determined by qRT-PCR for the indicated genes normalized to nontargeting controls in mDA neuron cultures differentiated for 30 days from the line L1-1Mut. Error bars show the variance from two parallel cultures.

(G and H) Knockdown of *CADPS2, CPNE8, MAP7,* and *UHRF2* but not *ANXA1* had a significant effect on the sensitivity of mDA neurons when treated with N2 medium alone (G) or N2 supplemented with 50 nM rotenone (H), as measured by the amount of cleaved CASPASE3 and TH double-positive neurons. Error bars represent SEM.

*p < 0.05 and **p < 0.01 according to t test.

cytotoxicity when treated with oxidative stress (Figures 7F and 7G). Finally, ERK-IN and LRRK2-IN1 increased neurite outgrowth of differentiated neurons compared to DMSO-treated controls (Figure 7H). Therefore, *LRRK2* G21019S leads to activation of ERK, which contributes to the mDA neurodegenerative phenotype observed in vitro.

We next tested whether activation of ERK contributed to the dysregulation of our newly identified genes. To do this, qRT-PCR was performed on cultures of mDA neurons treated with ERK-IN for 4 days. We observed that expression of *CADPS2, CPNE8*, and *UHRF2* was significantly altered by ERK inhibition in the opposite direction compared to that induced by *LRRK2* G2019S (Figure 7I). Taken together, these results suggest that *CADPS2, CPNE8*, and *UHRF2* expression is dysregulated by *LRRK2* G2019S through aberrant ERK activation. However, the results for *ANXA1* and *MAP7* suggest that *LRRK2* G2019S might also contribute to PD phenotypes through additional mechanisms.

DISCUSSION

Reprogramming is a breakthrough technology that enables the generation of patient-specific stem cells. By using patients with PD-causing mutations, such as *LRRK2* G2019S, it is possible to derive iPSCs that recapitulate aspects of PD pathology (Nguyen et al., 2011; Sánchez-Danés et al., 2012). However, because of variance in genetic backgrounds, which is likely to arise from polymorphisms in other genes, each individual might behave differently with respect to a given mutation. Recently, Liu et al. (2012) reported the derivation of iPSCs from PD patients harboring *LRRK2* G2019S as well as isogenic gene-corrected controls. The authors demonstrated phenotypic changes in the nuclear envelope. Although interesting, these changes lack a clear causal link to PD pathogenesis. In addition, the authors studied primitive neural stem cells, which are most closely related to cells present in early post-implantation-stage embryos that are not present in fetuses, neonates, or adults (Hitoshi et al., 2004; Liu et al., 2012). Therefore, there is still significant potential for gene-corrected iPSCs to elucidate the molecular mechanisms underlying PD pathogenesis in mDA neurons.

Here, we have demonstrated that neurons differentiated from iPSCs derived from patients with PD harboring *LRRK2* G2019S exhibit multiple phenotypes including reduced neurite outgrowth and increased sensitivity to stress. By using gene-corrected isogenic cultures and the introduction of the mutation into a control iPSC line, we show that these phenotypes were specifically associated with *LRRK2* G2019S. Because an inhibitor of LRRK2 kinase activity ameliorated these phenotypes, the G2019S mutation probably results in increased kinase activity, which is consistent with previous reports (Gloeckner et al., 2006; West et al., 2005).

Gene correction enabled the discovery of genes that contribute to PD-associated phenotypes in cultured mDA neurons induced by *LRRK2* G2019S. Expression profiling of multiple pairs of isogenic cultures resulted in the identification of a handful of genes that were consistently dysregulated by *LRRK2* G2019S including *CPNE8*, *CADPS2*, *MAP7*, and *UHRF2*. Western blotting confirmed differences in the level of protein, and siRNA experiments demonstrated that this dysregulation contributed to mDA degeneration.

Interestingly, these genes have previously been implicated in neurodegenerative phenotypes in multiple ways. Polymorphisms in *CPNE8* have been shown to affect the incubation time of prion disease in mice (Lloyd et al., 2010). Interestingly, PD has been proposed to be a prion-like disease involving αSYN (Polymenidou and Cleveland, 2012). We could confirm previous reports of increased levels of αSYN with mutant *LRRK2* (Nguyen et al., 2011; Sánchez-Danés et al., 2012). It is possible that the reported defects in autophagy induced by *LRRK2* G2019S contribute to the increased level of αSYN protein because there is no detectable increase in *SNCA* transcription.

UHRF2 is an E3 ubiquitin ligase with the same catalytic activity as *PARKIN*. Because loss-of-function mutations in *PARKIN* cause PD, the downregulation of *UHRF2* in cultures of mDA neurons containing the PD-associated mutation *LRRK2* G2019S is significant. In addition, UHRF2 has previously been shown to enhance clearance of polyglutamine aggregates, which cause neurodegeneration in several diseases (Iwata et al., 2009). It is tempting to speculate that UHRF2 could play a similar role for αSYN. Consequently, the increased levels of CPNE8 and αSYN and decreased levels of UHRF2 proteins suggest that *LRRK2* G2019S could act on multiple mechanisms to increase the initiation of synucleinopathy.

CADPS2 dysregulation also has potentially significant implications for mDA neurodegeneration. The protein CADPS2 has been demonstrated to regulate the neurotransmission of monoamines, of which dopamine is an example (Brunk et al., 2009). This is of interest because transgenic mice overexpressing *LRRK2* variants show dysregulation of dopamine release (Li et al., 2010). Dopamine is thought to increase oxidative stress in mDA neurons through the formation of reactive metabolites (Napolitano et al., 2011). Consequently, dysregulation of *CADPS2* by *LRRK2* G2019S could result in aberrant formation of toxic metabolites. Consistent with this idea, increased oxidative stress, for example by administration of rotenone, is known to induce PD-like pathogenesis and induced mDA-specific neurodegeneration in vitro in our differentiated hiPSC cultures (Inden et al., 2011).

Because LRRK2 is not a transcription factor, additional proteins probably mediate the transcriptional dysregulation we observed. We have shown that *LRRK2* G2019S resulted in increased phosphorylation of ERK in cultures of human mDA neurons. Inhibition of ERK activity rescued mDA neurons in our system, which suggests that ERK activity is crucial for the pathogenesis of mutant LRRK2. Two previously published reports could account for the link of LRRK2 with ERK. First, Ste20 family kinases, which are upstream of ERK and are induced by stress, are phosphorylated by LRRK2 protein (Zach et al., 2010). Second, it has been shown that Endophilin A1 is directly phosphorylated by LRRK2 (Matta et al., 2012). Consistent with this finding, knockdown of Endophilin A1 resulted in decreased ERK activation by BDNF (Fu et al., 2011). It is also significant to note that the autophagy defect caused by LRRK2 has also been linked to ERK activity (Bravo-San Pedro et al., 2013). Taken together, our results suggest possible targets for the development of new therapeutics for patients with PD.

EXPERIMENTAL PROCEDURES

Generation of Induced Pluripotent Stem Cells

Informed consent was obtained from all patients involved in our study prior to cell donation. The Ethics Committee of the Medical Faculty and the University Hospital Tübingen previously approved this consent form. Dermal fibroblasts, obtained from skin biopsies of patients with PD and healthy controls, were cultured. Reprogramming was adapted from Takahashi et al. (2007). Human iPSCs were cultured on mitomycin C (Tocris)-inactivated MEFs. Gene correction was performed by nucleofection of ZFN constructs targeting LRRK2 (Sigma). 50 μg/ml G418 (PAA) 2 μM ganciclovir (Sigma)-resistant colonies were picked and clonally expanded on MEFs.

iPSC Differentiation into mDA Neurons

mDA neurons were generated via adapted protocol (Chambers et al., 2009; Nguyen et al., 2011). Confluent iPSCs were cultured with 1 μM dorsomorphin (Tocris), 10 μM SB431542, and 0.5 μM purmorphamine (PMA, Alexis). mDA patterning was performed with N2 medium supplemented with 0.5 μM PMA, 100 ng/ml human FGF8, 20 ng/ml human BDNF (both Peprotech), and 200 μM ascorbic acid (AA, Sigma). Maturation was induced by culturing with BDNF, AA, GDNF, TGF-β, and dbcAMP. mDA neuron differentiation cultures were replated as single cells on about day 30 on Matrigel-coated 48-well plates.

Protein Analysis

Cell pellets of differentiated neurons were extracted with RIPA-Buffer containing protease inhibitors (Mini complete, Roche) on ice. Supernatant were mixed with 6× Laemmli buffer. 15 μg of the protein lysate were loaded on a 4%–12% gel (NuPAGE, Invitrogen) after incubation at 95°C for 5 min and then blotted on a PVDF membrane. The membrane was blocked and incubated with the indicated primary antibodies (listed in Supplemental Information). After 3× washing, the blot was incubated with HRP coupled secondary antibody. The membrane was washed and then developed with chemiluminescent HRP substrate solution (Millipore, GE). Protein bands were standardized on GAPDH, TBP, β-actin, or α-TUBULIN.

Quantification of the Cytotoxicity of 6-OHDA and Rotenone

mDA neuron differentiation cultures on days 27–35 were disaggregated and plated as single cells. 2 days later, cultures were fed with N2 medium without supplements for 6 hr. This medium was replaced with warm N2 medium supplemented with 10 μM 6-OHDA, 2 μM 6-OHDA, 50 nM rotenone, or 100 nM rotenone and incubated for 48 hr. Afterwards, the cell cultures were fixed and stained.

Quantitative RT-PCR

Total RNA was isolated from cell culture samples with RNeasy columns (QIAGEN) including on-column DNA digestion. cDNA was prepared with oligo-dT16 primers (Metabion) and M-MLV reverse transcriptase (USB). Cycling was carried out on an ABI 7300 Real-Time PCR system. Relative expression levels were calculated via the $2^{-2\Delta}$ method, based on biological reference samples and housekeeping genes for normalization. Primer sequences are listed in Table S2.

Whole-Genome Expression Analysis

DNA-free total RNA samples (500 ng) to be hybridized on Illumina human-12 V3 expression BeadChips were processed with a linear amplification kit (Ambion) generating biotin-labeled cRNA (IVT duration: 14 hr). Raw data were background subtracted and normalized via the "cubic spline" algorithm. Data analysis was done with MS Excel and R (Bioconductor, pvclust).

Gene Knockdown

Self-transfecting Accell siRNA (nontargeting green fluorescent control, *ANXA1*, *CADPS2*, *CPNE8*, *MAP7*, *UHRF2*; Thermo) SMARTPool are mixtures of four siRNAs targeting a single gene. siRNA was diluted in maturation medium and added to the cells twice every other day (for RNA extraction). For the cytotoxicity experiments, siRNA was added starting 2 days before reseeding, during reseeding, and 2 days later during the stressing procedure.

Inhibitor Treatment

For RNA and protein sample isolation, mDA neuron cultures were treated with maturation medium supplemented with 1.5 μM LRRK2-IN1 for 6 days and 0.5 μM PD0325901 (both Merck) for 2–4 days and compared to DMSO alone. Medium was changed every other day. For determining neural survival, cultures were treated starting 2 days before reseeding.

ACCESSION NUMBERS

The data have been deposited in GEO at NCBI under the accession number GSE43364.

SUPPLEMENTAL INFORMATION

Supplemental Information includes Supplemental Experimental Procedures, seven figures, and two tables and can be found with this article online at http://dx.doi.org/10.1016/j.stem.2013.01.008.

ACKNOWLEDGMENTS

This work was supported by grants from the German Research (WO 1610/2-1 to M.M. and T.G.; KR2119/8-1 to R.K. and T.G.); Fortuene (Nr. 1831-0-0-0-0 to M.M.); the German Research Council (DFG, KR2119/8-1 to R.K. and T.G.); Fritz Thyssen Foundation (10.11.2.153 to R.K.); the Michael J. Fox Foundation (LRRK2 Biology LEAPS Award, 2012); and by a doctoral scholarship from the charitable Hertie Foundation (to L.F.B.). Plasmids for reprogramming were obtained from Addgene: Addgene plasmids 8449, 8454, 17217, 17218, 17219, and 17220. We would like to acknowledge Ann-Kathrin Hauser for the sequencing analysis. We would like to thank Kerstin Hergarten and Rhea Brintrup for excellent technical support.

Received: August 21, 2012
Revised: December 6, 2012
Accepted: January 11, 2013
Published: March 7, 2013

REFERENCES

Badiola, N., de Oliveira, R.M., Herrera, F., Guardia-Laguarta, C., Gonçalves, S.A., Pera, M., Suárez-Calvet, M., Clarimon, J., Outeiro, T.F., and Lleó, A. (2011). Tau enhances α-synuclein aggregation and toxicity in cellular models of synucleinopathy. PLoS ONE *6*, e26609.

Berg, D., Schweitzer, K.J., Leitner, P., Zimprich, A., Lichtner, P., Belcredi, P., Brüssel, T., Schulte, C., Maass, S., Nägele, T., et al. (2005). Type and frequency of mutations in the LRRK2 gene in familial and sporadic Parkinson's disease*. Brain *128*, 3000–3011.

Botta-Orfila, T., Ezquerra, M., Pastor, P., Fernández-Santiago, R., Pont-Sunyer, C., Compta, Y., Lorenzo-Betancor, O., Samaranch, L., Martí, M.J., Valldeoriola, F., et al. (2012). Age at onset in LRRK2-associated PD is modified by SNCA variants. J. Mol. Neurosci. *48*, 245–247.

Bravo-San Pedro, J.M., Niso-Santano, M., Gomez-Sanchez, R., Pizarro-Estrella, E., Aiastui-Pujana, A., Gorostidi, A., Climent, V., Lopez de Maturana, R., Sanchez-Pernaute, R., Lopez de Munain, A., et al. (2013). The LRRK2 G2019S mutant exacerbates basal autophagy through activation of the MEK/ERK pathway. Cell. Mol. Life Sci. *70*, 121–136.

Brewer, G.J., Torricelli, J.R., Evege, E.K., and Price, P.J. (1993). Optimized survival of hippocampal neurons in B27-supplemented Neurobasal, a new serum-free medium combination. J. Neurosci. Res. *35*, 567–576.

Brunk, I., Blex, C., Speidel, D., Brose, N., and Ahnert-Hilger, G. (2009). Ca2+-dependent activator proteins of secretion promote vesicular monoamine uptake. J. Biol. Chem. *284*, 1050–1056.

Carballo-Carbajal, I., Weber-Endress, S., Rovelli, G., Chan, D., Wolozin, B., Klein, C.L., Patenge, N., Gasser, T., and Kahle, P.J. (2010). Leucine-rich repeat kinase 2 induces alpha-synuclein expression via the extracellular signal-regulated kinase pathway. Cell. Signal. *22*, 821–827.

Chambers, S.M., Fasano, C.A., Papapetrou, E.P., Tomishima, M., Sadelain, M., and Studer, L. (2009). Highly efficient neural conversion of human ES and iPS cells by dual inhibition of SMAD signaling. Nat. Biotechnol. *27*, 275–280.

Cookson, M.R. (2010). The role of leucine-rich repeat kinase 2 (LRRK2) in Parkinson's disease. Nat. Rev. Neurosci. *11*, 791–797.

Cookson, M.R., Hardy, J., and Lewis, P.A. (2008). Genetic neuropathology of Parkinson's disease. Int. J. Clin. Exp. Pathol. *1*, 217–231.

European Brain Council (2011). Parkinson's disease Fact Sheet. http://www.europeanbraincouncil.org/pdfs/Documents/Parkinson%27s%20fact%20sheet%20July%202011.pdf.

Fu, X., Yang, Y., Xu, C., Niu, Y., Chen, T., Zhou, Q., and Liu, J.J. (2011). Retrolinkin cooperates with endophilin A1 to mediate BDNF-TrkB early endocytic trafficking and signaling from early endosomes. Mol. Biol. Cell *22*, 3684–3698.

Gloeckner, C.J., Kinkl, N., Schumacher, A., Braun, R.J., O'Neill, E., Meitinger, T., Kolch, W., Prokisch, H., and Ueffing, M. (2006). The Parkinson disease causing LRRK2 mutation I2020T is associated with increased kinase activity. Hum. Mol. Genet. *15*, 223–232.

Golub, Y., Berg, D., Calne, D.B., Pfeiffer, R.F., Uitti, R.J., Stoessl, A.J., Wszolek, Z.K., Farrer, M.J., Mueller, J.C., Gasser, T., and Fuchs, J. (2009). Genetic factors influencing age at onset in LRRK2-linked Parkinson disease. Parkinsonism Relat. Disord. *15*, 539–541.

Greber, B., Coulon, P., Zhang, M., Moritz, S., Frank, S., Müller-Molina, A.J., Araúzo-Bravo, M.J., Han, D.W., Pape, H.C., and Schöler, H.R. (2011). FGF signalling inhibits neural induction in human embryonic stem cells. EMBO J. *30*, 4874–4884.

Hitoshi, S., Seaberg, R.M., Koscik, C., Alexson, T., Kusunoki, S., Kanazawa, I., Tsuji, S., and van der Kooy, D. (2004). Primitive neural stem cells from the mammalian epiblast differentiate to definitive neural stem cells under the control of Notch signaling. Genes Dev. *18*, 1806–1811.

Hotta, A., and Ellis, J. (2008). Retroviral vector silencing during iPS cell induction: an epigenetic beacon that signals distinct pluripotent states. J. Cell. Biochem. *105*, 940–948.

Inden, M., Kitamura, Y., Abe, M., Tamaki, A., Takata, K., and Taniguchi, T. (2011). Parkinsonian rotenone mouse model: reevaluation of long-term administration of rotenone in C57BL/6 mice. Biol. Pharm. Bull. *34*, 92–96.

Ishizawa, T., Mattila, P., Davies, P., Wang, D., and Dickson, D.W. (2003). Colocalization of tau and alpha-synuclein epitopes in Lewy bodies. J. Neuropathol. Exp. Neurol. *62*, 389–397.

Iwata, A., Nagashima, Y., Matsumoto, L., Suzuki, T., Yamanaka, T., Date, H., Deoka, K., Nukina, N., and Tsuji, S. (2009). Intranuclear degradation of polyglutamine aggregates by the ubiquitin-proteasome system. J. Biol. Chem. *284*, 9796–9803.

Li, X., Patel, J.C., Wang, J., Avshalumov, M.V., Nicholson, C., Buxbaum, J.D., Elder, G.A., Rice, M.E., and Yue, Z. (2010). Enhanced striatal dopamine transmission and motor performance with LRRK2 overexpression in mice is eliminated by familial Parkinson's disease mutation G2019S. J. Neurosci. *30*, 1788–1797.

Lin, X., Parisiadou, L., Gu, X.L., Wang, L., Shim, H., Sun, L., Xie, C., Long, C.X., Yang, W.J., Ding, J., et al. (2009). Leucine-rich repeat kinase 2 regulates the progression of neuropathology induced by Parkinson's-disease-related mutant alpha-synuclein. Neuron *64*, 807–827.

Liu, G.H., Qu, J., Suzuki, K., Nivet, E., Li, M., Montserrat, N., Yi, F., Xu, X., Ruiz, S., Zhang, W., et al. (2012). Progressive degeneration of human neural stem cells caused by pathogenic LRRK2. Nature *491*, 603–607.

Lloyd, S.E., Maytham, E.G., Grizenkova, J., Hummerich, H., and Collinge, J. (2010). A Copine family member, Cpne8, is a candidate quantitative trait gene for prion disease incubation time in mouse. Neurogenetics *11*, 185–191.

MacLeod, D., Dowman, J., Hammond, R., Leete, T., Inoue, K., and Abeliovich, A. (2006). The familial Parkinsonism gene LRRK2 regulates neurite process morphology. Neuron *52*, 587–593.

Maldonado, H., Ortiz-Riaño, E., Krause, B., Barriga, A., Medina, F., Pando, M.E., Alberti, C., Kettlun, A.M., Collados, L., García, L., et al. (2008). Microtubule proteins and their post-translational forms in the cerebrospinal fluid of patients with paraparesis associated with HTLV-I infection and in SH-SY5Y cells: an in vitro model of HTLV-I-induced disease. Biol. Res. *41*, 239–259.

Maldonado, H., Ramírez, E., Utreras, E., Pando, M.E., Kettlun, A.M., Chiong, M., Kulkarni, A.B., Collados, L., Puente, J., Cartier, L., and Valenzuela, M.A. (2011). Inhibition of cyclin-dependent kinase 5 but not of glycogen synthase kinase 3-β prevents neurite retraction and tau hyperphosphorylation caused by secretable products of human T-cell leukemia virus type I-infected lymphocytes. J. Neurosci. Res. *89*, 1489–1498.

Matta, S., Van Kolen, K., da Cunha, R., van den Bogaart, G., Mandemakers, W., Miskiewicz, K., De Bock, P.J., Morais, V.A., Vilain, S., Haddad, D., et al. (2012). LRRK2 controls an EndoA phosphorylation cycle in synaptic endocytosis. Neuron *75*, 1008–1021.

Napolitano, A., Manini, P., and d'Ischia, M. (2011). Oxidation chemistry of catecholamines and neuronal degeneration: an update. Curr. Med. Chem. *18*, 1832–1845.

Nguyen, H.N., Byers, B., Cord, B., Shcheglovitov, A., Byrne, J., Gujar, P., Kee, K., Schüle, B., Dolmetsch, R.E., Langston, W., et al. (2011). LRRK2 mutant iPSC-derived DA neurons demonstrate increased susceptibility to oxidative stress. Cell Stem Cell *8*, 267–280.

Ozelius, L.J., Senthil, G., Saunders-Pullman, R., Ohmann, E., Deligtisch, A., Tagliati, M., Hunt, A.L., Klein, C., Henick, B., Hailpern, S.M., et al. (2006). LRRK2 G2019S as a cause of Parkinson's disease in Ashkenazi Jews. N. Engl. J. Med. *354*, 424–425.

Paisán-Ruíz, C., Jain, S., Evans, E.W., Gilks, W.P., Simón, J., van der Brug, M., López de Munain, A., Aparicio, S., Gil, A.M., Khan, N., et al. (2004). Cloning of the gene containing mutations that cause PARK8-linked Parkinson's disease. Neuron *44*, 595–600.

Plowey, E.D., Cherra, S.J., 3rd, Liu, Y.J., and Chu, C.T. (2008). Role of autophagy in G2019S-LRRK2-associated neurite shortening in differentiated SH-SY5Y cells. J. Neurochem. *105*, 1048–1056.

Polymenidou, M., and Cleveland, D.W. (2012). Prion-like spread of protein aggregates in neurodegeneration. J. Exp. Med. *209*, 889–893.

Polymeropoulos, M.H., Lavedan, C., Leroy, E., Ide, S.E., Dehejia, A., Dutra, A., Pike, B., Root, H., Rubenstein, J., Boyer, R., et al. (1997). Mutation in the alpha-synuclein gene identified in families with Parkinson's disease. Science *276*, 2045–2047.

Rajput, A., Dickson, D.W., Robinson, C.A., Ross, O.A., Dächsel, J.C., Lincoln, S.J., Cobb, S.A., Rajput, M.L., and Farrer, M.J. (2006). Parkinsonism, Lrrk2 G2019S, and tau neuropathology. Neurology *67*, 1506–1508.

Ross, O.A., Toft, M., Whittle, A.J., Johnson, J.L., Papapetropoulos, S., Mash, D.C., Litvan, I., Gordon, M.F., Wszolek, Z.K., Farrer, M.J., and Dickson, D.W. (2006). Lrrk2 and Lewy body disease. Ann. Neurol. *59*, 388–393.

Sánchez-Danés, A., Richaud-Patin, Y., Carballo-Carbajal, I., Jiménez-Delgado, S., Caig, C., Mora, S., Di Guglielmo, C., Ezquerra, M., Patel, B., Giralt, A., et al. (2012). Disease-specific phenotypes in dopamine neurons from human iPS-based models of genetic and sporadic Parkinson's disease. EMBO Mol. Med. *4*, 380–395.

Schiesling, C., Kieper, N., Seidel, K., and Krüger, R. (2008). Review: Familial Parkinson's disease—genetics, clinical phenotype and neuropathology in relation to the common sporadic form of the disease. Neuropathol. Appl. Neurobiol. *34*, 255–271.

Simón-Sánchez, J., Schulte, C., Bras, J.M., Sharma, M., Gibbs, J.R., Berg, D., Paisan-Ruiz, C., Lichtner, P., Scholz, S.W., Hernandez, D.G., et al. (2009). Genome-wide association study reveals genetic risk underlying Parkinson's disease. Nat. Genet. *41*, 1308–1312.

Spillantini, M.G., Schmidt, M.L., Lee, V.M., Trojanowski, J.Q., Jakes, R., and Goedert, M. (1997). Alpha-synuclein in Lewy bodies. Nature *388*, 839–840.

Takahashi, K., and Yamanaka, S. (2006). Induction of pluripotent stem cells from mouse embryonic and adult fibroblast cultures by defined factors. Cell *126*, 663–676.

Takahashi, K., Tanabe, K., Ohnuki, M., Narita, M., Ichisaka, T., Tomoda, K., and Yamanaka, S. (2007). Induction of pluripotent stem cells from adult human fibroblasts by defined factors. Cell *131*, 861–872.

West, A.B., Moore, D.J., Biskup, S., Bugayenko, A., Smith, W.W., Ross, C.A., Dawson, V.L., and Dawson, T.M. (2005). Parkinson's disease-associated mutations in leucine-rich repeat kinase 2 augment kinase activity. Proc. Natl. Acad. Sci. USA *102*, 16842–16847.

Zach, S., Felk, S., and Gillardon, F. (2010). Signal transduction protein array analysis links LRRK2 to Ste20 kinases and PKC zeta that modulate neuronal plasticity. PLoS ONE *5*, e13191.

Zimprich, A., Biskup, S., Leitner, P., Lichtner, P., Farrer, M., Lincoln, S., Kachergus, J., Hulihan, M., Uitti, R.J., Calne, D.B., et al. (2004). Mutations in LRRK2 cause autosomal-dominant parkinsonism with pleomorphic pathology. Neuron *44*, 601–607.

nature COMMUNICATIONS

ARTICLE

Received 24 Jan 2014 | Accepted 2 May 2014 | Published 6 Jun 2014

DOI: 10.1038/ncomms5028

iPSC-derived neurons from GBA1-associated Parkinson's disease patients show autophagic defects and impaired calcium homeostasis

David C. Schöndorf[1,2], Massimo Aureli[3,*], Fiona E. McAllister[4,*], Christopher J. Hindley[5,*], Florian Mayer[6], Benjamin Schmid[1,2], S. Pablo Sardi[7], Manuela Valsecchi[3], Susanna Hoffmann[1,2], Lukas Kristoffer Schwarz[1,2], Ulrike Hedrich[2,8], Daniela Berg[1,2], Lamya S. Shihabuddin[7], Jing Hu[6], Jan Pruszak[5,9], Steven P. Gygi[4], Sandro Sonnino[3], Thomas Gasser[1,2] & Michela Deleidi[1,2]

Mutations in the acid β-glucocerebrosidase (*GBA1*) gene, responsible for the lysosomal storage disorder Gaucher's disease (GD), are the strongest genetic risk factor for Parkinson's disease (PD) known to date. Here we generate induced pluripotent stem cells from subjects with GD and PD harbouring *GBA1* mutations, and differentiate them into midbrain dopaminergic neurons followed by enrichment using fluorescence-activated cell sorting. Neurons show a reduction in glucocerebrosidase activity and protein levels, increase in glucosylceramide and α-synuclein levels as well as autophagic and lysosomal defects. Quantitative proteomic profiling reveals an increase of the neuronal calcium-binding protein 2 (NECAB2) in diseased neurons. Mutant neurons show a dysregulation of calcium homeostasis and increased vulnerability to stress responses involving elevation of cytosolic calcium. Importantly, correction of the mutations rescues such pathological phenotypes. These findings provide evidence for a link between *GBA1* mutations and complex changes in the autophagic/lysosomal system and intracellular calcium homeostasis, which underlie vulnerability to neurodegeneration.

[1] Department of Neurodegenerative Diseases, German Center for Neurodegenerative Diseases (DZNE), Tübingen 72076, Germany. [2] Hertie-Institute for Clinical Brain Research, University of Tübingen, Tübingen 72076, Germany. [3] Department of Medical Biotechnology and Translational Medicine, University of Milan, Milan 20090, Italy. [4] Department of Cell Biology, Harvard Medical School, Boston, Massacchusetts 02115, USA. [5] Emmy Noether-Group for Stem Cell Biology, Department of Molecular Embryology, Institute of Anatomy and Cell Biology, University of Freiburg, Freiburg 79104, Germany. [6] Werner Reichardt Center for Integrative Neuroscience (CIN), University of Tübingen, Tübingen 72076, Germany. [7] Genzyme, a Sanofi Company, Framingham, Massachusetts 01701, USA. [8] Department of Epileptology, Hertie Institute for Clinical Brain Research, University of Tübingen and German Center for Neurodegenerative Diseases, Tübingen 72076, Germany. [9] Center for Biological Signaling Studies (BIOSS), University of Freiburg, Freiburg 79104 Germany. * These authors contributed equally to this work. Correspondence and requests for materials should be addressed to M.D. (email:michela.deleidi@dzne.de) or to T.G. (email: thomas.gasser@uni-tuebingen.de).

Parkinson's disease (PD) is the second most common neurodegenerative disorder, with >1% of the population over 65 years of age affected and >4% affected by the age of 85 years. Several clues to understanding disease pathogenesis come from mutations in genes, which have been linked to familial forms of PD or identified as risk factors. Among these, heterozygous mutations in the acid β-glucocerebrosidase (*GBA1*) gene, which encodes the lysosomal enzyme β-glucocerebrosidase (GCase), have been linked to a higher risk of developing PD and other synucleinopathies[1,2]. GCase is a lysosomal enzyme that catalyses the hydrolysis of glucosylceramide (Glc-Cer) to ceramide and glucose. Homozygous mutations of *GBA1* are responsible for Gaucher's disease (GD), which is the most prevalent lysosomal storage disorder, characterized by decreased activity of GCase and subsequent accumulation of Glc-Cer in several organs including the brain. Different clinical forms are described depending on the absence (non-neuronopathic forms, GD type 1) or presence (neuronopathic forms, GD type 2 and 3) of neurological symptoms. GD type 1 is the most common type and is often associated with PD and parkinsonism, thus challenging such classification[3]. To date, over 300 mutations have been identified in *GBA1* and linked to GD. In recent years, GD and PD have been connected on account of the clinical observation of parkinsonism and Lewy Body (LB) pathology in patients with GD[3]. Compared with the general population, patients with GD type 1 have a 20-fold increased lifetime risk of developing parkinsonism[4], whereas individuals carrying heterozygous *GBA1* mutations have a five times greater risk of developing PD than non-carrier individuals[1]. The pathological mechanisms through which the mutant enzyme causes PD still remain elusive and both gain- and loss-of-function theories have been postulated. Such hypotheses are not mutually exclusive and include increased α-synuclein (α-syn) protein aggregation, sphingolipid accumulation and impaired trafficking as potential mechanisms involved in the pathogenesis of neurodegeneration[5,6].

Recent progress in the induced pluripotent stem cell (iPSC) technology has allowed the generation of functional dopaminergic (DA) neurons from familial and sporadic PD subjects[7–9], offering a unique opportunity to study the role of genetic mutations and risk factors in the pathogenesis of PD. Neurons from PD patients carrying heterozygous *GBA1* mutations have not yet been generated, and it is unknown whether such cells recapitulate the pathological phenotypes observed *in vivo*.

In this study, we demonstrate that iPSC-derived neurons from GD and PD individuals carrying *GBA1* mutations display relevant disease phenotypes, including a significant reduction of GCase enzymatic activity and protein levels as well as increased levels of α-syn and Glc-Cer. Furthermore, mutant neurons show defects in the autophagic/lysosomal system and impaired intracellular calcium homeostasis. Importantly, such phenotypes are reverted upon gene correction, thus supporting a direct link between *GBA1* mutations and disease-relevant phenotypes.

Results

Generation of iPSCs and isogenic gene-corrected controls. Skin fibroblasts were obtained from two healthy controls, four PD patients carrying heterozygous *GBA1* mutations (RecNcil/wt; L444P/wt; N370S/wt) and four GD patients (type 1: N370S/N370S; type 3: L444P/L444P) (Supplementary Table 1). Fibroblasts were reprogrammed by transduction with SOX2, OCT4, KLF4 and c-MYC retroviruses. After 4 to 5 weeks, iPSC colonies were isolated and further characterized (Supplementary Table 2). All generated iPSCs showed human embryonic stem cell (hESC)-like morphology and expressed alkaline phosphatase and the pluripotency markers SSEA4, TRA-1-81, TRA-1-60, OCT4, NANOG and LIN28 (Supplementary Figs 1 and 2a). iPSCs were genetically matched with their parental cells by PCR-based DNA fingerprinting analysis, maintained euploid karyotypes over several passages *in vitro* and showed effective silencing of the exogenous transgenes and upregulation of endogenous hESC markers (Supplementary Fig. 2b–d). All lines tested were efficiently differentiated to mesoderm, endoderm and ectoderm *in vitro* (Supplementary Fig. 3a) and formed teratomas consisting of the three germ layers when injected into the kidney capsule and testis of immune-compromised mice (Supplementary Fig. 3b).

Correction of *GBA1* mutations in iPSCs was performed by zinc-finger nuclease (ZFN)-mediated homologous recombination. Three iPSC lines (PD1-2, PD2-2 and PD4-2) were selected for gene-targeting experiments. iPSCs were nucleofected with ZFNs, which were designed to introduce a double-strand brake adjacent to the N370S and L444P mutations, along with a wild-type (wt)-GBA1 construct harbouring a neomycin resistance cassette (Fig. 1a). Single resistant colonies were selected, and corrected sequences at the mutation site were confirmed by DNA and RNA sequencing (Fig. 1b). Karyotype analysis revealed that no translocation had occurred in the clones after ZFN-mediated insertion.

Differentiation of iPSCs to mDA neurons. iPSCs from controls, GBA-PD and GD subjects were differentiated to mDA neurons by using a floor-plate-based neural differentiation protocol[10]. This early neural patterning protocol induces 70% FOXA2$^+$/OTX2$^+$ floor plate precursors by day 11 (ref. 10 and Supplementary Fig. 4). By day 40, all iPSC lines generated β-TubIII$^+$ neurons and cells expressing tyrosine hydroxylase (TH). At DIV 65, 15–20% of the cells were TH$^+$ and co-expressed markers of mDA phenotype (FOXA2, NURR1, GIRK2, VMAT2) (Fig. 2). No significant differences in differentiation potential were observed among control, GBA-PD, gene-corrected and GD lines (Supplementary Fig. 5a). Differentiated neurons showed a punctate staining of synapsin 1, indicating the presence of synaptically mature neurons (Supplementary Fig. 5b).

Enrichment of neuronal populations from differentiated iPSCs. To enrich neuronal populations from differentiated iPSC cultures, we included a neuronal cell isolation step using fluorescence-activated cell sorting (FACS)[11–14]. At DIV 65–70, differentiated neurons from iPSCs were purified based on a surface marker code of CD24^{high} CD29$^-$ CD184$^-$ CD44$^-$ CD15$^-$ (Fig. 3a). Analysis of post-FACS cell cultures revealed highly enriched neuronal populations (6.1-fold enrichment compared with unsorted cells), which expressed mature DA neuronal markers and could be kept *in vitro* for 3 weeks after sorting (Fig. 3b,c and Supplementary Fig. 6). Whole-cell patch clamp recordings showed that single neurons were able to fire action potentials (AP) repetitively. Importantly, around 50% of the patched neurons derived from iPSCs showed spontaneous firing activity (Supplementary Fig. 7a), whereas in 93% of the recorded cells AP could be elicited by current injections into the soma (Supplementary Fig. 7b). The mean resting membrane potential of all recorded neurons was -53.1 ± 1.5 mV. In addition, recorded cells showed sodium and potassium currents (Supplementary Fig. 7c). Importantly, differentiated neuronal cultures released DA (Supplementary Fig. 7d).

The polysialoganglioside content of iPSC-derived neurons. Gangliosides are sphingolipids (GSL) particularly abundant in the neuronal plasma membrane playing an important role in the pathogenesis of neurological disorders. With respect to

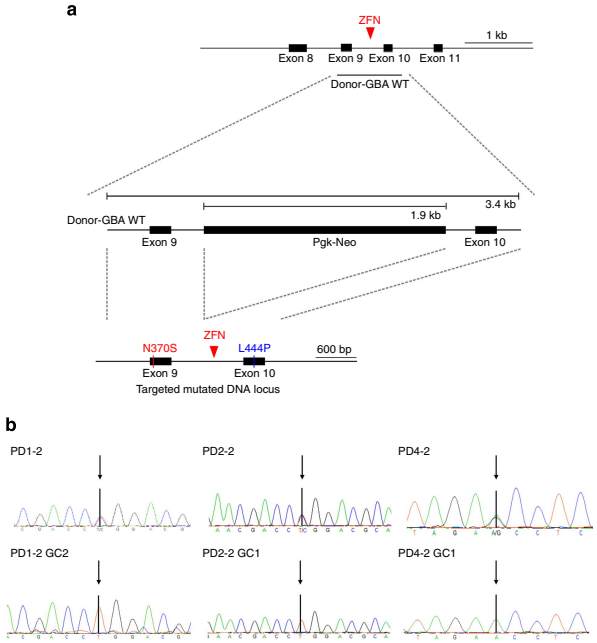

Figure 1 | Gene correction of GBA-PD iPSCs. (**a**) Structure of the *GBA1* gene on chromosome 1 and schematic overview of gene correction using ZFNs. Black boxes represent exons. (**b**) Mutated and gene-corrected (GC) iPSCs after sequencing (upper lanes: iPSCs with heterozygous mutations; lower lanes: iPSCs with homozygous wt-*GBA1* sequences as indicated by arrows).

synucleinopathies, alterations in the neuronal GSL composition cause impaired α-syn membrane binding and enhanced aggregation in the cytoplasm[15]. To study the link between GCase and α-syn and to investigate the pathogenesis of neurodegeneration in sphingolipidoses, it is therefore crucial to utilize cell models that resemble the GSL composition and pattern of adult human brain. The content and pattern of gangliosides markedly change during brain development[16] and the ganglioside concentration is ~10 times higher in the brain than in other organs[17]. The total brain ganglioside content is very low at the embryonic and fetal stage and then increases several folds with a shift from gangliosides of the Lac series, GM3 and GD3, to monosialo-, during development, and polysialo-species in the adult brain[16,17]. The GSL content and pattern are therefore useful markers to follow neural development both *in vivo* and *in vitro*[18,19]. To investigate whether iPSCs recapitulate such developmental changes during *in vitro* differentiation and whether iPSC-derived neurons have the GSL composition of developmentally mature neurons, we metabolically labelled gangliosides by feeding fibroblasts, iPSCs and iPSC-derived neurons (before and after FACS enrichment) from control, GBA-PD and GD type 3 subjects with isotopically tritium labelled [1–^{3}H]sphingosine[19]. After a 48-hour chase, gangliosides were purified from the total lipid extract, separated by HPTLC and analysed by radio-imaging[20]. As expected, the ganglioside pattern of fibroblasts was characterized by the presence of GM3 and a minor quantity of GD3 (Fig. 4a). Minor differences in the ganglioside pattern and in the GM3/GD3 ratio among fibroblast cell lines were detected (Fig. 4a), which have been described to be age and patient specific[21]. In iPSC cultures, GM3 still represented the main ganglioside, but low amounts of GM2, GM1 and GD1a components were identified (Fig. 4a). By contrast, differentiated iPSCs contained all the polysialogangliosides found in the CNS, even though high levels of GM3 and GD3 were still present[16] (Fig. 4a and Supplementary Fig. 8). After FACS enrichment, the levels of GD3 and GM3 were found to be significantly reduced compared with the total GSL composition and the levels of GM1, GD1a, GD1b and GT1b were in a percentage distribution similar to that found in the adult human and rodent brain (Fig. 4a and Supplementary Fig. 9)[22]. Importantly, the total ganglioside content in FACS-enriched iPSC-derived neurons was about 10 times higher than that in fibroblasts: the radioactivity associated with gangliosides ranged from 41,250 to 57,500 dpm mg^{-1} cell protein in fibroblasts (control, GD and GBA-PD) and from 330,650 to 415,000 dpm mg^{-1} cell protein in sorted neurons.

Glycohydrolases in human iPSCs and enriched neurons. The developmental changes of GSL content and patterns can be largely attributed to switches in the expression and activity of several enzymes involved in their synthesis and catabolism[16]. We therefore investigated the activities of enzymes involved in the catabolic pathway of GSL during human iPSC differentiation. Control iPSCs were differentiated for 65–70 days *in vitro*, neurons enriched by FACS and the activities of the main hydrolases involved in the metabolism of glycoconjugates (conduritol B

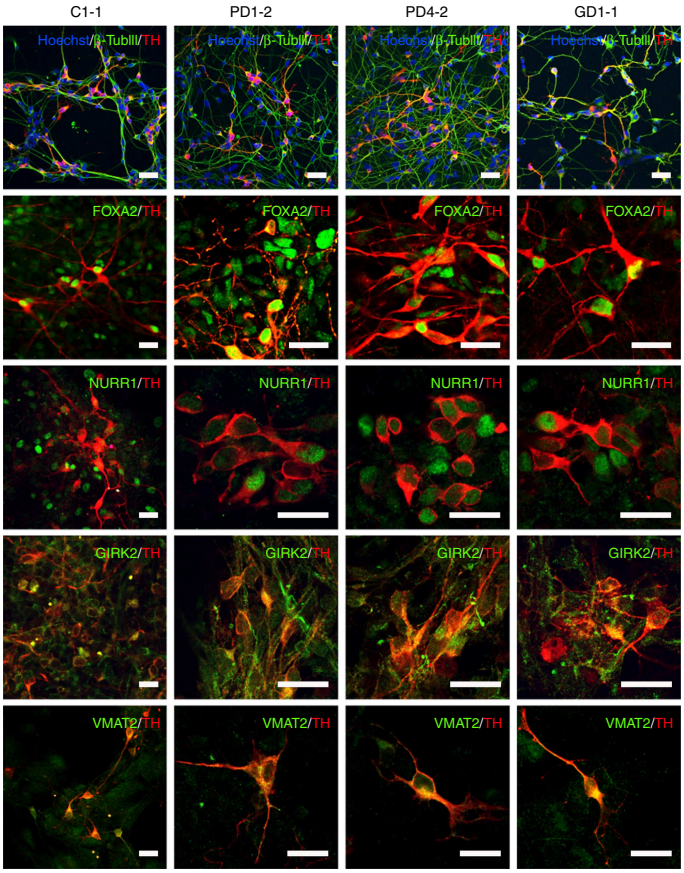

Figure 2 | Differentiation of iPSCs into mDA neurons. Immunostaining of indicated differentiated iPSC cultures at DIV65. Cells were stained for TH (red) and β-TubIII, FOXA2, NURR1, GIRK2 and VMAT2 (all green). Cell nuclei were counterstained with Hoechst (blue). (Bars, 20 μm).

epoxide (CBE)-sensitive β-glucosidase, non-lysosomal β-glucosyl ceramidase (GBA2), β-galactosidase and β-hexosaminidase) were investigated. Two different cellular compartment-specific β-glucosidase activities were analysed: the lysosomal β-glucocerebrosidase GCase and the non-lysosomal beta-glucosyl ceramidase GBA2 (ref. 23). By using CBE, a specific inhibitor of GCase, it was possible to evaluate the activity associated with GBA2, whereas, by application of the specific inhibitor *N*-(5-adamantane-1-yl-methoxy-pentyl)-deoxynojirimycin (AMP-DNM)[24], it was possible to determine the β-glucosidase activity due to GCase. We found that the activity of all tested enzymes was significantly increased in iPSC-derived neurons compared with iPSCs and fibroblasts, suggesting an important role of such enzymes in differentiation and maintenance of GSL composition in neurons (Fig. 4b and Supplementary Fig. 10a). Quantitative RT-PCR and immunoblot revealed an increase in GBA1, GBA2, β-galactosidase and β-hexosaminidase mRNA and protein levels in differentiated cultures compared with iPSCs (Fig. 4c,d).

Increased Glc-Cer and α-syn levels in *GBA1* mutant neurons. Recent studies using iPSC-derived neurons from GD patients showed that DA neurons accumulate glycosphingolipids[25,26]. To examine whether neurons from PD patients carrying heterozygous *GBA1* mutations also display such phenotypes, we carried out liquid chromatography (LC) and tandem mass spectrometry (MS) (LC-MS/MS) analysis on differentiated iPSCs from controls, GBA-PD and GD patients. Both homozygous and heterozygous *GBA1* mutant iPSC-derived neurons showed elevated levels of Glc-Cer compared with control cells (Fig. 5a). Importantly, gene-corrected isogenic controls showed reduced Glc-Cer levels compared with the parental lines (Fig. 5a).

A direct link between GCase and α-syn accumulation has previously been shown[25,27,28]. However, it has not yet been investigated whether heterozygous *GBA1* mutations are linked to increased levels of α-syn. We therefore sought to examine the effects of *GBA1* mutations on α-syn accumulation in

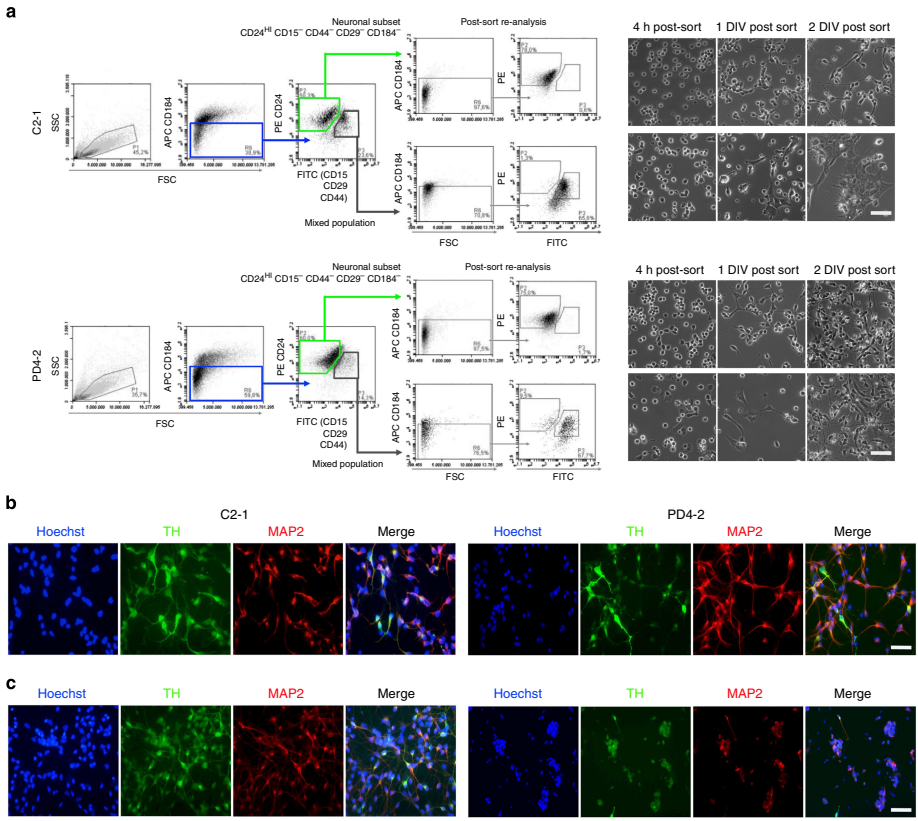

Figure 3 | FACS enriches for neuronal populations. (**a**) Gating strategy used for neuronal cell sorting. Live cells as determined by FSC/SSC gating were selected for CD184-APC-negative/low surface expression and subsequently separated for CD24-PE versus CD15/CD29/CD44 expression, detected in the FITC channel as indicated in the dot plots. Post-sort reanalysis shows representative samples of both fractions immediately after FACS enrichment, which were then plated for comparative *in vitro* analysis (phase contrast images. Bars, 50 μm). (**b**,**c**) Immunocytochemistry at DIV2 post-sort for TH (green) and the neuronal marker MAP2 (red) performed on the neuronal (**b**) and mixed (**c**) populations of a representative control and GBA-PD line. Nuclei were counterstained with Hoechst (blue). FACS enriches for both TH and neuronal marker positivity in the neuronal population compared with the non-neuronal population. (Bars, 50 μm.)

differentiated iPSCs. First, we examined the effect of loss of GCase activity in control iPSC-derived neurons. We found that CBE treatment induced an increase in α-syn protein levels in control iPSC-derived neurons (Fig. 5b). Next, iPSCs from controls, GBA-PD and GD subjects were differentiated to mDA neurons, and α-syn levels were measured by western blot. A significant increase in α-syn protein levels was found in GBA-PD neurons carrying the L444P allele and in GD neurons compared with controls (Fig. 5c,e). It is known that differences in expression levels of α-syn are influenced by individual genetic background, which could explain the high variability of α-syn expression in the general population[29]. Thus, we measured α-syn levels in neuronal cultures from GBA-PD iPSCs and corresponding isogenic gene-corrected controls. Interestingly, we found a significant reduction in α-syn levels in all gene-corrected neurons (RecNcil, L444P, N370S) compared with their parental lines (Fig. 5d,f).

Reduced GCase in *GBA1* mutant neurons. The GCase activity was significantly reduced in GBA-PD and GD fibroblasts compared with healthy control cells (Supplementary Fig. 11). Next, control, GBA-PD, isogenic gene-corrected controls and GD iPSCs were differentiated for 65 days and neuronal cultures were enriched by FACS. We found that the GCase enzymatic activity was significantly reduced in GBA-PD and GD neurons compared with controls (Fig. 6a). Importantly, isogenic gene-corrected lines showed a significantly higher average of enzymatic activity compared with non-corrected lines (Fig. 6a). Quantitative analysis of intracellular GCase protein levels in cells of

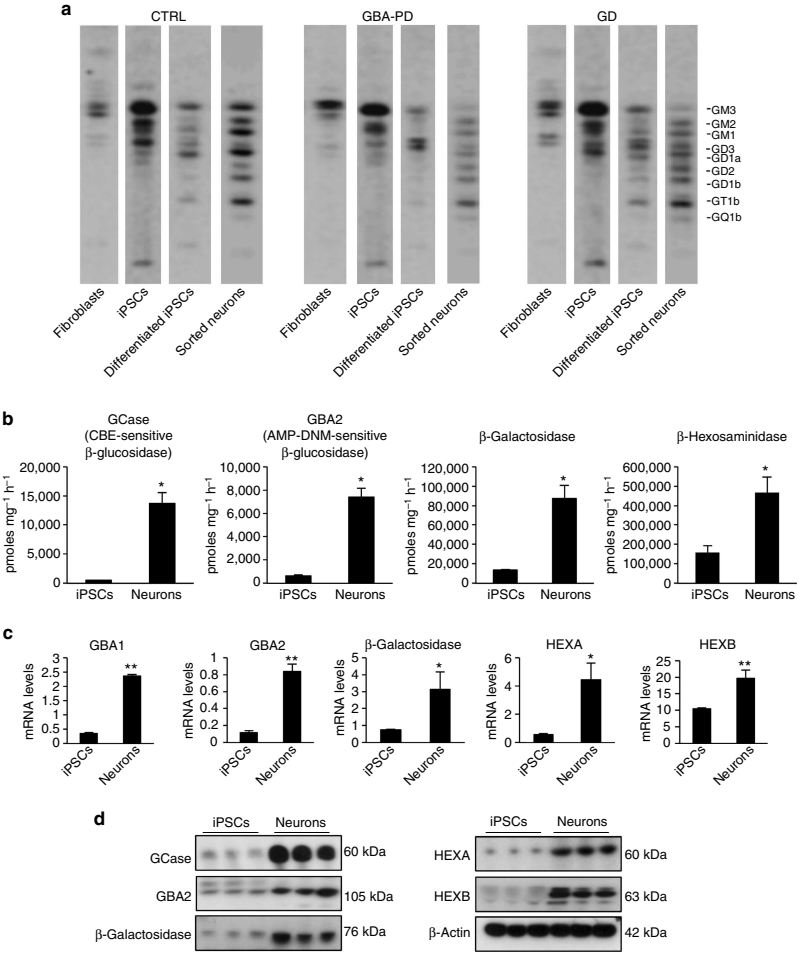

Figure 4 | Ganglioside and glycohydrolase changes during human iPSC differentiation recapitulate human brain development. (**a**) Ganglioside composition of human fibroblasts, iPSCs, differentiated iPSCs and enriched iPSC-derived neurons (after FACS) from control (line C1-1), GBA-PD (line PD1-1) and GD (line GD1-1) subjects. Cell lipids were metabolically labelled with [1-^{3}H]sphingosine and visualized by digital autoradiography. (**b**) Activities of glycohydrolases (GCase, GBA2, β-galactosidase, β-hexosaminidase) in control iPSCs and iPSC-derived enriched neurons at DIV65. Enzyme activities are expressed as pmoles mg^{-1} h^{-1}. Data are represented as mean + s.d.; experiments were independently repeated three times in triplicate. *$P<0.01$; Student's *t*-test. (**c**) GBA1, GBA2, β-galactosidase and HEXA and HEXB gene expression levels in control iPSCs and iPSC-derived enriched neurons at DIV65. Data are represented as mean + s.d.; experiments were independently repeated three times in triplicate. *$P<0.05$; **$P<0.01$, Student's *t*-test. (**d**) Representative western blots showing GCase, GBA2, β-galactosidase and HEXA and HEXB protein levels in control iPSCs and corresponding iPSC-derived neurons (DIV65).

different patients by western-blotting revealed that protein levels of the enzyme were also reduced in GBA-PD and GD patients compared with control individuals (Fig. 6b,c). ZFN-mediated gene correction rescued the levels of GCase (Fig. 6b,c).

Decreased glycohydrolase activities in *GBA1* mutant neurons. We next analysed the activity of additional glycohydrolases in iPSC-derived neurons from controls, GBA-PD, isogenic gene-corrected controls and GD subjects. Activity levels of the lysosomal enzymes β-galactosidase and β-hexosaminidase, as well as

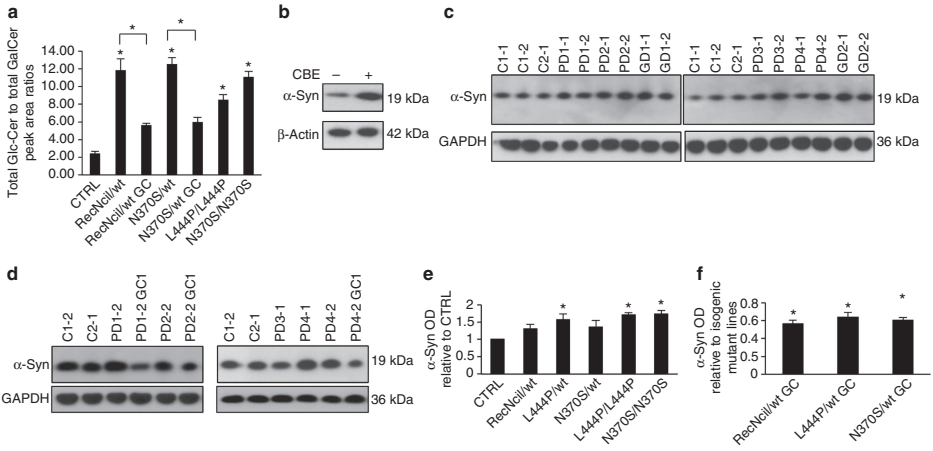

Figure 5 | Glc-Cer and α-syn levels are increased in GBA-PD and GD iPSC-derived neurons. (**a**) LC-MS/MS analysis showing the level of Glc-Cer in control, GBA-PD, isogenic controls and GD iPSC-derived neurons. Data are represented as mean + s.d.; $n = 3$, $^*P < 0.01$, One-way ANOVA. (**b**) Control iPSCs (line C1-1) were differentiated for 65 days and exposed to the GCase inhibitor CBE (25 μM) for 48 h. Representative western blot showing increased levels of α-syn in CBE-treated iPSC-derived neurons compared to untreated neurons. (**c**,**d**) Representative western blots showing the protein levels of α-syn in control, GBA-PD, gene-corrected isogenic controls and GD iPSC-derived neurons. (**e**) Optical densities of α-syn bands normalized by the averaged value of GAPDH and expressed as a percentage of the control (CTRL) line value. Data are represented as mean + s.d.; experiments were independently repeated five times. $^*P < 0.01$, one-way ANOVA. (**f**) Average α-syn protein levels normalized by the averaged value of GAPDH and expressed as a percentage of the respective isogenic mutant lines. Data are represented as mean + s.d.; experiments were independently repeated five times. $^*P < 0.01$, Student's *t*-test.

the activity of the non-lysosomal β-glucosylceramidase GBA2, were examined in differentiated iPSC-neurons after FACS enrichment. Our analysis revealed a significant decrease in the activity of GBA2 and β-galactosidase in GBA-PD and GD neurons compared with healthy controls, whereas activity levels of β-hexosaminidase remained unchanged (Fig. 6a). Interestingly, gene correction rescued such changes in RecNcil- and L444P-associated PD lines (Fig. 6a). Gene expression levels of GBA2 and β-galactosidase in patient neurons were unchanged compared with control neurons (Supplementary Fig. 10b).

An increase in the activity of GBA2, β-hexosaminidase and β-galactosidase has recently been described in GD fibroblasts and leukocytes[30,31]. We therefore examined the enzyme activities in respective fibroblast lines and found a significant increase in GBA2 activity in GBA-PD (L444P/wt) and GD (L444P/L444P) fibroblasts, while GD fibroblasts (L444P/L444P) showed in addition a significant increase in β-galactosidase activity compared with controls (Supplementary Fig. 11).

Glycohydrolase activities in the CSF of GBA-PD patients. Recent studies showed that GCase activity is lower in the cerebrospinal fluid (CSF) and brain samples of patients with PD or dementia with LB than that in healthy individuals[32–34]. To determine whether changes in iPSC-derived neurons were accompanied by changes in the glycohydrolase enzymatic activity in the CSF, we measured the activity of several glycohydrolases (GCase, GBA2, β-galactosidase, β-hexosaminidase, α-fucosidase, α- and β-mannosidase) in the CSF of PD patients carrying heterozygous RecNcil, L444P or N370S *GBA1* mutations, idiopathic PD patients as well as age-matched unaffected controls. Enzyme activity levels were normalized against total protein levels. The CSF of patients used for iPSC generation in this study was included in the analysis. No significant differences between idiopathic PD patients and controls were observed for all tested enzymes (Fig. 7); however, in GBA-PD patients the activities of GCase, GBA2 and β-galactosidase were significantly reduced compared with unaffected controls (Fig. 7). In addition, we found a significant reduction in the enzyme activity of GCase, GBA2, α- and β-mannosidase in GBA-PD patients compared with idiopathic PD patients (Fig. 7).

Lysosomal and autophagic defects in *GBA1* mutant neurons. To extend these findings, we analysed the autophagic/lysosomal machinery in *GBA1* mutant neurons. Immunofluorescent staining for LAMP1, a lysosomal marker, revealed a significant increase in number and size of $LAMP1^+$ particles in patient iPSC-derived neurons compared with healthy individuals, suggesting an accumulation of lysosomes (Fig. 8a,b and Supplementary Fig. 12a). To examine macroautophagy, we first investigated the autophagosome content by immunostaining for endogenous light chain type 3 protein (LC3), a marker of autophagosomes. Our analysis revealed a significant increase of $LC3^+$ vesicles in GBA-PD and GD neurons compared with control neurons (Supplementary Fig. 12b,d). These results were confirmed by immunoblot, which showed an increase in basal levels of LC3-II in GBA-PD and GD-derived neurons (Fig. 8c,d). Inhibition of lysosomal degradation by leupeptin and ammonium chloride (NH_4Cl) revealed that the autophagic flux was significantly reduced in GBA-PD and GD neurons (Fig. 8e). To examine autophagosome-lysosome fusion, we assessed the co-localization of LC3 and LAMP1 markers in iPSC-derived neurons. We observed a decreased degree of co-localization

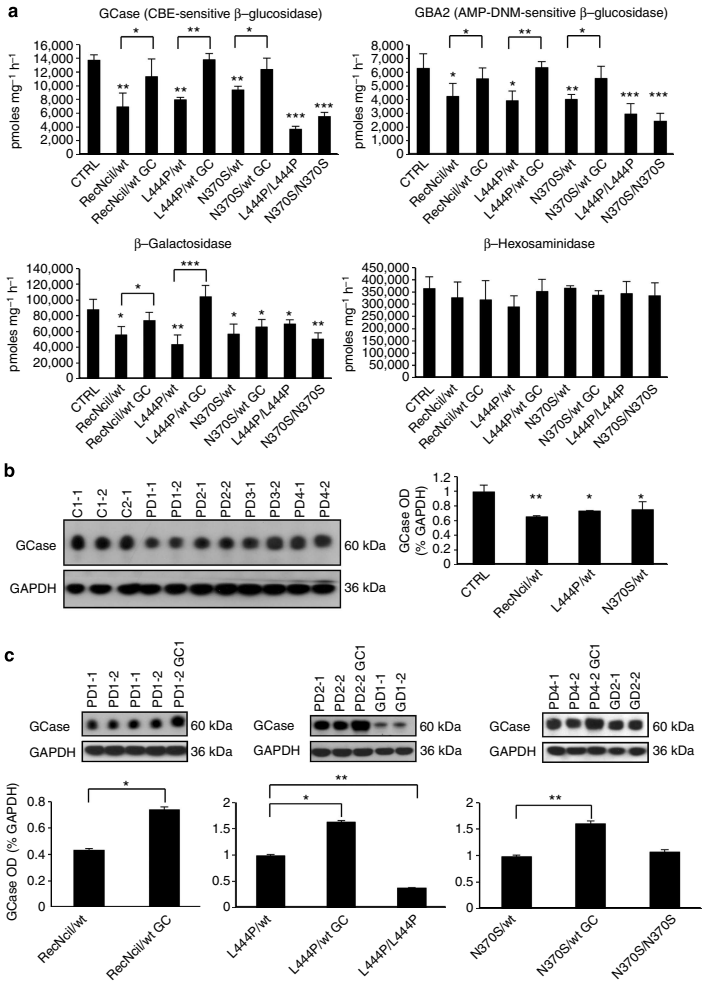

Figure 6 | GBA-PD and GD iPSC-derived neurons show decreased glycohydrolase enzyme activities and protein levels. (**a**) Glycohydrolase enzyme activities (GCase, GBA2, β-galactosidase, β-hexosaminidase) were measured in enriched neurons from control, GBA-PD, isogenic gene-corrected control and GD iPSC-derived neurons at DIV65. Enzyme activities are expressed as pmoles $mg^{-1} h^{-1}$. Data are represented as mean + s.d.; experiments were independently repeated three times in triplicate. $^{*}P<0.05$; $^{**}P<0.01$; $^{***}P<0.001$ compared with controls, one-way ANOVA. (**b**,**c**) Representative western blots of GCase protein levels in control, GBA-PD, corresponding gene-corrected and GD iPSC-derived neurons. Data are represented as mean + s.d.; experiments were independently repeated three times. $^{*}P<0.05$; $^{**}P<0.01$, one-way ANOVA and Student's *t*-test.

between $LC3^{+}$ vacuoles and $LAMP1^{+}$ vacuoles in GBA-PD and GD neurons, which suggests an impaired autophagosome-lysosome fusion in *GBA1* mutant neurons. (Supplementary Fig. 12c,e).

Impaired calcium homeostasis in *GBA1* mutant neurons. We next used quantitative mass spectrometry (MS)-based proteomics to search for proteins whose levels are affected by *GBA1* mutations in iPSC-derived neurons. Two independent iPSC lines harbouring the L444P allele and three independent control lines were differentiated and enriched by FACS. We extracted proteins and performed quantitative proteomic profiling by isotopic labelling (tandem mass tag, TMT) and MS analysis (Table 1, Supplementary Fig. 13a,b and Supplementary Data 1). In total, 7,069 proteins were identified from enriched neurons at a protein false-discovery rate (FDR) <1%. We calculated the differences in protein abundances between GBA-PD neurons and control lines,

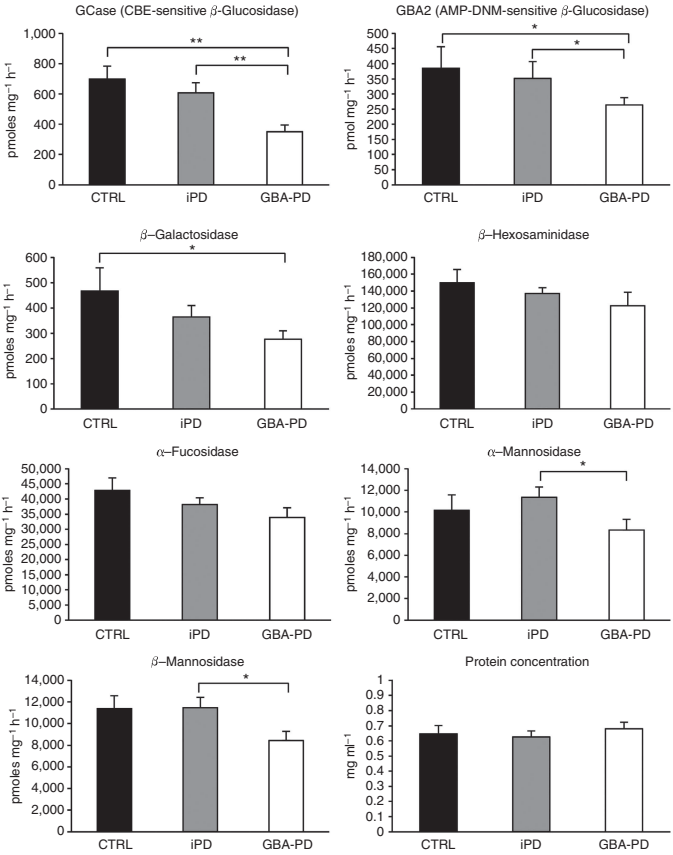

Figure 7 | Glycohydrolase enzyme activities in the CSF of unaffected individuals, GBA-PD and idiopathic PD patients. CSF glycohydrolase activities were measured in patients with idiopathic PD (iPD), GBA-PD patients and age-matched unaffected individuals (CTRL). Enzyme activities were normalized to total protein concentrations and expressed as pmoles $mg^{-1} h^{-1}$. Data are represented as mean + s.e.m.; CTRL, $n=14$; iPD, $n=15$; GBA-PD, $n=15$. Experiments were performed in triplicate. $^{*}P<0.05$; $^{**}P<0.01$, Mann–Whitney U test.

tested for statistical significance by t-test analysis and filtered for proteins whose levels changed by at least 1.2-fold (Table 1). To validate the MS proteomic data, immunoblotting of selected proteins was performed on three independent differentiated iPSC cultures (Supplementary Fig. 13a). Among the differentially expressed proteins, we found that the neuronal calcium-binding protein 2 (NECAB2) was significantly upregulated (1.9-fold) in lines harbouring the L444P allele (Table 1 and Supplementary Fig. 13a). Calcium-induced excitotoxicity plays a key role in the pathogenesis of several neurodegenerative diseases including PD[35]. To further investigate the potential role of calcium in the vulnerability of neurons harbouring *GBA1* mutations, we examined calcium homeostasis using the calcium dye Fura-2 acetoxymethyl ester and compared calcium levels in control and diseased neurons. Interestingly, we found a significant increase in the basal calcium levels in GBA-PD and GD iPSC-derived neurons compared with controls (Fig. 9a). We therefore investigated the effects of caffeine, a RyR agonist that increases the calcium release from the calcium-sensitive internal stores, namely the endoplasmic reticulum (ER), into the cytoplasm. Caffeine induced an increase in cytosolic calcium, which was significantly greater in GBA-PD (L444P/wt) and GD neurons compared with control neurons (Fig. 9b and Supplementary Fig. 14a). Although we also found a consistent trend for increased calcium levels in GBA-PD (RecNcil/wt) neurons, this increase was not statistically significant (Fig. 9b). However, intracellular calcium levels in response to caffeine stimulation were comparable between isogenic gene-corrected neurons (both L444P/wt and RecNcil/wt) and control neurons (Fig. 9b and Supplementary Fig. 14a), suggesting a role of *GBA1* mutations in regulating intracellular calcium concentration. Our data therefore indicate that RyR-mediated calcium release is increased in the

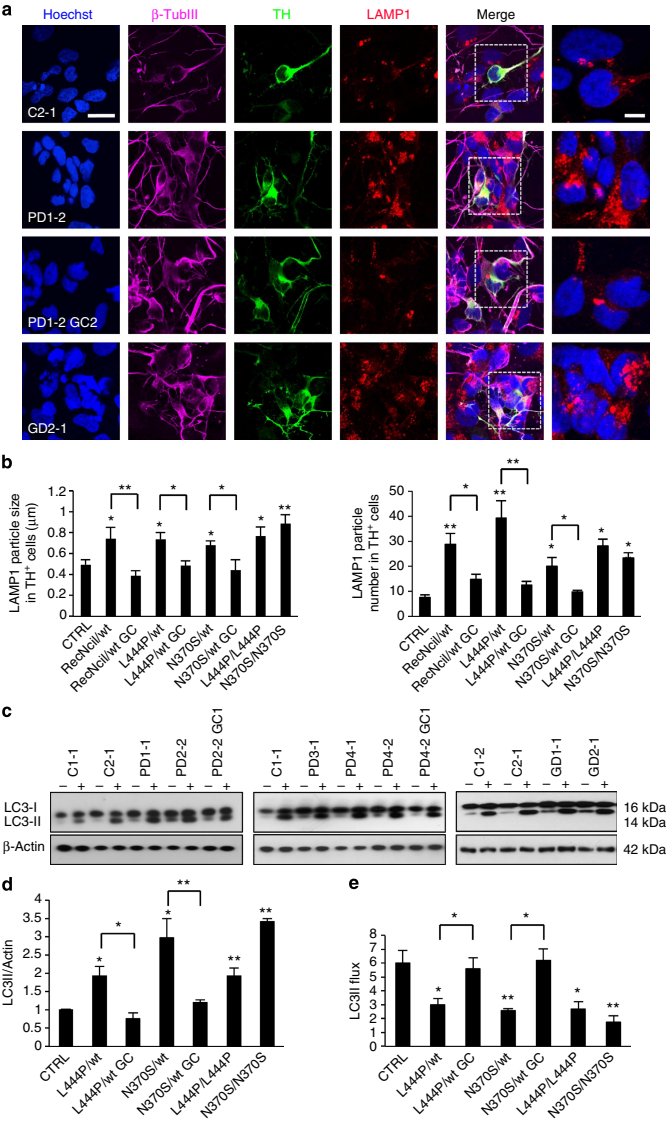

Figure 8 | GBA-PD and GD iPSC-derived neurons show alterations in the autophagic/lysosomal system. (**a**) Immunostaining of differentiated iPSC cultures at DIV65 under basal conditions. Cells were stained for TH (green), β-TubIII (magenta) and LAMP1 (red). Cell nuclei were counterstained with Hoechst (blue). High magnification insets are shown in the right lane. (Bars, 20 μm and 10 μm in the insets.) (**b**) Average size and number of LAMP1$^+$ particles in TH$^+$ neurons were quantified by ImageJ. Data are represented as mean + s.e.m.; experiments were independently repeated three times in triplicate. *$P<0.01$, **$P<0.001$, one-way ANOVA. (**c**) Western blot analysis for LC3 in iPSC-derived neuronal cultures at DIV65, untreated (−) or treated with 200 μM leupeptin and 20 mM NH_4Cl for 4 h (+). (**d**) Quantification of the basal levels of LC3-II relative to β-actin. Data are represented as mean + s.e.m.; experiments were independently repeated three times. *$P<0.01$; **$P<0.001$, one-way ANOVA. (**e**) Quantification of LC3 flux normalized to actin. Data are represented as mean + s.e.m.; experiments were independently repeated three times in triplicate. *$P<0.01$; **$P<0.001$, one-way ANOVA.

Table 1 | Identification of proteins with changed expression levels in iPSC-derived enriched neurons carrying *GBA1* mutations.

Protein	Gene symbol	Description	N. peptides	Fold change
Q7Z6G3	*NECAB2*	N-terminal EF-hand calcium-binding protein 2	4	1.9
Q15173-2	*PPP2R5B*	Serine/threonine-protein phosphatase 2 A 56 kDa regulatory subunit beta isoform	1	1.8
Q8NF91-4	*SYNE1*	Isoform 4 of Nesprin-1	1	1.7
Q8ND56-2	*LSM14A*	Isoform 2 of Protein LSM14 homolog A	5	1.7
Q9Y2Y0-2	*ARL2BP*	Isoform 2 of ADP-ribosylation factor-like protein 2-binding protein	2	1.4
P62979	*RPS27A*	Ubiquitin-40S ribosomal protein S27a	45	1.3
Q9BR76	*CORO1B*	Coronin-1B	5	1.3
Q8NC44	*FAM134A*	Protein FAM134A	1	−2.1
Q9HBL7	*C9orf46*	Transmembrane protein C9orf46	1	−1.5
Q9NUJ1	*ABHD10*	Abhydrolase domain-containing protein 10, mitochondrial	10	−1.2

Summary of the identified proteins from quantitative mass spectrometry proteomics that were significantly ($P<0.05$, Student's *t*-test) up- or downregulated in purified neurons from GBA-PD iPSCs compared with control neurons.

presence of *GBA1* mutations. We next examined the vulnerability of mutant neurons to ER stress responses by application of either A23187 (0–5 μM), a calcium ionophore that induces ER stress by increasing the cytosolic calcium concentration, or rotenone (0–200 nM), an inhibitor of complex I of the mitochondrial electron transport chain, which induces mitochondrial ROS production and elevation of intracellular levels of calcium[36,37]. Neuronal vulnerability was assessed by measuring cellular release of lactate dehydrogenase (LDH). Our results show that neurons carrying *GBA1* mutations were more sensitive to A23187 (1–2.5 μM) and rotenone (50–200 nM) than control cells (Fig. 9c and Supplementary Fig. 15a). Immunocytochemistry and cell counts of TH^+ cells confirmed the increased vulnerability of mutant neurons (Fig. 9d and Supplementary Fig. 15b). Importantly, such a phenotype was rescued by gene correction. To gain insight into the functional role of NECAB2, we knocked down NECAB2 in iPSC-derived neurons using lentiviral-mediated short hairpin RNA (shRNA). The gene expression and protein levels of NECAB2 were reduced by ~80% in knocked down iPSC-derived neurons (Fig. 9e,f). To further examine the functional role of NECAB2, iPSC-derived neurons were exposed to A23187 and neurotoxicity was assessed by immunostaining for TH. We found that knockdown of NECAB2 resulted in a statistically significant increase of calcium-mediated neurotoxicity (Fig. 9g,h). In addition, calcium-imaging experiments revealed an increase in caffeine-induced cytosolic calcium levels after NECAB2 knockdown (Supplementary Fig. 14b).

Discussion

Heterozygous *GBA1* mutations have been recognized as the strongest risk factor for PD and LB disorders[1]. In this study, we describe the generation and characterization of a collection of iPSC lines from GD patients, PD subjects harbouring heterozygous *GBA1* mutations, as well as unaffected individuals. The cells used for iPSC generation in this study were obtained from donors harbouring L444P, RecNcil and N370S alleles. L444P and N370S point mutations are the most frequent GD-causing alleles that have been linked to PD[1,38], whereas the RecNcil is a complex GBA-pseudogene recombinant allele composed of three point mutations, namely the 6433 T→C transition (L444P), 6468 G→C transition (A456P) and 6482 G→C transition (silent mutation). To identify PD phenotypes related to *GBA1* mutations, isogenic gene-corrected iPSC lines were generated for each mutation. iPSCs were efficiently differentiated to mDA neurons without significant differences and enriched by FACS.

For the first time, we report that iPSC neuronal differentiation recapitulates the developmental changes observed during human brain development and that enriched iPSC-derived neurons show the polysialoganglioside content of adult human brain. To examine the shift of the ganglioside pattern along *in vitro* differentiation of human iPSCs, we utilized a radioactive labelling method and compared the ganglioside composition of fibroblasts, iPSCs and iPSC-derived neurons before and after FACS enrichment. Unsorted iPSC-derived neurons showed an increased complexity of the ganglioside pattern compared with fibroblasts and iPSCs; however, they still had a high content of GM3, which is usually found at high levels in other cell types. Interestingly, unsorted neurons showed high levels of GD3, which is mainly associated with proliferating neural stem cells[16]. By contrast, despite the presence of low quantities of GM3 and GM2, the gangliosidic pattern of purified neurons mirrored the composition of human brain with GM1, GD1a, GD1b, GT1b as major compounds and GD3, GD2 and GQ1b in less abundance[39]. These findings show that using unsorted differentiated iPSCs, which are heterogeneous cell populations, significantly limits the analysis of disease-related pathways. This underlines the importance of cell sorting to reduce background noise in such experimental approaches[12,40]. Taken together, these data indicate that enriched iPSC-derived neurons represent a valuable tool to study the role of GSLs in neurodegeneration as well as in sphingolipidoses and disorders of brain development. In this context, we also show that the glycosyltransferases involved in the catabolic pathways of GSLs (GCase, GBA2, β-galactosidase, β-hexosaminidase) are upregulated on human iPSC neuronal differentiation. Activity and protein levels of these enzymes were almost absent in undifferentiated iPSCs, whereas mature neurons expressed high levels of such enzymes. This may suggest a key role of these glycohydrolases in brain development and maintenance of GSL pattern and composition in the adult human brain.

GD patients with parkinsonism and PD patients carrying *GBA1* mutations show classic PD pathology with widespread α-syn inclusions[41]. The exact mechanism is unknown, but *GBA1* mutants may contribute to the enhanced aggregation of α-syn via a direct interaction[5]. In support of such a gain of function hypothesis, post-mortem studies in PD and LB disease, along with GD or *GBA1* mutation carriers, have shown the presence of GCase in LBs and Lewy neurites[42]. Recent data suggest that loss of GCase activity may also lead to α-syn accumulation as a secondary effect of lysosomal dysfunction[25,27] and that the accumulation of Glc-Cer due to GCase deficiency induces increased α-syn oligomerization, which in turn decreases GCase activity[25,43]. By utilizing iPSC-derived neurons carrying heterozygous *GBA1* mutations and their isogenic gene-corrected controls, we show that *GBA1* mutations are directly linked to the increase of α-syn levels. For the first time, we report an increase of Glc-Cer in iPSC-derived neurons from PD patients carrying heterozygous *GBA1* mutations, which may in turn influence α-syn levels and aggregation.

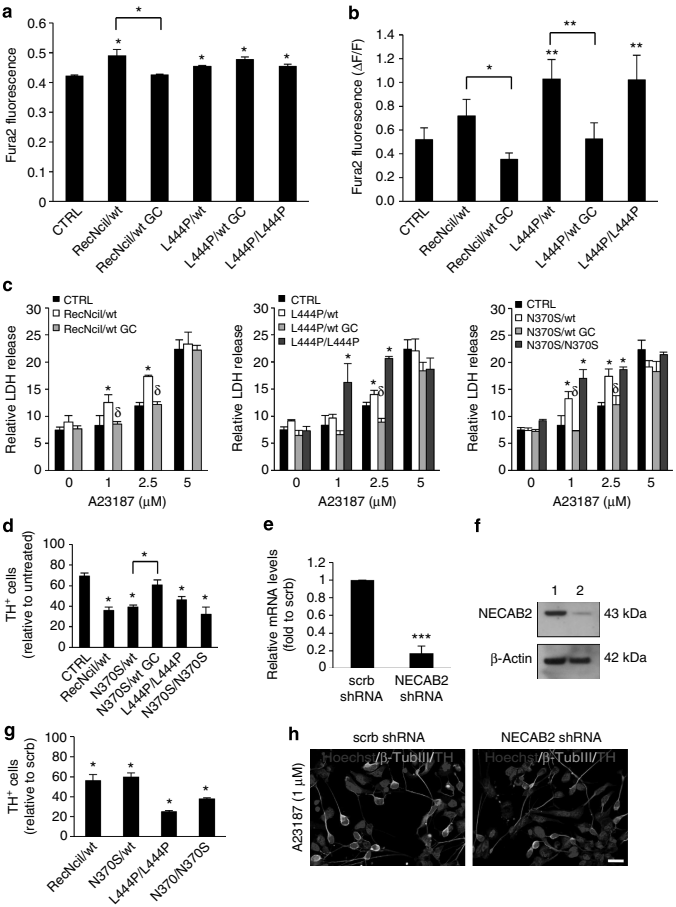

Figure 9 | Calcium homeostasis is dysregulated in GBA-PD and GD iPSC-derived neurons. (**a**) Cytosolic calcium levels were evaluated in iPSC-derived neurons at basal conditions by measuring the 340/380 nm ratio of Fura-2 acetoxymethyl ester. Data are represented as mean + s.e.m.; experiments were independently repeated three times in triplicate. *$P<0.01$; Student's *t*-test. (Number of cells analysed: CTRL, $n=58$; RecNcil/wt, $n=36$; RecNcil/wt GC, $n=107$; L444P/wt, $n=82$; L444P/wt GC, $n=33$; L444P/L444P, $n=62$). (**b**) Caffeine (10 mM) was applied to iPSC-derived neurons, and the peak cytosolic calcium concentration was measured as a change in Fura-2 fluorescence. Data are represented as mean + s.e.m.; experiments were independently repeated three times in triplicate. *$P<0.01$; **$P<0.001$, Student's *t*-test. (Number of cells analysed: CTRL, $n=58$; RecNcil/wt, $n=36$; RecNcil/wt GC, $n=107$; L444P/wt, $n=82$; L444P/wt GC, $n=33$; L444P/L444P, $n=62$). (**c**) iPSC-derived neurons were treated with A23187 (0–5 μM) for 4 h and cytotoxicity was evaluated by released LDH activity. LDH release values were calculated as the percentage of untreated cells lysed by incubation with Triton X-100. Data are represented as mean + s.e.m.; experiments were independently repeated four times in triplicate. *$P<0.05$, one-way ANOVA, control lines versus mutated lines; δ$P<0.05$, one-way ANOVA, mutated lines versus isogenic gene corrected controls. (**d**) Quantification of TH$^+$ cells treated with A23187 (1 μM) for 4 h expressed as a percentage of DMSO-treated controls. Data are represented as mean + s.d.; experiments were independently repeated three times in triplicate. *$P<0.01$, one-way ANOVA. (**e**) Knockdown efficiency of NECAB2 determined by qRT-PCR and normalized to scrambled non-targeting shRNA. Data are represented as mean + s.d.; experiments were independently repeated three times in triplicate. ***$P<0.0001$, Student's *t*-test. (**f**) Representative western blot for NECAB2 showing knockdown efficiency. 1, scrambled non-targeting shRNA; 2, NECAB2 shRNA. (**g**) Quantification of TH$^+$ cells in GBA-PD and GD iPSC-derived neuronal cultures infected with scrambled non-targeting shRNA or NECAB2 shRNA lentivirus and treated with A23187 (1 μM for 4 h). Values were calculated as a percentage of scrambled shRNA-treated cells. Data are represented as mean + s.e.m.; experiments were independently repeated three times in triplicate. *$P<0.01$, Student's *t*-test. (**h**) Representative images showing GBA-PD iPSC-derived DA neurons infected with scrambled non-targeting shRNA or NECAB2 shRNA lentivirus and treated with A23187 (1 μM for 4 h). Cells were stained for β-TubIII (green) and TH (red). Nuclei were counterstained with Hoechst (blue). (Bar, 20 μm.)

Our data show that *GBA1* mutations are linked to defects in the autophagic/lysosomal system characterized by an impairment of the autophagic flux with consequences for autophagosome clearance. Although we have observed an accumulation of lysosomes, the fusion between autophagosomes and lysosomes and the lysosomal hydrolytic function were impaired. This may explain the increased levels of α-syn in *GBA1* mutant neurons and α-syn pathology in GBA-PD patients. Interestingly, the reduction in the glycohydrolase lysosomal activity in iPSC-derived neurons was accompanied by a reduction in the enzymatic activity of these enzymes in the CSFs of GBA-PD patients compared with control individuals. PD and parkinsonism have been described in many lysosomal storage diseases, suggesting that impairment of the endolysosomal compartment is strictly correlated with the onset of neuronal degeneration[44]. In this context, *GBA1* mutations may alter the lysosomal function via several pathways. The intracellular lipid content strongly influences autolysosome formation as well as α-syn aggregation[15,45]. In contrast, increased levels of α-syn may cause lysosomal dysfunction in *GBA1* mutant neurons via a positive feedback loop[25]. Furthermore, our data in isogenic controls, along with previous reports[46], suggest the existence of a crosstalk between different enzymes involved in sphingolipid metabolism. Interestingly, we found that GBA2 enzyme activity was significantly decreased in iPSC-derived neurons harbouring *GBA1* mutations. GBA2 is a non-lysosomal enzyme with glucosylceramidase function localized at the ER and plasma membrane[47]. It is encoded by the *GBA2* gene and is highly expressed in the brain, testis and liver[48]. Notably, *GBA2* mutations cause a form of autosomal-recessive cerebellar ataxia and have been recently linked to motor neuron defects in hereditary spastic paraplegia[49,50]. Mutant GCase in the ER leads to ER stress and induces the unfolded protein response in skin fibroblasts from GD patients and mutation carriers[51]. Since GBA2 is also located in the ER, such perturbations may affect its activity. Even though the mechanisms responsible for the observed impairment of GBA2 function remain unclear, our data show that the decrease in GBA2 enzymatic activity was reverted on ZFN-mediated *GBA1* gene correction, suggesting a crosstalk between GCase and GBA2 activity. In favour of this hypothesis, a recent report shows that GBA2 activity depends on GCase, whereas GCase activity is independent of GBA2 (ref. 52). Further studies are needed to better elucidate such crosstalk and its role in disease onset and progression. GBA-PD and GD parental fibroblast lines showed an upregulation of the enzymatic activity of GBA2 and β-galactosidase compared with control cells. Such discrepancy can be attributed to the different sphingolipid metabolism in fibroblasts and neurons. As described above, neurons have high glycohydrolase enzymatic activity and a unique GSL content and distribution. Alternatively, even though only low passage fibroblasts were used in this study, such findings may also be due to the changes of the GSL pattern observed during subculture progression[21]. These data further support the importance of using iPSC-derived neurons as the ideal tool to model neurological diseases and in particular neurodegeneration associated with sphingolipidoses.

In this study, we have generated a proteome profile of differentiated iPSCs. This is the first report of multiplexed quantitative proteomics being performed on a highly enriched neuronal fraction. As little as 15 μg for each cell line was used for quantitative proteomics using TMT labelling, leading to the identification of over 7,000 proteins from 12 LC-mass spectrometry runs. Such analysis enabled the identification of a protein, namely NECAB2, whose levels were increased in human iPSC-derived neurons harbouring mutations in the *GBA1* gene. NECAB2 belongs to the family of neuronal calcium-binding proteins containing an N-terminal EF-hand domain (NECAB). It is highly expressed in the striatopallidal structures where it interacts with the adenosine A2A receptor[53,54]. Interestingly, a recently published microarray data set for putative novel mDA neuron-related transcription factors and membrane-associated proteins has shown that NECAB1 is a marker for mDA neurons, and it is highly expressed in the dorsal ventral tegmental area and dorsal substantia nigra[55]. Adult mDA neurons are autonomous pacemakers and rely on the activation of L-type Ca(V)1.3 calcium channels, leading to elevated intracellular calcium concentrations[56]. In addition, mDA neurons lack significant intrinsic calcium-buffering properties, which may explain their selective vulnerability to neurodegeneration[57]. A recent study demonstrates that the levels of calcium-binding proteins are reduced in cell bodies of neurons in areas selectively vulnerable to degeneration in PD. However, the surviving cells upregulate such proteins suggesting a compensatory mechanism[58]. Interestingly, we found increased basal levels of calcium and an increased calcium release from the ER on caffeine stimulation in GBA-PD and GD neurons. Such findings are in line with previous observations in pharmacological models of neuronopathic GD showing that Glc-Cer accumulation leads to overactivation of the ryanodine receptor[59].

The dysregulation of calcium homeostasis in diseased neurons was accompanied by an increased vulnerability to ER stress responses involving elevation of cytosolic calcium by the calcium ionophore A23187 and rotenone. Recently, mitochondrial impairment has been linked to GCase dysfunction providing a further rationale for the increased susceptibility to rotenone described in this study[60]. Importantly, increased neurotoxicity was observed in *GBA1* mutant neurons exposed to A23187 on NECAB2 knockdown. These data demonstrate the calcium-buffering properties of NECAB2 and support the hypothesis that the increase of NECAB2 in neurons harbouring *GBA1* mutations represents a compensatory mechanism in such vulnerable neurons.

In summary our studies showed that both GD and PD iPSC-derived neurons have increased levels of α-syn and Glc-Cer as well as complex changes in the autophagic/lysosomal system and calcium homeostasis, which may underlie the selective vulnerability of mDA neurons to degeneration in PD. Taken together, our results suggest possible targets for the development of disease-modifying drugs for patients with familial and idiopathic PD.

Methods

Sample collection. Informed consent was obtained from all patients involved in our study before cell donation or CSF collection. The Ethics Committee of the Medical Faculty and the University Hospital Tübingen previously approved this consent form. PD was diagnosed according to UK Brain Bank criteria[61]. The open-reading frame (11 exons) of the *GBA1* gene was entirely sequenced in cases and controls. See Supplementary Table 3 for primer sequences. For CSF studies, control individuals underwent spinal taps for exclusion of vascular events or inflammatory conditions. Any clinical sign of a neurodegenerative disorder led to exclusion from the study. Dermal fibroblasts were cultured in fibroblast medium, which consisted of DMEM (Biochrom) supplemented with 10% fetal calf serum, 1% penicillin/streptomycin/glutamine, 1% nonessential amino acids, 1% sodium pyruvate (all PAA) and 0.5 mM β-mercaptoethanol (Invitrogen). GD fibroblasts were obtained from the Telethon Genetic Biobank Network (02FFF0491979, 02FFF0352006, 02FFF0201995, 02FFF0361999).

Generation of iPSCs and gene correction. Fibroblasts were infected with a mix of retroviruses encoding OCT4, SOX2, KLF4 and c-MYC. Five days after infection, cells were split into six-well plates pre-seeded with irradiated mouse embryonic fibroblasts (MEF, GlobalStem). Seven days after infection the medium was changed to human embryonic stem cell (hESC) medium consisting of KO-DMEM (Gibco) supplemented with 20% KO-Serum Replacement (Invitrogen), 2 mM Glutamax (Invitrogen), 50 μM β-mercaptoethanol (Invitrogen), non-essential amino acids

(Cambrex) and 10 ng ml^{-1} b-FGF (Peprotech). Individual colonies were isolated and clonally expanded on MEFs.

For gene correction, iPSCs were dissociated into single cells using Accutase (PAA). In total, 1.5×10^6 cells were diluted in hESC medium and collected by centrifugation. Cells were transfected with 0.83 μg of each ZFN construct (Sigma), as well as 3.3 μg linearized targeting vector, using the Stem cell Nucleofection Kit and the Amaxa Nucleofector I (both Lonza), according to the manufacturer's instructions (program B16). The transfected cells were replated onto MEF-coated plates in hESC medium supplemented with 10μM ROCK inhibitor Y27632 (Ascent Scientific). From day 2 on, medium was changed on a daily basis. After colony formation (5–7 days), 250 μg ml^{-1} G418 (Biochrom) was added to select for homologous recombined clones. Resistant colonies were transferred to 12-well plates and expanded on MEFs for further characterization. To confirm gene correction, genomic DNA was extracted from the gene-targeted clones and sequenced at the corresponding locus. Final characterization was achieved by extraction of RNA using the RNeasy kit (Qiagen), transcription into cDNA and sequencing of the cDNA. See Supplementary Table 4 for primer sequences.

Karyotyping. Karyotyping was performed by G-banding to examine the integrity of the chromosomes by the Cytogenetics Laboratory at the University of Tübingen.

***In vitro* differentiation of human iPSCs.** To test *in vitro* pluripotency, embryoid bodies (EBs) were generated from iPSCs by culturing the colonies in hESC medium in the absence of b-FGF. After 5 days, EBs were transferred to gelatin-coated plates and subsequently cultured for another 14 days in N2/B27 supplemented with 10 μM SB431542 (Tocris) (ectoderm) or knockout DMEM (Invitrogen) supplemented with 20% FBS, 1 mM L-glutamine (L-glut), 1% non-essential amino acids, 0.1 mM β-mercaptoethanol and 1% penicillin/streptomycin (endoderm/mesoderm). After 2 weeks, cultures were fixed and stained as indicated.

Teratoma assay. Teratoma assays were performed by Applied Stem Cell (Menlo Park)[62]. In brief, 10^6 iPSCs were injected into the kidney capsule and testis of Fox Chase SCID-beige mice. Animals were killed ~6–12 weeks after injection and haematoxylin-eosin (H&E) stainings were used to analyse harvested tissues.

Differentiation of iPSCs into midbrain DA neurons. iPSCs were differentiated into DA neurons following a floor plate-based mDA neuron induction protocol[10], with minor modifications. iPSC colonies were dissociated into a single-cell suspension using Accutase and 10 μM ROCK inhibitor Y-27632. Cells were collected by centrifugation and seeded at a density of 1.5×10^5 cells per well on Matrigel (BD Biosciences)-coated 12-well plates. Differentiation was based on exposure to LDN193189 (100 nM, Stemgent) from days 0–11, SB431542 (10 μM, Tocris) from days 0–5, SHH C25II (100 ng ml^{-1}, R&D), purmorphamine (2 μM, EMD) and FGF8 (100 ng ml^{-1}, Peprotech) from days 1–7 and CHIR99021 (CHIR; 3 μM, Stemgent) from days 3–13. Cells were grown for 11 days on Matrigel in knockout serum replacement medium (KSR) containing KO-DMEM, 15% knockout serum replacement, 2 mM L-glutamine and 10 μM β-mercaptoethanol. KSR medium was gradually shifted to N2 medium starting on day 5 of differentiation. On day 11, media was changed to Neurobasal/B27/L-glut containing medium (NB/B27; Invitrogen) supplemented with CHIR (until day 13), BDNF (brain-derived neurotrophic factor, 20 ng ml^{-1}; R&D), ascorbic acid (0.2 mM, Sigma), GDNF (glial cell line-derived neurotrophic factor, 20 ng ml^{-1}; R&D), TGFβ3 (transforming growth factor type β3, 1 ng ml^{-1}; R&D), dibutyryl cAMP (dbcAMP, 0.5 mM; Sigma) and DAPT (10 μM; Tocris,) for 9 days. On day 21, cells were dissociated using Accutase and replated on dishes pre-coated with poly-L-ornithine (PLO; 15 μg ml^{-1}) and laminin (1 μg ml^{-1}) in differentiation medium (NB/B27 + BDNF, ascorbic acid, GDNF, dbcAMP, TGFβ3 and DAPT).

Quantitative Real-Time PCR. Total RNA was extracted with an RNeasy kit and quantitative RT–PCR reaction was performed using the SYBR GREEN Kit (Qiagen). The expression level of each gene was normalized to endogenous HMBS levels. Fold-change in gene expression was calculated using the $2^{-\Delta\Delta CT}$ method, based on biological reference samples and housekeeping genes for normalization. All the results were obtained from the evaluation of three technical replicates of three independent experiments. See Supplementary Table 5 for primer sequences.

Flow cytometry. Cells were harvested and gently dissociated using TrypLE (Life Technologies) to obtain a single-cell suspension of $0.5–2 \times 10^6$ cells ml^{-1} and resuspended in Ca^{2+}/Mg^{2+} free phosphate buffered saline (PBS; PAA Laboratories) with 2% FBS and distributed into 1.5 ml microcentrifuge tubes. Centrifugation steps were conducted using a refrigerated table microcentrifuge (Peqlab Perfect Spin 24 R) at 2,400 r.p.m. (542 g) for 3–5 min. Surface antigens were labelled by incubating with the primary antibodies for 30 min in the dark at room temperature. The following conjugated primary antibodies were used in the study: CD15-FITC, CD29-FITC, CD44-FITC, CD24-PE, CD184-APC. See Supplementary Table 6 for the list of antibodies. All antibodies were carefully titrated. The stained cells were analysed on a BD Accuri C6 benchtop cytometer equipped with FL1 (533/30), FL2 (585/40) and FL4 (675/25) bandpass filters. Data were analysed and are presented using BD CFlow software version 1.0.227.4. Neuronal cell sorting was performed on a Beckman Coulter MoFlo instrument using a 100 μm nozzle and sheath pressure of 20 to 25 psi (ref. 11). Excluding debris and the minor amount of cells observed to be dead after harvesting, a primary gate based on forward and side scatter was set to select the overall population of interest. FSC-peak (height) versus FSC-integral (area) gating was applied to exclude doublets for cell sorting. Gates for detecting positive staining were set against unstained controls for surface antigens. Where appropriate, compensation was applied according to single-stained controls of the same cell type included in each individual experiment.

Electrophysiology. For whole-cell patch clamp experiments, neurons derived from iPSCs were plated on 35 mm petri-dishes (Greiner-bio-one). Recordings of cultured neurons were performed at room temperature using an Axopatch 200B amplifier (Molecular devices). Data were digitized using a DigiData 1320A (Molecular devices). During electrophysiological recordings, cells were kept in extracellular solution containing (in mM): 142 NaCl, 8.09 KCl, 6 $MgCl_2$, 1 $CaCl_2$, 10 glucose, 10 HEPES and a final pH of 7.4. Patch pipettes were pulled from borosilicate glass (Science products) using a Sutter P97 Puller (Sutter Instruments Company). Their resistance ranged from 3 to 5 MΩ. Patch pipettes were filled with intracellular solution containing (in mM): 5 KCl, 4 ATP-Mg, 10 phosphocreatine, 0.3 GTP-Na, 10 HEPES, 125 K-gluconate, 2 $MgCl_2$, 10 EGTA with a final pH of 7.2 and an osmolarity of 290 mosmol. The sampling rate was 50 kHz and data were low-pass filtered at 10 kHz. Series resistance (< 20 MΩ) was monitored during the experiment. Cells showing unstable series resistance or resting membrane potential were discarded.

HPLC analysis. Differentiated neuronal cultures at DIV65 of differentiation were washed once with HBSS and then treated with 56 mM KCl in HBSS for 30 min; control cultures were exposed to HBSS. Supernatants were collected, snap-frozen and stored at − 80 °C until analysis. Concentrations of DA were determined by column liquid chromatography with electrochemical detection. The HPLC system (HTEC-500, Eicom Corp.) including a pulse-free microflow pump, a degasser and an amperometric detector equipped with a glassy-carbon electrode, operating at + 0.45 V versus an Ag/AgCl electrode, was used. Samples were injected by use of a CMA/200 Refrigerated Microsampler (CMA/Microdialysis). The chromatograms were recorded and integrated by a computerized data acquisition system (DataApex). DA was separated on a 150 × 2.1 i.d. mm column (CA5-ODS, Eicom Corp.). The mobile phase consisted of 0.1 M phosphate buffer at pH 6.0, 0.13 mM EDTA, 2.3 mM sodium-1-octanesulfonate and 20% methanol. The detection limit (signal-to-noise ratio = 3) for DA was estimated to 0.5 fmol in 15 μl (0.03 nM) injected onto the column. Well to well variations were adjusted by concentration of cleared protein lysates.

Glc-Cer and Gal-Cer analysis by mass spectrometry. Quantitative analysis of Glc-Cer was carried out by LC-MS/MS. In brief, frozen cell pellets were suspended in 50 μl of water and extracted with 1 ml of a solution of acetonitrile: methanol: water (97:2:1, v v^{-1} v^{-1}) at room temperature. Extracts were injected onto an Atlantis HILIC silica column (Waters Corp.) for separation of Glc-Cer and Gal-Cer, and respective molecules were detected using MRM mode tandem mass spectrometry with an AB Sciex API-5000 mass spectrometer. Analytes were quantitated against standard curves using standards obtained from Matreya, LLC (Pleasant Gap).

Enzymatic activity assays. Total cell associated GCase activities were analysed using 4-methylumbelliferyl-β-D-glucopyranoside (MUB-Glc), β-galactosidase and β-hexosaminidase activities were assayed using the artificial substrates 4-methylumbelliferyl β-D-galactopyranoside (MUB-Gal) and 4-methylumbelliferyl N-acetyl-β-D-glucosaminide (MUG) (all Glycosynth)[30]. Differentiated iPSCs at DIV65-70 were enriched by FACS and plated into Matrigel-coated 48-well assay plates in differentiation medium (500 μl per well). Media was changed every 3 days. Seven days after plating, cells were washed twice with PBS, harvested and lysed in water containing complete protease inhibitor cocktails (Roche). Total cell protein was measured using the Micro BCA assay reagent (Pierce). Cell lysates were transferred to a 96-well microplate and enzymatic assays were performed in triplicates. The activities of β-galactosidase and β-hexosaminidase were measured in McIlvaine Buffer (0.1 M Citrate/0.2 M Phosphate) pH 5.2 using 0.5 mM MUB-Gal and 1 mM MUG, respectively. For CBE-sensitive GCase and GBA2 assays, the cells were pre-incubated for 30 min at room temperature in McIlvaine Buffer (0.1 M Citrate/0.2 M Phosphate) pH 6.0 containing 5 nM AMP-DNM *N*-(5-adamantane-1-yl-methoxy-pentyl)-deoxynojirimycin)[24] and 1 mM CBE (conduritol B epoxide, Calbiochem), respectively. GCase and GBA2 activities were also determined using 150 nM AMP-DNJ (Miglustat, Zavesca) as an inhibitor (no significant differences were found compared with AMP-DNM). No enzymatic activity was detected after the concomitant use of CBE and AMP-DNM or AMP-DNJ. After incubation with the inhibitors, MUB-Glc was added at a final concentration of 3 mM. The reaction mixtures were incubated at 37 °C under gentle shaking. The fluorescence was recorded after transferring 20 μl of the

reaction mixtures to a microplate and adding 180 µl of 0.25 M glycine, pH 10.7. Data were calculated as pmoles of converted substrate mg^{-1} of cell protein h^{-1}.

Sphingolipid analyses. Fibroblasts, undifferentiated iPSCs, differentiated iPSCs, sorted neurons and granule cells obtained from the cerebellum of 8-day-old Harlan Sprague–Dawley rats at DIV 8 were plated on poly-L-ornithine (PLO)/laminin-coated 48 wells. Two days (fibroblasts, undifferentiated iPSCs and primary granule cells, unsorted differentiated iPSCs) or seven days (sorted neurons) after plating, cells were incubated with 3×10^{-8} [1-^{3}H]-D-erythro-C18/C20-sphingosine in the appropriate culture medium (2-h pulse followed by a 48-h chase). Fresh brains from three 2-month-old C57BL/6j mice and three Harlan Sprague–Dawley rats were weighted, minced with a razor blade, homogenized in iced water (500 mg of fresh tissue ml^{-1}), sonicated and then lyophilized. Lipids were extracted from cells and brains with chloroform/methanol/water in the ratio 2:1:0.1 by volume and subjected to a two-phase partitioning. Radioactive gangliosides were separated by mono- or two-dimensional HPTLC carried out with the solvent systems chloroform/methanol/0.2% aqueous $CaCl_2$, 50: 42: 11 or 55: 45: 10[63]. Brain endogenous gangliosides were recognized using Ehrlich's reagent[64]. Radioactive lipids were identified and quantified with a Beta-Imager 2000 instrument (Biospace) using an acquisition time of about 48 h. The use of animal models was approved by the Italian Government (D.M. 33/2004).

Immunofluorescence. Cells were fixed in 4% paraformaldehyde for 10 min, rinsed with PBS and blocked by 10% normal goat or donkey serum in PBST (PBS + 0.1% TritonX-100) for 60 min[62]. Alkaline phosphatase staining was performed using the Alkaline Phosphatase Kit (Millipore), according to the manufacturer's protocol. For LC3, LAMP1 and LAMP2 analysis, cells were co-stained for β-TubIII and TH, and images were acquired with a Zeiss LSM 510 (Carl Zeiss) confocal microscope using a 63 × 1.4NA plan-apochromat oil objective. Images were processed in ImageJ (NIH) and brightness/contrast was adjusted equally. The particle size and number in β-TubIII and TH^+ cells were quantified with the 'analyse particles' plug-in in ImageJ (NIH). Quantification was carried out on at least 50 cells per condition from independent experiments. Co-localization of LC3/LAMP1 in TH^+ neurons was quantified in threshold images with the 'JACoP' plug-in of the ImageJ software. See Supplementary Table 6 for the list of antibodies used.

Protein extraction and western blotting. Proteins were extracted using RIPA protein extraction buffer (50 mM Tris pH 8, 150 mM NaCl, 0.5% natriumdeoxycholate, 1% NP40, 0.1% SDS) containing protease and phosphatase inhibitors (Roche) on ice. In total, 15–30 µg of the protein lysate was loaded on a 4–12% Bis-Tris Gel (NuPAGE, Invitrogen) and transferred on a PVDF membrane (Millipore). Blots were incubated with primary antibodies overnight at 4 °C on a shaker platform and were then probed with anti-mouse (Dianova), anti-rabbit (Dako) or anti-goat (JacksonLab) IgG-HRP (H + L) secondary antibody (all 1:10.000) for 1 h at room temperature. Visualization was done by using Amersham ECL Western Blotting Detection Reagent (GE Healthcare). Densitometry analyses on the immunoblots from multiple experiments were performed by ImageJ software. See Supplementary Table 6 for the list of antibodies used. Full-length images of immunoblots are shown in Supplementary Figs 16–18.

Autophagy studies. Where indicated, cells were treated with NH_4Cl (20 mM) and leupeptin (200 µM) (EMD, Millipore) for 4 h and then fixed or lysed for western blot analysis. LC3-II levels were quantified by densitometry and normalized for β-actin. LC3 flux was quantified by dividing levels of LC3-II after lysosomal inhibitor treatment for 4 h by the level of LC3-II without treatment.

Calcium imaging. Cells were loaded with Fura-2 acetoxymethyl ester (Sigma) for 30 min at RT in recording medium (NaCl 140 mM, KCl 4 mM, $CaCl_2$ 2 mM, $MgCl_2$ 1 mM, Glucose 4 mM, HEPES 10 mM). KCl (60 mM) and caffeine (10 mM, Sigma) were prepared in recording medium. For baseline recordings, scans were acquired every 10 s for 5 min. Fluorescence measurements were obtained on an epi-fluorescence inverted microscope (Zeiss Axio Observer). All imaging data were collected and analysed using AxioVision (rel. 4.8) software.

Cytotoxicity assays. After 63–65 days *in vitro*, cells were plated on PLO/laminin-coated 96-well plates at a density of 30.000 cells per well. Two days later, cells were incubated with A23187 (1 to 5 µM, Tocris), or rotenone (50 to 200 nM, Sigma) in N2 medium for 4 h and 24 h, respectively. Dimethyl sulfoxide (DMSO) was used as vehicle and control conditions. The LDH assay (Promega) was performed as per the manufacturer's instructions. For knockdown experiments, cytotoxicity assays were performed 72 h after non-targeting shRNA or NECAB2 shRNA lentiviral infection.

Proteomic analysis. Cells were resuspended in 100 µl lysis buffer (8 M urea, 5 mM DTT, 50 mM HEPES pH 8.5, 1 × Roche Protease Inhibitors, 1 × Roche PhosphoStop phosphatase inhibitors) and cell debris was removed by centrifugation (10 min, 9,000 *g*). The clarified lysate was allowed to incubate at room temperature for 30 min for reduction of disulphide bonds. Cysteines were then alkylated with 15 mM iodoacetamide (45 min, RT, dark). Excess iodoacetamide was quenched with DTT (15 min, RT, dark). The proteins were precipitated using methanol-chloroform and then resuspended in a small volume of 8 M urea, 50 mM HEPES pH 8.5. Before digestion, they were diluted to 1 M urea, 50 mM HEPES pH 8.5. The protein concentrations were measured using the BCA assay (Pierce). Samples were digested overnight at 37 °C with trypsin, which was added at a 1:100 protease-to-protein ratio. This reaction was subsequently quenched with 1% formic acid, the sample desalted using C18 solid-phase extraction (Sep-Pak, Waters) and then dried by vacuum-centrifugation. To perform tandem mass tag labelling, desalted peptides were resuspended in 35 µl of 100 mM HEPES pH 8.5 and 8 µl of acetonitrile. TMT reagents (0.8 mg) were dissolved in anhydrous acetonitrile (40 µl) of which 4 µl was added to the peptides. The mixture was incubated at room temperature for 1 h. The labelling reaction was then quenched by the addition of hydroxylamine to a final concentration of 0.3% (v/v). Each of the TMT-labelled samples were combined at a 1:1:1:1:1:1:1:1 ratio, dried, desalted and fractionated using high pH reversed-phase (HPRP). Following fractionating the samples were acidified to 1% formic acid (v/v), dried, desalted using StageTips, dried and then reconstituted in 5% acetonitrile and 5% formic acid. LC-MS/MS was performed on an LTQ Orbitrap Elite mass spectrometer (Thermo-Fisher Scientific)[65]. The total LC-MS run length for each sample was 180 min consisting of a 150 min gradient from 6 to 33% acetonitrile in 0.125% formic acid. A recently developed MS3 method was used to overcome the interference problem in acquisition of TMT data[66].

Data analysis. Mass spectrometry data were processed using an in-house software pipeline[67]. Raw files were converted to mzXML files and searched using the Sequest algorithm[68] against a composite database containing all sequences from the human International Protein Index (IPI) database (version 3.6) in forward and reverse orientations. Database searching matched MS/MS spectra with fully tryptic peptides from this composite database with a precursor ion tolerance of 20 p.p.m. and a product ion tolerance of 1 Da. Carbamidomethylation of cysteine residues (+ 57.02146 Da) and TMT tags on peptide N-termini (+ 229.162932 Da) were set as static modifications. Oxidation of methionines (+ 15.99492 Da) was set as a variable modification. Linear discriminant analysis was used to filter peptide spectral matches to a 1% FDR, as described previously[67]. For analysis of TMT data, the reporter ion counts of the peptide spectral matches for each protein were summed, as described previously[66,69]. Statistical significance was calculated by *t*-test analysis adjusted using the Benjamini and Hochberg method to control for false-discovery rate and filtered for proteins whose levels changed by at least 1.2-fold. Expression changes were considered significantly up- or downregulated when the *P*-value was ≤ 0.05.

Cerebrospinal fluid enzyme assays. Total protein amounts were measured using a DC protein assay in triplicate according to the manufacturer's instructions (Biorad). β-Glucosidase activities were analysed by using 4-methylumbelliferyl-β-D-glucopyranoside (MUB-Glc). β-Galactosidase and β-hexosaminidase activities were assayed by using the artificial substrates 4-Methylumbelliferyl β-D-galacto-pyranoside (MUB-Gal) and 4-Methylumbelliferyl N-acetyl-β-D-glucosaminide (MUG). β-Mannosidase, α-mannosidase and α-fucosidase activities were determined using 4-methylumbelliferyl-β-D-mannopyranoside (MUB-β-Man), 4-methylumbelliferyl-α-D-mannopyranoside (MUB-α-Man) and 4-methyl-umbelliferyl-α-L-fucopyranoside, respectively (MUB-Fuc) (all Glycosynth). Same amounts of CSF protein was transferred to a 96-well microplate and enzymatic assays performed in triplicate. Determination of the β-galactosidase, β-hexosaminidase, β-mannosidase, α-mannosidase and α-fucosidase activities were performed in McIlvaine Buffer (0.1 M Citrate/0.2 M Phosphate) pH 5.2 using 0.5 mM MUB-Gal and 3 mM MUG, 3 mM MUB-β-Man, 3 mM MUB-α-Man and 3 mM MUB- Fuc, respectively. For CBE-sensitive β-glucosidase and GBA2 assays, cells were pre-incubated for 30 min at room temperature in McIlvaine Buffer (0.1 M Citrate/0.2 M Phosphate) pH 6.0 with 5 nM AMP-DNM and 1 mM CBE, respectively. The activity of the CBE-sensitive β-glucosidase was determined in the presence of 0.5% Triton X-100. After 30 min, MUB-Glc was added at a final concentration of 6 mM. After 30 to 180 min of incubation at 450 r.p.m. stirring and 37 °C, fluorescence was detected by transferring 20 µl of the reaction mixtures to a microplate and adding 180 µl of 0.25 M glycine, pH 10.7.

Lentivirus-mediated shRNA. The verified Mission lentiviral plasmids encoding turbo GFP (SHC003), non-targeting shRNA (SHC016) and NECAB2 shRNA (TRCN0000056234, TRCN0000056236) in pLKO.1-puro vector backbone were purchased from Sigma-Aldrich. Lentiviral stocks were prepared by calcium phosphate transfection and the packaging vectors pLP1, pLP2 and pLP/VSVG using the ViraPower HiPerform T-REx Gateway Expression System (Invitrogen). In brief, 80% confluent HEK 293T cells were transfected with 3 µg of plasmid DNA and 9 µg of the ViraPower packaging mix using the TransIT-LT1 Transfection Reagent (Mirus). The following day, the medium was replaced with fresh culture medium and cells were incubated at 37 °C in a humified 5% CO_2 incubator. After 48 h, medium was changed and the virus-containing supernatant was harvested, filtered through a 0.45 µm PVDF filter membrane (Millipore) and concentrated by centrifugation in a Vivaspin column (Sartorius Stedim Biotech) at 4,000 r.p.m. at 4 °C

for 15 min. Supernatants were collected over 48 to 60 h and titred used at an MOI of five to infect cells.

Statistical analysis. The Statistical Package GraphPad Prism version 4.00 (GraphPad Software, San Diego California USA) was used to analyse the data. Statistical testing involved a two-tailed paired or unpaired Student's *t*-test, One-way Anova with Bonferroni's multiple comparison test or Mann–Whitney U test, as appropriate. Data are expressed as mean + s.e.m. (or + s.d.) as indicated. Significance was considered for $P<0.05$.

References

1. Sidransky, E. *et al.* Multicenter analysis of glucocerebrosidase mutations in Parkinson's disease. *N. Engl. J. Med.* **361,** 1651–1661 (2009).
2. Nalls, M. A. *et al.* A multicenter study of glucocerebrosidase mutations in dementia with lewy bodies. *JAMA Neurol.* **70,** 727–735 (2013).
3. Neudorfer, O. *et al.* Occurrence of Parkinson's syndrome in type I Gaucher disease. *QJM* **89,** 691–694 (1996).
4. Bultron, G. *et al.* The risk of Parkinson's disease in type 1 Gaucher disease. *J. Inherit. Metab. Dis.* **33,** 167–173 (2010).
5. Westbroek, W., Gustafson, A. M. & Sidransky, E. Exploring the link between glucocerebrosidase mutations and parkinsonism. *Trends Mol. Med.* **17,** 485–493 (2011).
6. Sardi, S. P., Singh, P., Cheng, S. H., Shihabuddin, L. S. & Schlossmacher, M. G. Mutant GBA1 expression and synucleinopathy risk: first insights from cellular and mouse models. *Neurodegener. Dis.* **10,** 195–202 (2012).
7. Park, I. H. *et al.* Disease-specific induced pluripotent stem cells. *Cell* **134,** 877–886 (2008).
8. Cooper, O. *et al.* Pharmacological rescue of mitochondrial deficits in iPSC-derived neural cells from patients with familial Parkinson's disease. *Sci. Transl. Med.* **4,** 141ra190 (2012).
9. Reinhardt, P. *et al.* Genetic correction of a LRRK2 mutation in human iPSCs links parkinsonian neurodegeneration to ERK-dependent changes in gene expression. *Cell Stem Cell* **12,** 354–367 (2013).
10. Kriks, S. *et al.* Dopamine neurons derived from human ES cells efficiently engraft in animal models of Parkinson's disease. *Nature* **480,** 547–551 (2011).
11. Pruszak, J., Sonntag, K. C., Aung, M. H., Sanchez-Pernaute, R. & Isacson, O. Markers and methods for cell sorting of human embryonic stem cell-derived neural cell populations. *Stem Cells* **25,** 2257–2268 (2007).
12. Pruszak, J., Ludwig, W., Blak, A., Alavian, K. & Isacson, O. CD15, CD24, and CD29 define a surface biomarker code for neural lineage differentiation of stem cells. *Stem Cells* **27,** 2928–2940 (2009).
13. Yuan, S. H. *et al.* Cell-surface marker signatures for the isolation of neural stem cells, glia and neurons derived from human pluripotent stem cells. *PLoS ONE* **6,** e17540 (2011).
14. Turac, G. *et al.* Combined flow cytometric analysis of surface and intracellular antigens reveals surface molecule markers of human neuropoiesis. *PLoS ONE* **8,** e68519 (2013).
15. Jo, E., McLaurin, J., Yip, C. M., St George-Hyslop, P. & Fraser, P. E. Alpha-Synuclein membrane interactions and lipid specificity. *J. Biol. Chem.* **275,** 34328–34334 (2000).
16. Ngamukote, S., Yanagisawa, M., Ariga, T., Ando, S. & Yu, R. K. Developmental changes of glycosphingolipids and expression of glycogenes in mouse brains. *J. Neurochem.* **103,** 2327–2341 (2007).
17. Svennerholm, L. *et al.* Human brain gangliosides: developmental changes from early fetal stage to advanced age. *Biochim. Biophys. Acta* **1005,** 109–117 (1989).
18. Yavin, Z. & Yavin, E. Immunofluorescent patterns of dissociated rat embryo cerebral cells during development in surface culture: distinctive reactions with neurite and perikaryon cell membranes. *Dev. Neurosci.* **1,** 31–40 (1978).
19. Prinetti, A. *et al.* Changes in the lipid turnover, composition, and organization, as sphingolipid-enriched membrane domains, in rat cerebellar granule cells developing *in vitro*. *J. Biol. Chem.* **276,** 21136–21145 (2001).
20. Chigorno, V., Sciannamblo, M., Mikulak, J., Prinetti, A. & Sonnino, S. Efflux of sphingolipids metabolically labeled with [1-3H]sphingosine, L-[3- 3H]serine and [9,10- 3H]palmitic acid from normal cells in culture. *Glycoconj. J.* **23,** 159–165 (2006).
21. Sciannamblo, M. *et al.* Changes of the ganglioside pattern and content in human fibroblasts by high density cell population subculture progression. *Glycoconj. J.* **19,** 181–186 (2002).
22. Riboni, L. *et al.* Ganglioside pattern of normal human brain, from samples obtained at surgery. A study especially referred to alkali labile species. *J. Biochem.* **96,** 1943–1946 (1984).
23. van Weely, S., Brandsma, M., Strijland, A., Tager, J. M. & Aerts, J. M. Demonstration of the existence of a second, non-lysosomal glucocerebrosidase that is not deficient in Gaucher disease. *Biochim. Biophys. Acta* **1181,** 55–62 (1993).
24. Overkleeft, H. S. *et al.* Generation of specific deoxynojirimycin-type inhibitors of the non-lysosomal glucosylceramidase. *J. Biol. Chem.* **273,** 26522–26527 (1998).
25. Mazzulli, J. R. *et al.* Gaucher disease glucocerebrosidase and alpha-synuclein form a bidirectional pathogenic loop in synucleinopathies. *Cell* **146,** 37–52 (2011).
26. Panicker, L. M. *et al.* Induced pluripotent stem cell model recapitulates pathologic hallmarks of Gaucher disease. *Proc. Natl Acad. Sci. USA* **109,** 18054–18059 (2012).
27. Manning-Bog, A. B., Schule, B. & Langston, J. W. Alpha-synuclein-glucocerebrosidase interactions in pharmacological Gaucher models: a biological link between Gaucher disease and parkinsonism. *Neurotoxicology* **30,** 1127–1132 (2009).
28. Sardi, S. P. *et al.* CNS expression of glucocerebrosidase corrects alpha-synuclein pathology and memory in a mouse model of Gaucher-related synucleinopathy. *Proc. Natl Acad. Sci. USA* **108,** 12101–12106 (2011).
29. Fuchs, J. *et al.* Genetic variability in the SNCA gene influences alpha-synuclein levels in the blood and brain. *FASEB J.* **22,** 1327–1334 (2008).
30. Aureli, M. *et al.* Cell surface associated glycohydrolases in normal and Gaucher disease fibroblasts. *J. Inherit. Metab. Dis.* **35,** 1081–1091 (2012).
31. Burke, D. G. *et al.* Increased glucocerebrosidase (GBA) 2 activity in GBA1 deficient mice brains and in Gaucher leucocytes. *J. Inherit. Metab. Dis.* (2012).
32. Balducci, C. *et al.* Lysosomal hydrolases in cerebrospinal fluid from subjects with Parkinson's disease. *Movement Disorders* **22,** 1481–1484 (2007).
33. Parnetti, L. *et al.* Cerebrospinal fluid beta-glucocerebrosidase activity is reduced in Dementia with Lewy Bodies. *Neurobiol. Dis.* **34,** 484–486 (2009).
34. Gegg, M. E. *et al.* Glucocerebrosidase deficiency in substantia nigra of parkinson disease brains. *Ann. Neurol.* **72,** 455–463 (2012).
35. Schapira, A. H. Calcium dysregulation in Parkinson's disease. *Brain* **136,** 2015–2016 (2013).
36. Freestone, P. S. *et al.* Acute action of rotenone on nigral dopaminergic neurons-involvement of reactive oxygen species and disruption of Ca2 + homeostasis. *Eur. J. Neurosci.* **30,** 1849–1859 (2009).
37. Pal, R., Monroe, T. O., Palmieri, M., Sardiello, M. & Rodney, G. G. Rotenone induces neurotoxicity through Rac1-dependent activation of NADPH oxidase in SHSY-5Y cells. *FEBS Lett.* **588,** 472–481 (2013).
38. Brockmann, K. *et al.* GBA-associated PD presents with nonmotor characteristics. *Neurology* **77,** 276–280 (2011).
39. Kracun, I., Rosner, H., Cosovic, C. & Stavljenic, A. Topographical atlas of the gangliosides of the adult human brain. *J. Neurochem.* **43,** 979–989 (1984).
40. Israel, M. A. *et al.* Probing sporadic and familial Alzheimer's disease using induced pluripotent stem cells. *Nature* **482,** 216–220 (2012).
41. Velayati, A., Yu, W. H. & Sidransky, E. The role of glucocerebrosidase mutations in Parkinson disease and Lewy body disorders. *Curr. Neurol. Neurosci. Rep.* **10,** 190–198 (2010).
42. Goker-Alpan, O., Stubblefield, B. K., Giasson, B. I. & Sidransky, E. Glucocerebrosidase is present in alpha-synuclein inclusions in Lewy body disorders. *Acta Neuropathol.* **120,** 641–649 (2010).
43. Xu, Y. H. *et al.* Accumulation and distribution of alpha-synuclein and ubiquitin in the CNS of Gaucher disease mouse models. *Mol. Genet. Metab.* **102,** 436–447 (2011).
44. Shachar, T. *et al.* Lysosomal storage disorders and Parkinson's disease: Gaucher disease and beyond. *Movement Disorders* **26,** 1593–1604 (2011).
45. Koga, H., Kaushik, S. & Cuervo, A. M. Altered lipid content inhibits autophagic vesicular fusion. *FASEB J.* **24,** 3052–3065 (2010).
46. Valaperta, R. *et al.* Plasma membrane production of ceramide from ganglioside GM3 in human fibroblasts. *FASEB J.* **20,** 1227–1229 (2006).
47. Boot, R. G. *et al.* Identification of the non-lysosomal glucosylceramidase as beta-glucosidase 2. *J. Biol. Chem.* **282,** 1305–1312 (2007).
48. Yildiz, Y. *et al.* Mutation of beta-glucosidase 2 causes glycolipid storage disease and impaired male fertility. *J. Clin. Investig.* **116,** 2985–2994 (2006).
49. Hammer, M. B. *et al.* Mutations in GBA2 cause autosomal-recessive cerebellar ataxia with spasticity. *Am. J. Hum. Genet.* **92,** 245–251 (2013).
50. Martin, E. *et al.* Loss of function of glucocerebrosidase GBA2 is responsible for motor neuron defects in hereditary spastic paraplegia. *Am. J. Hum. Genet.* **92,** 238–244 (2013).
51. Maor, G. *et al.* Unfolded protein response in Gaucher disease: from human to Drosophila. *Orphanet. J. Rare Dis.* **8,** 140 (2013).
52. Korschen, H. G. *et al.* The non-lysosomal beta-glucosidase GBA2 is a non-integral membrane-associated protein at the endoplasmic reticulum (ER) and Golgi. *J. Biol. Chem.* **288,** 3381–3393 (2013).
53. Sugita, S., Ho, A. & Sudhof, T. C. NECABs: a family of neuronal Ca(2 +)-binding proteins with an unusual domain structure and a restricted expression pattern. *Neuroscience* **112,** 51–63 (2002).
54. Canela, L. *et al.* The neuronal Ca(2 +) -binding protein 2 (NECAB2) interacts with the adenosine A(2A) receptor and modulates the cell surface expression and function of the receptor. *Mol. Cell Neurosci.* **36,** 1–12 (2007).
55. Ganat, Y. M. *et al.* Identification of embryonic stem cell-derived midbrain dopaminergic neurons for engraftment. *J. Clin. Investig.* **122,** 2928–2939 (2012).

56. Guzman, J. N., Sanchez-Padilla, J., Chan, C. S. & Surmeier, D. J. Robust pacemaking in substantia nigra dopaminergic neurons. *J. Neurosci.* **29,** 11011–11019 (2009).
57. Foehring, R. C., Zhang, X. F., Lee, J. C. & Callaway, J. C. Endogenous calcium buffering capacity of substantia nigral dopamine neurons. *J. Neurophysiol.* **102,** 2326–2333 (2009).
58. Hurley, M. J., Brandon, B., Gentleman, S. M. & Dexter, D. T. Parkinson's disease is associated with altered expression of CaV1 channels and calcium-binding proteins. *Brain* **136,** 2077–2097 (2013).
59. Pelled, D. *et al.* Enhanced calcium release in the acute neuronopathic form of Gaucher disease. *Neurobiol. Dis.* **18,** 83–88 (2005).
60. Osellame, L. D. *et al.* Mitochondria and quality control defects in a mouse model of Gaucher disease-links to Parkinson's disease. *Cell Metab.* **17,** 941–953 (2013).
61. Litvan, I. *et al.* Movement disorders society scientific issues committee report: SIC Task Force appraisal of clinical diagnostic criteria for Parkinsonian disorders. *Movement Disorders* **18,** 467–486 (2003).
62. Deleidi, M., Hargus, G., Hallett, P., Osborn, T. & Isacson, O. Development of histocompatible primate-induced pluripotent stem cells for neural transplantation. *Stem Cells* **29,** 1052–1063 (2011).
63. Scandroglio, F. *et al.* Lipid content of brain, brain membrane lipid domains, and neurons from acid sphingomyelinase deficient mice. *J. Neurochem.* **107,** 329–338 (2008).
64. Partridge, S. M. Filter-paper partition chromatography of sugars: 1. General description and application to the qualitative analysis of sugars in apple juice, egg white and foetal blood of sheep. with a note by R. G. Westall. *Biochem. J.* **42,** 238–250 (1948).
65. McAllister, F. E. *et al.* Mass spectrometry based method to increase throughput for kinome analyses using ATP probes. *Anal. Chem.* **85,** 4666–4674 (2013).
66. McAlister, G. C. *et al.* Increasing the multiplexing capacity of TMTs using reporter ion isotopologues with isobaric masses. *Anal. Chem.* **84,** 7469–7478 (2012).
67. Huttlin, E. L. *et al.* A tissue-specific atlas of mouse protein phosphorylation and expression. *Cell* **143,** 1174–1189 (2010).
68. Eng, J. K., McCormack, J. R. & Yates, 3rd J. R. An approach to correlate tandem mass spectral data of peptides with amino acid sequences in a protein database. *J. Am. Soc. Mass Spectrometry* **5,** 976–989 (1994).
69. Ting, L., Rad, R., Gygi, S. P. & Haas, W. MS3 eliminates ratio distortion in isobaric multiplexed quantitative proteomics. *Nat. Methods* **8,** 937–940 (2011).
70. Vizcaino, J. A. *et al.* The PRoteomics IDEntifications (PRIDE) database and associated tools: status in 2013. *Nucleic Acid Res.* **41,** D1063–D1069 (2013).

Acknowledgements

We thank Daniela M. Arduino for helping with the autophagy studies; Ann-Kathrin Hauser for the sequencing analysis; Dr Marie Follo and Klaus Geiger of the Core Facility, University Medical Center Freiburg for cell sorting; Lindsay Sweet, Genzyme Corporation for LC-MS measurements. Gaucher's disease samples were obtained from the 'Cell Line and DNA Biobank from Patients affected by Genetic Diseases' (G. Gaslini Institute)—Telethon Genetic Biobank Network (Project No. GTB07001)'. We thank the PRIDE team for assistance in the submission of the mass spectrometry proteomics data. This work was supported by the Marie Curie Career Integration Grant MC CIG304108 (M.D.), Fritz Thyssen Foundation grant 10.13.1.155 (M.D.), German Research Foundation (D.F.G.) grant KR2119/8-1 (T.G.), Eva-Theers-Stiftung (T.G. and M.D.) and by German Research Foundation (D.F.G.) grant PR1132/3-1 (J.P.). C.H. and M.D. were each supported by an Alexander von Humboldt-Foundation Postdoctoral Fellowship.

Author contributions

D.C.S. performed the experiments and analysed the data; M.A. performed the experiments and analysed the data, participated in writing the manuscript; F.E.M. performed the MS experiments and analysed the data, participated in writing the manuscript; C.J.H. performed the FACS experiments and analysed the data; F.M. performed experiments; B.S. performed experiments; S.P.S. provided LC/MS data; M.V. performed experiments; S.H. performed experiments; L.K.S. performed experiments; U.H. performed experiments; D.B. oversaw patient sample collection; L.S. provided LC/MS data; J.H. designed calcium imaging experiments; J.P. performed experiments, designed the FACS experiments and participated in writing the manuscript; S.P.G. carried out mass spectrometry; S.S. participated in designing experiments and writing the manuscript; T.G. supervised part of the study and wrote the manuscript; M.D. designed and coordinated the study, performed experiments, analysed the data and wrote the manuscript.

Additional information

Accession codes The mass spectrometry proteomics data have been deposited in ProteomeXchange *via* the PRIDE partner repository[70] under the accession code PXD000866.

Supplementary Information accompanies this paper at http://www.nature.com/naturecommunications

Competing financial interests: The authors declare no conflict of interest.

Reprints and permission information is available online at http://npg.nature.com/reprintsandpermissions/

How to cite this article: Schöndorf, D. C. *et al.* iPSC-derived neurons from GBA1-associated Parkinson's disease patients show autophagic defects and impaired calcium homeostasis. *Nat. Commun.* 5:4028 doi: 10.1038/ncomms5028 (2014).

Article

Cell Reports

The NAD+ Precursor Nicotinamide Riboside Rescues Mitochondrial Defects and Neuronal Loss in iPSC and Fly Models of Parkinson's Disease

Graphical Abstract

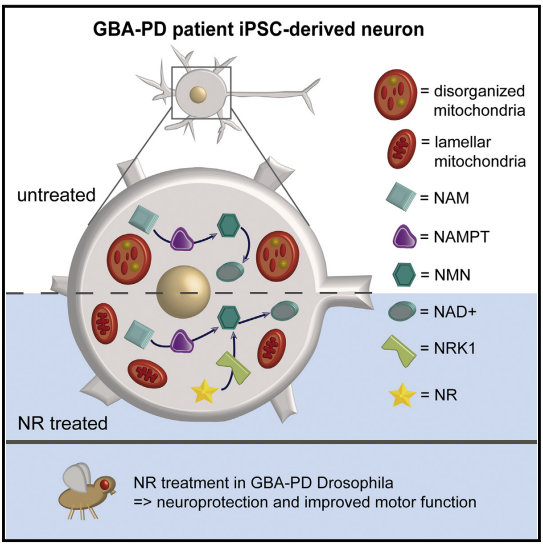

Highlights

- NAD+ metabolism and mitochondrial function are altered in GBA-PD neurons
- Human iPSC-derived neurons are responsive to NAD+ precursors
- Nicotinamide riboside improves mitochondrial function in GBA-PD iPSC neurons
- Nicotinamide riboside rescues neuronal loss and motor deficits in GBA-PD flies

Authors

David C. Schöndorf, Dina Ivanyuk, Pascale Baden, ..., Thomas Gasser, Alexander J. Whitworth, Michela Deleidi

Correspondence

michela.deleidi@dzne.de

In Brief

Mitochondrial damage is a key feature in Parkinson's disease. Schöndorf et al. demonstrate that nicotinamide riboside, an NAD+ precursor, boosts mitochondrial function in neurons derived from Parkinson's disease patient stem cells and is neuroprotective in Parkinson's disease fly models. These findings support use of NAD+ precursors in Parkinson's and other neurodegenerative diseases.

Schöndorf et al., 2018, Cell Reports *23*, 2976–2988
June 5, 2018
https://doi.org/10.1016/j.celrep.2018.05.009

CellPress

OPEN ACCESS
CellPress

Cell Reports
Article

The NAD+ Precursor Nicotinamide Riboside Rescues Mitochondrial Defects and Neuronal Loss in iPSC and Fly Models of Parkinson's Disease

David C. Schöndorf,[1,2] Dina Ivanyuk,[1,2,8] Pascale Baden,[1,2,8] Alvaro Sanchez-Martinez,[3] Silvia De Cicco,[1,2] Cong Yu,[1,2] Ivana Giunta,[3] Lukas K. Schwarz,[1,2] Gabriele Di Napoli,[1,2] Vasiliki Panagiotakopoulou,[1,2] Sigrun Nestel,[4] Marcus Keatinge,[5] Jan Pruszak,[6,7] Oliver Bandmann,[5] Bernd Heimrich,[4] Thomas Gasser,[1,2] Alexander J. Whitworth,[3] and Michela Deleidi[1,2,9,*]

[1]German Center for Neurodegenerative Diseases (DZNE), Helmholtz Association, Tübingen 72076, Germany
[2]Hertie-Institute for Clinical Brain Research, University of Tübingen, Tübingen 72076, Germany
[3]Medical Research Council Mitochondrial Biology Unit, University of Cambridge, Cambridge Biomedical Campus, Hills Road, Cambridge CB2 0XY, UK
[4]Department of Neuroanatomy, Institute of Anatomy and Cell Biology, University of Freiburg, Freiburg 79104, Germany
[5]Sheffield Institute for Translational Neuroscience (SITraN), University of Sheffield, Sheffield, UK
[6]Emmy Noether-Group for Stem Cell Biology, Department of Molecular Embryology, Institute of Anatomy and Cell Biology, Faculty of Medicine, University of Freiburg, Freiburg, Germany
[7]Center for Biological Signaling Studies (BIOSS), University of Freiburg, Freiburg 79104, Germany
[8]These authors contributed equally
[9]Lead Contact
*Correspondence: michela.deleidi@dzne.de
https://doi.org/10.1016/j.celrep.2018.05.009

SUMMARY

While mitochondrial dysfunction is emerging as key in Parkinson's disease (PD), a central question remains whether mitochondria are actual disease drivers and whether boosting mitochondrial biogenesis and function ameliorates pathology. We address these questions using patient-derived induced pluripotent stem cells and *Drosophila* models of *GBA*-related PD (*GBA*-PD), the most common PD genetic risk. Patient neurons display stress responses, mitochondrial demise, and changes in NAD+ metabolism. NAD+ precursors have been proposed to ameliorate age-related metabolic decline and disease. We report that increasing NAD+ via the NAD+ precursor nicotinamide riboside (NR) significantly ameliorates mitochondrial function in patient neurons. Human neurons require nicotinamide phosphoribosyltransferase (NAMPT) to maintain the NAD+ pool and utilize NRK1 to synthesize NAD+ from NAD+ precursors. Remarkably, NR prevents the age-related dopaminergic neuronal loss and motor decline in fly models of *GBA*-PD. Our findings suggest NR as a viable clinical avenue for neuroprotection in PD and other neurodegenerative diseases.

INTRODUCTION

Mitochondrial dysfunction has been proposed as a key mechanism in many neurodegenerative diseases. Among others, Parkinson's disease (PD) stands out due to the role of PD-linked genes in mitochondrial function and dynamics (Exner et al., 2012). Evidence for mitochondrial dysfunction in PD was first described in the 1980s by Schapira et al., who showed complex I (CI) defects in cells and tissues from PD patients (Schapira et al., 1989). Substantial progress has been made since, and genetic and biochemical studies now indicate that mitochondrial dysfunction and cellular energy failure are key to PD (Jansen et al., 2017). In this respect, recent studies have shown that the activation of pathways related to mitochondrial biogenesis and energy metabolism, such as the NAD+/sirtuin 1 (SIRT1) pathway, provides protection against aging-related disease (Rajman et al., 2018). Similar approaches could be easily translated into treatment for PD. However, it is still unclear whether mitochondrial defects are actual disease drivers and increasing mitochondrial biogenesis provides neuroprotection in PD. In addition, little is known about NAD+ metabolism and availability of NAD+ precursors in human neurons. Here, we have addressed these fundamental questions in an induced pluripotent stem cell (iPSC) neuronal model of PD bearing mutations in the lysosomal enzyme β-Glucocerebrosidase (*GBA*) gene (*GBA*-PD), the most common genetic risk for PD (Sidransky et al., 2009). β-Glucocerebrosidase (GCase) activity is reduced not only in mutation carriers but also in idiopathic PD and healthy individuals at older age (Gegg et al., 2012; Rocha et al., 2015), pointing toward a general role for GCase in brain aging and neurodegenerative processes. Importantly, patients with *GBA* mutations represent an etiologically homogeneous subgroup of PD, therefore providing the ideal cohort for precision medicine approaches.

The pathogenetic mechanisms involved in *GBA*-PD are only partially understood and include autophagic defects, increased α-synuclein aggregation, calcium dyshomeostasis,

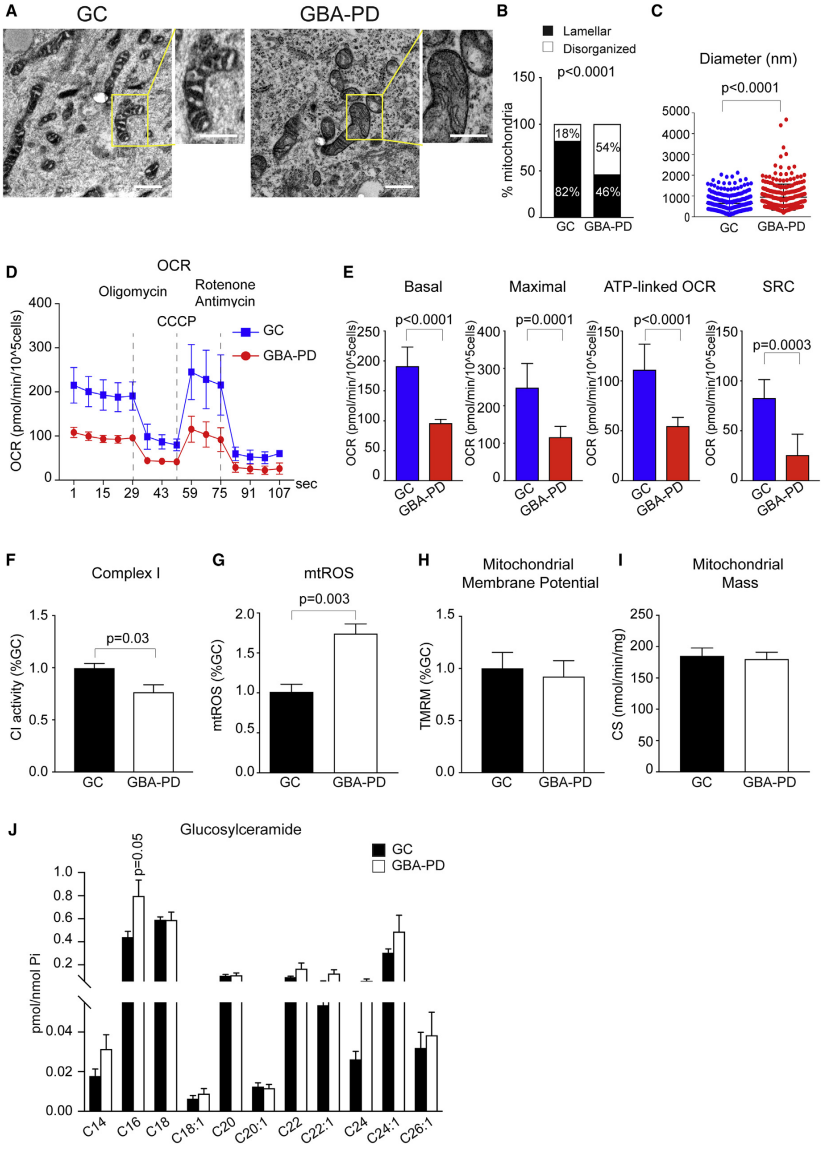

(legend on next page)

and endoplasmic reticulum (ER) stress (Migdalska-Richards and Schapira, 2016). GCase is a lysosomal enzyme that catalyzes the hydrolysis of glucosylceramide (GlcCer), a membrane glycosphingolipid, to ceramide and glucose, and both loss and gain of its enzymatic function may contribute to disease. According to the loss-of-function hypothesis, GCase deficiency causes substrate accumulation that alters lysosomal function and promotes α-synuclein aggregation (Jo et al., 2000; Velayati et al., 2010; Mazzulli et al., 2011). GCase is glycosylated and folded in the ER and subsequently trafficked through the Golgi to the lysosome. According to the gain-of-function hypothesis, *GBA* mutations interfere with the folding process in the ER, leading to ER-associated degradation, ER stress, and activation of the unfolded protein response (UPR) (Maor et al., 2013; Fernandes et al., 2016). Interestingly, mitochondrial dysfunction has been described in experimental models of GCase deficiency (Osellame et al., 2013; Keatinge et al., 2015; Cleeter et al., 2013). However, whether mitochondrial function is altered in PD patients with *GBA* mutations (*GBA*-PD) and the mechanisms underlying such demise are still unknown. Furthermore, whether improving mitochondrial biogenesis and function represents an effective therapeutic strategy for PD needs to be investigated.

RESULTS

iPSC-Derived Neurons from *GBA*-PD Patients Show Defects in Mitochondrial Function

To investigate whether *GBA* is linked to mitochondrial function in human neurons, iPSC lines from PD patients with heterozygous *GBA* mutations (N370S, L444P, and RecNcil), as well as corresponding isogenic gene-corrected (GC) and unaffected controls (Schöndorf et al., 2014) (Table S1), were differentiated into dopaminergic (DA) neurons, and mitochondrial morphology was examined by transmission electron microscopy (TEM). Morphometric analysis revealed altered cristae morphology in *GBA*-PD neurons compared to isogenic GC and healthy controls (Figures 1A, 1B, and S1A). In addition, *GBA*-PD neurons showed a significant increase in mitochondrial diameter (Figure 1C). Next, we measured oxygen consumption rates (OCRs) and found that *GBA*-PD neurons displayed significantly reduced basal respiration and decreased maximal OCR as well as ATP-linked OCR and spare respiratory capacity (SRC) compared to isogenic controls (Figures 1D and 1E). Similarly, basal respiration, maximal OCR, and ATP-linked OCR and SRC were significantly reduced in *GBA*-PD neurons compared to unrelated unaffected controls (Figure S1B). Western blot analysis revealed an increase in the level of respiratory chain complex subunits in *GBA*-PD neurons compared to isogenic controls, but this increase did not reach statistical significance (Figures S1C and S1D). We next measured CI activity in enriched mitochondrial fractions from *GBA*-PD iPSC neurons and GC controls. CI activity was significantly reduced in *GBA*-PD neurons compared to isogenic controls (Figure 1F). Consistent with these findings, *GBA*-PD neurons produced significantly higher amounts of mitochondrial reactive oxygen species (mtROS) than isogenic controls (Figure 1G). However, mitochondrial membrane potential and mitochondrial mass were not significantly changed in *GBA*-PD neurons (Figures 1H and 1I). Of note, no significant difference in the degree of mitochondrial function was observed among different *GBA* genotypes, suggesting that the genotypes examined in this study (RecNcil, L444P, and N370S) equally affect mitochondria (Figures S1E–S1I). To get further insight into the mechanisms underlying mitochondrial dysfunction in *GBA*-PD, we examined the GCase substrate sphingolipid composition of mitochondria from *GBA*-PD neurons and isogenic controls by high-performance liquid chromatography tandem mass spectrometry (HPLC-MS/MS). To this end, mitochondria were isolated from iPSC neurons with a high degree of purity. Western blot analysis showed high level of enrichment of isolated mitochondria with a small amount of non-mitochondrial organelle contamination (Figure S1J). Quantification of individual species of GlcCer revealed the absence of GlcCer accumulation in patient mitochondria with only a significant increase of C16-GlcCer (Figure 1J).

iPSC-Derived Neurons from *GBA*-PD Patients Show Defects in Mitochondrial Dynamics

Next, we examined the level of mitochondrial fission (DRP1 and Fis1) and fusion (OPA1 and Mfn1) proteins in *GBA*-PD iPSC neurons and isogenic controls. Immunoblot analysis revealed a

Figure 1. Mitochondrial Function in *GBA*-PD iPSC Neurons

(A–C) Mitochondrial morphology in isogenic gene-corrected (GC) controls and *GBA*-PD iPSC neurons.

(A) Representative TEM images of mitochondria are shown (L444P *GBA*-PD and GC controls) (scale bar, 500 nm).

(B) Quantification of mitochondrial cristae morphology in isogenic GC and *GBA*-PD (N370S, L444P) iPSC-derived neurons (n = 3; two-sided Fisher's exact test).

(C) Mitochondrial major diameter. Data are presented as mean ± SD (n = 299 GC and n = 264 *GBA*-PD mitochondria from 3 independent experiments were analyzed; two-tailed t test).

(D) Oxygen consumption rate (OCR) trace for isogenic GC and *GBA*-PD (N370S, L444P, RecNcil) iPSC neurons. Data are normalized to cell number and presented as mean ± SD (n = 8; two-tailed t test).

(E) Quantification of basal, maximal, ATP-linked respiration, and spare respiratory capacity (SRC). Data are normalized to cell number and presented as mean + SD (n = 8; two-tailed t test).

(F) Complex I (CI) activity in enriched mitochondria from isogenic *GBA*-PD (N370S, L444P) and GC iPSC neurons. Data are expressed as mean + SEM (n = 5; two-tailed t test).

(G) Mitochondrial ROS (mtROS) levels in *GBA*-PD (N370S, L444P, RecNcil) and GC iPSC neurons. Data are normalized to GC and represented as mean + SEM (n = 5; two-tailed t test).

(H) Mitochondrial membrane potential in isogenic GC and *GBA*-PD (N370S, L444P, RecNcil) iPSC neurons. Data are normalized to GC and presented as mean + SEM (n = 5; two-tailed t test).

(I) Citrate synthase (CS) activities in GC and *GBA*-PD (N370S, L444P, RecNcil) iPSC neurons. Data are presented as mean + SEM (n = 5; two-tailed t test).

(J) Mitochondrial sphingolipid profile of isogenic GC and *GBA*-PD (N370S, L444P) iPSC neurons. Data are normalized to inorganic phosphate (Pi) and presented as mean + SEM (n = 7 independent mitochondrial purifications; two-tailed t test).

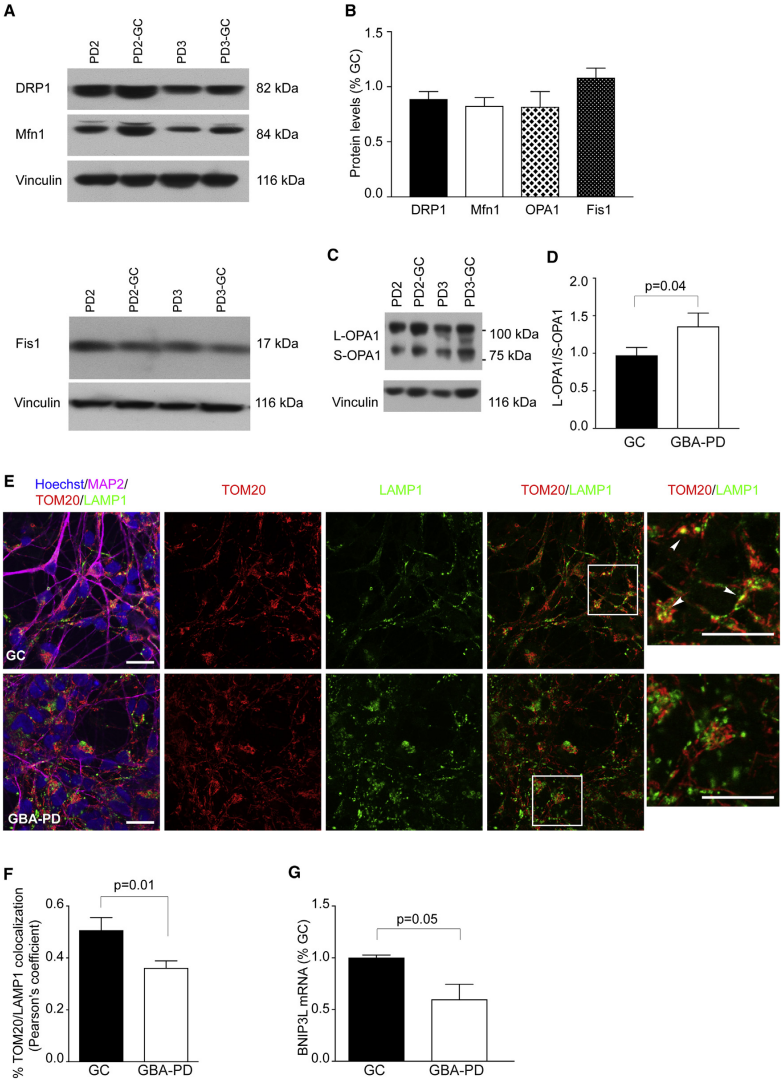

Figure 2. Mitochondrial Dynamics in *GBA*-PD iPSC Neurons

(A and B) Western blot of DRP1, Mfn1, and Fis1 in isogenic *GBA*-PD (N370S, L444P) and gene-corrected (GC) iPSC neurons (A). Vinculin was used as a loading control. Quantification of western blots is shown in (B). Data are normalized to GC and presented as mean + SEM (n = 5).

(C and D) Western blot analysis of OPA-1 processing (C). The L-OPA1/S-OPA-1 ratio is shown in (D). Data are presented as mean + SEM (n = 5; two-tailed t test).

(legend continued on next page)

reduction in DRP1, OPA1, and Mfn1 levels in *GBA*-PD neurons (Figures 2A–2D). On the other hand, there was an increase of Fis1 in *GBA*-PD neurons (Figures 2A and 2B). However, these differences did not reach statistical significance. Interestingly, the ratio between the long and short form of OPA1 was significantly increased in *GBA*-PD neurons compared to isogenic controls, suggesting an impairment of mitophagy (MacVicar and Lane, 2014) (Figures 2C and 2D). *GBA*-PD neurons showed a significant reduction of mitochondrial-lysosomal co-localization compared to GC controls, as assessed by confocal microscopy and Amnis ImageStream flow cytometry (Figures 2E, 2F, S2A, and S2B). In line with these findings, the expression of the mitophagy adaptor protein BNIP3L/NIX was significantly reduced in *GBA*-PD compared to isogenic controls (Figure 2G).

Mitochondrial Function Is Altered in *GBA* Knockout iPSC-Derived Neurons

To assess the impact of loss of GCase enzymatic function on mitochondria in the absence of gain-of-function mechanisms, we generated *GBA* knockout (KO) iPSCs using clustered regularly interspaced short palindromic repeats (CRISPR)-Cas9 (Figures S3A–S3F). *GBA* was knocked out in two healthy control iPSC lines and one *GBA-PD* N370S iPSC line (Table S2). All *GBA* KO clones showed complete loss of GCase protein and its enzymatic activity (Figures S3E and S3F). No significant difference in DA neuronal differentiation potential was observed among *GBA* KO iPSCs and corresponding parental lines as assessed by quantification of βIII-tubulin- and tyrosine hydroxylase (TH)-positive neurons (>80% neurons, of which on average 40% of cells in both controls and *GBA* KO lines expressed TH). *GBA* KO iPSC-derived neurons exhibited accumulation of the GCase substrates GlcCer and glucosylsphingosine as revealed by HPLC-MS/MS (Figures S3G). A significant increase of C16-galactosylceramide was also observed (Figure S3I). No significant change in levels of other sphingolipids was detected (Figures S3H and S3I). Two *GBA* KO clones were selected from each parental iPSC line and used for further experiments (Table S2). As observed in *GBA*-PD neurons, morphometric analysis revealed ultrastructural abnormalities in *GBA* KO iPSC-neurons compared to isogenic controls (Figures 3A and 3B). Similar to what we observed in *GBA*-PD neurons, *GBA* KO neurons showed significantly reduced basal and maximal respiration as well as ATP-linked OCR and SRC (Figure 3C). Despite the consistent trend for decreased CI activity in *GBA* KO neurons, the values did not reach statistical significance (Figure 3D). *GBA* KO neurons showed elevated levels of mtROS (Figure 3E). Furthermore, we did not observe significant changes of mitochondrial membrane potential (Figure 3F). HPLC-MS/MS analysis of mitochondria purified from *GBA* KO iPSC-derived neurons showed a significant accumulation of all subtypes of the GCase substrates GlcCer and glucosylsphingosine (Figure 3G).

GBA-PD, but Not *GBA* Knockout, iPSC-Derived Neurons Show Increased ER Stress and UPR

Interestingly, when comparing OCRs and CI activity in the isogenic lines (*GBA*-PD N370S, GC control and *GBA* KO), no gene dosage effect was found (Figures S3J and S3K). These data suggest that different mechanisms contribute to mitochondrial defects in heterozygous *GBA*-PD patient and *GBA* KO neurons. One of such mechanisms could be the UPR and ER stress that have been previously observed in *GBA-PD* (Fernandes et al., 2016). To dissect the contribution of gain- and loss-of-function of mutant GCase, we measured the levels of the ER chaperone immunoglobulin-binding protein (BiP) by western blot in *GBA*-PD N370S iPSC-derived neurons as well as isogenic controls and isogenic *GBA* KO neurons. Levels of BiP were increased in *GBA*-PD neurons compared to isogenic controls and isogenic *GBA* KO neurons (Figure 4A). Consistent with these findings, RNA levels of spliced X-box-binding protein-1 (XBP1s) were significantly increased in *GBA*-PD, but not in isogenic *GBA* KO neurons, suggesting activation of the IRE1 related branch of ER stress (Figure 4B). Healthy control-derived *GBA* KO neurons showed levels of BiP similar to their isogenic controls (Figure S3L). In addition, levels of phospho-eIF2α were significantly increased in *GBA*-PD, but not in isogenic *GBA* KO neurons, as compared to GC controls (Figure 4C). Consistent with these findings, levels of phospho-PERK were increased only in *GBA*-PD neurons as compared to GC controls (Figure 4D).

NAD+ Metabolism Is Altered in *GBA*-PD iPSC-Derived Neurons

Mitochondrial dysfunction and increased oxidative stress are hallmarks of aging and have been linked to the decline of intracellular levels of NAD+ (Mouchiroud et al., 2013). To examine whether *GBA* mutations lead to changes in NAD+ metabolism, we measured the expression of the NAD+ biosynthetic enzymes nicotinamide mononucleotide adenylyltransferases (NMNATs). mRNA levels of NMNAT2 were significantly decreased in *GBA*-PD neurons compared to isogenic controls, whereas levels of NMNAT1 and NMNAT3 were unchanged (Figure 5A). NMNAT2 levels were unchanged in *GBA* KO neurons (Figure S3M). Levels of nicotinamide phosphoribosyltransferase (NAMPT), the rate-limiting enzyme in the NAD+ salvage synthesis pathway, were similar in both groups (*GBA*-PD and GC controls), as assessed by qRT-PCR (Figure 5A). Next, we measured the adenine and pyridine nucleotide pool in *GBA*-PD and isogenic control as well as *GBA* KO iPSC-neurons by targeted metabolomics using liquid chromatography-mass spectrometry (LC-MS). The intracellular NAD+ content was maintained in *GBA*-PD and *GBA* KO neurons (Figure S4). To exclude that the observed absence of significant changes of NAD+ levels could be linked to the absence of overt neurodegeneration in our stem cell-based model system, we also examined the NAD+ metabolome in adult *gba*$^{+/+}$, *gba*$^{-/-}$, and gba$^{+/-}$ whole zebrafish brains. Adult *gba*$^{-/-}$

(E) Immunostaining of differentiated iPSC cultures for MAP2 (magenta), TOM20 (red), and LAMP1 (green). Cell nuclei were counterstained with Hoechst (blue). Scale bar, 20 μm.

(F) Colocalization between LAMP1 and TOM20. Data are presented as mean + SEM (n = 5; two-tailed t test).

(G) BNIP3L mRNA levels in isogenic GC and *GBA*-PD (N370S, L444P) iPSC-derived neurons. Data are normalized on Rplp0 and OAZ1 and to GC and presented as mean + SEM (n = 5; two-tailed t test).

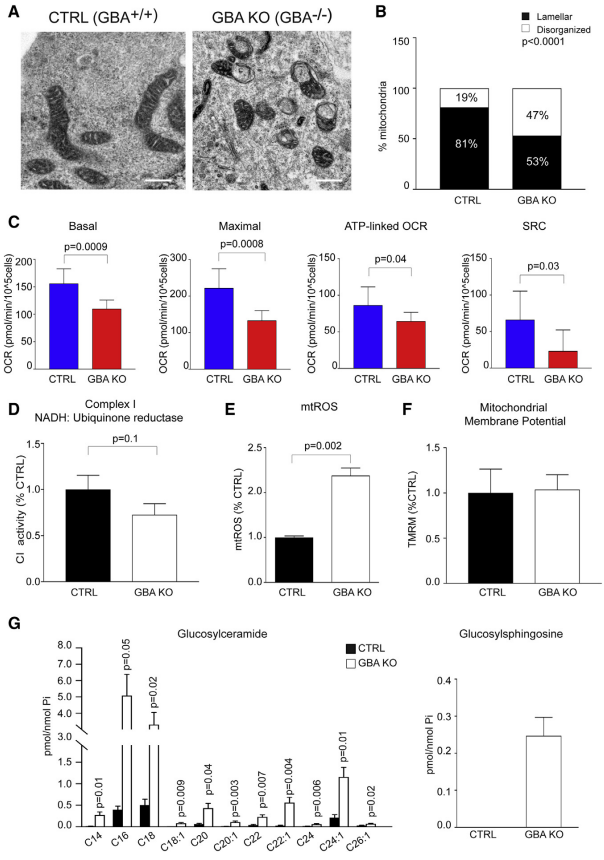

Figure 3. Mitochondrial Function in Human *GBA* KO iPSC Neurons

(A and B) Mitochondrial morphology in isogenic healthy control (CTRL) and *GBA* KO iPSC neurons. Representative TEM images of mitochondria (A; scale bar, 500 nm). Quantification of mitochondrial cristae morphology in isogenic CTRL and *GBA* KO iPSC-neurons (B). Data are presented as mean + SEM (n = 3; two-sided Fisher's exact test).

(C) Mitochondrial respiration. Data are presented as mean + SD (n = 5–7; two-tailed t test).

(D) CI activity in isogenic CTRL and *GBA* KO iPSC neurons. Data are expressed as mean + SEM (n = 5; two-tailed t test).

(E) mtROS levels normalized to CTRL and presented as mean + SEM (n = 5; two-tailed t test).

(F) Mitochondrial membrane potential. Data are presented as mean + SEM (n = 5; two-tailed t test).

(G) Mitochondrial sphingolipid profile of CTRL and *GBA* KO iPSC-neurons. GlcCer and glucosylsphingosine levels normalized by inorganic phosphate (Pi). Glucosylsphingosine was below detection limit in control mitochondria. Data are presented as mean + SEM (n = 4 independent mitochondrial purifications; two-tailed t test).

zebrafish recapitulate the key pathological aspects of PD, including DA neuronal loss, early microglial activation, and mitochondrial dysfunction (Keatinge et al., 2015). Metabolomic analyses revealed that the NAD+ pool was maintained in brains of adult *gba*$^{+/-}$ and *gba*$^{-/-}$ zebrafish (Figure S5). However, a significant increase in nicotinamide mononucleotide (NMN) was observed in *gba*$^{-/-}$ compared to *gba*$^{+/+}$ zebrafish brains as well as in *gba*$^{-/-}$ compared to *gba*$^{+/-}$ brains (Figure S5), suggesting an alteration of NAD+ metabolism. To rule out the possibility that the heterogeneity of the cell culture and whole brain tissues influences the results, we then employed the biosensor Peredox to monitor the cytosolic NADH/NAD+ ratio in single iPSC-derived neurons with live-cell imaging (Hung et al., 2011). The NAD+/NADH redox state was significantly reduced in *GBA*-PD iPSC neurons, suggesting reduced level of available NAD+ (Figure 5B). No significant change was observed in *GBA* KO neurons (Figure S3N).

The NAD+ Precursor Nicotinamide Riboside Rescues Mitochondrial Defects in *GBA*-PD iPSC-Derived Neurons

Next, we tested the ability of different NAD+ precursors to increase NAD+ levels in human iPSC-derived neurons. Control iPSC-derived neurons were treated with nicotinamide (NAM), NMN, or nicotinamide riboside (NR), and NAD+ levels were measured using a NAD+ cycling assay. NR and NMN showed the strongest effect in boosting NAD+ levels (Figure S6A). As NR represents a promising approach, as shown by pharmacokinetic studies in healthy subjects (Trammell et al., 2016), we investigated the ability of NR to rescue *GBA*-linked mitochondrial defects. NR significantly increased NAD+ and NADH levels in *GBA*-PD neurons (Figures S6B and S6C). NR treatment resulted in an increase in expression of markers of mitochondrial biogenesis (TFAM) and mitochondrial UPR (mtUPR) (HSP60) (Figure 5C). Consistent with these findings, mitochondrial DNA content and mitochondrial mass were increased after 48 hr in NR-treated samples (Figures 5D and 5E). The effect of NR was abrogated by EX527, a SIRT1-specific inhibitor, suggesting that SIRT1 is one of the mediators of NR function (Figure S6D). Importantly, NR restored mitochondrial cristae morphology and significantly reduced mtROS production in *GBA*-PD neurons (Figures 5F–5H). In parallel, NR

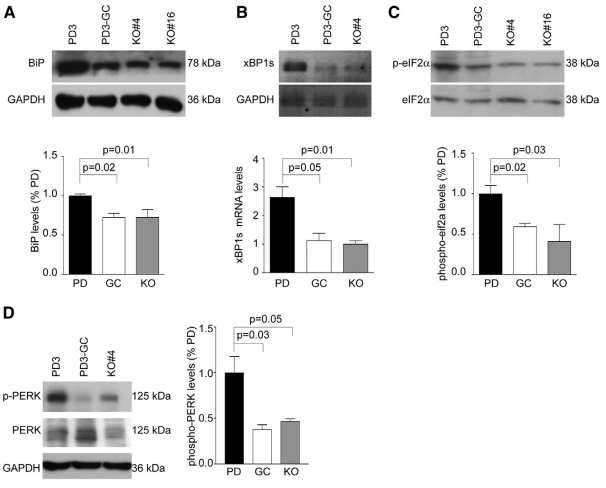

Figure 4. ER Stress Responses in *GBA*-PD and *GBA* KO iPSC Neurons

Analysis of ER stress responses and UPR was performed in isogenic *GBA*-PD (N370S), gene-corrected (GC) controls, and isogenic *GBA* KO (clones 4 and 16) iPSC neurons.

(A) Representative western blots showing BiP levels in isogenic *GBA*-PD, GC, and *GBA* KO iPSC neurons. BiP intensity bands were normalized to GAPDH and the corresponding isogenic control. Data are expressed as mean + SEM (n = 5; one-way ANOVA).

(B) Analysis of XBP1 splicing (XBP1s). mRNA levels of XBP1s were measured by qPCR. Representative agarose gel electrophoresis of qRT-PCR products is shown. For quantification, GAPDH served as reference gene. Data are expressed as mean + SEM (n = 5; one-way ANOVA).

(C) Representative western blots showing phospho-eIF2α/eIF2α levels in isogenic *GBA*-PD, GC, and *GBA* KO iPSC-derived neurons. For quantification, phospho-eIF2α intensity bands were normalized to total eif2α and the corresponding isogenic control. Data are expressed as mean + SEM (one-way ANOVA). Gel loading as in (A).

(D) Representative western blots showing phospho-PERK/PERK levels in isogenic *GBA*-PD, GC, and *GBA* KO iPSC-derived neurons. Data are expressed as mean + SEM (n = 5; one-way ANOVA).

treatment significantly reduced the mitochondrial membrane potential (Figure 5I). Similar results were observed when *GBA* KO neurons were treated with NR (Figures S6E–S6G). With regard to the observed defects in mitochondrial dynamics, NR altered the levels of mitochondrial shaping proteins, with a nonsignificant increase in DRP1, Mfn1, and OPA1 and a slight decrease in Fis1 (Figures 5J and 5K). The decreased levels of mitochondrial DNA content observed at 24 hr after NR treatment would suggest an increased mitochondrial clearance (Figure 5D). In line with these findings, NR was able to increase the levels of BNIP3L/NIX in *GBA*-PD neurons (Figure 5L). NR did not enhance mitochondrial respiration (Figures S6H and S6I). On the contrary, a significant decrease in basal respiration was observed in *GBA*-PD iPSC-derived neurons treated with NR (Figure S6H). In addition, NR treatment did not alter protein levels of BiP in *GBA*-PD neurons (Figure S6J). To confirm that increased NAD+ levels are responsible for the phenotypic rescue, we treated cells with the poly(ADP-ribose)-polymerase (PARP) inhibitor PJ34 that, differently from NAD+ precursors, increases NAD+ levels by inhibiting its consumption. Similar to NR, PJ34 significantly increased NAD+ levels in human-iPSC-derived neurons and rescued mitochondrial defects in *GBA*-PD neurons (Figures S7A–S7E). Taken together, these results suggest that increasing NAD+ levels rescues mitochondrial dysfunction via increased levels of NAD+ in patient-derived *GBA*-PD and *GBA* KO neurons.

Increasing NAD+ Improves Autophagy in *GBA*-PD and *GBA* KO Neurons

GBA mutations affect autophagy and lysosomal function, leading to autophagic block, defects in autophagosome clearance, and altered lysosomal recycling (Schöndorf et al., 2014; Magalhaes et al., 2016). To examine the effects of NR on autophagy, we treated *GBA*-PD and *GBA* KO neurons with NR and assessed parameters of autophagic function. NR treatment did not alter the levels of LC3II at basal conditions; however, it significantly increased LC3II levels in patient neurons treated with leupeptin and ammonium chloride, suggesting an increase of synthesis and clearance of autophagosomes (Figures S7F–S7I). The autophagic flux was significantly increased in *GBA* KO neurons and showed a nonsignificant increase in *GBA*-PD neurons after NR treatment (Figures S7F–S7I).

NR Metabolism and NAD+ Availability in Human iPSC-Derived Neurons

To examine pathways of NAD+ maintenance and NAD+ precursors utilization, control iPSC-derived neurons were treated with the NAMPT inhibitor FK866, and NAD+ levels were measured. FK866 treatment decreased intracellular NAD+ levels by more than 90% (Figure 6A). However, FK866 treatment did not alter the sensitivity of human neurons to NR treatment (Figure 6A), indicating that NR is metabolized into NAD+ in a NAMPT-independent pathway. We next measured the expression levels of the NAD+ biosynthesis enzymes NR kinase 1 and 2 (NRK1 and NRK2) (Bieganowski and Brenner, 2004). In undifferentiated iPSCs, NRK2 showed higher expression levels; on the contrary, levels of NRK1 were significantly higher in iPSC-derived neurons (Figure 6B). The role of NRKs in NAD+ metabolism in human neurons is still unknown. Given its high expression, we aimed to investigate whether NRK1 is essential for NR metabolism into NAD+ in human neurons. Of note, mRNA levels of NRK1 were not affected by NR treatment (Figure 6C). Next, we knocked down NRK1 in control iPSC-derived neurons using

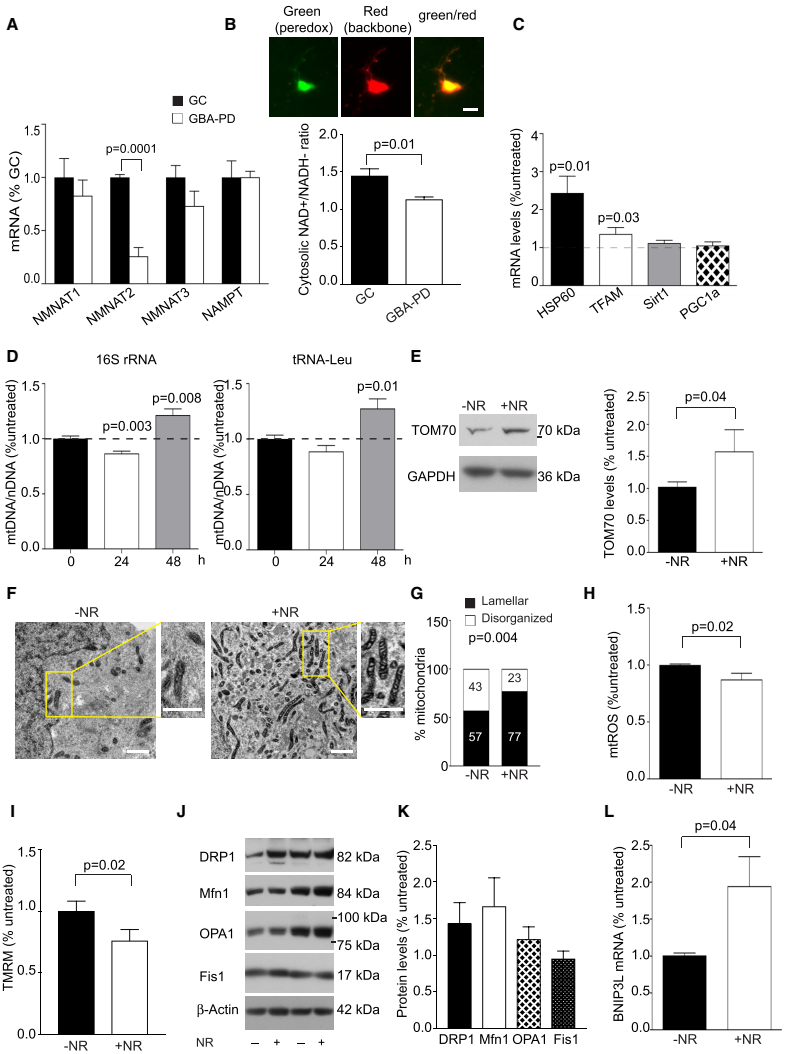

Figure 5. Nicotinamide Riboside Reverts Mitochondrial Defects in *GBA*-PD iPSC Neurons

(A) NMNAT1, NMNAT2, NMNAT3, and NAMPT mRNA levels in isogenic GC and *GBA*-PD (N370S, L444P) iPSC neurons. Data were normalized to the level of the housekeeping genes Rplp0 and OAZ and expressed as fold change over PD. Data are expressed as mean + SEM (n = 5; two-tailed t test).

(B) The NAD+/NADH redox state was measured in iPSC-derived neurons using the biosensor Peredox. Results are presented as mean + SEM (n = 5; two-tailed t test).

(legend continued on next page)

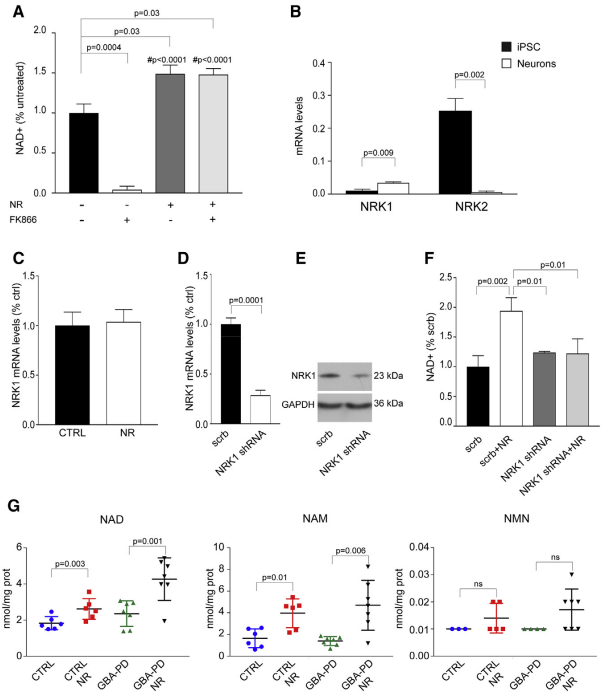

Figure 6. NR Metabolism and Availability in Human iPSC Neurons

(A) Control iPSC neurons were treated with NR with or without the NAMPT inhibitor FK866, and NAD+ levels were measured using a NAD+ cycling assay. Data are expressed as fold changes over untreated neurons and presented as mean + SEM (n = 3; one-way ANOVA). #, significance compared with FK866-treated neurons.

(B) NRK1 and NRK2 mRNA levels were measured in control undifferentiated human iPSCs and iPSC-derived neurons. Data are normalized to Rplp0 levels and expressed as mean + SEM (n = 3; two-tailed t test).

(C) NRK1 mRNA levels were measured in control iPSC neurons with or without NR treatment. Data are normalized to control and presented as mean + SEM (n = 3).

(D) Knockdown efficiency of NRK1 in iPSC neurons was determined by qRT-PCR and normalized to non-targeting shRNA. Data are presented as mean + SEM (n = 3; two-tailed t test).

(E) Representative western blot for NRK1 showing knockdown efficiency in iPSC neurons.

(F) Scramble (Scrb) or NRK1 knockdown control iPSC neurons were treated with NR, and NAD+ levels were measured using a NAD+ cycling assay. Data are expressed as fold changes over untreated and presented as mean + SEM (n = 3; one-way ANOVA).

(G) Control and *GBA*-PD (N370S) iPSC neurons were treated with 0.5 mM NR for 24 hr and LC-MS-based targeted NAD+ metabolomics was performed. Levels of NAD, NAM, and NMN are shown. Data are normalized on protein concentration and presented as mean ± SD (n = 7 independent differentiations; two-tailed t test).

lentiviral-mediated short hairpin RNA (shRNA) (Figures 6D and 6E). NRK1 knockdown did not affect basal levels of NAD+ in neurons, as assessed by a NAD+ cycling assay, whereas NR treatment was unable to significantly increase NAD+ levels in NRK1 knockdown neurons (Figure 6F). These data suggest that NRK1 is essential for exogenous NR metabolism in human neurons. To further examine the metabolism of exogenous NR, we treated control and *GBA*-PD iPSC neurons with 0.5 mM NR and performed LC-MS-based targeted quantitative metabolomics (Figures 6G and S7J). NR treatment significantly increased the levels of NAD+ in control and patient cells. In addition, we found a significant increase of NAM in both groups. On the other

(C) iPSC-derived neurons with *GBA* mutations (N370S and L444P) were treated with NR, and mRNA expression levels of mtUPR and mitochondrial biogenesis markers were measured by qRT-PCR. Data are normalized to untreated and expressed as mean + SEM (n = 5; two-tailed t test).

(D) qRT-PCR was performed to determine mtDNA content as mitochondrial (16S rRNA and tRNA-Leu) to nuclear (β-2M) DNA ratio in untreated samples or after 24- or 48-hr treatment with NR. Data are normalized to untreated and expressed as mean + SEM (n = 5; two-tailed t test).

(E) Western blot showing TOM70 levels. Protein levels are normalized to GAPDH and the corresponding untreated control. Data are presented as mean + SEM (n = 3; two-tailed t test).

(F and G) Mitochondrial morphology was assessed by TEM. Representative TEM images of mitochondria in *GBA*-PD (L444P) iPSC-derived neurons untreated or treated with NR (F; scale bar 500 nm). Quantification of mitochondrial cristae morphology in NR treated and untreated *GBA*-PD iPSC neurons (G; n = 3; two-sided Fisher's exact test).

(H) mtROS in *GBA*-PD (N370S, L444P) iPSC neurons after NR treatment. Data are normalized to the corresponding untreated control and presented as mean + SEM (n = 3; Student's t test).

(I) Mitochondrial membrane potential in *GBA*-PD (N370S, L444P) iPSC neurons after NR treatment. Data are normalized to untreated samples and presented as mean + SEM (n = 5; two-tailed t test).

(J and K) *GBA*-PD (N370S, L444P) iPSC-neurons were treated with NR, and the levels of OPA1, Mfn1, Fis1, and DRP1 were assessed by western blot (J). β-Actin was used as a loading control. Quantification is depicted in (K). Data are represented as mean + SEM (n = 5).

(L) BNIP3L mRNA levels. Data are normalized on Rplp0 and OAZ1 and expressed as fold changes over untreated. Values are presented as mean + SEM (n = 5; Student's t test).

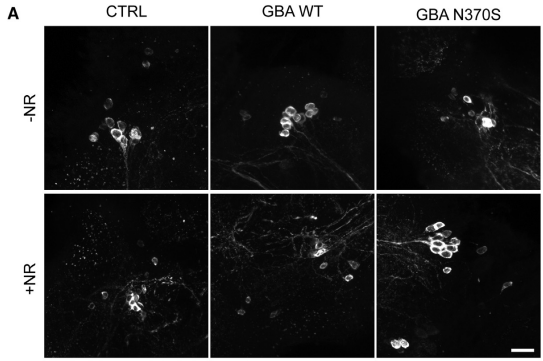

Figure 7. Nicotinamide Riboside Prevents Dopaminergic Neuronal Loss and Rescues Climbing Deficits in *GBA*-PD Flies

(A) Representative confocal images of adult *Drosophila* brains stained with anti-TH antibody. Control and transgenic flies expressing human wild-type (WT) or N370S *GBA* with and without NR treatment (500 μM for 30 days) are shown (scale bar, 10 μm).

(B) Graphs show DA cell counts in absence or presence of NR in PPL1 clusters. Data are presented as mean + SEM (ns, non-significant, n = 8–12 clusters; Kruskal-Wallis with Dunn's multiple comparisons test).

(C) Analysis of climbing ability in adult flies expressing N370S *GBA* variants in the presence or absence of NR (500 μM for 10 days). Data are presented as mean + 95% confidence interval (n = ~50 animals per condition ;Kruskal-Wallis with Dunn's multiple comparisons test).

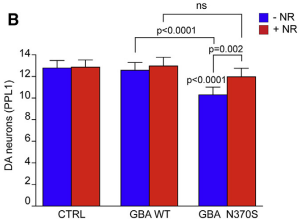

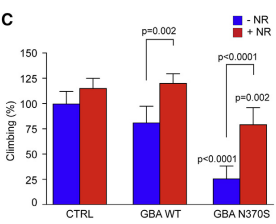

hand, levels of NMN, the immediate downstream product of NR, tended to be higher in NR-treated cells, but this difference was not statistically significant (Figure 6G).

NR Rescues Motor Deficits in a *Drosophila* Model of *GBA*-PD

To assess the neuroprotective effect of NAD+ precursors *in vivo*, we employed a *Drosophila* model of *GBA*-PD. Flies expressing human N370S *GBA* show increased ER stress, an age-dependent loss of DA neurons accompanied by progressive defects in climbing activity (Sanchez-Martinez et al., 2016). To explore neuroprotection, flies expressing wild-type (WT) or N370S *GBA* were first raised on normal food, and then adult flies were aged on food containing NR (500 μM). At 30 days, expression of N370S *GBA* caused loss of DA neurons in the protocerebral posterial lateral 1 (PPL1) cluster. Strikingly, feeding NR significantly prevented DA neuronal loss compared to untreated controls (Figures 7A and 7B). Importantly, NR treatment also significantly prevented the decline in climbing ability in mutant N370S *GBA* flies (Figure 7C).

DISCUSSION

Mounting evidence suggests that mitochondrial dysfunction plays a key role in PD. Here, we report that neurons from *GBA*-PD patients and *GBA* KO neurons exhibit mitochondrial dysfunction characterized by morphological changes, reduced respiration, and increased oxidative stress. As mitochondrial membrane lipid composition regulates many of these functions (Aufschnaiter et al., 2017) and changes in lipid metabolism have been observed in *GBA*-PD (Schöndorf et al., 2014; Fernandes et al., 2016; García-Sanz et al., 2017), we examined the mitochondrial sphingolipid profile of *GBA*-PD and *GBA* KO neurons. Lipidomic analysis revealed the absence of a significant accumulation of sphingolipids in patient mitochondria. However, we observed a significant increase of C16-GlcCer. On the contrary, the mitochondrial sphingolipid profile of *GBA* KO neurons was profoundly altered, with significant accumulation of GlcCer and glucosylsphingosine. Given the role of sphingolipids in the regulation of mitochondrial properties, substrate accumulation or even subtle changes in lipid composition of mitochondrial membranes, as observed in patient mitochondria, may interfere with their biophysical properties and signaling pathways. However, we are not able to unambiguously define the exact subcellular localization of these alterations. Even though we have isolated mitochondria to the highest degree of purity, a small amount of contamination with lysosomes and ER was still present. The low degree of non-mitochondrial proteins and the complete absence of additional lysosomal markers (other than LAMP1) suggest the residual presence of organelle contact sites in mitochondrial preparations. Given the importance of contact sites in interorganelle communication (Wong et al., 2018), further studies are needed to investigate the role of distinct sphingolipids in such inter-organelle communication and mitochondrial dysfunction.

Overall, we did not observe a gene dosage effect when comparing mitochondrial function in heterozygous *GBA*-PD with *GBA* KO neurons. Thus, distinctly different mechanisms

likely contribute to mitochondrial dysfunction in these models. One such mechanism could be the alteration of mitochondria sphingolipid composition, which we observed in *GBA* KO, but not *GBA*-PD, cells. Interestingly, in other lysosomal storage diseases, the loss of lysosomal enzymatic function leads to substrate accumulation at the ER membranes and subsequent activation of the UPR (Tessitore et al., 2004). However, despite significant substrate accumulation in our model, the complete loss of GCase enzymatic function in *GBA* KO neurons is not sufficient to trigger ER stress responses that were instead observed in heterozygous *GBA*-PD neurons. This points toward a key role of gain-of-function mechanisms in ER stress responses in *GBA*-PD. On the other hand, GCase deficiency results in sphingolipid accumulation and mitochondrial dysfunction including increased mtROS.

GBA-PD neurons showed an imbalance of mitochondrial shaping proteins DRP1, OPA1, Mfn1, and Fis1 and an increased ratio of L-OPA1/S-OPA1. As L-OPA1 processing and impaired DRP1 activity contribute to the dysfunction of mitophagy (MacVicar and Lane, 2014), our results would suggest an impairment of mitochondrial clearance in *GBA*-PD. This was further supported by the reduced mitochondria-lysosome colocalization and reduced expression of the mitophagy adaptor NIX/BNIP3L. Unexpectedly, we did not observe a significant increase of mitochondrial content in patient neurons. The mitochondrial membrane potential was also preserved in *GBA*-PD neurons. As BNIP3L/NIX plays a role in the loss of mitochondrial membrane potential (Sandoval et al., 2008), reduced levels of BNIP3L in *GBA*-PD neurons could explain the lack of decreased mitochondrial membrane potential. Taken together, our data suggest an imbalance of mitochondrial dynamics in *GBA*-PD neurons that leads to mitochondrial dysfunction in the absence of accumulation of damaged mitochondria. As mitophagy occurs locally in distal neuronal axons, we cannot exclude accumulation of dysfunctional mitochondria within axons (Ashrafi et al., 2014).

Increasing intracellular NAD+ concentrations has been shown to be protective against age-related metabolic decline and disease (Rajman et al., 2018; Katsyuba and Auwerx, 2017). NAD+ is a coenzyme for several enzymes, including SIRT1, which regulates mitochondrial biogenesis, autophagy, and cellular stress responses (Chang and Guarente, 2014; Prola et al., 2017). Several mechanisms lead to NAD+ consumption, including oxidative stress. To examine whether NAD+ decline is involved in *GBA*-PD, we have first used targeted metabolomics and found that NAD+ levels were maintained in both *GBA*-PD and *GBA* KO iPSC-derived neurons, as well as whole brains from *gba*$^{-/-}$ zebrafish. As cellular energy metabolism and the cytosolic NADH/NAD+ redox state differ in various tissues or different cells within the same tissue, we have employed a genetically encoded NADH/NAD+ biosensor for live-cell imaging in iPSC-derived neurons. *GBA*-PD neurons showed a significant reduction of the NAD+/NADH redox state. The reduction of NMNAT2 in *GBA*-PD neurons further supports an alteration of NAD+ metabolism in *GBA*-PD. Besides its role in NAD+ synthesis, NMNAT2 also acts as a chaperone to reduce proteotoxic stress and its levels decline prior to the onset of neurodegeneration (Ali et al., 2016). Thus, the reduction of NMNAT2 in *GBA*-PD neurons could also explain the increased proteotoxic stress observed in these cells. The zebrafish metabolomics data further support an alteration of NAD+ metabolism. *GBA* deficiency led to a significant increase in NMN in zebrafish brains. This strongly suggests reduced NMNAT activity in the zebrafish brain when lacking *GBA*. We were unable to reliably detect NMN at basal conditions in iPSC-derived neurons, as NMN is a low abundance metabolite in cellular extracts. In conclusion, even though we cannot yet conclude definitively that NAD+ decline occurs in *GBA*-PD, our data suggest alterations of NAD+ metabolism in these models. Given the existence of different cellular NAD+ pools and the relevance of mitochondrial NAD+ for mitochondrial and cellular function, an important question remains how these NAD+ cellular pools communicate with each other and modulate the aging process and disease risk.

Here, we report that human iPSC-derived neurons rely on NAMPT for maintenance of the NAD+ pool, they are responsive to NAD+ precursors and utilize NRK1 as the main metabolic pathway to synthetize NAD+ from exogenous NR in a NAMPT-independent manner. NR administration caused a significant increase of NAD+. Besides NAD+, levels of NAM were also increased upon NR treatment, suggesting an increase of the activity of NAD+ consuming enzymes that convert NAD+ to NAM. However, we cannot exclude a partial conversion of exogenous NR into NAM before synthesis to NAD+. Levels of the immediate downstream product of NR, NMN, tended to be higher in NR-treated cells, but this difference was not statistically significant. This would suggest a rapid conversion of NMN into NAD+. In our model systems, NR ameliorated mitochondrial function and rescued mitochondrial quality control. We also observed an increased expression of BNIP3L/NIX after NR treatment. In line with this, mitochondrial content decreased after 24 hr of NR treatment, which points toward increased mitophagy. However, prolonged NR treatment boosted mitochondrial content and increased TFAM, which underlines the dual role of NAD+ and sirtuins in maintaining mitochondrial biogenesis and quality control. Furthermore, supporting an increase in mitophagy, NR positively regulated autophagic function. Importantly, we found that NAD+ supplementation rescues the age-dependent loss of DA neurons and decline in motor ability in a *GBA*-PD *Drosophila* model.

In summary, our study elucidates the mechanisms involved in *GBA*-PD and reveals mitochondrial dysfunction as a key driver of disease. Our findings show that NAD+ precursors ameliorate *GBA*-related defects. Among the available NAD+ precursors, NR may be a valuable therapeutic approach due to its high bioavailability, minimal toxicity, and evidence of its ability to cross the blood-brain barrier (Trammell et al., 2016). Future studies will explore the potential therapeutic benefits of combining NAD+ boosters with chaperones and GCase activators (Migdalska-Richards et al., 2016).

EXPERIMENTAL PROCEDURES

Cell Culture

iPSC lines (Table S1) were previously generated and characterized (Schöndorf et al., 2014).

Generation of *GBA* Knockout Human iPSCs

CRISPR-Cas9 constructs were generated as described previously (Ran et al., 2013).

Measurement of Mitochondrial Membrane Potential and mtROS

Neurons were washed once with Hank's balanced salt solution (HBSS) (Invitrogen) following incubation with 200 nM tetramethylrhodamine methylester perchlorat (TMRM) (Invitrogen). For measurements of mtROS, cells were incubated with 5 μM MitoSOX Red (Invitrogen). Cytofluorimetric analysis was performed using MACSQuant Analyzer 10 (Miltenyi).

Seahorse XF^{e}96 Metabolic Flux Analysis

OCR was analyzed using an XF^{e}96 Extracellular Flux Analyzer (Seahorse Biosciences).

NAD/NADH Measurements and Metabolomics

NAD+ levels were measured using the NAD/NADH-Glo Assay Kit (Promega). NADH levels were measured using the NAD/NADH Assay Kit (Abcam). The cytosolic NADH/NAD+ redox state of iPSC neurons was measured as described previously (Hung et al., 2011).

Enzymatic Activities

GCase activity was tested using the intact cell lysosomal β-Glu assay (Sawkar et al., 2006). Citrate synthase and mitochondrial CI activities were measured following the protocol reported by Spinazzi et al. (2012).

Drosophila Studies

Transgenic *Drosophila* lines expressing human WT or N370S *GBA* were previously generated (Sanchez-Martinez et al., 2016).

Statistical Analysis

The Statistical Package GraphPad Prism version 7.0b (GraphPad Software, San Diego, CA) was used to analyze the data. Statistical testing involved a two-sided Fisher's exact test, two-tailed Student's t test, one-way ANOVA with Bonferroni's multiple comparison test, or Kruskal-Wallis with Dunn's multiple comparisons test, as appropriate. Data are expressed as mean + SEM or SD as indicated.

SUPPLEMENTAL INFORMATION

Supplemental Information includes Supplemental Experimental Procedures, seven figures, and two tables and can be found with this article online at https://doi.org/10.1016/j.celrep.2018.05.009.

ACKNOWLEDGMENTS

We are grateful to Katharina Demandt, Ulrike Ulmer, Selina Reich, and Maria Zarani for their excellent experimental help and Simone Pöschel from the Imaging Flow Cytometry Core Facility, University of Tübingen for excellent assistance with the Amnis ImageStream. This work was made possible through funding by the German Research Council (DFG; DE 2157/2-1; M.D.), Helmholtz Association (VH-NG-1123; M.D.), Marie Curie Career Integration Grant (CIG304108; M.D.), Medical Research Council core funding (MC-A070-5PSB0; A.J.W.), and the European Research Council (starting grant 309742; AJW). Research was supported in part by the Medical University of South Carolina's Lipidomics Shared Resource through funding of laboratory space for the Analytical Unit located in 505 Children's Research Institute (CRI): Hollings Cancer Center (P30 CA138313), the Lipidomics Shared Resource in the South Carolina Lipidomics and Pathobiology COBRE; MUSC Department of Biochemistry (P20 RR017677), and the National Center for Research Resources and Office of the Director of the National Institutes of Health (C06 RR018823)

AUTHOR CONTRIBUTIONS

M.D. conceived, designed, and supervised the study. A.J.W. designed *Drosophila* studies. D.C.S., D.I., P.B., S.D.C., C.Y., L.K.S., G.D.N., V.P., and J.P. performed *in vitro* experiments. D.C.S., D.I., P.B., S.D.C., and L.K.S. analyzed data. S.N. and B.H. performed TEM, A.S.-M. and I.G. performed *Drosophila* studies and analyzed data, and M.K. and O.B. performed zebrafish experiments. T.G. oversaw patient sample collection. M.D. wrote the manuscript with input from all authors. All authors contributed to proofreading of the manuscript.

DECLARATION OF INTERESTS

The authors declare no competing interests.

Received: September 7, 2017
Revised: March 5, 2018
Accepted: May 2, 2018
Published: June 5, 2018

REFERENCES

Ali, Y.O., Allen, H.M., Yu, L., Li-Kroeger, D., Bakhshizadehmahmoudi, D., Hatcher, A., McCabe, C., Xu, J., Bjorklund, N., Taglialatela, G., et al. (2016). NMNAT2:HSP90 complex mediates proteostasis in proteinopathies. PLoS Biol. *14*, e1002472.

Ashrafi, G., Schlehe, J.S., LaVoie, M.J., and Schwarz, T.L. (2014). Mitophagy of damaged mitochondria occurs locally in distal neuronal axons and requires PINK1 and Parkin. J. Cell Biol. *206*, 655–670.

Aufschnaiter, A., Kohler, V., Diessl, J., Peselj, C., Carmona-Gutierrez, D., Keller, W., and Büttner, S. (2017). Mitochondrial lipids in neurodegeneration. Cell Tissue Res. *367*, 125–140.

Bieganowski, P., and Brenner, C. (2004). Discoveries of nicotinamide riboside as a nutrient and conserved NRK genes establish a Preiss-Handler independent route to NAD+ in fungi and humans. Cell *117*, 495–502.

Chang, H.C., and Guarente, L. (2014). SIRT1 and other sirtuins in metabolism. Trends Endocrinol. Metab. *25*, 138–145.

Cleeter, M.W., Chau, K.Y., Gluck, C., Mehta, A., Hughes, D.A., Duchen, M., Wood, N.W., Hardy, J., Mark Cooper, J., and Schapira, A.H. (2013). Glucocerebrosidase inhibition causes mitochondrial dysfunction and free radical damage. Neurochem. Int. *62*, 1–7.

Exner, N., Lutz, A.K., Haass, C., and Winklhofer, K.F. (2012). Mitochondrial dysfunction in Parkinson's disease: molecular mechanisms and pathophysiological consequences. EMBO J. *31*, 3038–3062.

Fernandes, H.J., Hartfield, E.M., Christian, H.C., Emmanoulidou, E., Zheng, Y., Booth, H., Bogetofte, H., Lang, C., Ryan, B.J., Sardi, S.P., et al. (2016). ER stress and autophagic perturbations lead to elevated extracellular α-synuclein in GBA-N370S Parkinson's iPSC-derived dopamine neurons. Stem Cell Reports *6*, 342–356.

García-Sanz, P., Orgaz, L., Bueno-Gil, G., Espadas, I., Rodríguez-Traver, E., Kulisevsky, J., Gutierrez, A., Dávila, J.C., González-Polo, R.A., Fuentes, J.M., et al. (2017). N370S-GBA1 mutation causes lysosomal cholesterol accumulation in Parkinson's disease. Mov. Disord. *32*, 1409–1422.

Gegg, M.E., Burke, D., Heales, S.J., Cooper, J.M., Hardy, J., Wood, N.W., and Schapira, A.H. (2012). Glucocerebrosidase deficiency in substantia nigra of Parkinson disease brains. Ann. Neurol. *72*, 455–463.

Hung, Y.P., Albeck, J.G., Tantama, M., and Yellen, G. (2011). Imaging cytosolic NADH-NAD(+) redox state with a genetically encoded fluorescent biosensor. Cell Metab. *14*, 545–554.

Jansen, I.E., Ye, H., Heetveld, S., Lechler, M.C., Michels, H., Seinstra, R.I., Lubbe, S.J., Drouet, V., Lesage, S., Majounie, E., et al.; International Parkinson's Disease Genetics Consortium (IPGDC) (2017). Discovery and functional prioritization of Parkinson's disease candidate genes from large-scale whole exome sequencing. Genome Biol. *18*, 22.

Jo, E., McLaurin, J., Yip, C.M., St George-Hyslop, P., and Fraser, P.E. (2000). alpha-Synuclein membrane interactions and lipid specificity. J. Biol. Chem. *275*, 34328–34334.

Katsyuba, E., and Auwerx, J. (2017). Modulating NAD$^+$ metabolism, from bench to bedside. EMBO J. *36*, 2670–2683.

Keatinge, M., Bui, H., Menke, A., Chen, Y.C., Sokol, A.M., Bai, Q., Ellett, F., Da Costa, M., Burke, D., Gegg, M., et al. (2015). Glucocerebrosidase 1 deficient

Danio rerio mirror key pathological aspects of human Gaucher disease and provide evidence of early microglial activation preceding alpha-synuclein-independent neuronal cell death. Hum. Mol. Genet. *24*, 6640–6652.

MacVicar, T.D., and Lane, J.D. (2014). Impaired OMA1-dependent cleavage of OPA1 and reduced DRP1 fission activity combine to prevent mitophagy in cells that are dependent on oxidative phosphorylation. J. Cell Sci. *127*, 2313–2325.

Magalhaes, J., Gegg, M.E., Migdalska-Richards, A., Doherty, M.K., Whitfield, P.D., and Schapira, A.H. (2016). Autophagic lysosome reformation dysfunction in glucocerebrosidase deficient cells: relevance to Parkinson disease. Hum. Mol. Genet. *25*, 3432–3445.

Maor, G., Rencus-Lazar, S., Filocamo, M., Steller, H., Segal, D., and Horowitz, M. (2013). Unfolded protein response in Gaucher disease: from human to Drosophila. Orphanet J. Rare Dis. *8*, 140.

Mazzulli, J.R., Xu, Y.H., Sun, Y., Knight, A.L., McLean, P.J., Caldwell, G.A., Sidransky, E., Grabowski, G.A., and Krainc, D. (2011). Gaucher disease glucocerebrosidase and α-synuclein form a bidirectional pathogenic loop in synucleinopathies. Cell *146*, 37–52.

Migdalska-Richards, A., and Schapira, A.H. (2016). The relationship between glucocerebrosidase mutations and Parkinson disease. J. Neurochem. *139* (*Suppl 1*), 77–90.

Migdalska-Richards, A., Daly, L., Bezard, E., and Schapira, A.H. (2016). Ambroxol effects in glucocerebrosidase and α-synuclein transgenic mice. Ann. Neurol. *80*, 766–775.

Mouchiroud, L., Houtkooper, R.H., Moullan, N., Katsyuba, E., Ryu, D., Cantó, C., Mottis, A., Jo, Y.S., Viswanathan, M., Schoonjans, K., et al. (2013). The NAD(+)/sirtuin pathway modulates longevity through activation of mitochondrial UPR and FOXO signaling. Cell *154*, 430–441.

Osellame, L.D., Rahim, A.A., Hargreaves, I.P., Gegg, M.E., Richard-Londt, A., Brandner, S., Waddington, S.N., Schapira, A.H., and Duchen, M.R. (2013). Mitochondria and quality control defects in a mouse model of Gaucher disease: links to Parkinson's disease. Cell Metab. *17*, 941–953.

Prola, A., Pires Da Silva, J., Guilbert, A., Lecru, L., Piquereau, J., Ribeiro, M., Mateo, P., Gressette, M., Fortin, D., Boursier, C., et al. (2017). SIRT1 protects the heart from ER stress-induced cell death through eIF2α deacetylation. Cell Death Differ. *24*, 343–356.

Rajman, L., Chwalek, K., and Sinclair, D.A. (2018). Therapeutic potential of NAD-boosting molecules: the in vivo evidence. Cell Metab. *27*, 529–547.

Ran, F.A., Hsu, P.D., Wright, J., Agarwala, V., Scott, D.A., and Zhang, F. (2013). Genome engineering using the CRISPR-Cas9 system. Nat. Protoc. *8*, 2281–2308.

Rocha, E.M., Smith, G.A., Park, E., Cao, H., Brown, E., Hallett, P., and Isacson, O. (2015). Progressive decline of glucocerebrosidase in aging and Parkinson's disease. Ann. Clin. Transl. Neurol. *2*, 433–438.

Sanchez-Martinez, A., Beavan, M., Gegg, M.E., Chau, K.Y., Whitworth, A.J., and Schapira, A.H. (2016). Parkinson disease-linked GBA mutation effects reversed by molecular chaperones in human cell and fly models. Sci. Rep. *6*, 31380.

Sandoval, H., Thiagarajan, P., Dasgupta, S.K., Schumacher, A., Prchal, J.T., Chen, M., and Wang, J. (2008). Essential role for Nix in autophagic maturation of erythroid cells. Nature *454*, 232–235.

Sawkar, A.R., Schmitz, M., Zimmer, K.P., Reczek, D., Edmunds, T., Balch, W.E., and Kelly, J.W. (2006). Chemical chaperones and permissive temperatures alter localization of Gaucher disease associated glucocerebrosidase variants. ACS Chem. Biol. *1*, 235–251.

Schapira, A.H., Cooper, J.M., Dexter, D., Jenner, P., Clark, J.B., and Marsden, C.D. (1989). Mitochondrial complex I deficiency in Parkinson's disease. Lancet *1*, 1269.

Schöndorf, D.C., Aureli, M., McAllister, F.E., Hindley, C.J., Mayer, F., Schmid, B., Sardi, S.P., Valsecchi, M., Hoffmann, S., Schwarz, L.K., et al. (2014). iPSC-derived neurons from GBA1-associated Parkinson's disease patients show autophagic defects and impaired calcium homeostasis. Nat. Commun. *5*, 4028.

Sidransky, E., Nalls, M.A., Aasly, J.O., Aharon-Peretz, J., Annesi, G., Barbosa, E.R., Bar-Shira, A., Berg, D., Bras, J., Brice, A., et al. (2009). Multicenter analysis of glucocerebrosidase mutations in Parkinson's disease. N. Engl. J. Med. *361*, 1651–1661.

Spinazzi, M., Casarin, A., Pertegato, V., Salviati, L., and Angelini, C. (2012). Assessment of mitochondrial respiratory chain enzymatic activities on tissues and cultured cells. Nat. Protoc. *7*, 1235–1246.

Tessitore, A., del P Martin, M., Sano, R., Ma, Y., Mann, L., Ingrassia, A., Laywell, E.D., Steindler, D.A., Hendershot, L.M., and d'Azzo, A. (2004). GM1-ganglioside-mediated activation of the unfolded protein response causes neuronal death in a neurodegenerative gangliosidosis. Mol. Cell *15*, 753–766.

Trammell, S.A., Schmidt, M.S., Weidemann, B.J., Redpath, P., Jaksch, F., Dellinger, R.W., Li, Z., Abel, E.D., Migaud, M.E., and Brenner, C. (2016). Nicotinamide riboside is uniquely and orally bioavailable in mice and humans. Nat. Commun. *7*, 12948.

Velayati, A., Yu, W.H., and Sidransky, E. (2010). The role of glucocerebrosidase mutations in Parkinson disease and Lewy body disorders. Curr. Neurol. Neurosci. Rep. *10*, 190–198.

Wong, Y.C., Ysselstein, D., and Krainc, D. (2018). Mitochondria-lysosome contacts regulate mitochondrial fission via RAB7 GTP hydrolysis. Nature *554*, 382–386.